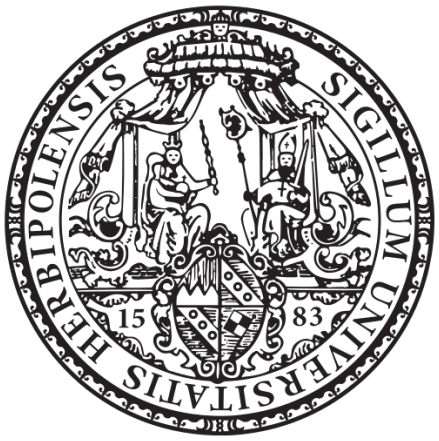

Activation of the Interleukin-5 receptor and its inhibition by cyclic peptides

Aktivierung des IL-5 Rezeptors und dessen Inhibierung durch zyklische Peptide

Doctoral thesis for a doctoral degree
at the Graduate School of Life Sciences,
Julius-Maximilians-Universität Würzburg,
Section: Biomedicine

submitted by

Jan-Philipp Scheide-Nöth

from

Göttingen

Würzburg 2019

Submitted on: ……..……..

Office stamp

Members of the *Promotionskomitee*:

Chairperson: Prof. Dr. Jörg Schultz

Primary Supervisor: Prof. Dr. Thomas Müller

Supervisor (Second): Prof. Dr. Hermann Schindelin

Supervisor (Third): PD Dr. rer. nat. Heike Hermanns

Date of Public Defense: ……

Date of Receipt of Certificates: ……

Table of contents

1 INTRODUCTION 1
1.1 Overview of the immune system 1
1.2 Eosinophils 2
1.3 Interleukin-5 4
1.3.1 A member of the common beta chain family 4
1.3.2 Structure of IL-5 5
1.4 Mechanism of interleukin-5 signaling 7
1.5 Structural and functional aspects of the IL-5 receptor subunits 9
1.5.1 IL-5 receptor α and the binary IL-5•IL-5Rα complex 9
1.5.2 Common beta chain and the ternary IL-5•IL-5Rα•βc complex 14
1.6 Eosinophil associated diseases and the role of IL-5 18
1.6.1 Helminth infections 18
1.6.2 Asthma 18
1.6.3 Hypereosinophilic syndrome 19
1.7 Therapeutic approaches for HES and asthma 21
1.7.1 Targeting IL-5 as a therapeutic approach for asthma and HES 22

2 AIMS 25

3 MATERIALS AND METHODS 27
3.1 Materials 27
3.1.1 Chemicals and Enzymes 27
3.1.2 Bacterial Strains 27
3.1.3 Vectors 27
3.1.4 Oligonucleotides 28
3.1.5 Antibiotics 30
3.2 Molecular biology methods 31
3.2.1 Single mutation by rapid PCR site-directed mutagenesis 31
3.2.2 Two-step PCR 31
3.2.3 Restriction endonuclease reaction 32
3.2.4 Agarose gel electrophoresis 33
3.2.5 Ligation 33
3.2.6 Preparation of competent cells (Rubidium chloride method) 34
3.2.7 Transformation of *E. coli* 34
3.2.8 Colony-PCR 35
3.2.9 Plasmid preparation 36
3.3 Protein chemical methods 37
3.3.1 SDS-polyacrylamide gel electrophoresis (SDS-PAGE) 37
3.3.2 Protein precipitation 38
3.3.3 Staining methods for SDS-PAGE gels 38
3.3.4 Western Blot 39
3.3.5 Dot blot 40
3.3.6 Photometric determination of the protein concentration 40
3.3.7 Labeling of proteins with biotin or fluorescent dye using NHS conjugates 41
3.3.8 Site-specific coupling of proteins with biotin or fluorescent dye using Sfp synthase 41
3.3.9 Mass spectrometry 42
3.4 Production of recombinant proteins using a baculovirus-insect cell expression system 43
3.4.1 Insect cell cultivation 43
3.4.2 Cell counting 43
3.4.3 Co-transfection 43
3.4.4 Plaque assay 44

3.4.5 Plaque assay staining ... 45
3.4.6 Virus amplification ... 45
3.4.7 Determination of the viral titer ... 46
3.4.8 Expression of proteins using High-Five™ insect cells ... 47
3.5 *E. coli* recombinant protein expression ... 48
3.5.1 Expression of insoluble proteins (inclusion-bodies) ... 48
3.5.2 Expression of soluble proteins ... 48
3.5.3 Cell lysis and extraction of insoluble proteins ... 49
3.5.4 Cell lysis of soluble proteins ... 49
3.5.5 Renaturation ... 50
3.6 Protein purification using chromatographic methods ... 51
3.6.1 Immobilized metal ion affinity chromatography ... 51
3.6.2 IL-5 affinity chromatography ... 52
3.6.3 Gel filtration chromatography ... 53
3.6.4 Anion-exchange chromatography ... 53
3.6.5 Reversed-phase high-performance liquid chromatography ... 54
3.7 Auto-processing of the AF17121-CPD fusion protein ... 55
3.8 Thermofluor ... 55
3.9 TF-1 cell proliferation assay ... 56
3.10 Surface plasmon resonance ... 57
3.11 Microscale thermophoresis ... 58
3.12 Crystallization ... 59
3.12.1 AF17121/hIL-5Rα complex crystallization ... 59
3.12.2 X-ray data analysis ... 59

4 RESULTS ... 60
4.1 Recombinant expression of Interleukin-5 and its receptor ectodomains ... 60
4.1.1 Purification of the human Interleukin-5 protein ... 60
4.1.1.1 Bacterial expression of hIL-5 ... 60
4.1.1.2 Refolding of the hIL-5 ... 62
4.1.1.3 Purification of the hIL-5 protein ... 64
4.1.2 Purification of the Interleukin-5 receptor ectodomain ... 66
4.1.2.1 Bacterial expression of the ectodomain of hIL-5Rα C66A ... 66
4.1.2.2 Refolding of the hIL-5Rα C66A ectodomain protein ... 67
4.1.2.3 Anion exchange chromatography of the hIL-5Rα C66A ... 69
4.1.3 Purification of the ectodomain of the common beta chain ... 71
4.1.3.1 Recombinant virus generation of βc N346Q ... 71
4.1.3.2 Expression and purification of the ectodomain of βc N346Q using High-Five insect cells ... 72
4.1.3.3 Final purification of the ectodomain of βc N346Q via gel filtration ... 73
4.2 Structural and functional studies of the ternary IL-5 complex ... 75
4.2.1 Functional analysis of protein-protein interactions employing surface plasmon resonance (SPR) ... 75
4.2.2 Purification of the IL-5 ternary ligand-receptor complex via gel filtration ... 78
4.2.3 Functional studies show βc binds to IL-5•IL-5Rα with micromolar affinity ... 79
4.3 Structural and functional analysis of the ectodomain of hIL-5Rα in its unbound state ... 82
4.3.1 Unfolding analyses of hIL-5Rα C66A$_{ECD}$ indicate a local domain flexibility ... 82
4.3.2 Crystallization trials of IL-5Rα$_{ECD}$ in the unbound state ... 84
4.3.3 Establishing a purification protocol for IL-5Rα C66A derived from baculovirus-infected insect cells ... 86
4.3.3.1 Recombinant virus generation of IL-5Rα C66A ... 86
4.3.3.2 Semi-preparative production of hIL-5Rα C66A in suspension-adapted High Five insect cells ... 87
4.3.3.3 Purification of insect-cell derived IL-5Rα C66A using metal chelate affinity chromatography ... 87

4.3.3.4 Anion exchange chromatography of insect-cell derived IL-5Rα C66A ... 88
4.3.4 Functional analysis of insect-cell derived IL-5Rα C66A using surface plasmon resonance (SPR) ... 89
4.3.5 Optimization of the IL-5Rα C66A protein yield ... 90
4.4 Structure/function analysis of IL-5Rα bound to IL-5 inhibitory peptides ... 92
4.4.1 Functional analysis of the peptide AF17121 using surface plasmon resonance ... 92
4.4.2 Preparation of the IL-5Rα•AF17121 complex ... 93
4.4.3 Crystallization of the IL-5Rα•AF17121 complex ... 97
4.4.4 Structure of IL-5Rα•AF17121 receptor-peptide complex shares the wrench-architecture with IL-5•IL-5Rα ... 98
4.4.5 Differences and similarities of IL-5Rα recognition between IL-5 and AF17121 ... 108
4.4.6 Is the IL-5Rα wrench-architecture prefixed or formed upon ligand binding? ... 113
4.4.7 Mutagenesis study of AF17121: Establishing a recombinant production of the peptide ... 116
4.4.7.1 Bacterial expression of the AF17121-cysteine protease domain (CPD) fusion protein ... 116
4.4.7.2 Purification of the AF17121-CPD fusion protein ... 117
4.4.7.3 Auto-processing of the peptide-protease fusion protein ... 117
4.4.7.4 Purification of AF17121 using gel filtration ... 118
4.4.8 Functional analysis of recombinantly produced AF17121 peptide ... 120
4.4.9 Structure-based improvement of the AF17121 mediated IL-5 inhibition ... 121

5 DISCUSSION ... 128
5.1 Recombinant production of the IL-5 protein and the ectodomains of IL-5Rα and βc ... 129
5.2 Cryo-EM required to determine the structure of the ternary IL-5 complex? ... 132
5.3 A bi-dentate salt bridge is the key determinant for the strong AF17121•IL-5Rα interaction ... 134
5.4 The IL-5Rα ectodomain wrench-like architecture requires a certain degree of flexibility ... 137
5.5 A similar recognition epitope for AF17121 and IL-5 but with different residues being involved ... 142
5.6 A rational design approach to AF17121 variants with improved IL-5Rα binding ... 145

6 SUMMARY ... 150

7 ZUSAMMENFASSUNG ... 152

8 REFERENCES ... 154

9 APPENDIX ... 168
9.1 Abbreviations ... 168
9.2 cDNA sequences and the respective amino acid sequences ... 170
9.2.1 Human Interleukin-5 ... 170
9.2.2 Human Interleukin-5 receptor α variant C66A ... 170
9.2.3 Common beta chain variant N346Q ... 172
9.2.4 Common beta chain wild type ... 172
9.2.5 AF17121 ... 173
9.3 Molecular weights and molar extinction coefficients ... 174
9.3.1 Molecular weight and extinction coefficients of Interleukin-5 receptor α variants 174
9.3.2 Molecular weight and extinction coefficients of AF17121-CPD fusion protein variants ... 175
9.3.3 Molecular weight and extinction coefficients of AF17121 peptide variants ... 176
9.4 Thermofluor buffer composition ... 177
9.5 Buffer composition of the sub-screens ... 178
9.6 Copyright clearance ... 179

10 CURRICULUM VITAE 180
11 LIST OF PUBLICATIONS 181
12 ACKNOWLEDGEMENT 182
13 AFFIDAVIT 183

1 INTRODUCTION

1.1 Overview of the immune system

Our immune system is challenged everyday by pathogens or foreign compounds that are either inhaled/swallowed or inhabit/penetrate our skin and mucous membrane. Whether these organisms and compounds are capable of defeating the different levels of defense (s. Figure 1*) and causing disease depends on their pathogenicity and the integrity of host defense mechanisms. Infectious substance(s) that breach the first levels of barriers and successfully invade the body will subsequently encounter cellular defense mechanisms of innate and adaptive immunity. The term innate immunity includes anatomic and chemical barriers, proteins located in the blood stream (including members of the complement system) and the innate lymphoid cells. These components provide rapid and immediate host defense and are found even in the simplest animals, highlighting their importance in survival. Adaptive immunity is characteristic for higher animals (vertebrates), but requires days to develop an efficient defense. Adaptive immunity is represented by B- and T-lymphocytes and develops continuously during the lifetime of an individual as a response to infection and adapts to infections encountered. This results in a precise immune response and also enables generating an immunological memory to provide a more vigorously and rapid response to repeated exposures of the same infectious agent. (Parkin, J. *et al.*, 2001, Abbas, A.K. *et al.*, 2015, Murphy, K.M. *et al.*, 2017)

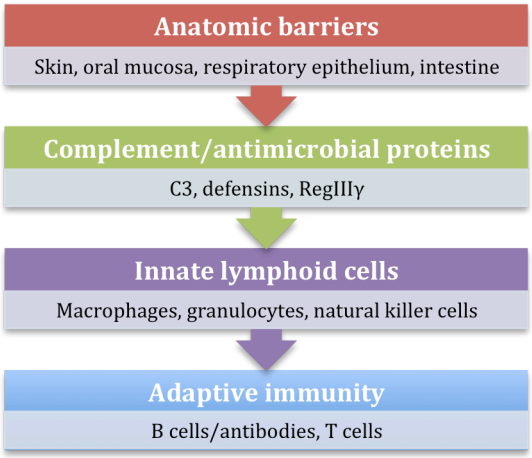

Figure 1: Different levels of defense. [Murphy, K.M. *et al.* 2017*]

* Copyright s. 9.6 (page 179)

1.2 Eosinophils

Granulocytes, including eosinophils, basophils and neutrophils, are generally accounted to the cells of innate immunity. The term “eosinophil” was introduced by Paul Ehrlich in 1879 describing cells with granules (intracellular vesicular compartments) having an affinity for eosin and other acid dyes (Ehrlich, P., 1879). Eosinophils are bone marrow-derived granulocytes found in peripheral blood and tissues. They usually represent about 1-4% of circulating leukocytes. In healthy individuals eosinophils predominately reside in the lamina propria of the gastrointestinal tract (Mishra, A. *et al.*, 1999), but are also found in the lung, thymus, uterus, adipose tissues, mammary gland and spleen (s. review: (Rothenberg, M.E. *et al.*, 2006)). Due to their capacity to release cytotoxic granule cationic proteins, which are involved in killing parasites, but also capable of inducing host tissue damage and dysfunction, eosinophils have merely been associated as end-stage effector cells in parasitic helminth infections and allergic diseases such as atopic asthma. But new data obtained especially during the last decade instead revealed the multifaceted roles of eosinophils in innate immunity and additional functions in regulating inflammation, affecting tissue remodeling, bridging innate and adaptive immunity and maintaining epithelial barrier function as well as tissue homeostasis and repair (Furuta, G.T. *et al.*, 2005, Pegorier, S. *et al.*, 2006, Lotfi, R. *et al.*, 2008, Goh, Y.P. *et al.*, 2013, Chu, V.T. *et al.*, 2014). Many of these multiple immunomodulatory functions stem from their capacity to synthesize and store a vast arsenal of cytokines, chemokines, growth factors and lipid mediators, available for immediate release (s. Figure 2). (s. reviews: (Rothenberg, M.E. *et al.*, 2006, Shamri, R. *et al.*, 2011, Leru, P.M., 2015, Varricchi, G. *et al.*, 2016, Wen, T. *et al.*, 2016))

Granulocyte-Macrophage Colony-Stimulating Factor (GM-CSF), Interleukin-3 (IL-3) and Interleukin-5 (IL-5) were identified as important regulator of eosinophil maturation in the bone marrow (Lopez, A.F. *et al.*, 1986, Lopez, A.F. *et al.*, 1988, Rothenberg, M.E. *et al.*, 1988). IL-5 is specific for the eosinophil lineage and induces selective differentiation of eosinophils (Sanderson, C.J., 1992). In addition, IL-5 stimulates the release of eosinophils into the blood and is also important for eosinophil priming, survival and activation ((Collins, P.D. *et al.*, 1995, Takatsu, K., 2004), s. review: (Wen, T. *et al.*, 2016)). IL-5 and the

chemokines of the eotaxin family regulate selectively eosinophil trafficking to inflammatory sites (s. review: (Rankin, S.M. *et al.*, 2000)), even though a number of cytokines (Horie, S. *et al.*, 1997), adhesion molecules (s. review: (Bochner, B.S. *et al.*, 1994)) and chemokines are also involved. Genetic manipulation of mice, i.e. transgenic IL-5 overexpression or IL-5 deletion, underlined the role of IL-5 for eosinophil development. Genetic deletion of IL-5 resulted in strongly reduced levels of eosinophils in the blood and lungs upon allergen challenge (Foster, P.S. *et al.*, 1996, Kopf, M. *et al.*, 1996), whereas transgenic overexpression of IL-5 led to development of eosinophilia, i.e. highly increased numbers of eosinophils in the blood or body tissues (Dent, L.A. *et al.*, 1990, Tominaga, A. *et al.*, 1991, Lee, J.J. *et al.*, 1997).

Therefore, it is not surprising that the cytokine IL-5 has become a highly interesting target for pharmaceutical intervention, as it functions as key regulator of eosinophils.

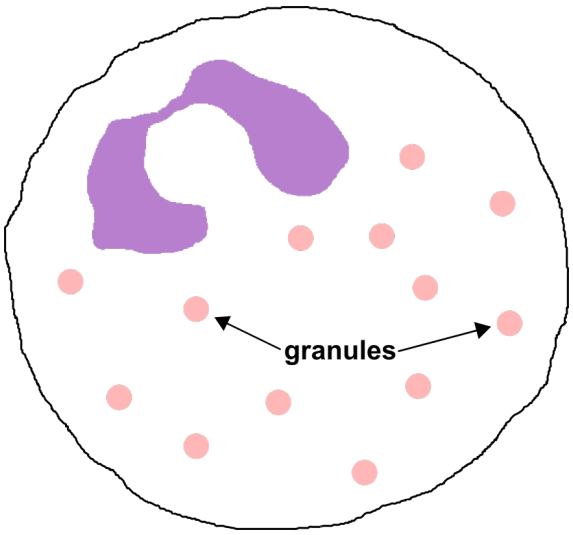

Cationic proteins:
MBP, ECP, EDN, EPX

Cytokines:
IL-1α/-β, IL-2 to IL-6, IL-12, IL-13, IL-16, IL-17, IL17E / IL-25, GM-CSF, IFNγ, TNF-α, APRIL

Chemokines:
CCL3, CCL5, CCL11/Eotaxin, CCL13, CCL 17, CCL22, CCL23, CXCL1, CXCL5, CXCL8, CXCL9, CXCL10, CXCL11, SCF

Growth factors:
NGF, PDGF-β, TGF-α/-β

Lipid mediators:
Leukotrienes (LTC_4, LTE_4, LTD_4), 15-HETE, Prostaglandins (PGE_1, PGE_2), PAF, Thromboxane B_3,

Figure 2: Scheme of an eosinophil providing an overview of the wide array of preformed and stored mediators important for their effector functions. [Varricchi, G. *et al.* 2016]

1.3 Interleukin-5

1.3.1 A member of the common beta chain family

Interleukin-5 (IL-5), IL-3 and Granulocyte-Macrophage Colony-Stimulating Factor (GM-CSF) represent class I cytokines and are encoded on the long arm of chromosome 5 (Huebner, K. *et al.*, 1985, Le Beau, M.M. *et al.*, 1987, Sutherland, G.R. *et al.*, 1988). Their amino acid sequences do not share significant homology. However, all three cytokines share a common architecture comprising a bundle of four anti-parallel α-helices and two β-strands. While IL-3 (Feng, Y. *et al.*, 1996) and GM-CSF (Walter, M.R. *et al.*, 1992) form monomers just like most other class I cytokines, IL-5 folds into a homodimer assembly (Milburn, M.V. *et al.*, 1993) and is therefore rather unique (s. Figure 3).

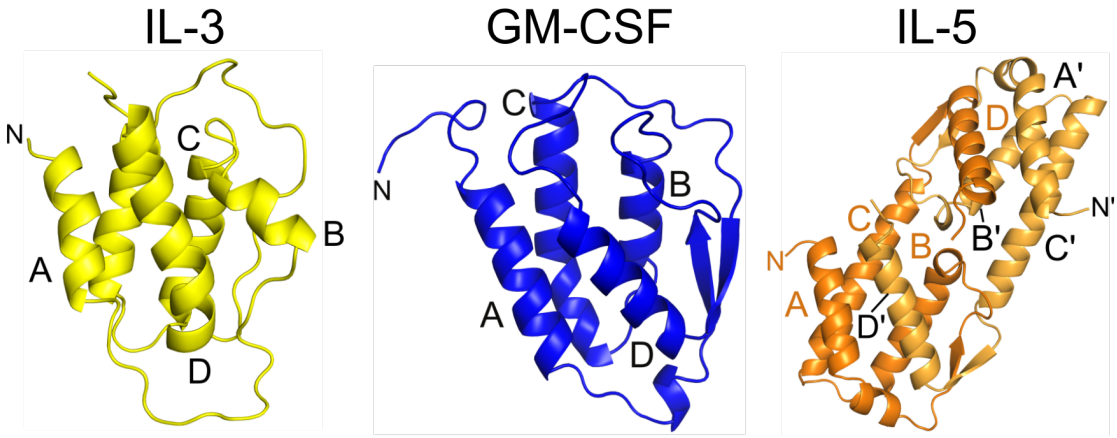

Figure 3: βc family cytokines: IL-3, GM-CSF and IL-5. The IL-3, GM-CSF and IL-5 architecture is presented as cartoon with the α-helices labeled A-D, and A'-D' for the second IL-5 monomer. [PDB ID: 1JLI (IL-3); 2GMF (GM-CSF), 1HUL (IL-5); Feng, Y. *et al.* 1996, Rozwarski, D.A. *et al.* 1996, Milburn, M.V. *et al.* 1993; Hercus, T.R. *et al.* 2013*]

IL-5, IL-3 and GM-CSF signal through assembling two different cell surface receptors, a cytokine specific α chain and a shared β chain therefore named common β chain (Kitamura, T. *et al.*, 1991, Tavernier, J. *et al.*, 1991). Due to sharing the so-called common beta chain (βc), the three cytokines together form the common beta chain (βc) family (s. review: (Hercus, T.R. *et al.*, 2013)).

All three cytokines are produced by activated T_H2 cells (T-cells). IL-3 regulates the production and function of hemopoietic cells and hemopoietic stem cells (Mach, N. *et al.*, 1998). It is important for basophil production and activation (Lantz, C.S. *et al.*, 1998, Kim, S. *et al.*, 2010b). IL-3 is also involved in generating mast cells and regulates mast cell function (Dahl, C. *et al.*, 2004). In

* Copyright s. 9.6 (page 179)

addition to activated T-helper cells also mast cells produce IL-3 (s. reviews: (Ihle, J.N., 1992, Hercus, T.R. *et al.*, 2013)).

The cytokine GM-CSF stimulates the function and production of myeloid hemopoietic progenitor cells as well as macrophages, neutrophils, eosinophils, basophils and certain dendritic cells ((Mellman, I. *et al.*, 2001), s. reviews: (Metcalf, D., 2008, Hercus, T.R. *et al.*, 2013)).

While IL-5 can also regulate basophil development (Denburg, J.A. *et al.*, 1991), it is more involved in the synthesis and function of eosinophils (Lopez, A.F. *et al.*, 1988, Sanderson, C.J., 1992). Besides T_H2 cells, also mast cells and eosinophils synthesize small amounts of IL-5 (Broide, D.H. *et al.*, 1992, Ying, S. *et al.*, 1997). More recently type 2 innate lymphoid cells (ILC-2) have been identified as additional source of IL-5 ((Fort, M.M. *et al.*, 2001), s. review: (Klose, C.S. *et al.*, 2016)).

The similar biologic activities of the βc family cytokines on the above-mentioned myeloid cells depend on the presence (expression) of their corresponding cellular receptors. The pattern of receptor expression is tissue-specific and defines the immune responses and functions of the three cytokines.

Generating mice lacking the entire IL-3/GM-CSF/IL-5 system resulted mainly in reduced numbers of eosinophils (Nishinakamura, R. *et al.*, 1996). Indicating that the members of the βc family are not essential for maintaining a functional immune system, but play a role in emergency situations (inflammation and infection) (Guthridge, M.A. *et al.*, 1998).

1.3.2 Structure of IL-5

Interleukin-5 (IL-5) is one of the few known homodimeric interleukins. Each monomeric subunit contains 115 amino acids after secretion peptide removal and folds into a typical four-helix bundle, which is however unusually intertwined. Two short β-sheets are found on opposite sides of the molecule. The two β-sheets are located between the helices A and B (β1), and C and D (β2). Two interchain disulfide bonds stabilize the architecture (s. Figure 4). The fourth helices of the monomers are domain-swapped between the two monomers, resulting in the head-to-head architecture as revealed by structure analysis. (Milburn, M.V. *et al.*, 1993) Glycosylation occurs at four N-glycosylation sites in the homodimeric human IL-5, but it is not required for dimerization and does not affect biological activity (Proudfoot, A.E. *et al.*, 1990).

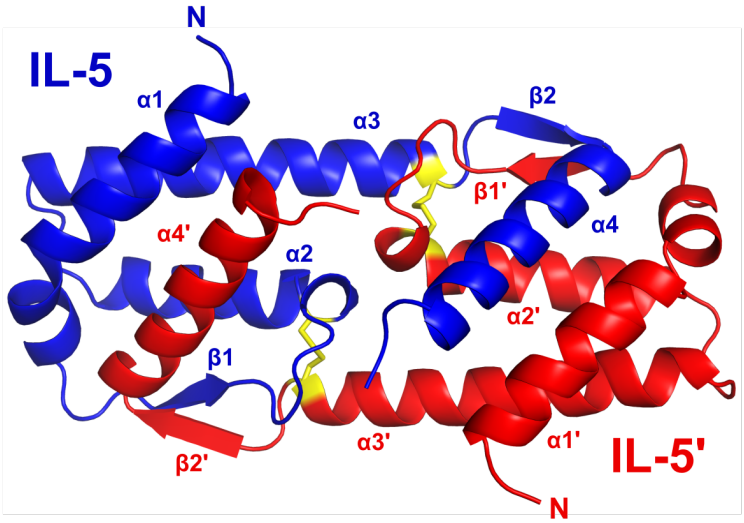

Figure 4: Homodimeric human Interleukin-5. The IL-5 architecture is presented as cartoon with the α-helices labeled α1-α4 (A-D) and α1'-α4' (A'-D') and the β-sheets are labeled β1-β2 and β1'-β2'. Monomer subunits are colored in blue and red. Interchain disulfide bonds shown in yellow. [PDB ID: 1HUL; Milburn, M.V. *et al.* 1993]

1.4 Mechanism of interleukin-5 signaling

Interleukin-5 (IL-5) signaling occurs via a sequential receptor assembly and activation mechanism. The same mechanism also applies to the other two βc family members, IL-3 and GM-CSF. The ligand IL-5 binds first to its specific α-receptor subunit IL-5Rα with high affinity (low nanomolar to subnanomolar range), thereby forming a binary membrane-localized complex. In the second step, this intermediate complex recruits the homodimeric common beta chain (βc) thereby forming a ternary assembly (s. Figure 5). The exact composition (stoichiometry) of the IL-5 receptor assembly is not yet known.

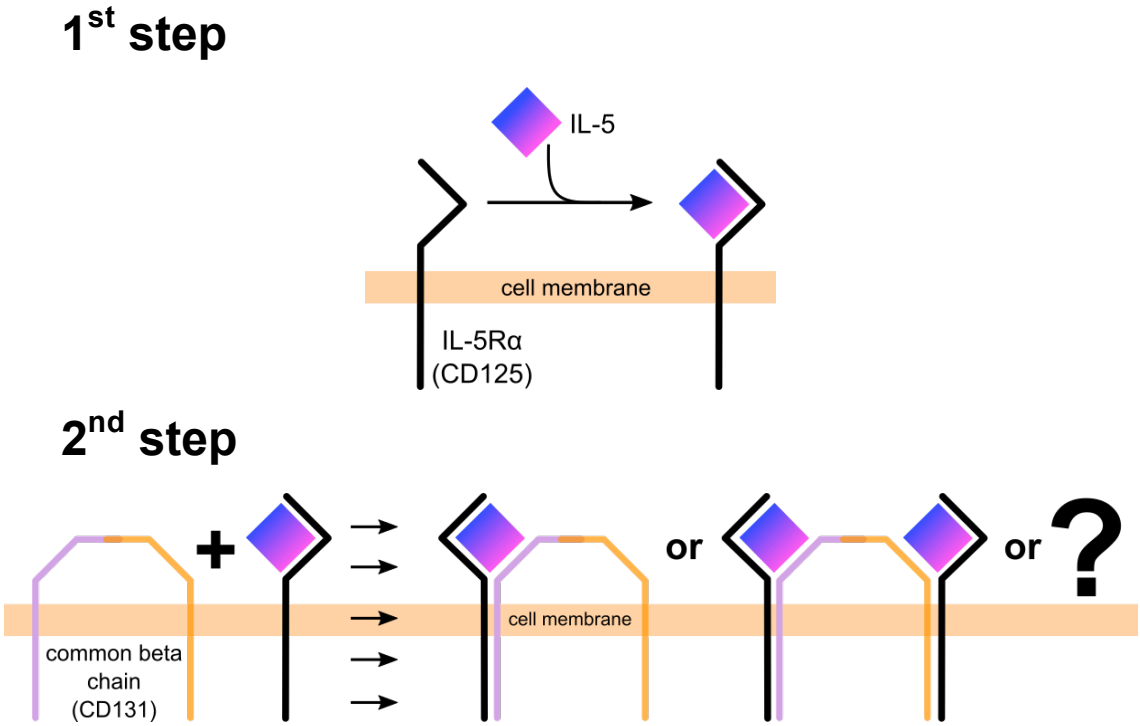

Figure 5: Schematic illustration of the sequential interaction mechanism of IL-5 signaling. 1st Step: IL-5 binds to IL-5Rα, thereby forming the binary complex. **2nd Step:** The binary complex recruits βc, thereby the ternary complex is assembled. Possible assemblies of the IL-5 ternary complex are shown, but the exact composition is yet not known.

Formation of the ternary ligand-receptor complex is assumed to trigger signal transduction in the cytoplasm. Thereby several signaling pathways are activated, including JAK/STAT (Janus kinases / signal transducers and activators of transcription), MAPK (mitogen-activated protein kinases), PI3K (phosphoinositide 3-kinase) and NF-κB (nuclear factor kappa-light-chain-enhancer of activated B cells) (s. Figure 6; s. review (Pelaia, G. *et al.*, 2016)).

In unstimulated conditions, IL-5Rα and the βc are constitutively associated with JAK2 and JAK1, respectively (Ogata, N. *et al.*, 1998). Binding of the ligand and

subsequent receptor assembly brings both receptor-associated JAK kinases in close proximity triggering the trans-phosphorylation between JAK2 and JAK1 (Rawlings, J.S. *et al.*, 2004). The JAK activation results in tyrosine phosphorylation of the signal transducers and activators of transcription (STAT) 1, 3 and 5, which enhance the gene expression of pim-1, cyclin D3 and other IL-5 inducible genes involved in survival and proliferation of eosinophils (Pazdrak, K. *et al.*, 1995, Stout, B.A. *et al.*, 2004). The cytoplasmic βc domain is also subsequently phosphorylated at different tyrosine residues through the activated JAKs. Phosphorylation of βc activates the ERK (extracellular signal regulated kinase) and MAPK pathway. The mitogen-activated protein kinases p38 and ERK 1/2 are important for eosinophil differentiation, cytokine production and degranulation (Adachi, T. *et al.*, 2000). Members of the Ras/ERK pathway play pivotal roles in eosinophil proliferation and survival (Hall, D.J. *et al.*, 2001). During inflammation, NF-κB together with p38 MAPK induces adhesion and chemotaxis of human eosinophils (Wong, C.K. *et al.*, 2003, Ip, W.K. *et al.*, 2005). PI3K is also involved in IL-5 induced eosinophil adhesion (Sano, M. *et al.*, 2005).

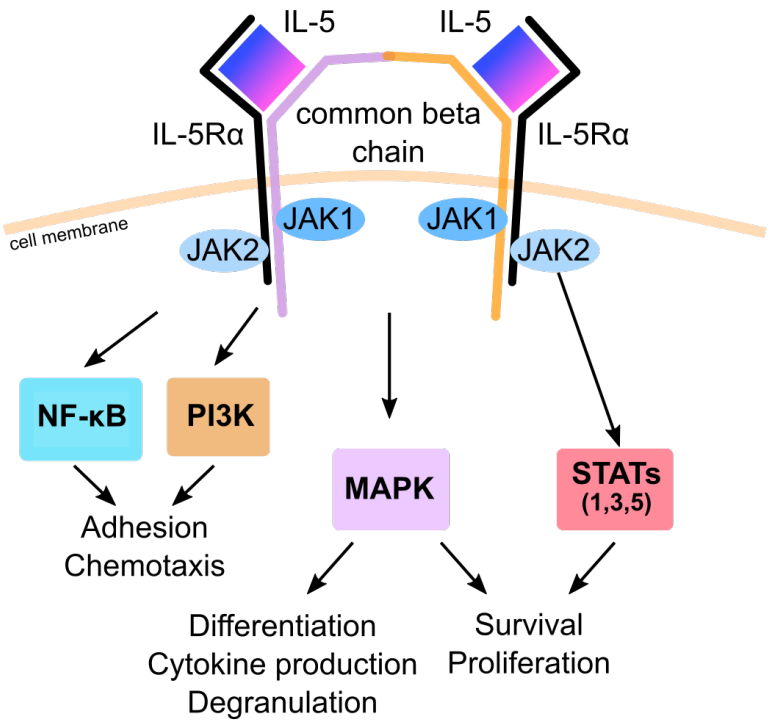

Figure 6: Schematic illustration of the activated pathways by IL-5 signaling in eosinophils. [Pelaia, G. *et al.* 2016*]

* Copyright s. 9.6 (page 179)

1.5 Structural and functional aspects of the IL-5 receptor subunits

1.5.1 IL-5 receptor α and the binary IL-5•IL-5Rα complex

The Interleukin-5 receptor α (IL-5 Rα) gene encodes for a glycoprotein of 420 amino acids (aa) length. The IL-5Rα protein has a signal peptide (20 aa), followed by an extracellular domain (ectodomain, 322 aa) involved in IL-5 recognition and binding, a single-span transmembrane segment (20 aa) and a short intracellular domain (58 aa) with no intrinsic enzymatic activity. The intracellular domain serves as an adapter module for the binding of cytoplasmic proteins such as the JAK kinases or the STAT proteins and therefore plays an important role in the activation of the signaling cascade (s. reviews (Molfino, N.A. *et al.*, 2012, Hercus, T.R. *et al.*, 2013)).

IL-5 and IL-5Rα interact with a 1:1 stoichiometry despite IL-5's dimeric nature (Devos, R. *et al.*, 1993, Patino, E. *et al.*, 2011, Kusano, S. *et al.*, 2012). Structure analysis revealed that on each side of the two-fold symmetry axis of IL-5 one potential IL-5Rα epitope is located face to face. However, one IL-5Rα bound to IL-5 already covers parts on both sides of the two-fold axis. Therefore two IL-5Rα moieties cannot bind simultaneously to IL-5 due to the large size of IL-5Rα. (Patino, E. *et al.*, 2011)

The structure of the complex of IL-5 bound to the IL-5Rα ectodomain furthermore revealed that the IL-5Rα ectodomain adopts a new wrench-like architecture (Patino, E. *et al.*, 2011). Here, IL-5Rα "wraps" around IL-5 figuratively spoken like a wrench around a nut. The wrench-like architecture consists of three Fibronectin type III-like (FNIII) domains (D1-D3). Each FNIII domain comprises seven β strands arranged in two anti-parallel β sandwiches (Patino, E. *et al.*, 2011, Kusano, S. *et al.*, 2012). Most other cytokine receptor ectodomains, e.g. the IL-4Rα (Hage, T. *et al.*, 1999) or the growth hormone receptor (GHR) (de Vos, A.M. *et al.*, 1992) only contain two FNIII domains, which together form the so-called cytokine recognition motif (CRM) (Bazan, J.F., 1990). These cytokine receptors bind their ligands solely via the CRM arrangement, which folds into an architecture resembling an upside-down L letter. Thus, the IL-5Rα receptor presents one of the few known class I cytokine receptors that contain an extra motif in addition to the CRM (s. Figure 7).

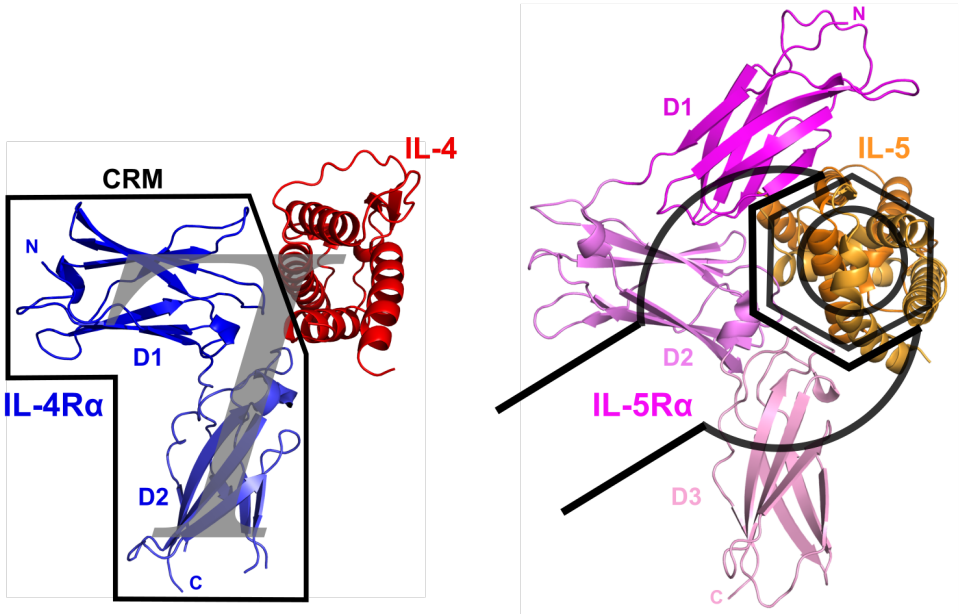

Figure 7: Structures of IL-4•IL-4Rα (left) and IL-5•IL-5Rα (right) complex (cartoon representation). On the left site the cytokine recognition motif (CRM) and on the right side the wrench-like architecture of the IL-5 receptor α are shown. **[**PDB ID: 1IAR (left) and 3QT2 (right); Hage, T. *et al*. 1999, Patino, E. *et al.* 2011[*]]

The structure analysis also revealed three contact patches in IL-5Rα comprising three β-sheet connecting loops in FNIII domain D3 (patch 3), two β-sheet connecting loops in FNIII domain D2 (patch 2) and β-strand 4 in FNIII domain D1 (patch 1) (s. Figure 8). Most noticeable are the interactions between the IL-5Rα FNIII domain D1 and β2 of IL-5 (patch 1). Eleven out of 15 direct intermolecular hydrogen bonds formed between IL-5 and IL-5Rα are found here, with the epitopes showing a pronounced charge-charge complementarity. Interactions from patch 2 and 3 of IL-5Rα with corresponding parts in IL-5 are less tightly interweaved. Only one intermolecular H-bond is observed in patch 2, instead most interactions seem to be of hydrophobic nature. Patch 3 seems likewise the smallest with most interactions being of hydrophobic nature. Only a single residue, Met295, significantly contributes to binding in patch 3. (Patino, E. *et al.*, 2011)

Surprisingly, the architecture of the ectodomains of IL-5Rα and the IL-13 receptors IL-13Rα1 and IL-13Rα2 are highly similar (s. Figure 9) even though the amino acid sequence homology among class I cytokine receptors is quite low (LaPorte, S.L. *et al.*, 2008, Lupardus, P.J. *et al.*, 2010, Patino, E. *et al.*, 2011). Since the ligands differ vastly, with IL-5 being a homodimer and IL-4 and IL-13 being monomers, this is even more remarkably.

[*] Copyright s. 9.6 (page 179)

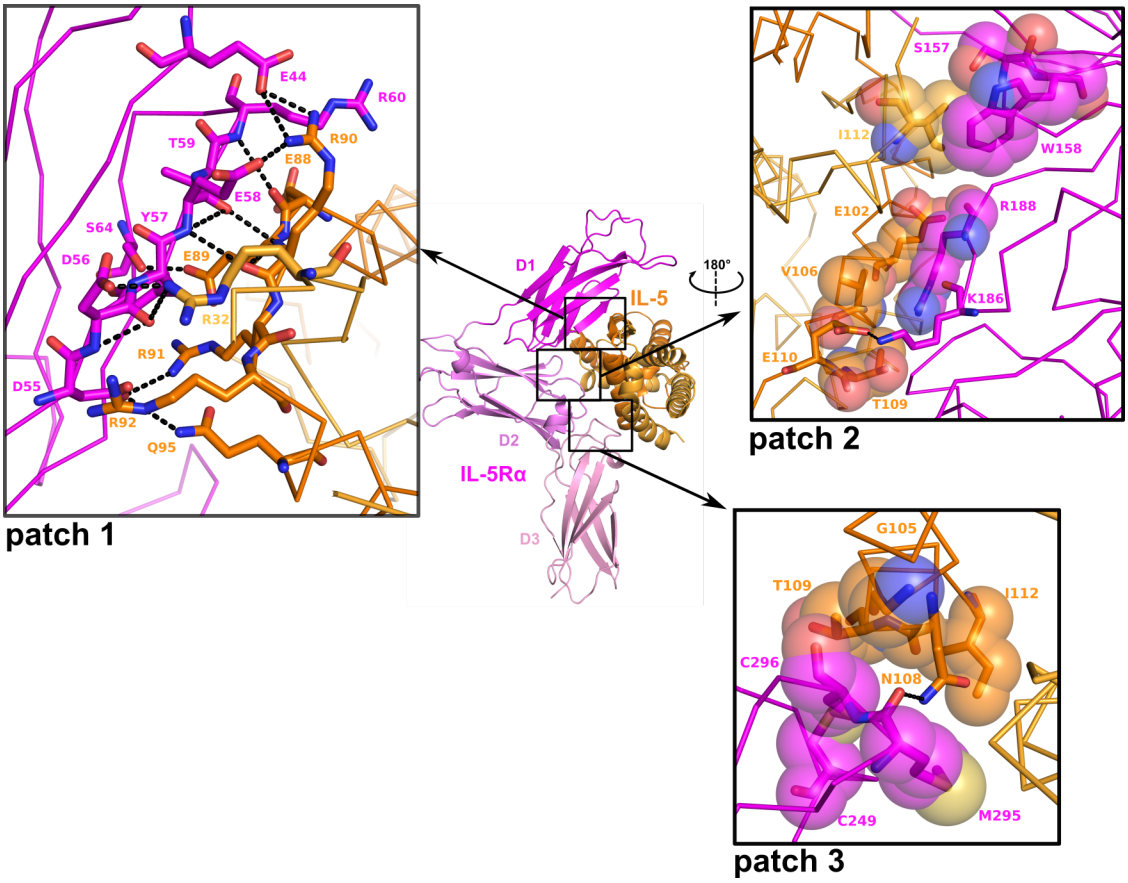

Figure 8: Diagram showing the three patches found in the interface of the IL-5•IL-5Rα complex. IL-5 (orange and light orange) and IL-5Rα (magenta) are presented as ribbons. H bonds presented as stippled lines in black. Hydrophobic contacts and van der Waals interactions are shown as spheres. [PDB ID: 3QT2; Patino, E. *et al.* 2011*]

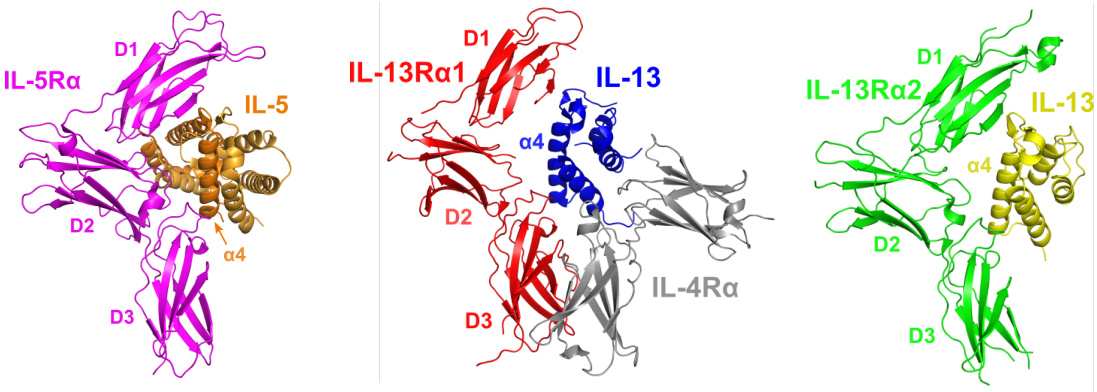

Figure 9: Representation of the similar wrench-like architecture of the receptor ectodomains of IL-5Rα bound to IL-5 (left), IL-13Rα1 in complex with IL-13 and IL-4Rα (middle) and IL-13Rα2 bound to IL-13 (right). Structures are presented as cartoon. [PDB ID: 3QT2 (left); 3BPO (middle), 3LB6 (right); Patino, E. *et al.* 2011, LaPorte, S.L. *et al.* 2008, Lupardus, P.J. *et al.* 2010]

* Copyright s. 9.6 (page 179)

The receptor ectodomains in complex with their ligand can be superimposed well, whereas the ligands align only very limited. Only the fourth helix (α4) of IL-5 and IL-4/IL-13 structurally superimposes with the receptor ectodomains aligned, most likely due to the fact that the fourth helix also makes the largest contact with the receptor. The ligands position rather differently into the binding pocket formed by the structurally highly similar receptor ectodomains. This can be explained by the fact that the interhelical angles between the other helices differ vastly. In addition, β-strand 2, which makes important contacts with the FNIII domain D1 of the receptors, differs in length and orientation between the three ligands. The β-strand 2 in the IL-5•IL-5Rα complex forms far more polar contacts between the receptor and the ligand is longer compared to the interaction found in the complexes IL-4Rα•IL-13•IL-13Rα1 and IL-13•IL-13Rα2. This could explain why mutations in the D1 domain of IL-13Rα1 affect IL-13 or IL-4 binding to a lesser extend compared to equivalent mutations in IL-5Rα, which completely abrogate IL-5 binding (LaPorte, S.L. *et al.*, 2008, Ito, T. *et al.*, 2009, Patino, E. *et al.*, 2011).

More recently the structures of the GM-CSFRα bound to GM-CSF (Broughton, S.E. *et al.*, 2016) and IL-3Rα without a ligand, but in complex with a Fab fragment of the receptor neutralizing mAb CSL362 (Broughton, S.E. *et al.*, 2014) have been solved thereby completing the set of receptor α subunit structures for the βc family of cytokines (s. Figure 10). The ectodomains of the GM-CSF, IL-3 and IL-5 α-receptors selectively bind its respective cytokine through unique structural features (Broughton, S.E. *et al.*, 2016).

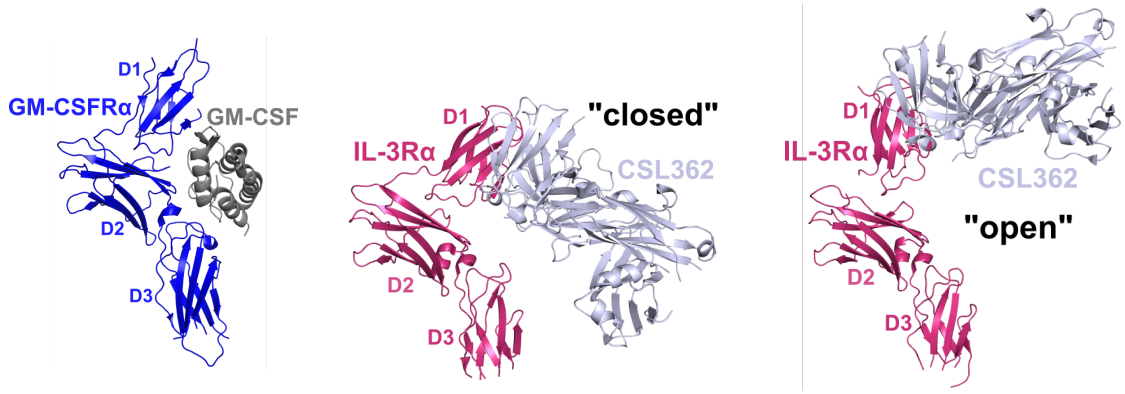

Figure 10: Representation of the receptor α subunit structures of the GM-CSFRα bound to GM-CSF (left) and IL-3Rα in complex with the Fab fragment CSL362 in "closed" (middle) and "open" conformation (right). Structures are presented as cartoon. [PDB ID: 4RS1 (left); 4JZJ (middle + right); Broughton, S.E. *et al.* 2016, Broughton, S.E. *et al.* 2014]

Interestingly the structure of IL-3Rα in complex bound to the Fab antibody fragment showed an alternative “open” conformation (s. Figure 10 right), with an altered orientation of the FNIII domain D1 (Broughton, S.E. *et al.*, 2014). This “open” conformation has not been seen in the related GM-CSF receptor (Broughton, S.E. *et al.*, 2016), IL-5 (Patino, E. *et al.*, 2011, Kusano, S. *et al.*, 2012) or the IL-13 receptors α1 and α2, however, these receptors were analyzed in their ligand-bound state (LaPorte, S.L. *et al.*, 2008, Lupardus, P.J. *et al.*, 2010).

When the structure of the IL-5Rα ectodomain bound to IL-5 was solved, revealing its unusual receptor architecture, the authors also wondered whether the wrench-like architecture is preformed or whether the wrench can switch between an open state and closed state upon IL-5 binding. A preformed closed wrench might present an obstacle for efficient ligand binding due to blocking unobstructed access to the binding epitope, since the three FNIII domains of IL-5Rα cover more than 170° of the IL-5 torus. Thus, an opening and closing of the wrench would likely facilitate complex formation. On the contrary the observed fast association rate for the IL-5 ligand-receptor interaction would require a very fast closing mechanism making a ligand-induced conformational rearrangement with large movements implausible. Additional observations then pointed towards a preformed wrench-like architecture. Several amino acid residues located in the D1D2 interface are highly conserved in IL-5Rα from different species. In the structurally similar IL-13Rα1 and IL-13Rα2 receptors equivalent residues in the domain interface seem also conserved or are replaced by residues with similar chemistry or functionality as found in the IL-5Rα D1D2 interface. (Patino, E. *et al.*, 2011) Mutating these residues in the IL-13Rα1 linker region or changing the length of the linker abrogated binding of IL-13 completely (Kraich, M and Mueller, T.D., unpublished data). Mutation studies of the IL-5Rα receptor detailed in Patino, E. *et al*. (2011) revealed that the residues Leu23, Ile69 and His71 in FNIII domain D1 and Asp208 in FNIII domain D2 occupy key positions. (s. Figure 11). Functional studies of these residues suggest that the wrench-architecture is presumably preformed and destabilization of this ‘‘closed’’ architecture leads to the observed loss of IL-5 binding. (Patino, E. *et al.*, 2011)

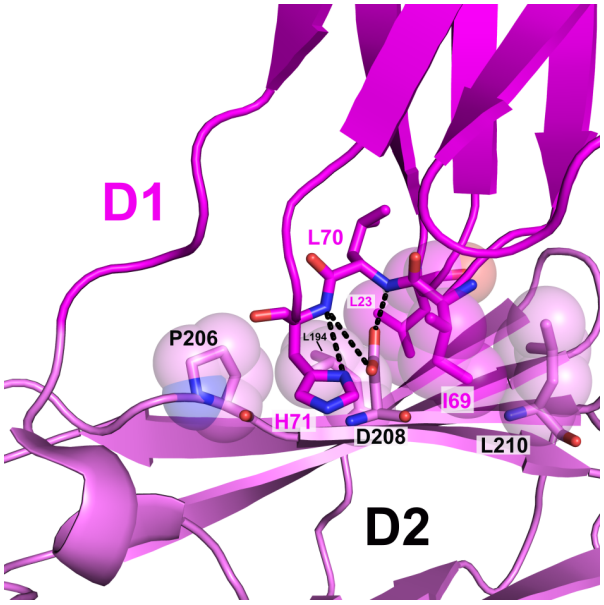

Figure 11: Conserve residues in IL-5Rα FNIII domains D1 (C atoms, magenta) and D2 (C atoms, light pink) possibly fix the domain orientation in IL-5Rα ectodomain. Residue Asp208 is completely buried in the D1D2 interface and engages in two H-bonds with the backbone amide groups of Leu70 and His71. This bi-dentate H-bond is effectively shielded from solvent by residues Leu23, Ile69, His71 in FNIII domain D1 and Leu194, Pro206 and Leu210 in FNIII domain D2. H bonds are shown as stippled black lines. Hydrophobic contacts shielding Asp208 are indicated as spheres. [PDB ID: 3QT2; Patino, E. *et al.* 2011*]

1.5.2 Common beta chain and the ternary IL-5•IL-5Rα•βc complex

The gene for the common beta chain (βc) encodes for a glycoprotein of 881 amino acids (aa) length. The common beta protein has a signal peptide (16 aa), an extracellular domain (ectodomain, 427 aa), a single-span transmembrane segment (17 aa) and an intracellular domain (437 aa). The intracellular domain is important for mediating the biological activities of IL-5, as well as IL-3 and GM-CSF, through recruiting downstream signaling molecules (s. reviews: (Molfino, N.A. *et al.*, 2012, Hercus, T.R. *et al.*, 2013)).

Structure analysis of the ectodomain of the βc receptor revealed a unique non-covalent homodimer structure, forming an arc-like architecture. Each monomer subunit consists of four Fibronectin type III-like (FNIII) domains (D1-D4) (s. Figure 12). The arc-like architecture places the two membrane-proximal domains approximately 90-140 Å apart. (Carr, P.D. *et al.*, 2001)

* Copyright s. 9.6 (page 179)

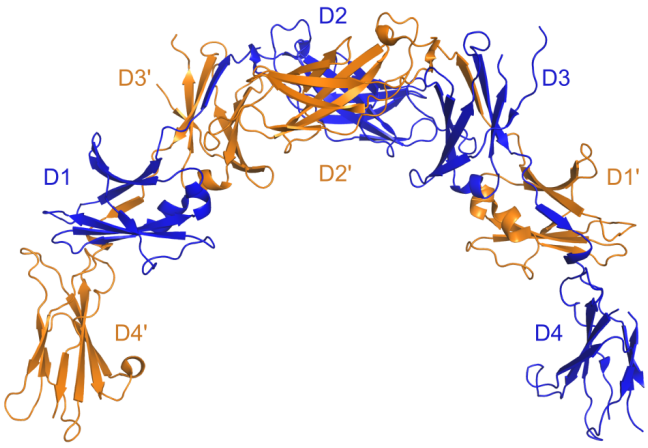

Figure 12: Structure of the human βc. Monomer D colored blue and monomer D' colored orange. The four FNIII-like domains of each monomer are labeled as D1-D4 or D1'-D4'. Represented as cartoon. [PDB ID: 2GYS; Carr, P.D. *et al.* 2006]

The βc receptor is unable to bind directly to IL-5, IL-3 or GM-CSF (Hayashida, K. *et al.*, 1990, Scibek, J.J. *et al.*, 2002, Ishino, T. *et al.*, 2008). Cells expressing only the α chain receptors bind with "low affinity" to their corresponding cytokine (IL-3 K_D = 120 nM (Kitamura, T. *et al.*, 1991); GM-CSF K_D = 2-8 nM (Gearing, D.P. *et al.*, 1989); IL-5 K_D = 1 nM (Tavernier, J. *et al.*, 1991)). The presence of the βc receptor converts the ligand-receptor interaction to a high affinity binding (IL-3 K_D = 140 pM (Kitamura, T. *et al.*, 1991); GM-CSF K_D = 100-200 pM (Hayashida, K. *et al.*, 1990); IL-5 K_D = 250 pM (Tavernier, J. *et al.*, 1991)).

In 2008, Hansen *et al.* determined the structure of the ternary complex of GM-CSF bound to its receptor subunits GM-CSFRα and βc, which revealed an unexpected assembly. A detailed analysis of the crystal lattice suggested that ternary complex formation might trigger assembly of an even higher-ordered complex consisting of two βc dimers, four GM-CSFRα and four GM-CSF ligand moieties noted as a dodecameric complex. Crystal lattice contacts alone did not explain the large size of the interface (termed site 4) between the membrane-proximal FNIII domains of two adjacent βc moieties involved in the dodecameric ligand-receptor assembly. Instead the dodecamer formation was found crucial for GM-CSF signaling as mutations introduced at site 4, disrupting these interactions, as well as antibodies raised against βc and blocking site 4 showed. Physiologically this observation might be explained by the fact that the receptor-associated kinase JAK2 involved in GM-CSF signaling seems to be solely associated with the βc chain as shown from co-immunoprecipitation experiments (Brizzi, M.F. *et al.*, 1994, Quelle, F.W. *et al.*, 1994, Hansen, G. *et al.*, 2008). Due to the arc-like structure of βc the cytoplasmic parts within a

single dimeric βc are separated by 120Å, thus formation of a hexameric assembly would not allow two JAK2 kinases attached to either end of the βc cytoplasmic domains to trans-phosphorylate each other. However, in a dodecameric assembly the cytoplasmic parts of two βc receptors are in direct neighborhood bringing two JAK2 kinases in very close proximity (s. Figure 13). (Hansen, G. *et al.*, 2008)

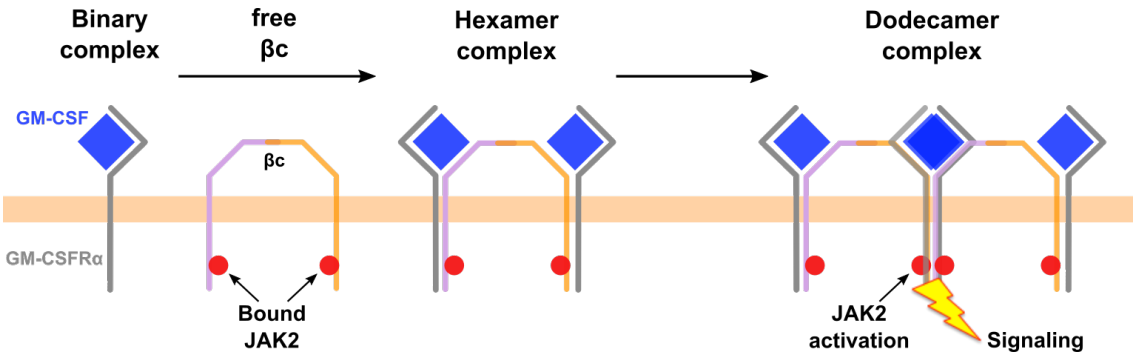

Figure 13: Schematic illustration of the proposed receptor formation of GM-CSF signal transduction. Dimerization and trans-phosphorylation of the JAK2 kinases associated with βc (red spheres) is only possible in the dodecamer complex but not in the hexamer complex. [Hansen, G. *et al.* 2008*]

Based on the ternary GM-CSF complex and previous mutagenesis studies six interaction sites important for complex assembly have been identified (s. Figure 14). Three of the six interaction sites (sites 1-3) between GM-CSF, GM-CSFRα and the βc mediate hexamer formation and the other three (sites 4-6) are involved in the dodecameric arrangement of the GM-CSF complex. Similar receptor assembly and interactions have been proposed for the ternary complex of IL-3 and IL-5. Modeling based on the ternary GM-CSF•GM-CSFRα•βc complex indeed showed that formation of such a higher-ordered assembly is also possible for IL-5 despite its homodimeric nature (Patino, E. *et al.*, 2011). However, a hexameric formation of the ternary IL-5 (and IL-3) complex might be sufficient for receptor activation. To answer this question structure data of the IL-5•IL-5Rα•βc ternary complex are needed, which will yield insights into whether IL-5 leads to a similar higher order receptor assembly as found for GM-CSF or whether there are ligand-specific differences that could also explain ligand specific signals. ((Hansen, G. *et al.*, 2008), s. reviews: (Broughton, S.E. *et al.*, 2012, Hercus, T.R. *et al.*, 2013))

* Copyright s. 9.6 (page 179)

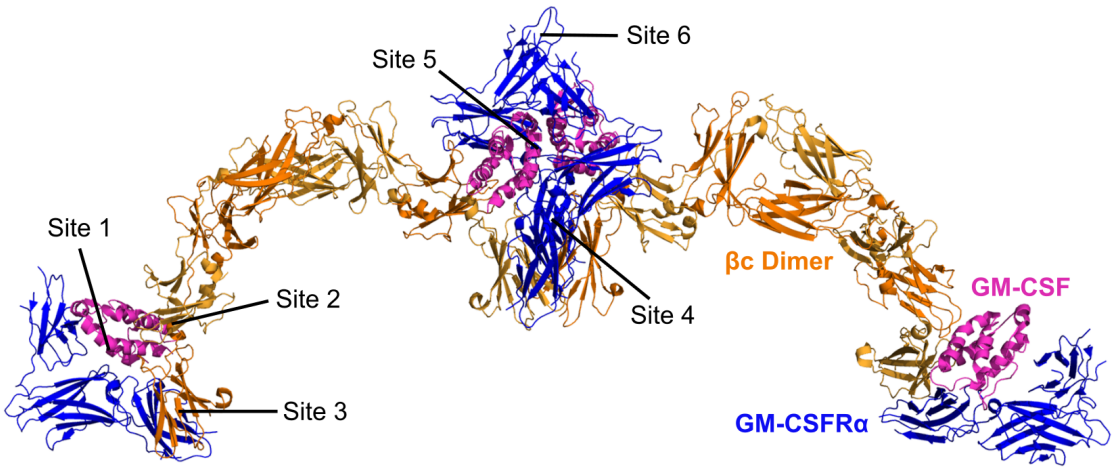

Figure 14: Postulated dodecamer assembly of the ternary GM-CSF•GM-CSFRα•βc complex. Site 1 includes all interactions between GM-CSF and GM-CSFRα occurring during the "binary" complex formation. Helix A of GM-CSF and the composite βc surface comprising the A-B and E-F loops of domain 1 from one βc chain and the B-C and F-G loops of domain 4 of the second βc chain form the interface in site 2. The hydrogen bond formed between Glu21 of GM-CSF and Tyr421 is critical for site 2 interactions. Site 3 is formed between βc domain 4 and the GM-CSFRα domain 3. Interactions via site 4 occur between the membrane-proximal domain 3 of GM-CSFRα and βc domain 4 in each hexamer. Site 5 is formed through interactions of GM-CSF molecules from neighboring hexamers in the dodecamer. Site 6 interactions occur between GM-CSFRα domain 1 (NTD) from adjacent hexamers. Structures are presented as cartoon. (Hercus, T.R. *et al.* 2013[*]) [PDB ID: 4NKQ; Hansen, G. *et al.* 2008]

[*] Copyright s. 9.6 (page 179)

1.6 Eosinophil associated diseases and the role of IL-5

In addition to the basic understanding of the structure and composition of the ternary IL-5 complex, knowledge of the underlying mechanism is even more important to enable the development of new interventional therapies against IL-5 associated diseases.

Eosinophilic diseases have a broad spectrum and can potentially involve all organ systems. A common characteristic is the dramatically elevated number of eosinophils circulating (blood eosinophilia) and/or present at sites of inflammation (tissue eosinophilia). Except for degranulation, other mechanisms by which eosinophils might also cause disease have not been fully elucidated. But understanding of the interplay of eosinophil biology with disease pathogenesis caused by blood and tissue eosinophilia could be improved. While some eosinophilia are caused by atopic diseases others, such as eosinophilic pneumonia, remain idiopathic despite exhaustive investigations. (s. review: (Akuthota, P. *et al.*, 2012))

1.6.1 Helminth infections

Based on histopathologic evidence and through demonstrating *in vitro* killing of parasites by eosinophils (Kazura, J.W. *et al.*, 1978, David, J.R. *et al.*, 1980, Haque, A. *et al.*, 1981) and eosinophil granule products (Butterworth, A.E. *et al.*, 1979, Hamann, K.J. *et al.*, 1990), eosinophils were proposed as end-stage effector cells with the primary function to protect the host against helminth parasites. However, defining the role of eosinophils *in vivo* has been much more difficult, suggesting that eosinophils do play a role in killing of some helminths, particularly those with tissue-migratory stages. (s. review: (Klion, A.D. *et al.*, 2004b))

1.6.2 Asthma

Asthma is a chronic inflammatory disease of the respiratory tract. Characteristics of this complex disorder are reversible airway obstruction, airway inflammation and bronchial hyper-responsiveness. Eosinophils have been shown to likely contribute to the pathology of asthma through accumulation in the inflamed tissue and the release of granule proteins and pro-inflammatory mediators. The effector proteins eosinophilic cationic protein (ECP), major basic protein (MBP) and eosinophil peroxidase (EPO) are

responsible for the tissue damage of the respiratory epithelium, due to their cytotoxic properties (Gleich, G.J. *et al.*, 1979, Gleich, G.J. *et al.*, 1986). Mucus production is stimulated and vascular permeability is increased through their granule proteins, resulting in airway obstruction and tissue edema. The release of a broad range of cytokines and chemokines additionally promotes airway inflammation (Lim, K.G. *et al.*, 1995, Kita, H., 1996, Woerly, G. *et al.*, 1999). (s. reviews: (Walsh, G.M. *et al.*, 2003, Molfino, N.A. *et al.*, 2012)

It was thought that blocking IL-5 and thereby reducing eosinophil numbers would positively affect the pathology of asthma, especially for the treatment of allergic asthma, in which IL-5, along with IL-4, IL-9 and IL-13, drive asthma pathogenesis (Wills-Karp, M. *et al.*, 2004). However, several clinical trials targeting these cytokines showed limited correlation between targeting eosinophils and clinical response. For instance the anti-IL-5 monoclonal antibody mepolizumab led to reduced peripheral eosinophil numbers, but showed no anti-asthmatic efficacy on the late asthmatic response or on airway hyper-responsiveness to histamine in patients with mild asthma (Leckie, M.J. *et al.*, 2000). In contrast, the use of the anti-IL-4Rα antibody dupilumab showed improved lung function, but no decrease in eosinophil numbers (Wenzel, S.E. *et al.*, 2013). Similar studies blocking different cytokines and transcriptomic profiling of cells in the lungs helped revealing different asthma endotypes (Haldar, P. *et al.*, 2008, Haldar, P. *et al.*, 2009, Woodruff, P.G. *et al.*, 2009, Raedler, D. *et al.*, 2015). These endotypes form several subgroups with similar aetiology, but show varying responsiveness to treatment and involve different cell types (Anderson, G.P., 2008, Wenzel, S.E., 2012). Therefore, targeting IL-5 seemingly provides a promising treatment approach for patients with an eosinophil-dependent asthma endotype, especially in the case of eosinophilic asthma. (s. review: (Amin, K. *et al.*, 2016)

1.6.3 Hypereosinophilic syndrome

Hypereosinophilic syndrome (HES) presents a rather heterogeneous class of rare disorders characterized by blood and tissue eosinophilia resulting in a wide variety of clinical manifestations that range from fatigue and other nonspecific complaints to potentially fatal endomyocardial fibrosis and neurologic involvement (Weller, P.F. *et al.*, 1994). HES was first defined by Chusid *et al.* (1975) and nowadays HES must adhere to the following criteria:

Firstly; markedly elevated blood hypereosinophilia (HE) (eosinophils >1.5 x 10^9/l blood on two examinations; interval ≥1 month), secondly; organ damage and/or dysfunction attributable to tissue HE and thirdly; exclusion of other disorders or conditions as major reason for organ damage (e.g. parasitic infection, drug hypersensitivity reaction or non-hematologic malignancy) (Chusid, M.J. *et al.*, 1975, Valent, P. *et al.*, 2012). Together with this redefinition the Working Conference on Eosinophil Syndromes (2011) proposed a new terminology for eosinophilic syndromes in consideration of the recently identified HES subtypes or variants with distinct etiologies (Rioux, J.D. *et al.*, 1998, Roufosse, F. *et al.*, 2000, Cools, J. *et al.*, 2003, Valent, P. *et al.*, 2012). Variants of HES include idiopathic HES (HES_{US}), primary HES (HES_N) and secondary HES (HES_R). Since eosinophils are believed to play a primary role in HES pathogenesis and since in some patients IL-5 overproduction was observed, IL-5 presents a potential target for treatment of HES (Owen, W.F. *et al.*, 1989, Straumann, A. *et al.*, 2001). This could recently be confirmed for the humanized anti-IL-5 antibody mepolizumab showing clinical efficacy for controlling eosinophilia in HES in clinical trials (Klion, A.D. *et al.*, 2004a, Klion, A.D. *et al.*, 2006). (s. reviews: (Klion, A., 2009, Leru, P.M., 2015))

1.7 Therapeutic approaches for HES and asthma

Corticosteroids represent the first-line treatment for patients with asthma and HES. In asthma, it was shown that most of the beneficial effects result from the modulation of T_H2 cytokines, even though the activity of corticosteroids is broad and nonspecific (Wu, C.Y. *et al.*, 1991, Kunicka, J.E. *et al.*, 1993, Maneechotesuwan, K. *et al.*, 2009). Most but not all patients with HES respond rapidly to corticosteroid treatment and can be maintained on low doses of corticosteroids for long periods. Due to substantial side effects, including weight gain, thinning skin, increased risk of infection, adrenal suppression, osteoporosis, cataracts, glaucoma, hyperglycemia and depression, that patients undergoing chronic steroid therapy bear, alternative therapies are needed (Kim, S. *et al.*, 2010a). (s. reviews: (Klion, A., 2009, Wenzel, S.E., 2012))

Follow-up therapies of HES include a variety of cytotoxic and immunomodulatory therapies, as well as tyrosine kinase inhibitors and monoclonal antibodies, targeting specific molecules involved in disease pathogenesis of HES. The cytotoxic agent hydroxyurea is rather inefficient as a single agent for HES (Butterfield, J.H., 2007) and does not immediately reduce eosinophil count, but has been shown to enhance the efficacy of other agents like prednisone (Parrillo, J.E. *et al.*, 1978), interferon-alpha (Coutant, G. *et al.*, 1993) and imatinib (Butterfield, J.H. *et al.*, 2006). Immunomodulatory agents like interferon-alpha, cyclosporine, and immunoglobulin modulate T cell proliferation and T_H2 cytokine production thereby showing therapeutic effects in HES (Butterfield, J.H., 2007). Systemic toxicity is however a drawback of this therapy. The more recently developed tyrosine kinase inhibitors including imatinib (Klion, A.D. *et al.*, 2004c), nilotinib (Verstovsek, S. *et al.*, 2006) and sorafenib (Lierman, E. *et al.*, 2006) have shown to be efficient in FIP1L1/PDGFRA-positive HES *in vitro* and in animal models. In this subgroup an interstitial deletion in chromosome 4q12 results in the generation of a fusion protein between the platelet-derived growth factor receptor alpha (PDGFRα) gene and a previously uncharacterized gene, Fip1-like1 (FIP1L1). The fusion protein acts as a constitutively active tyrosine kinase (Cools, J. *et al.*, 2003, Griffin, J.H. *et al.*, 2003, Yamada, Y. *et al.*, 2006). In addition, imatinib showed promising results in the treatment of eosinophilic leukemia and is approved by

the U.S. Food and Drug Administration (FDA) for the treatment of HES. (s. review: (Klion, A., 2009))

Antibodies targeting the T_H2 pathway in asthma, like anti-IgE (Fahy, J.V. *et al.*, 1997), anit-IL-4Rα (dupilumab) (Wenzel, S.E. *et al.*, 2013) or anti-IL-13 (Gauvreau, G.M. *et al.*, 2011) antibodies, also demonstrated promising results. (s. review: (Wenzel, S.E., 2012)

1.7.1 Targeting IL-5 as a therapeutic approach for asthma and HES

Several strategies have been developed to block IL-5 signaling. One of the strategies uses neutralizing antibodies that either bind directly to IL-5 or to the IL-5 receptor α subunit (s. Figure 15). Mepolizumab and reslizumab are two monoclonal antibodies that bind to IL-5 and impede IL-5 binding to IL-5Rα (Cook, R., Applebaum, R., Cusimano, D., 1998, Egan, R.W. *et al.*, 1999, Hart, T.K. *et al.*, 2001).

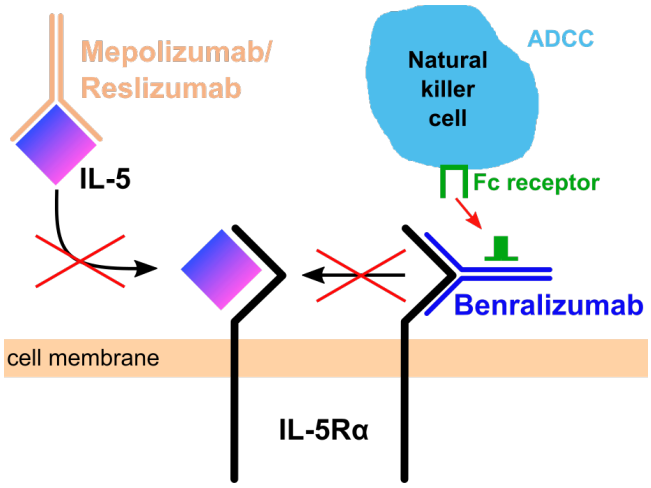

Figure 15: Illustration of the inhibitory effects of the antibodies mepolizumab, reslizumab and benralizumab in IL-5 signaling on eosinophils. Mepolizumab and reslizumab bind to different epitopes of interleukin-5 and prevent IL-5 binding to IL-5Rα. Benralizumab directly binds the IL-5 receptor α and induces apoptosis of eosinophils through antibody-dependent cell mediated cytotoxicity (ADCC).

These IL-5 antibodies were initially developed for treatment of asthma. While first studies showed reduced levels of blood and sputum eosinophilia, the antibodies did however not show convincing improvement in clinical endpoints (Leckie, M.J. *et al.*, 2000, Kips, J.C. *et al.*, 2003, Flood-Page, P. *et al.*, 2007). More recent studies identified beneficial effects of mepolizumab and reslizumab as therapies in the treatment of patients with serve eosinophilic asthma. Here, mepolizumab reduced the overall rate of exacerbations as well as the number of severe exacerbations requiring hospitalization and hence improved control of

asthma symptoms (Pavord, I.D. *et al.*, 2012, Bel, E.H. *et al.*, 2014, Ortega, H.G. *et al.*, 2014). Application of reslizumab resulted in improvements in the forced expiratory volume in one second (FEV_1) in all studies and Castro, M. *et al.* (2015) reported also a reduction of exacerbations (Castro, M. *et al.*, 2015, Bjermer, L. *et al.*, 2016, Corren, J. *et al.*, 2016). In the majority of HES patients, irrespective of the underlying IL-5 baseline level or etiology studies, application of mepolizumab or reslizumab showed a prolonged reduction of eosinophil number as well as reduced exacerbations and improvement of clinical and quality of life measurements (Garrett, J.K. *et al.*, 2004, Klion, A.D. *et al.*, 2004a). (s. reviews: (Klion, A., 2009, Molfino, N.A. *et al.*, 2012, Lam, C. *et al.*, 2017)

Benralizumab, an anti-IL-5Rα monoclonal antibody, binds with high affinity to the IL-5Rα and induces apoptosis of eosinophils and basophils through antibody-dependent cell mediated cytotoxicity (ADCC) (Kolbeck, R. *et al.*, 2010). So far only a few studies have been performed that showed a reduction of exacerbation rates, improved pre-bronchodilator FEV_1 and asthma symptoms for patients with uncontrolled eosinophilic asthma (Bleecker, E.R. *et al.*, 2016, FitzGerald, J.M. *et al.*, 2016). A phase II study with HES patients receiving benralizumab is currently performed (NCT02130882, http://clinicaltrials.gov).

As an alternative to the classical approach of developing neutralizing antibodies, screening of random recombinant peptide-on-plasmid libraries identified agonistic and antagonistic peptides of several cytokine receptors, e.g. erythropoietin, thrombopoietin and type I IL-1 receptors (Wrighton, N.C. *et al.*, 1996, Yanofsky, S.D. *et al.*, 1996, Cwirla, S.E. *et al.*, 1997). The peptide library used to identify potential IL-5 antagonists contained two cysteine residues allowing the formation of conformationally constrained cyclic peptides. Two distinct sets of IL-5 antagonizing peptides were identified, cyclic monomers and disulfide-linked homodimers (s. Figure 16). Both peptide sets directly bound IL-5Rα and thereby block IL-5 signaling (England, B.P. *et al.*, 2000). The IL-5 neutralizing peptide AF17121 is currently the smallest “high-affinity” IL-5 antagonist of the cyclic monomer family (Ruchala, P. *et al.*, 2004). The peptide AF20016 is the most efficient peptide within the group of disulfide-bridged homodimers (Uings, I.J. *et al.*, 2001).

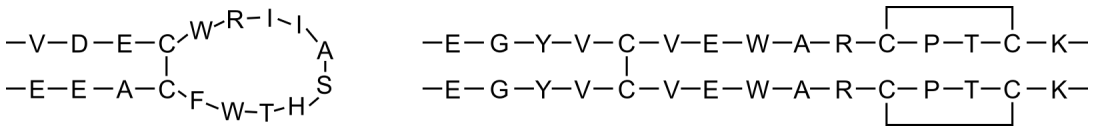

Figure 16: Left: IL-5 antagonizing peptide AF17121, which is cyclized through an intramolecular disulfide bond. **Right:** The homodimeric peptide AF20016, which binds two IL-5Rα moieties. The dimer formation is initiated through an intermolecular disulfide bond.

Further analyses of the AF17121 peptide identified a number of residues important for the interaction with IL-5Rα suggesting that AF17121 might mimic IL-5 binding (Ruchala, P. *et al.*, 2004, Ishino, T. *et al.*, 2005).

Investigations of the disulfide-linked homodimers revealed that these peptides can bind two IL-5 receptor α chains at the same time and showed that the peptide is highly specific for the human IL-5Rα (England, B.P. *et al.*, 2000, Uings, I.J. *et al.*, 2001). However, no studies identifying important residues for the interaction between the IL-5Rα and AF20016 have been reported so far.

2 AIMS

Cytokines represent important mediators of various immune regulatory functions. Interleukin-5 (IL-5) plays a key role in T_H2-mediated immune response. As a key regulator of eosinophilic granulocytes (eosinophils), it controls several key aspects of eosinophil life, i.e. differentiation, migration, proliferation, survival and activation. Asthma and hypereosinophilic diseases are frequently associated with highly increased levels of eosinophils and the observed tissue damage is assumingly linked to eosinophil activation. Therefore, targeting IL-5 and/or its receptors, IL-5 receptor α-chain (IL-5Rα) and common beta chain (βc), present new promising therapeutic strategies to block IL-5 signaling and to abrogate eosinophil activity. The structure of the binary IL-5•IL-5Rα complex determined in 2011 provided first data that might be exploited for rational drug design for the development of IL-5 inhibitors. However, several questions remained unanswered. Firstly, it is unclear whether the wrench-architecture of IL-5Rα is flexible or preformed and fixed. Thus, structure data of either the unbound IL-5Rα or IL-5Rα bound to ligands other than IL-5 might provide additional information on this question. Structure data for the IL-5•IL-5Rα•βc ternary complex will yield insights into whether IL-5 leads to a similar higher order receptor assembly as found for GM-CSF or not.

To answer these questions and to gain further insights into the underling receptor activation mechanism, IL-5 and its receptor subunits need to be further functionally and structurally analyzed. Since these types of analyzes require large amounts of highly purified protein, purification procedures for IL-5 and for the IL-5Rα and βc ectodomain proteins should be established and optimized. To reveal the composition and architecture of the IL-5•IL-5Rα•βc ternary complex the structure determination of the IL-5 ternary complex by X-ray crystallography was planned. Information about the flexibility of the IL-5Rα ectodomain is needed for subsequent IL-5 inhibitor design hence structure analyzes of unbound IL-5Rα should be performed. Finally no structure data is currently available on the set of small IL-5 inhibiting peptides, which however present a valuable alternative to neutralizing antibodies against IL-5 and IL-5 receptors that currently enter the clinics. Thus one major aim of this project was the structure/function analysis of the small peptides AF17121 and/or AF20016 ideally in complex bound to IL-5Rα. From these data structure-based rational

design of peptidomimetics or optimized peptides might be performed, which can help to develop these peptides to therapeutics in eosinophil-driven diseases.

3 MATERIALS AND METHODS

3.1 Materials

3.1.1 Chemicals and Enzymes

If not listed separately all chemicals and enzymes were obtained in highest purity and quality from Carl Roth GmbH and Co. KG, AppliChem GmbH, Sigma-Aldrich Chemie, Fermentas/ThermoScientific, New England Biolabs, Finnzymes/Biozym, Roche and QA-Bio GmbH.

3.1.2 Bacterial Strains

Escherichia coli NovaBlue^{TM} (Novagen)	*endA1 hsdR17* ($rK12^{-}$ $mK12^{+}$) *supE44 thi-1 recA1 gyrA96 relA1 lac* F′[*proA*$^{+}$*B*$^{+}$*lacI*^{q}ZΔ*M15*::Tn*10*] (Tet^{R})
Escherichia coli BL21 Star^{TM} (DE3) (Novagen)	F^{-}*omp*T *hsd*S$_B$ (r_B^{-} m_B^{-}) *gal dcm rne*131 (DE3)
Escherichia coli BL21 Gen-X^{TM} (Gentlantis):	F^{-}*omp*T *hsd*S$_B$ (r_B^{-} m_B^{-}) *gal dcm rne*131 (DE3)
Escherichia coli Rosetta^{TM} (DE3) (Novagen)	F^{-} *ompT hsdS*$_B$(r_B^{-} m_B^{-}) *gal dcm* (DE3) pRARE (Cam^{R})
Escherichia coli JM109 (DE3) (Promega)	*end*A1, *rec*A1, *gyr*A96, *thi, hsd*R17 (r_k^{-}, m_k^{+}), *rel*A1, *sup*E44, Δ(*lac-pro*AB), [F´ *tra*D36, *pro*AB, *laq*I^{q}ZΔM15]

3.1.3 Vectors

pET28b_ybbR (Novagen)	*E. coli* expression vector, T7/lac-promotor, Kan^{R}, N-terminal ybbR-tag coding sequence
pET3d (Novagen)	*E. coli* expression vector, T7/lac-promotor, Amp^{R}
pET22b-CPD$_{BamHI-Leu}$ (Novagen)	*E. coli* expression vector, T7/lac-promotor, Amp^{R} C-terminal His_6-tag coding sequence. The *Vibrio cholerae* MARTX toxin cysteine protease domain was additionally added (Shen, A. *et al.*, 2009)
pMK1 (Modified by former teammate)	Baculovirus transfection and expression vector for insect cells, polh-promotor, Amp^{R}, N- or C-terminal $His_{6\text{-tag}}$ coding sequence, N-terminal His_6-tag sequence can be cleaved via thrombin protease sequence
pAB-bee-8xHis (AB Vector)	Baculovirus transfection and expression vector for insect cells, polh-promotor, Amp^{R}, N- or C-terminal $His_{8\text{-tag}}$ coding sequence

3.1.4 Oligonucleotides

Red: added restriction enzyme recognition sequence
Purple: inserted mutation (codon)
Green: inserted stop codon
Blue: 5'/3' extension for technical reasons

hIL-5Rα C66A

Cloning into pET28b_ybbR from pET3d:

BamHI hIL-5Ra s: 5'-GGATCCgacttacttcctgatgaaaag
XhoI hIL-5Ra as: 5'-CTCGAGttatcttgagaaccccac

Mutation:

Q25A: 5'-ctggtttggctGCAgttcttttacaatgg
E44A: 5'-ggaatgttaatctaGCAtatcaagtgaa
I49A: 5'-gaatatcaagtgaaaGCAaacgctccaaaag
P52A: 5'-gaaaataaacgctGCAaaagaagatgactatg
K53A: 5'-aaataaacgctccaGCAgaagatgactatg
E54A: 5'-cgctccaaaaGCAgatgactatgaaacc
D55A: 5'-cgctccaaaagaaGCTgactatgaaaccag
D55N: 5'-cgctccaaaagaaAATgactatgaaacc
D55E: 5'-cgctccaaaagaaGAAgactatgaaacc
D56A: 5'-ctccaaaagaagatGCCtatgaaaccagaa
Y57A: 5'-caaaagaagatgacGCTgaaaccagaatcac
Y57F: 5'-caaaagaagatgacTTTgaaaccagaatc
Y57W: 5'-caaaagaagatgacTGGgaaaccagaatc
E63A: 5'-aaccagaatcactGCAagcaaagctgtaac
K65A: 5'-gaatcactgaaagcGCAgctgtaaccatcc
V67A: 5'-ctgaaagcaaagctGCAaccatcctccaca
T68A: 5'-gcaaagctgtaGCCatcctccacaaaggc
I69A: 5'-gcaaagctgtaaccGCCctccacaaaggc
I69C: 5'-gcaaagctgtaaccTGCctccacaaagg
H71C: 5'-gtaaccatcctcTGCaaaggcttttcagc
F74A: 5'-cctccacaaaggcGCTtcagcaagtgtgc
Y155A: 5'-tctctactataggGCTggctcttggactga
K186A: 5'-cttttatcctcagcGCAgggcgtgactggc
R188A: 5'-cctcagcaaagggGCTgactggcttgcgg
R188K: 5'-cctcagcaaagggAAGgactggcttgcgg
D189A: 5'-cagcaaagggcgtGCCtggcttgcggtgct
W190A: 5'-gcaaagggcgtgacGCGcttgcggtgcttg
L194A: 5'-ctggcttgcggtgGCTgttaacggctccag
P206A: 5'-cactctgctatcaggGCCtttgatcagctg
D208A: 5'-gctatcaggcccttGCTcagctgtttgcc
D208C: 5'-gctatcaggcccttTGTcagctgtttgc
L210A: 5'-gcccttgatcagGCGtttgcccttcacgc
M295A: 5'-gcagtgagctccGCGtgcagagaggcagg
R297A: 5'-gagctccatgtgcGCAgaggcagggctctg

βc N346Q

Cloning of the βc N346Q cDNA into the pMK1 vector from pAB-bee vector

BamHI βc s: 5′-**GGATCC**tgggagcgttccctggctggtgc
XhoI +Stop βc as: 5′-**CTCGAGTTA**ggactcggtgtcccaggaacg

Mutation:

N346Q to WT:

s: 5′-cccccatccctg**AAC**gtgaccaaggac

as: 5′-gtccttggtcac**GTT**cagggatggggg

AF17121$_{CPD}$

Cloning into pET22b-CPD$_{BamHI-Leu}$:

AF17121 WT + Leu:

s: 5′-tttt**CATATG**gttgacgaatgctggcgtatc**ATCGCTTCCCAC**

as: 5′-aaaa**GGATCC**gagttcttcagcgcagaaccaggt**GTGGGAAGCGAT**

AF17121 WT two-step PCR:

pET22b CPD s: 5′-**CGCTGAAGAACTC**ggatccggaaaaatactc
pJET AF17121as: 5′-**GAGTATTTTTCC****GGATCC**gagttcttcagcg

Mutation:

E3Q: 5′-catatggttgac**CAA**tgctggcgtatcatcg
W5Y: 5′-ggttgacgaatgc**TAC**cgtatcatcgcttcc
I7F: 5′-cgaatgctggcgt**TTC**atcgcttcccacacc
I7H: 5′-cgaatgctggcgt**CAC**atcgcttcccacacc
I7M: 5′-cgaatgctggcgt**ATG**atcgcttcccacacc
I7L: 5′-cgaatgctggcgt**TTG**atcgcttcccacacc
I7Y: 5′-cgaatgctggcgt**TAC**atcgcttcccacacc
I8F: 5′-cgaatgctggcgtatc**TTC**gcttcccacacc
I8M: 5′-cgaatgctggcgtatc**ATG**gcttcccacacc
I8V: 5′-cgaatgctggcgtatc**GTC**gcttcccacacc
I8Y: 5′-cgaatgctggcgtatc**TAC**gcttcccacacc
A9F: 5′-gctggcgtatcatc**TTT**tcccacacctgg
A9I: 5′-gctggcgtatcatc**ATT**tcccacacctgg
A9M: 5′-gctggcgtatcatc**ATG**tcccacacctgg
S10A: 5′-cgtatcatcgct**GCC**cacacctggttctgc
S10G: 5′-cgtatcatcgct**GGC**cacacctggttctgc
S10P: 5′-cgtatcatcgct**CCT**cacacctggttctgc
H11K: 5′-cgtatcatcgcttcc**AAG**acctggttctgc
H11R: 5′-cgtatcatcgcttcc**CGC**acctggttctgc
T12E: 5′-catcgcttcccac**GAG**tggttctgcgctg
T12Q: 5′-catcgcttcccac**CAG**tggttctgcgctg
F14W: 5′-cttcccacacctgg**TGG**tgcgctgaagaac
A16G: 5′-cacctggttctgc**GGT**gaagaactcggatcc
A16P: 5′-cacctggttctgc**CCT**gaagaactcggatcc
E17D: 5′-cctggttctgcgct**GAC**gaactcggatccg
E18G: 5′-ggttctgcgctgaa**GGA**ctcggatccgg

3.1.5 Antibiotics

Ampicillin	Stock solution: 100 mg/ml in ddH_2O Working concentration: 100 µg/ml
Kanamycin	Stock solution: 100 mg/ml in ddH_2O Working concentration: 30 µg/ml
Tetracycline	Stock solution: 5 mg/ml in Ethanol Working concentration: 12.5 µg/ml

3.2 Molecular biology methods

3.2.1 Single mutation by rapid PCR site-directed mutagenesis (Weiner, M.P. *et al.*, 1994)

Table 1: Pipetting scheme for one PCR reaction.

Component	Concentration/ Amount	Volume
DNA template	20 ng	x µl
dNTP-Mix (25 mM)	0.25 mM	0.5 µl
Primer sense (10 µM)	0.1 µM	0.5 µl
Primer antisense (10 µM)	0.1 µM	0.5 µl
Phusion HF-Buffer (5x)	1x	10 µl
Phusion-Polymerase (2 U/µl)	0.012 U/µl	0.3 µl
ddH_2O		add to 50µl

Table 2: Thermal cycling profile of the PCR.

Cycle step	Time	Temperature	Cycles
Initial denaturation	5 min	95 °C	1
Denaturation	1 min	95 °C	
Annealing	30 s	x °C	25
Extension	30 s/kb	72 °C	
Final extension	5min	72 °C	1
Store final PCR product	Hold	4°	1

x = calculated annealing temperature based on the sequence composition of the primer pair used (the lower temperature was used).

DpnI digestion:

45 µl of the final PCR product are mixed with 5 µl Tango-Puffer (10x) and 1 µl DpnI (10 U/µl) restriction enzyme and incubated for 1 hour at 37°C.

3.2.2 Two-step PCR

1st step PCR: reaction I and II

The 1st step PCR of the two-step PCR is divided into two reactions using different pairs of oligonucleotides to produce the DNA fragments down- and upstream of the mutation introduced. Reaction I uses a 5' sense primer annealing at the 5' end of the DNA fragment and a 3' antisense primer harboring the mutation(s). In reaction II the annealing location of the oligonucleotides is mirrored.

Table 3: Pipetting scheme for two-step PCR reaction.

Component	Concentration/ Amount	Volume
DNA template	10 ng	x µl
dNTP-Mix (25 mM)	0.83 mM	1 µl
Primer sense (10 µM)	0.33 µM	1µl
Primer antisense (10 µM)	0.33 µM	1 µl
Phusion HF-Buffer (5x)	1x	6 µl
Phusion-Polymerase (2 U/µl)	0.02 U/µl	0.3 µl
ddH_2O		add to 30µl

Table 4: Thermal cycling profile for two-step PCR.

Cycle step	Time	Temperature	Cycles
Initial denaturation	5 min	95 °C	1
Denaturation	1 min	95 °C	
Annealing	30 s	x °C	30
Extension	30 s/kb	72 °C	
Final extension	5min	72 °C	1
Store final PCR product	Hold	4°	1

x = calculated annealing temperature based on the sequence composition of the primer pair used (the lower temperature was used).

2nd step PCR:

The overlap of the two PCR products from the 1st step PCR match and the mutation (mismatch) is used to assemble both fragments into a single PCR fragment. For the 2nd PCR step 1 µl (diluted 1:100) of each of the final PCR products from the 1st PCR step were used as the DNA template. The 5' sense primer and 3' antisense primer annealing at the 5' or 3' end of the DNA fragment were used. The PCR reaction and cycling instruction are the same as used in the 1st PCR step (s. Table 3 and Table 4).

3.2.3 Restriction endonuclease reaction

Table 5: Pipetting scheme for restriction endonuclease reaction.

Component	PCR product	Plasmid DNA
DNA	25 µl	3-5 µg
***Fast Digest* enzyme I** (Fermentas)	1 µl (10U)	1-1.5 µl (10-15U)
***Fast Digest* enzyme II** (Fermentas)	1 µl (10U)	1-1.5 µl (10-15U)
10x *Fast Digest* buffer (Fermentas)	4 µl	4 µl
ddH_2O	add to 40 µl	add to 40 µl

The restriction reactions (s. Table 5) are incubated at 37°C for 15-30 min. Afterwards, the linearized vector DNA is dephosphorylated by adding 1 µl alkaline phosphatase (FastAP, Fermentas) and incubating for 10 min at 37°C.

Inactivation of the enzymes is achieved by incubation at 65 °C for 15 min if applicable to the enzyme used. The digestion products are analyzed via agarose gel electrophoresis (s. 3.2.4) and purified using a PCR Clean-Up & Gel-Extraction Kit (Süd-Laborbedarf).

3.2.4 Agarose gel electrophoresis

50x TAE-buffer:	2 M Tris-HCl, 1 M sodium acetate, 50 mM EDTA, pH 8.0
6x DNA loading dye:	0.25% (w/v) bromophenol blue, 0.025% (w/v) xylene cyanol FF, 30% (v/v) glycerol
DNA-Marker:	MassRuler DNA Ladder Mix (Fermentas #SM0403) (for use 1 part of DNA-Marker mixed with 1 part of 6x DNA loading dye and 4 parts of ddH_2O)

Agarose gels (1%, agarose dissolved in 1x TAE-buffer) stained with GelGreen Nucleic Acid Stain (BIOTIUM; 2.5 µl per 50 ml) were used for the agarose gel electrophoresis. The DNA samples are treated with 6x DNA loading dye in the ratio 1:5 and up to 20 µl are loaded per sample well. To estimate the molecular size of the DNA fragments 7 µl of a DNA standard is loaded into one well. Separation of the DNA fragments is carried out at 100 V (250 mA, 50 W) for 30-60 min using 1xTAE-buffer as running buffer. DNA bands are visualized using a blue light transilluminator (Dark Reader®, Clare Chemical).

3.2.5 Ligation

Table 6: Pipetting scheme for ligation reaction.

Component	Amount / Volume
DNA fragment	variable
Linearized vector	100ng / x µl
T4 DNA Ligase (5 U/µl)	0.5 µl (2.5 U9
10x T4 DNA Ligase buffer	2 µl
ddH_2O	add to 20 µl

The amount of the DNA fragment needed is calculated based on the measured concentration at 260nm and the following formula.

$$ng(fragment) = \frac{ng(vector) \times kb(fragment)}{kb(vector)} \times molar\ ratio\ \left(\frac{fragment}{vector}\right)$$

Molar ratio of DNA fragment to vector (3:1) is chosen.

The ligation reaction is incubated for 30 min at room temperature or at 4°C overnight. 10 µl of the ligation mixture is used for transformation.

3.2.6 Preparation of competent cells (Rubidium chloride method)

TfbI-buffer:	30 mM potassium acetate, 100 mM RbCl, 10 mM $CaCl_2$, 50 mM $MnCl_2$, 15% (v/v) glycerol; adjust pH to 5.8 using 0.1 M acetic acid
TfbII-buffer:	10 mM MOPS, 75 mM $CaCl_2$, 10mM RbCl, 15% (v/v) glycerol, adjust pH to 6.5 with 0.1 M sodium hydroxide
LB-medium	Ready-to-use mix (Melford), 25 g dissolved in 1 l ddH_2O result into the following formation: 10 g/l Tryptone, 5 g/l Yeast extract, 10 g/l NaCl, pH 7.0 (sterilize by autoclaving)

1 ml of an overnight culture of the desired *E. coli* strain with specific antibiotic(s) (if needed) are used to inoculate a 50 ml LB-Medium culture with respective antibiotic(s). The cells are incubated at 37°C with shaking (130 rpm, Multitron Standard, INFORS HT) until an OD_{600} 0.4 is reached. Then cells are incubated for 15 min on ice and centrifuged for 5 min at 4°C and 4500xg. The supernatant is discharged and the cells are resuspended in 20 ml TfbI-buffer. Afterwards the cells are incubated on ice for 5 min and centrifuged again. The cells were resuspended in 4ml TfbII-buffer incubated for 15 min. After that, the cell suspension is split in 50 µl aliquots and immediately frozen in liquid nitrogen. The aliquots are stored at -80°C.

3.2.7 Transformation of *E. coli*

LB-agar plates	Read-to-use mix (Roth) 35 g dissolved in 1 l ddH_2O result into the following formation: 10 g/l Tryptone, 5 g/l Yeast extract, 5 g/l NaCl, 15 g/l agar-agar, pH 7.0 (sterilize by autoclaving; add antibiotic(s) at 45°C)
SOB-medium	20 g/l Tryptone, 5 g/l Yeast extract, 0.5 g/l NaCl (sterilize by autoclaving)
SOC-medium	SOB-medium with 10 mM $MgSO_4$, 10 mM $MgCl_2$ and 0.4% (v/v) Glucose (Stock solution sterile filtrated) added (stored at -20°C)

10-20 ng of plasmid DNA or 10µl of a ligation reaction are added to one aliquot of competent *E. coli* cells and incubated on ice for 30 min. Afterwards the cells are incubated for 45 sec at 42°C (heat shock) in a block heater. 150 µl of SOC-medium are added immediately after the heat shock and the cells are incubated on ice for 2 min. Then cells are incubated for 30-45 min at 37°C with shaking (130 rpm). Transformed cells are plated on LB-agar plates containing the specific antibiotic(s). The plates are incubated at 37°C overnight.

3.2.8 Colony-PCR

LB-medium s. 3.2.6

A 1 ml LB-medium culture containing the specific antibiotic(s) is inoculated with a single colony picked from a LB-agar plate and incubated for 3-4 h at 37°C with shaking (130 rpm). After that the culture is centrifuged for 5 min at room temperature and 13.000xg, cells are resuspended in 50 µl ddH_2O and incubated for 5 min at 95°C (block heater). The cell suspension is then centrifuged again and 2 µl of the supernatant is used as the DNA template for subsequent PCR analysis (s. Table 7 and Table 8).

Table 7: Pipetting scheme for one colony PCR reaction.

Component	Concentration/ Amount	Volume
DNA template	-	2 µl
$MgCl_2$ (25 mM)	2mM	2 µl
dNTP-Mix (25 mM)	0.25 mM	0.25 µl
Primer sense (10 µM)	0.4 µM	1µl
Primer antisense (10 µM)	0.4 µM	1 µl
TureStart *Taq* buffer (10x)	1x	2.5 µl
TureStart Hot Start *Taq* DNA Polymerase (5 U/µl)	0.03 U/µl	0.15 µl
ddH_2O		add to 25µl

Table 8: Thermal cycling profile for colony PCR.

Cycle step	Time	Temperature	Cycles
Initial denaturation	5 min	95 °C	1
Denaturation	1 min	95 °C	
Annealing	30 s	x °C	25
Extension	1 min/kb	72 °C	
Final extension	5min	72 °C	1
Store final PCR product	Hold	4°	1

x = calculated annealing temperature based on the sequence composition of the primer pair used (the lower temperature was used).

Sequencing oligonucleotides (e.g. T7 sense and anti-sense) are used. PCR products are subsequently analyzed via agarose gel electrophoresis (s. 3.2.4).

3.2.9 Plasmid preparation

LB-medium s. 3.2.6

Multiplication of plasmid DNA can be done at different scales. 5 ml (high copy vector) or 10 ml (low copy vector) LB-medium overnight cultures with specific antibiotic(s) are used for the preparation of up to 20 µg of plasmid DNA. The DNA is isolated and purified after the manufactures' instructions using the GeneJET Plasmid Miniprep Kit (Fermentas).

The Plasmid Plus Midi Kit (Qiagen) was used for purifying up to 250 µg of plasmid DNA using 50 ml (high copy vector) or 100 ml (low copy vector) LB-medium overnight cultures with specific antibiotic(s).

3.3 Protein chemical methods

3.3.1 SDS-polyacrylamide gel electrophoresis (SDS-PAGE)

Rotiphorese Gel 40 (29:1):	40% (v/v) acrylamide/bisacrylamide stock solution at a ratio of 29:1 (Roth)
4x Upper Tris buffer:	0.5 M Tris-HCl pH 6.8, 0.4% (w/v) SDS
4x Lower Tris buffer:	1.5M Tris-HCl pH 8.8, 0.4% (w/v) SDS
SDS running buffer:	25 mM Tris-HCl, 0.19 M glycine, 0.15% (w/v) SDS
6x protein sample buffer:	375mM Tris-HCl pH 6.8, 9% (w/v) SDS, 60% (v/v) glycerol (87%), 0.015% (w/v) bromophenol blue
Protein size-standard:	Unstained Protein Molecular Weight Marker (Fermentas, #26610)

Table 9 shows the pipetting scheme for the preparation of the stacking- and running-gel. The components are pipetted in a 15ml (stacking-gel) or 50 ml (running-gel) reaction tube in the order listed below. The solution of the running-gel is first filled between the two glass plates, and the solution is covered with isopropanol to prevent oxygen access. After the polymerization of the separating gel the isopropanol is poured off and the stacking gel solution is filled between the glass plates and a comb is used to form the sample wells. The fully polymerized gel is inserted into the chamber filled with SDS running buffer (Mini PROTEAN Electrophoresis System, Biorad). The protein samples are treated with 6x protein sample buffer in a ratio 1:5 and up to 20 µl are loaded per sample well. To estimate the apparent molecular weight of the proteins 7 µl of the protein size-standard are loaded into one of the sample wells. The proteins are separated at 300 V (max. 25 W per gel). The electrophoresis is ended shortly before the migrating colored band (dye + sample) exits the lower end of the gel. (Laemmli, U.K., 1970)

Table 9: Pipetting scheme for stacking and running gel. Amount sufficient for two gels (10x10 cm, 0.75 mm thickness)

Component	Running-gel (12%)	Stacking-gel (4%)
Rotiphorese Gel 40 (29:1)	3.0 ml	0.5 ml
4x Upper Tris buffer	-	1.25 ml
4x Lower Tris buffer	2.5 ml	-
87% glycerol	2.0 ml	-
ddH_2O	2.5 ml	3.2 ml
TEMED	20 µl	20 µl
40% APS	20 µl	20 µl

3.3.2 Protein precipitation

If protein samples were highly diluted or the protein was in a buffer that is not compatible with SDS-PAGE, buffer was exchanged by precipitating the protein via methanol/ chloroform precipitation. The protein is diluted 1:10 in 400 µl ddH_2O and 300 µl methanol and 100 µl chloroform are added. The solution is vigorously mixed and centrifuged (2 min, 16800xg). The upper phase is carefully removed and 300 µl of methanol is added. The solution is again vigorously mixed and centrifuged. The supernatant is removed and the pellet is incubated (with open lid) until it is completely dry. The pellet is resuspended in 40 µl 2x protein sample buffer.

3.3.3 Staining methods for SDS-PAGE gels

Coomassie staining:

Coomassie blue staining buffer:	10% (v/v) acetic acid, 40% (v/v) ethanol, 50% (v/v) water, 0.12% (w/v) brilliant blue R250, 0.12% (w/v) brilliant blue G250
De-staining buffer:	30% (v/v) ethanol, 6% (v/v) acetic acid, 64% (v/v) water

Detecting protein quantities greater than or equal 1 µg coomassie staining is used. The SDS-PAGE gel is heated in the coomassie blue staining buffer in the microwave for 20 s and afterwards incubated for 15 min at room temperature with shaking. The staining solution is removed and the gel is washed with water. The gel is incubated in de-staining solution until the blue protein bands are visible and the background is completely decolorized.

Silver staining:

Table 10: Instructions and solutions for silver staining of one SDS-PAGE gel. Stock solution prepared in/with ddH_2O. w = washing step (with water)

Solution	Composition	Incubation time
1	30 ml 50% (v/v) acetone, 0.75 ml 50% (v/v) TCA, 12.5 µl 37% (w/v) formaldehyde	5 min + w
2	30 ml ddH_2O	5 min + w
3	30 ml 50% (v/v) acetone	5 min
4	30 ml ddH_2O, 50 µl 10% (w/v) $Na_2S_2O_3$	1 min + w
5	30 ml ddH_2O, 0.4ml 20% (w/v) $AgNO_3$, 0.3 ml 37% (w/v) formaldehyde	8 min + w
6	30 ml ddH_2O, 0.6 g (w/v) $NaCO_3$, 12.5 µl 37% (w/v) formaldehyde, 25 µl 10% (w/v) $Na_2S_2O_3$	Until protein bands are visible
7	1% (v/v) acetic acid	15 min

Gels stained via coomassie blue or silver staining are incubated for 30 min in drying gel solution (30% (v/v) methanol, 6% (v/v) glycerol) before being placed between two cellophane membranes (soaked in water) and put into frame using four clamps to hold the frames together. The gel is dried after 24h and ready for long-term storage.

3.3.4 Western Blot

Blot buffer:	24 mM Tris-HCl, 200mM glycine, 20% (v/v) methanol
TBS buffer:	10 mM Tris-HCl pH 7.5, 150 mM NaCl
TBST/T buffer:	20 mM Tris-HCl pH 7.5, 500 mM NaCl, 0.05% (v/v) Tween20, 0.2% (v/v) Triton X-100
Blocking buffer:	0.5% (w/v) Blocking Reagent (5prime) are dissolved in 1x Blocking Reagent buffer (10x; 5prime) at 70°C. After cooling down of the solution to room temperature 0.1% (v/v) Tween20 were added
Antibody solution:	Penta-His HRP Conjugate (5prime) 1:2000 diluted in blocking buffer
Detection solution:	1ml (per Blot) prepared after manufactures' instructions (WesternBright^{TM} ECL Kit, Biozym)

To detect proteins via specific antibodies they are transferred electrophoretically to a nitrocellulose membrane (Protran 0.45 µm, Whatman) following the SDS-PAGE (s. 3.3.1) using the wet blot method (Rotiphoresis® PROclamp MINI Tank Blotting System, Carl Roth). The gel and all other components of the transfector (blot mats, filter papers, membrane) are equilibrated for 10min in blot buffer before use. After assembly of the transfector, the proteins are transferred by applying an electric field of 80 V for 1 h in the blot chamber filled with blot buffer. The detection of proteins with His_6 sequence is done using the Penta His HRP Conjugate Kit (5prime). Since the horseradish peroxidase (HRP), required for the chemiluminescent detection reaction, is directly coupled to the primary antibody a secondary antibody is not needed. Afterwards the membrane is washed in TBST/T buffer for 10 min and TBS buffer for 10 min with shaking. In order to saturate nonspecific binding sites of the membrane it is then incubated for 1 h in 5 ml block buffer at room temperature with shaking. After that the membrane is washed twice in TBST/T and once in TBS buffer for 10 min each. The antibody is bound to the immobilized proteins on the membrane by incubating the membrane in the antibody solution with shaking at room temperature for 1 h or 4°C overnight. Afterwards the membrane is washed once

with TBST/T buffer and twice with TBS buffer for 10 min. The membrane is then incubated for 10 min in the detection solution and placed in a polythene foil. Detection of the chemiluminescence signal can be done using X-ray films (Cronex 5, AGFA) or a CCD camera system (ChemiDoc MP, BioRad).

3.3.5 Dot blot

PBST buffer:	137 mM NaCl, 2.7 mM KCl, 10 mM Na_2HPO_4, 2 mM KH_2PO_4, pH 7.4 + 0.05% Tween20
Blocking buffer:	5% (w/v) BSA in PBST buffer
Antibody solution:	Streptavidin-HRP (High Sensitivity, PIERCE) 1:10.000 diluted in blocking buffer

The positions of the protein samples are marked with a pencil on the nitrocellulose membrane (Protran 0.45 µm, Whatman). Protein samples are applied two to three times (5 µl). After that the membrane is washed twice with PBST buffer for 10 min with shaking. To block unspecific binding sites the membrane is then incubated for 1 h in 5 ml blocking buffer with shaking. Afterwards the membrane is washed three times with PBST for 10 min before incubated for 1 h in 5 ml antibody solution with shaking. The wash step is repeated five times. The membrane is then incubated for 10 min in the detection solution and placed in a polythene foil. Detection of the chemiluminescence signal is done using a CCD camera (ChemiDoc MP, BioRad).

3.3.6 Photometric determination of the protein concentration

The protein concentration (c) can be calculated using the Beer-Lambert equation. An UV absorption spectrum in the range of 250 – 320 nm is recorded (Evolution 300UV Visible or Nanodrop 2000c Spectrophotometer, Thermo).

$$c = \frac{A_{280} - A_{320}}{\varepsilon_{280} \times d}$$

where:

A_{280} = Absorption at 280 nm (protein specific)
A_{320} = Absorption at 320 nm (stray light effects)
ε_{280} = Extinction coefficient at 280 nm (protein specific) [M^{-1} cm^{-1}]
d = the path length [cm]

The protein specific extinction coefficient ε_{280} was determined based on the amino acid sequence with the aid of the ExPASy ProtParam Tool (Wilkins, M.R. *et al.*, 1999) (http://web.expasy.org/protparam/).

Table 11: Overview of the molecular weights and molar extinction coefficients calculated with ExPASy ProtParam Tool of the proteins used in the work. For the different variants s. 9.3.

Protein	Molecular weight [Da]	Extinction coefficient ε_{280} [M-1 cm-1]
hIL-5	26472.6	17210
hIL-5Rα_{ECD}	36040.7	69245
hIL-5Rα_{ECD} ybbR	37346.1	69245
βc N346Q	99350.8	202260
AF17121	2195.4	11125
AF17121-CPD	26125.8	37595
AF17121 (CPD)	2308.6	11125
AF20016	3470.0	14355

3.3.7 Labeling of proteins with biotin or fluorescent dye using NHS conjugates

Fluorescent dye: Alexa Fluor™ 647 NHS Ester (Thermo Fischer, A20006)
Biotin: EZ-Link™ Sulfo-NHS-Biotin (Thermo Fischer, 21217)

Proteins with no specific tag were labeled with NHS conjugates in a 1:2 molar ration (protein/NHS conjugate) using the following formula:

$$ml\ protein\ x\ \frac{mg\ protein}{ml\ protein}\ x\ \frac{mmol\ protein}{MW\ protein}\ x\ \frac{mmol\ conjugate}{mmol\ protein}$$

mmol conjugate = 2x mmol protein

The stock solution (1 mmol) of the NHS conjugate is prepared and the calculated volume is added to the protein solution. The reaction is incubated for 2 h on ice. Afterwards unbound NHS conjugate is removed via ultrafiltration (washing 5x with buffer). Aliquots (50 µl) are prepared and stored at -20°C.

3.3.8 Site-specific coupling of proteins with biotin or fluorescent dye using Sfp synthase

Fluorescent dye: CoA-647 (NEB, S9350S)
Biotin: CoA-Biotin (NEB, S9351S)

Fusion proteins encoding the ybbR tag sequence (DSLEFIASKLA) were specifically labeled by small molecule-CoA conjugates using the Sfp phosphopantetheinyl transferase (Yin, J. *et al.*, 2005, Yin, J. *et al.*, 2006).

Highly purified ybbR fusion protein and all other components (s. Table 12) are mixed and incubated for 2 h at 22°C (water bath and in the dark). Afterwards the solution is incubated for 72 h at 4°C. Unbound CoA conjugate is removed

via gel filtration chromatography (s. 3.6.3). Aliquots are prepared and stored at -20°C.

Table 12: Components and concentrations for one coupling reaction.

Components	Concentration in reaction
1 M HEPES pH 7.4	50 mM
1 M $MgCl_2$	10 mM
YbbR fusion protein	5 µM
40 µM Sfp synthase	0.5 µM
1 mM CoA conjugate	7.5 µM

3.3.9 Mass spectrometry

The molecular weight of proteins can be determined by mass spectrometric analysis. The proteins or peptides were purified and desalted via reversed-phase HPLC (s. 3.6.5) in order to be suitable for subsequent electron-spray ionization (ESI) mass spectrometry analysis. The mass spectra were recorded with a Bruker APEX II Fourier-transform ion cyclotron resonance (FT-ICR) mass spectrometer equipped with a 7.5 T magnet. For the measurement, 1 µl of the protein sample is dissolved in 50% ethanol and 1% acetic acid. The ionization of the sample is done using an Apollo electron spray electron source and detection is carried out in positive ion mode. Data acquisition was performed by Dr. Werner Schmitz (Institute of Biochemistry and Molecular Biology, University of Würzburg).

3.4 Production of recombinant proteins using a baculovirus-insect cell expression system

3.4.1 Insect cell cultivation

All cell lines used were cultured adherently in 75 cm^2 or 175 cm^2 cell culture flask (Greiner BioOne) at 27°C (Incubator, Memmert). The cells are passaged every 3-4 days as soon as they are confluent. Medium is removed and 10 ml of fresh medium are added to the cells. The adherent growing cells are gently dislodged and are then diluted in a ratio of 1:4. Afterwards the cell suspension volume is adjusted to 15 ml (75 cm^2) or 30 ml (175 cm^2) with fresh medium. Pooling adherent cells from several cell culture and adjusting the concentration to $5.5*10^5$ cells/ml enables cultivating of cells in larger volumes. The cells are incubated in erlenmeyer flasks with screw closure (Isolab) at 27°C and 80 rpm (Multitron Standard, INFORS HT). Every 3-4 days cells are counted and adjusted to a concentration of $5.5*10^5$ cells/ml with fresh medium until the desired volume is reached.

3.4.2 Cell counting

Trypan blue solution: 0.5% (w/v) trypan blue, 0.9% (w/v) NaCl in ddH_2O

20 µl cell suspension are mixed with 80 µl of the trypan blue solution and counted using a hemocytometer. Dead cells are stained blue due to the permeability of their cell membrane. The cell concentration can be determined as follows:

$$Cell\ concentration\ \left(\frac{cells}{ml}\right) = \frac{number\ of\ cells\ alive\ \cdot\ 10^4}{number\ of\ large\ squares}\ \cdot dilution\ factor$$

10^4 = hemocytometer-dependent constant multiplication factor

3.4.3 Co-transfection

*Sf*9 cells:	*Spodoptera frugiperda* (origin, Novagen)
*Sf*9 culture medium:	Insect-Xpress + 1% Pen/Strep (Lonza) + 5% FCS (Biochrome)
Serum free medium:	Insect-Xpress (Lonza)
Transfection Kit:	BacVector®-3000 Transfection Kit (Novagen)

*Sf*9 cells are gently dislodged, adjusted to $2.5*10^5$ cells/ml and 5ml of the cell suspension were transferred into a new 25 cm^2 flask. The cells are incubated for 20 min at 27°C. In the meantime, the transfection mix is prepared. Therefore 20-x µl serum free medium, x µl vector DNA (500 ng) and 5 µl Triple cut

virus-DNA (100 ng) are pipetted into one eppendorf tube (A) and 20 µl of sterile water and 5 µl of Insect GeneJuice® transfection reagent are added into another eppendorf tube (B). Afterward A and B are mixed and incubated for 15 min at room temperature. The adherently *Sf*9 cells are washed twice with 2 ml of serum free medium before 1 ml of serum free medium is added to the cells. 450 µl of serum free medium is added to the transfection mix and then it is added to the cells and incubated for 1 h at room temperature. After that 6 ml of *Sf*9 culture medium is added to the cells and incubated for 5 days at 27°C. Cells are centrifuged (5 min, 400xg). The supernatant is transferred into sterile 15 ml falcon tubes and stored at 4°C in the dark (wrapped in aluminum foil).

3.4.4 Plaque assay

*Sf*9 cells:	*Spodoptera frugiperda* (Novagen)
*Sf*9 culture medium:	Insect-Xpress + 1% Pen/Strep (Lonza) + 5% FCS (Biochrome)

A plaque assay is used to isolate single recombinant viruses obtained from co-transfection. *Sf*9 cells are gently dislodged in fresh medium and adjusted to $1.5*10^6$ cells/ml. 1ml of the cell suspension and 1ml of fresh medium are added to each well of a 6-well plate and incubated at 27°C for 1 h. In the meantime, a dilution series of the virus solution from the co-transfection with a volume of 1 ml each of 10^{-1} to 10^{-4} are produced. The medium is aspirated and 1 ml of the virus solution, a dilution or medium is added (s. Table 13) and incubated at 27°C for 1 hour. The virus solutions are aspirated and the cells in each well are coated with 1.5 ml of the agarose mixture. Preparation of the agarose mixture: 2.7% (w/v) Sea Plaque Agarose (Biozym) is melted and kept at 60°C. 6.6 ml of SF-900 1.3x medium (Invitrogen) are added to 700 µl of Fetal Calf Serum (charge 0991L, Biochrome) and mixed with 3.3 ml of agarose prior to overcoating of the cells. After the agarose mixture is solidified 2 ml of sterile water are added into the space between the single wells of the 6-well plate for moisturization. The plate is welded in thermoplastic foil and incubated at 27°C for 4 days.

Table 13: Virus dilution scheme for the plaque assay

Undiluted (positive control)	10^{-1}	10^{-2}
10^{-3}	10^{-4}	Medium (negative control)

3.4.5 Plaque assay staining

Staining of the plaque assay is done by adding 1 ml of MTT solution (1 mg/ml in ddH2O, AppliChem) per well and incubation for 1 h at 27°C. After aspiration of the staining solution infected cells appear as white spots (plaques). Single plaques can be picked for the first virus amplification.

3.4.6 Virus amplification

TriEx™ *Sf*9 cells:	*Spodoptera frugiperda* (Novagen)
TriEx™ *Sf*9 culture medium:	Insect-Xpress + 1% Pen/Strep (Lonza) + 5% FCS (Biochrome)

First virus amplification

Six single plaques colonies from the plaque assay are picked, transferred into a 1.5 ml eppendorf tube containing 1 ml fresh medium and incubated for 2 h at 27°C. In the meantime, TriEx cells are gently dislodged in fresh medium and adjusted to $1.5*10^6$ cells/ml. 1ml of the cell suspension and 1ml of fresh medium are added to each well of a 6-well plate and incubated at 27°C for 1 h. The virus solutions are centrifuged for 5 min at 400xg. After the medium is aspirated 1 ml of the supernatant of one virus solution is added into one well. Sterile water (2 ml) is added to the interspace of the 6-well plate and the plate is welded. After incubation for 4 days at 27°C the virus solutions are each transferred into a 1.5 ml eppendorf tube and centrifuged for 5 min at 180xg. The supernatants are transferred into new 1.5 ml eppendorf tubes and directly used for the second virus amplification.

Second virus amplification

The second virus amplification is prepared analogue to the initial one, here 1 ml of medium is additionally added to 1 ml of virus solution per well. After incubation, centrifugation and transferring of the virus supernatants into new 1.5 ml eppendorf tubes the virus solutions are stored at 4°C in the dark (wrapped in aluminum foil). Verification of protein expression level is done by western blot (s. 3.3.4) analyzing 20 µl of the virus solutions. The virus solution with the strongest signal is used for further virus amplifications.

Third virus amplification

TriEx cells are gently dislodged in fresh medium and adjusted to $5.5*10^5$ cells/ml. 15 ml of the cell suspension is transferred into a 75 cm^2 culture flask and incubated for 1 h at 27°C. The medium is replaced with fresh medium

and 1 ml of the second virus amplification is added. After incubation for 5 days at 27°C the virus solution is transferred into a sterile 15 ml falcon tube and centrifuged for 5 min at 1600xg. The supernatant is transferred into new sterile 15 ml falcon tube and stored at 4°C in the dark. 200 µl of the supernatant is used for determining the viral titer (s. 3.4.7).

Fourth virus amplification

TriEx cells cultured without FCS are used if the fourth virus amplification will be used for protein expression. The TriEx cells are gently dislodged with fresh medium and adjusted to $5.5*10^5$ cells/ml. 30 ml of the cell suspension is transferred into a 175 cm^2 culture flask and incubated for 1 h at 27°C. The medium is replaced with fresh medium. The amount of virus that needs to be added from the third virus amplification is calculated from the following equation.

$$MOI = \frac{Volume\ (virus)\ x\ Concentration\ (virus)}{Volume\ (cells) x\ Concentration\ (cells)} = \frac{V_V\ x\ c_V}{V_c\ x\ c_c}$$

$$V_V = \frac{V_c\ x\ c_c\ x\ MOI}{c_V}$$

To generate a high titer stock solution a Multiplicity of Infection (MOI, ratio of virus to cells) of 0.1 is used. After incubation for 5 days at 27°C the virus solution is transferred into a sterile 50 ml falcon tube and centrifuged for 5 min at 1600xg. The supernatant is transferred into new sterile 50 ml falcon tube and stored at 4°C in the dark. 200 µl of the supernatant is used for determining the viral titer (s. 3.4.7).

3.4.7 Determination of the viral titer

200 µl of the supernatant from the virus amplification are transferred into a sterile 1.5 ml eppendorf tube. The NucleoSpin Tissue Kit (Macherey-Nagel) was used to isolate and purify the virus DNA according to the manufacturers' manual. Real-time-PCR (RT-PCR) was used to determine the viral titer. All components from Table 14 are mixed, the virus DNA is replicated and analyzed using a LightCycler (Roche) employing the cycling instructions as listed in Table 15.

Table 14: Pipetting scheme for one qRT-PCR reaction

Component	Volume
Absolute qPCR SYBR® Green Capillary Mix (Thermo Scientific)	10 µl
ie1 oligonucleotide primer Mix (0.75 µM) **ie1 forward** TGGATATTGTTTCAGTTGCAAG **ie1 reverse** CAACAACGGCCCCTCGATA	8 µl
Template (virus DNA or ddH_2O)	2 µl

Table 15: Cycling instruction for RT-PCR

Step	Temperature	Time	Cycles
Initial denaturation	95°C	15 min	1
Denaturation	95°C	15s	40
Annealing	60°C	20s	
Extension	72°C	20s	
Detection	79°C	5s	
	95°C	5s	
Analysis melting	95°C	5s	1
	75°C	30s	1
Cooling	40°C	10s	1

Using the LightCycler software (version 3.5) the evaluated crossing point is inserted into the standard curve determined beforehand.

$$10^{\left(\frac{CP-38.5}{-3.2}\right)} = c_{virus}\left(\frac{Virus}{ml}\right)$$

3.4.8 Expression of proteins using High-Five™ insect cells

High-Five™ cells: *Trichoplusia ni* (origin, R. Grabherr, VIBT, Wien)
High-Five™ culture medium: 25.63 g/l IPL-41 powder medium (Gennaxxon), 4 g/l Yeast extract, adjust pH to 6.1 and filtrate sterile + 1% Pen/Strep (Lonza) + 1.5% lipid medium supplement (Sigma) + 0.15% Pluronic (F-68, Sigma)

High-Five™ suspension cultures were used for the expression of recombinant proteins. Cells are adjusted to $5.5*10^5$ cells/ml. Depending on the expression volume and viral titer x ml of the supernatant of a serum free virus amplification is added so that an MOI of 5 will be achieved. After incubating for 5 days at 27°C and 80 rpm the cells are centrifuged (6.000xg, 4°C, 15min). The supernatant is dialyzed according to the subsequent purification strategy.

3.5 *E. coli* recombinant protein expression

LB-medium	Ready-to-use mixture (Melford), 25 g dissolved in 1 l ddH_2O result into the following formulation: 10 g/l Tryptone, 5 g/l Yeast extract, 10 g/l NaCl, pH 7.0 (sterilize by autoclaving)
TB-broth	12 g/l Tryptone, 24 g/l Yeast extract, 4.4 ml/l glycerol (sterilized by autoclaving)
Pi Buffer (10x)	170mM KH_2PO_4, 720 mM K_2HPO_4 (sterilized by autoclaving)
TB-medium	9 volumes of TB-broth mixed with 1 volume of Pi Buffer

LB-medium or TB-medium (25 ml per 1 l expression culture) containing the respective antibiotic(s) are inoculated with a single colony from transformed *E. coli* cells (s. 3.2.7) and the culture is incubated for 15-17 h at 37°C with shaking (130 rpm). The next day 20 ml of the overnight culture are transferred per 2 l Erlenmeyer flask (baffled) containing 800ml (1:40) fresh LB- or TB-medium.

3.5.1 Expression of insoluble proteins (inclusion-bodies)

Lysis buffer

IL-5 (STE buffer)	50 mM Tris-HCl, 375 mM Sucrose, 1 mM EDTA, adjust pH to 8.0 (filtrate)
IL-5Rα (TBSE buffer)	10 mM Tris-HCl, 150 mM NaCl, 1 mM EDTA adjust pH to 8.0 (filtrate)

The expression cultures (LB-medium) are incubated at 37°C and 130 rpm until an optical density (OD_{600nm}) of 0.6 – 0.7 is reached. A final concentration of 1 mM Isopropyl β-D-1-thiogalactopyranoside (IPTG) is added to induce protein expression. The cultures are incubated for 3 h at 37°C and 130 rpm before the cells are harvested via centrifugation (4.500xg, 20 min, 4°C). The supernatant is discarded and the cells are resuspended in 25 ml lysis buffer (maximum 15 g per 25 ml) and stored at -20°C.

3.5.2 Expression of soluble proteins

Lysis buffer

CPD buffer	50 mM Tris-HCl, 500 mM NaCl, adjust pH to 7.5 (filtrate)

The expression of the soluble proteins was carried out similar to the expression of the insoluble proteins (s. 3.5.1) except for TB-medium was used. After induction of protein expression, the cultures are incubated at 18°C overnight (ca. 18h) and 130 rpm and the cells are resuspended in 45 ml of lysis buffer.

3.5.3 Cell lysis and extraction of insoluble proteins

Lysis buffer

IL-5 (STE buffer)	s. 3.5.1 + 5 mM DTT
IL-5Rα (TBSE buffer)	s. 3.5.1 + 5 mM DTT

Wash buffer

IL-5 (TE buffer)	STE buffer without Sucrose (s. 3.5.1)
IL-5Rα (TBS buffer)	TBSE buffer without EDTA (s. 3.5.1)

Extraction buffer

IL-5	50 mM NaOAc pH 5.0 + 8 M Urea
IL-5Rα	50 mM NaOAc pH 5.0 + 6 M GuHCl

The stored cells (-20°C) are thawed in pre-warmed water and resuspended with 200 ml (final volume, max. 15 g of cells) lysis buffer containing DTT. To isolate the inclusion bodies (IB's) the cells are lysed via sonication (10 min at 70% 30s/30s, sonotrode 70T) on ice and centrifuged afterwards (30 min, 4°C, 33.000xg). The cells are resuspended in 200 ml lysis buffer (with DTT) and the cell lysis is repeated. Afterwards the pellet (IB) is washed twice with 200 ml wash buffer, the first time 1% Triton® X 100 (v/v) is added to the wash buffer. Each wash is followed by a centrifugation step. To extract the protein the pellet is resuspended in extraction buffer (50 ml/g pellet). Resuspended IL-5 IB's are incubated for 2 h at room temperature and then overnight at 4°C under mild stirring (all the time). IL-5Rα IB's are incubated at room temperature under mild stirring overnight. On the next day the extraction solution is centrifuged (30 min, 10°C, 69.000xg) to separate insoluble components.

For longer storage of extracted IL-5 protein the buffer is exchanged via ultra-filtration (Amicon 8400 + 8050, Millipore; Hydrosart® 10kDa cut off, Sartorius) to IL-5Rα extraction buffer.

3.5.4 Cell lysis of soluble proteins

Lysis buffer

CPD buffer	s. 3.5.2

The stored cells (-20°C) are thawed in pre-warmed water and resuspended with 150 ml (final volume, max. 15 g of cells) lysis buffer. 40 mg lysozyme (dissolved in 1ml lysis buffer) is added and the mixture is incubated for 15 min at room temperature. Afterwards the cells are lysed via sonication (10 min at 10-80%

30s/30s, sonotrode 70T) and centrifuged (45 min, 4°C, 33.800xg). The supernatant is filtrated using a fluted filter and incubated overnight at 4°C. If cloudiness is observed the next day the protein solution is centrifuged (30min, 4°C, 55900xg) and filtrated using syringe filter (Rotilabo® PES unsterile, 0.22 µm, Roth).

3.5.5 Renaturation

Before renaturation the protein solutions are concentrated via ultra-filtration (Amicon 8400, Millipore; Hydrosart® 10kDa cut off, Sartorius) to achieve a concentration of up to 10-20 mg/ml.

IL-5

Renaturation buffer	100 mM Tris-HCl pH 8.5, 2 M Urea, 1 mM reduced glutathione, 0.1 mM oxidized glutathione
Dialysis buffer	100 mM Tris-HCl pH 8.5

50 mg of the concentrated IL-5 protein solution are diluted drop-wise into one-liter of pre-cooled (4°C) refolding buffer and the solution is incubated for at least 72 h at 4°C under mild stirring. The renaturation solution is then twice dialyzed against the dialysis buffer (1:10). The first time, the renaturation solution is incubated for 24 h in the dialysis buffer at 4°C and the second time for 4 days. After the dialysis the protein solution is centrifuged (30min, 4°C, 33.000xg) and filtrated (Bottle Top filter, Sarstedt) before being stored at 4°C.

IL-5Rα

Renaturation buffer	50 mM Tris-HCl pH 9.5, 7.5 M Urea, 0.1 mM reduced glutathione
Dialysis buffer I	50 mM Tris-HCl pH 9.5, 3 M Urea, 1 mg/l $CuSO_4$
Dialysis buffer II	50 mM Tris-HCl pH 9.5
Dialysis buffer III	50 mM Tris-HCl pH 8.1

100 mg of the concentrated IL-5Rα protein solution are diluted drop-wise into one-liter of renaturation buffer. The renaturation solution is incubated for 2 h at room temperature under mild stirring. Afterwards the solution is dialyzed against the dialysis buffer I (1:10) for 24 h at 4°C. The urea concentration of dialysis buffer I is reduced by 50% every day by replacing the dialysis bath with 50% of fresh dialysis buffer II until a urea concentration of 0.75 M is reached. After that the solution is dialyzed in 10-fold volume of dialysis buffer II for 24 h and 4°C before dialyzing it against dialysis buffer III for at least 24 h at 4°C.

3.6 Protein purification using chromatographic methods

3.6.1 Immobilized metal ion affinity chromatography

Column: HisTrap™ excel 5ml (GE Healthcare)

The polyhistidine-tag (6xHis-tag, N- or C-terminally linked) of proteins binds to the immobilized Ni^{2+}-ions of the column matrix. Unspecific bound proteins can be removed by washing with binding buffer and/or a defined percentage of elution buffer. The protein is eluted and collected with elution buffer. Collected fractions are analyzed via SDS-PAGE (s. 3.3.1) and protein-containing fractions are pooled and dialyzed. All steps should be done at 4°C.

βc

Binding buffer: 20mM Na_2HPO_4 pH 7.4, 500 mM NaCl

Elution buffer: 20mM Na_2HPO_4 pH 7.4, 500 mM NaCl, 500 mM Imidazole

Dialysis buffer: 100 mM Tris-HCl pH 8.5

The column is equilibrated with at least 5 column volumes (CV) binding buffer. The protein is loaded at a flow rate of 2 ml/min. Afterwards the column is washed with binding buffer until the absorption at 280 nm reaches it initial value. To remove further impurities the column is washed with 10 CV 4% elution buffer (2 ml/min, 4 ml fractions). Afterwards the protein is eluted and collected with 100% elution buffer (2 ml/min; 2.5 ml fractions) until the absorption at 280 nm reaches a plateau. Protein-containing fractions are dialyzed against dialysis buffer (1:100) overnight at 4°C.

IL-5Rα C66A (High-Five)

Binding buffer: 20mM Na_2HPO_4 pH 7.4, 500 mM NaCl

Elution buffer: 20mM Na_2HPO_4 pH 7.4, 500 mM NaCl, 500 mM Imidazole

Dialysis buffer: 50 mM Tris-HCl pH 8.1

The column is equilibrated with at least 5 CV binding buffer. The protein is loaded at a flow rate of 2.5 ml/min. Afterwards the column is washed with 10 CV of binding buffer. The protein is eluted with a linear gradient from 0 to 100% elution buffer (10 CV) and 2 ml fractions are collected (2.5 ml/min). Protein-containing fractions are dialyzed against dialysis buffer (1:100) overnight at 4°C.

$AF17121_{CPD}$

Binding buffer: 50 mM Tris-HCl pH 7.5, 500 mM NaCl

Elution buffer: 50 mM Tris-HCl pH 7.5, 500 mM NaCl, 500 mM Imidazole

The column is equilibrated as described above. The protein is loaded at a flow rate of 1.5 ml/min. The column is washed as described above (2.5 ml/min). The protein is eluted and collected with 100% elution buffer (2 ml/min, 5ml fractions). Protein-containing fractions are dialyzed against binding buffer (1:100) overnight at 4°C.

3.6.2 IL-5 affinity chromatography

Preparation:

The IL-5 protein was previously dialyzed overnight at 4°C against 0.1 M $NaHCO_3$ pH 8.3, 0.5 mM NaCl (1:1000). 0.5 g of the CNBr-activated Sepharose 4 fast flow matrix is added into 30 ml of 1mM HCl and mixed gently but thoroughly by inverting for 5 min. After that, the suspension is centrifuged at 1377xg at 4°C for 5 min. The matrix is then washed four times with 50 ml coupling buffer (0.1 M $NaHCO_3$ pH 8.3, 0.5 mM NaCl). The IL-5 protein is immediately immobilized onto activated matrix by adding 1 ml (5 mg/ml) of the IL-5 protein solution. The solution is incubated for 1 h at 4°C with agitation. To remove the unbound protein the solution is centrifuged (86xg, 5 min, 4°C). The matrix is resuspended in 10 ml 0.1M Tris-HCl pH 8.0 and transferred into a glass econo column (Biorad). The matrix is washed with 20 ml 0.1 M Tris-HCl pH 8.0 before being stored at 4°C.

IL-5Rα

Running buffer: 50 mM Tris, pH 8.1

Elution buffer: 4 M $MgCl_2$

The column is equilibrated with 10 CV running buffer at a slow flow rate (wait for the resin to settle). The protein solution is loaded onto the column and then transferred into a falcon tube and incubated for 1 h at 4°C under agitation. Transfer the solution back into the column and collect the flow through. Wash the column with 5 CV running buffer. The protein is eluted five times with 2 ml elution buffer. The elution fractions are immediately placed in the dialysis solution.

3.6.3 Gel filtration chromatography

Proteins migrate through a matrix with differently sized pores and are separated according to their Stokes radius. Collected fractions are analyzed via SDS-PAGE (s. 3.3.1) and protein-containing fractions are pooled.

Column: Superdex 200 26/70 (GE Healthcare)

βc

Running buffer: 10 mM HEPES pH 7.4, 150 mM NaCl, 3.4 mM EDTA

The column is equilibrated with 1.5 CV running buffer at a flow rate of 2.0 ml/min. For sufficient separations maximal 5 ml of the protein solution is loaded onto the column (2.5 ml/min). Fractions are collected as followed:
0-130 ml 4 ml fractions; 130-170 ml 2.5 ml fractions; 170-270 ml 4ml fractions

IL-5

Running buffer: 100 mM Tris-HCl pH 8.0

See above. The protein solution is loaded onto the column at a flow rate of 2.5 ml/min and 2.5 ml fractions are collected.

$AF17121_{CPD}$ and IL-5Rα•AF17121 complex

Running buffer: 10 mM HEPES pH 7.4, 150 mM NaCl, 3.4 mM EDTA

Column: Superdex peptide 10/300 (GE Healthcare)

The column is equilibrated with 1.5 CV running buffer at a flow rate of 0.5 ml/min. For sufficient separations maximal 500 µl of the protein solution is loaded onto the column (0.5 ml/min). Fractions are collected as followed:

$AF17121_{CDP}$: 0-9 ml 3 ml fractions, 9-22 ml 1 ml fractions

IL-5Rα•AF17121: 0-10 ml 1 ml fractions, 10-25 ml 0.5 ml fractions

3.6.4 Anion-exchange chromatography

Binding buffer: 50 mM Tris-HCl pH 8.1

Elution buffer: 50 mM Tris-HCl pH 8.1, 500 mM NaCl

Column: HiTrap™ Q-HP 5ml (GE Healthcare)

The column is equilibrated with 5 column volumes (CV) binding buffer at a flow rate of 5.0 ml/min. The protein solution is loaded onto the column (IL-5Rα *E. coli* 1.5 ml/min; High-Five 2.5 ml/min) and afterwards washed with binding buffer (2.5 ml/min) until the absorption at 280 nm reaches it initial value (5-10 CV). A linear gradient (10 CV, *E. coli* 1.5 ml/min; High-Five 2.5 ml/min) leading to a

final concentration of 100% elution buffer elutes the bound protein. Collected fractions are analyzed via SDS-PAGE (s. 3.3.1) and protein-containing fractions are pooled and if needed dialyzed. All steps were done at 4°C.

3.6.5 Reversed-phase high-performance liquid chromatography

Binding buffer: 0.1% (v/v) TFA in ddH_2O

Elution buffer: 0.1% (v/v) TFA in 100% Acetonitrile

Reversed-phase high-performance liquid chromatography was used for desalting protein samples prior to mass spectrometric analysis.

IL-5Rα and IL-5Rα•AF17121 complex

Column: Phenomenex Jupiter C4, 250x4.6 mm, 5 µm, 300 Å

$AF17121_{CPD}$

Column: Phenomenex Jupiter Proteo, 250 x 4.6 mm, 4 µm, 90 Å

The column is equilibrated with 1.5 CV binding buffer at a flow rate of 1 ml/min. The protein solution is adjusted to a final concentration of 0.1% TFA (v/v) using a 10% (v/v) TFA stock solution and centrifuged (10min, 16.800xg, 4°C) before loaded onto the column. A linear gradient leading to a final concentration of 100% elution buffer elutes the bound protein. Collected fractions are analyzed via SDS-PAGE (s. 3.3.1) and protein-containing fractions are lyophilized.

3.7 Auto-processing of the AF17121-CPD fusion protein

500 µl of the concentrated AF17121-CPD protein solution via ultrafiltration with an extinction of 80-90 are transferred into a 1.5 ml eppendorf cap. 5 µl of the 100 mM InsP6 stock-solution (dissolved in 50 mM Tris pH 7.5, 500 mM NaCl, Santa Cruz) are added and the reaction mixture is incubated for 1 h at 37°C in a water bath. Afterwards the solution is cooled on ice for 5 min before being centrifuged (10 min, 16.800xg, 4°C). The supernatant is transferred into a new 1.5ml eppendorf cap and purified via gel filtration chromatography.

3.8 Thermofluor

Solutions of 22 µl buffer, 1 µl SYPRO Orange (SO, 1:40 diluted in H_2O) and 2 µl of 7.3 mg/ml IL-5Rα protein were added to the wells (first 5 columns) of a 96 well plate. The first five rows of the 6^{th} column contained mixed solutions using the reference buffer (same buffer as the protein, 1x PBS) and the last three rows 24 µl of water mixed with 1µl SO. The plates were sealed with a plastic tape and heated in the Mx3005P Real Time PCR System (Agilent) from 25 to 95°C in increments of 1°C per min. Fluorescence changes in the wells of the plate were detected via a Photomultiplier tube. 40 different buffers each at a concentration of 100 mM and with a pH range from 4.5 to 9.8 have been used (s. Appendix Table 36, page 177).

3.9 TF-1 cell proliferation assay

Culture medium:	RPMI 1640 + GlutaMAX™-I (Gibco) + 10% FCS (Charge 0027S, Biochrome) + 1 % Pen/Strep (Lonza) + 5 ng/ml hIL-5 protein
Assay medium:	RPMI 1640 (Gibco) + 10% FCS (Biochrome) + 1 % Pen/Strep (Lonza)
96-well plates:	Greiner® Microplates Cellstar Cat.-No.: 655180
Resazurin solution:	0.15 mg/ml Resazurin sodium salt (VWR) dissolved in 1x PBS (137 mM NaCl, 2.7 mM KCL, 10 mM Na_2HPO_4, 2 mM KH_2HPO_4, pH 7.4)

TF-1 culture cells are seeded every 3-4 days at a density of $1x10^5$ cells/ml in culture medium (37°C, 5% CO_2, 85% relative humidity). TF-1 cells are mixed 1:1 with fresh culture medium one day before the TF-1 assay is set up. The cells are washed two times with assay medium (300xg, 5 min, 21°C) and afterwards adjusted to $3x10^5$ cells/ml (7ml per 96-well plate) with fresh assay medium and incubated 4 h at 37°C. In the meantime the protein or peptide dilutions are prepared (final volume per well 100 µl) and incubated for 1 ½ h at 37°C. 100 µl of the cell suspension are added to each well and the 96-well plates are incubated for at least 72h. 10 µl of the resazurin solution are added per well and incubated for 4 h at 37°C. Absorption of each well is measured using an ELISA plate reader (Multiskan Ascent, Thermo) at 571 and 749 nm. Half maximal effective concentration (EC_{50}) or half maximal inhibitory concentration (IC_{50}) is plotted using the statistic program “Prism” (Graphpad).
Table 16 summarizes the pipetting scheme of the competition assay. Measurements of the IC50 values for each peptide variant were done as triplicates.

Table 16: Pipetting scheme of the TF-1 cell proliferation assay.

<table>
<tr><th></th><th>1</th><th>2</th><th>3</th><th>4</th><th>5</th><th>6</th><th>7</th><th>8</th><th>9</th><th>10</th><th>11</th><th>12</th></tr>
<tr><td>A</td><td colspan="11">PBS</td></tr>
<tr><td>B</td><td rowspan="7">PBS</td><td colspan="9">hIL-5 200 pM constant + 10 µM AF17121 peptide variant log 3 dilution</td><td rowspan="7">PBS</td></tr>
<tr><td>C</td><td colspan="9">hIL-5 200 pM constant + 10 µM AF17121 peptide variant log 3 dilution</td></tr>
<tr><td>D</td><td colspan="9">hIL-5 200 pM constant + 10 µM AF17121 peptide variant log 3 dilution</td></tr>
<tr><td>E</td><td colspan="9">hIL-5 5 nM log 3 dilution</td></tr>
<tr><td>F</td><td colspan="9">hIL-5 5 nM log 3 dilution</td></tr>
<tr><td>G</td><td colspan="5">Medium</td><td colspan="4">hIL-5 200 pM constant</td></tr>
<tr><td>H</td><td colspan="11">PBS</td></tr>
</table>

3.10 Surface plasmon resonance

Measuring buffer: 10 mM HEPES pH 7.4, 150 mM NaCl, 3.4 mM EDTA, 0.005% Tween20

Device: ProteOn™ XPR36 (BioRad)

The surface plasmon resonance spectroscopy (SPR) is used for the quantitative analysis of protein-protein interactions *in vitro*. It allows to monitor the interaction of proteins in real time and to determine their binding kinetics.

The matrix of the ProteOn™ GLC biosensor chip (Bio-Rad) is activated by perfusing an EDC/sulfo-NHS solution (100 mM 1-ethyl-3-(3-dimethylaminopropyl) carbodiimid / 25 mM N-hydroxysulfosuccinimide) for 180 s with a flow rate of 30 µl/min. Subsequently the activated biosensor surface is coated with the ligand or neutravidin (diluted in 10 mM Na-acetate buffer pH 4.0) until the corresponding loading density is reached (30 µl/min). Free activated carboxyl groups of the biosensor surface are then quenched by perfusion (300 s, 30 µl/min) of 1 M ethanolamine HCl. The biotinylated ligand diluted in measuring buffer is perfused at a flow rate of 30 µl/min until the desired loading density is reached. At least six different dilutions of the analyte are prepared in measuring buffer to analyze the binding properties (100 µl/min). Evaluation of the binding kinetics was accomplished using a simple Langmuir 1:1 interaction model. Adjustments to the parameter settings are stated in the corresponding result part (s. Table 17). The regeneration of the ligand for the next measurement cycle is achieved by washing with 10 mM glycine pH 2.5 (30 s, 100 µl/min) followed by an equilibration step with measuring buffer (200s contact time, 300s dissociation, 100 µl/min).

Table 17: Summary of the default parameter settings for SPR data analysis.

Parameter	Unit	Scope	Type
Concentration	M	Local	Constant
k_a	1/Ms	Grouped	Fitted
k_d	1/s	Grouped	Fitted
K_D	M	Grouped	Calculated
Rmax	RU	Grouped	Fitted
Chi^2	RU	Local	Calculated
T_0 dissociation	s	Local	Constant
RI	RU	Local	Constant
Begin association	s	Grouped	Constant
End association	s	Grouped	Constant
Begin dissociation	s	Grouped	Constant
End dissociation	s	Grouped	Constant

3.11 Microscale thermophoresis

Measuring buffer: 10 mM HEPES pH 7.4, 150 mM NaCl, 3.4 mM EDTA, 0.05% Tween20

Device: Monolith NT.115 (NanoTemper)

Microscale thermophoresis (MST) can be used to quantify biomolecular interactions. It measures the motion of molecules along microscopic temperature gradients and detects changes in their hydration shell, charge or size.

For all measurements standard capillaries (MO-AK002, NanoTemper) were used. Proteins and peptides were labeled either randomly (s. 3.3.7) or side specific (s. 3.3.8) with the fluorescent dye Alexa-647. For protein or peptide measurement log 2 dilutions and the fluorescent-coupled protein stock solution (at least 200µl) are prepared in measuring buffer. 10 µl of the fluorescent-coupled protein are added to each of the 16 prepared dilutions (10 µl) and incubated at room temperature for 5 min. Afterwards the capillaries are loaded and immediately analyzed.

The protein and peptide solutions are first diluted 1:1 with $HBST20X_{150}$ (10 mM HEPES pH 7.4, 150 mM NaCl, 3.4 mM EDTA, 0.1% Tween20) and then further using $HBST10X_{150}$ (10 mM HEPES pH 7.4, 150 mM NaCl, 3.4 mM EDTA, 0.05% Tween20) to reach the desired concentration.

AF17121 & variants

The interaction of AF17121 and the different AF1721 variants is first analyzed at 25°C with the thermophoresis temperature gradient set to 60% and the fluorescence excitation with 60% of the LED energy. The temperature is then set to 37°C and after 5 min the MST analysis is performed with 60% of thermophoresis temperature gradient and 70% of the LED energy. Afterwards the temperature is set again to 25°C and new capillaries are loaded from the same serial dilution and the MST analysis is repeated.

3.12 Crystallization

3.12.1 AF17121/hIL-5Rα complex crystallization

Buffer: 10 mM HEPES pH 7.4, 150 mM NaCl, 3.4 mM EDTA

Column: Superdex 200 10/300 (GE Healthcare)

Purified hIL-5Rα protein and commercially obtained (chemical synthesis, Centic Biotec) AF17121 peptide were used for complex formation. The complex is formed using a molar ratio of 1:1.2 of the receptor to peptide. The complex solution is incubated on ice for 30 min and afterwards concentrated via ultrafiltration (Vivaspin Turbo, MWCO 3 kDa, Sartorius). The concentrated complex solution is incubated overnight at 4°C. The complex is purified by gel filtration chromatography (s. 3.6.3). 500 µl of the complex solution are loaded onto the column (0.5 ml/min). Protein fractions are analyzed via SDS-PAGE and protein containing fractions are pooled. The purified complex is concentrated up to 7 mg/ml by ultrafiltration (s. above). Initial crystallization screens were/are set up by the sitting drop vapor diffusion method at room temperature using the Honeybee 963 crystallization robot (Rudolf Virchow Center, University of Würzburg, ISOGEN). Each drop was prepared by mixing 0.3 µl of purified complex (5 mg/ml) and 0.3 µl of reservoir solution. 40 µl of the reservoir solution was filled in each well of the 96-well plate (Crystalquick™ LP Plate, Greiner Bio-One). The plates are sealed using a plastic film.

3.12.2 X-ray data analysis

Datasets from single crystals were collected at the beam line of the home source (Rudolf Virchow Center, University of Würzburg, Rigaku). Crystals were mounted using nylon loops and flash-frozen in liquid nitrogen without further soaking. Data collection was performed at 100 K. High-resolution datasets were collected at the MX1 beam line at the DESY Petra III (Hamburg, Germany) from single crystals. Data processing was performed using the software iMosfilm, the CPP4 suite, Phenix and Quanta.

4 RESULTS

4.1 Recombinant expression of Interleukin-5 and its receptor ectodomains

For structural and functional analyses large amounts of highly purified proteins are needed. As determining structures of the free Interleukin-5 receptor α chain (IL-5Rα), in the complex of IL-5Rα with inhibitory peptides and the complex of IL-5Rα with Interleukin-5 (IL-5) and the common beta chain (βc) was attempted in this project, the purification protocols for IL-5 and for the IL-5Rα and βc ectodomain proteins were optimized.

4.1.1 Purification of the human Interleukin-5 protein

As a first step towards improving the yield for human Interleukin-5 (IL-5), expression in four different *E. coli* expression strains was tested. As IL-5 is expressed insoluble as inclusion bodies in *E. coli* requiring refolding to obtain biologically active protein, increasing the yield and purity of protein starting material seemed a potential measure to increase the overall yield.

4.1.1.1 Bacterial expression of hIL-5

The cDNA encoding human IL-5 (Uniprot: P05113, 21-134) had been cloned into the pET3d expression vector (Patino, E. *et al*., 2011; s. 9.2.1). Four different expression strain cells, i.e. Rosetta (DE3), BL21 Gen-X (DE3), BL21 Star (DE3) and JM109 (DE3) were transformed with the expression vector pET3d hIL-5 (s. 3.2.7). A test expression was performed in baffled Erlenmeyer flasks using 400 ml LB-medium supplemented with the respective antibiotic(s) (s. 3.5 + 3.5.1). The cells were incubated at 37°C until an optical density (OD_{600nm}) of 0.6 was obtained. Overexpression of the protein was initiated by addition of 1mM IPTG. Protein expression proceeded for 3 h at 37°C. The cells were disrupted by sonication and the inclusion bodies were purified by mechanical washing (s. 3.5.3). The inclusion bodies were then re-suspended in 40 ml TE buffer per gram pellet (cells wet weight). SDS-PAGE analysis (s. 3.3.1) revealed that the Rosetta strain previously used showed the highest expression rate of all strains tested (s. Figure 17).

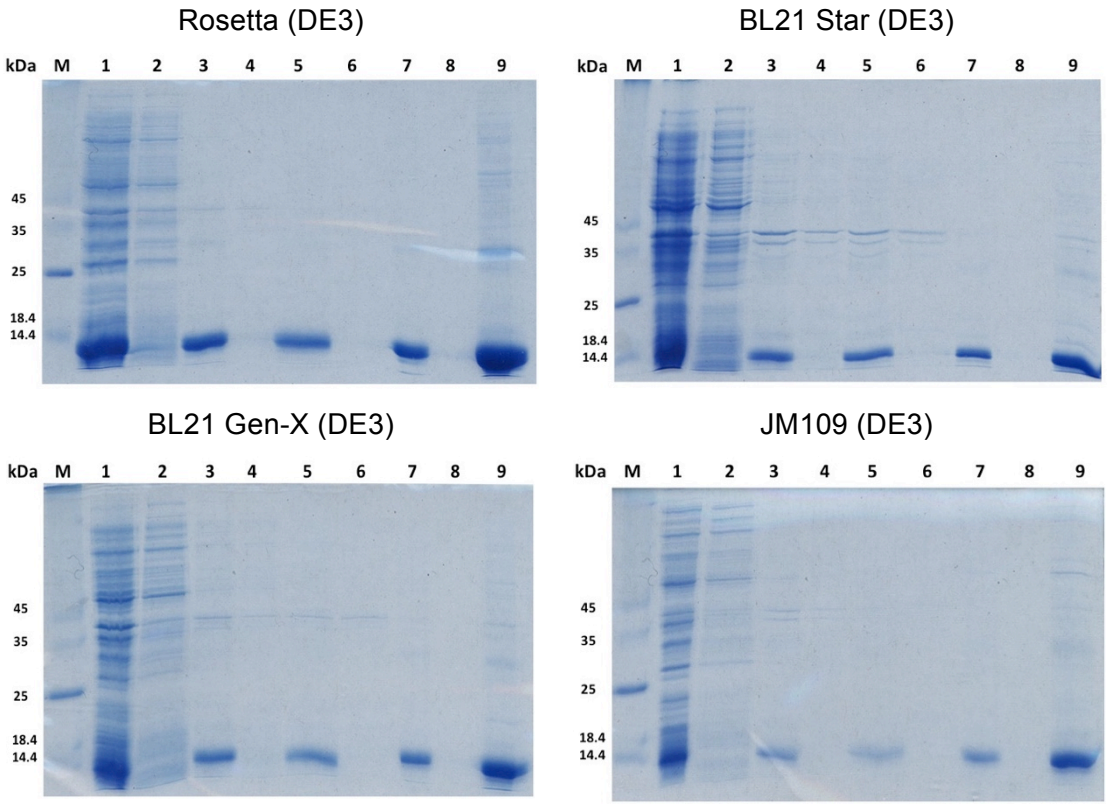

Figure 17: SDS-PAGE analysis of the 4 different *E. coli* strains tested for the expression of the IL-5 protein. M: protein standard **1:** after induced protein expression for 3 h. **2:** supernatant after 1st cell lysis step **3:** re-suspended inclusion bodies (IB's) after 1st cell lysis step **4:** supernatant after 2nd cell lysis step **5:** re-suspended IB's after 2nd cell lysis step **6:** supernatant after 1st washing step **7:** re-suspended IB's after 1st washing step **8:** supernatant after 2nd washing step **9:** re-suspended IB's after 2nd washing step

To reveal the molecular cause for this expression strain requirement a bioinformatic analysis was performed that showed that the cDNA of IL-5 contains several tripled codons rarely found in *E. coli*, which are however frequent in human genes (s. Figure 18). The Rosetta strain contains an additional plasmid that encodes for these underrepresented human tRNAs in *E. coli.*

Hence subsequent preparative scale protein expression of IL-5 was done using *E. coli* cells of the Rosetta (DE3) strain. Two-liter baffled Erlenmeyer flask containing 800 ml LB-Medium, supplemented with 100 µg/ml ampicillin and 34 µg/ml chloramphenicol, were inoculated with 20 ml of an overnight culture. Protein expression and cell lysis were performed as described. After protein expression about 2 g bacteria (wet weight) per liter bacterial culture could be obtained and around 0.6 g/l of inclusion bodies after cell lysis and purification of the inclusion bodies.

ATG GCA CCT ACT GAA ATT CCC ACT AGT GCA TTG GTG AAA GAG ACC TTG GCA CTG CTT TCT ACT CAT CGA
ACT CTG CTG AUA GCC AAT GAG ACT CTC CGG ATT CCT GTT CCT GTA CAT AAA AAT CAC CAA CTG TGC ACT GAA
GAA ATC TTT CAG GGA AUA GGC ACA CTC GAG AGT CAA ACT GTG CAA GGG GGT ACT GTG GAA AGA CUA TTC
AAA AAC TTG TCC TTA AUA AAG AAA TAC ATC GAT GGC CAA AAA AAA AAG TGT GGA GAA GAA CGT CGC CGT
GTA AAC CAA TTC CUA GAC TAT CTG CAG GAG TTT CTT GGT GTA ATG AAC ACC GAG TGG ATT ATT GAA AGT TGA

Amino Acid	Rare Codon	Frequency of Occurrence
Arginine	CGA	1
	CGG	1
	AGG	0
	AGA	1
Glycine	GGA	2
	GGG	1
Isoleucine	AUA	3
Leucine	CUA	2
Proline	CCC	1
Threonine	ACG	0

Repeated and/or Consecutive Rare Codons

GGA AUA = 1

AGA CUA = 1

Figure 18: Analysis of the presence of rare codons in the cDNA of human IL-5. http://svkdipmpps-rarecodon-analysis.blogspot.de/ (last visited: 15.07.2017)

4.1.1.2 Refolding of the hIL-5

Next different concentrations of urea and guanidine hydrochloride (GuHCl) to extract the IL-5 protein from the inclusion bodies were tested. This should allow to identify conditions yielding highly pure denatured, monomeric IL-5 protein, which should reduce the number of purification steps before and after refolding. Similar amounts of IL-5 inclusion bodies were resuspended in extraction buffer (50 mM NaOAc pH 5.0 supplemented with 2-6 M GuHCl or 2-8 M urea; concentrations were varied in 1 M steps). The extracts were incubated for 1 h (panned) at room temperature, and extract solution was cleaved from insoluble residues by centrifugation. The supernatants of the extracts were then analyzed by SDS-PAGE (s. Figure 19, top). Increasing concentrations of urea only extracted IL-5 protein from inclusion body aggregates, whereas GuHCl solubilized *E. coli* endogenous proteins. UV absorption spectrum analysis revealed that the 6 M GuHCl extract also contained much higher amounts of nucleic acids compared to the 8 M urea extract (s. Figure 19, bottom). Nucleic acid and host protein contaminations can induce aggregation during the refolding process and should therefore be avoided. Thus, as improvement we used 8 M of urea instead of 6 M GuHCl for extraction. This allowed us to omit the gel filtration under denaturing conditions. The extraction solution was first stirred for 2 h at room temperature and then incubated overnight at 4°C to allow maximal extraction of IL-5 from the insoluble inclusion body fraction (s. 3.5.3.).

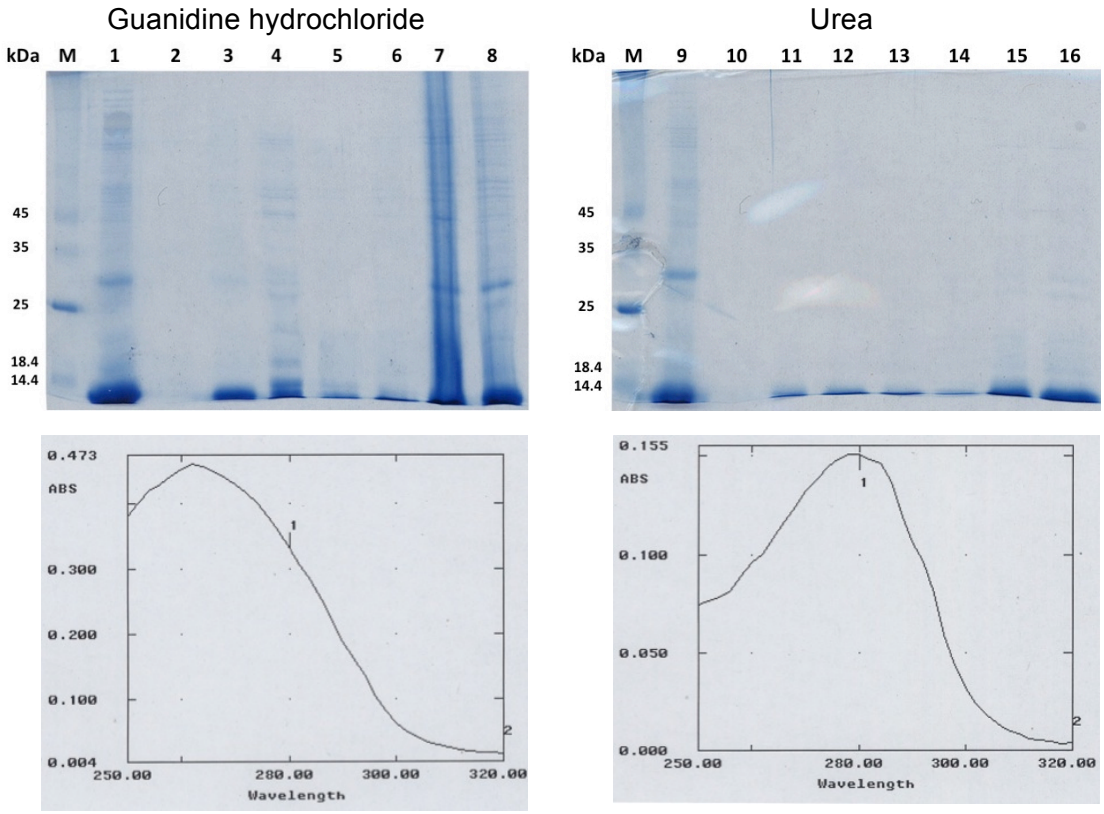

Figure 19: SDS-PAGE analysis and UV absorption spectrum of the extraction test of the IL-5 protein. Top: SDS-PAGE analysis of the IL-5 protein extraction using guanidine hydrochloride (GuHCl; left) and urea (right). **M:** protein standard **1:** re-suspended IL-5 inclusion bodies (IB's) after last washing step **2:** empty lane **3:** re-suspended IB's after extraction with 2 M GuHCl **4-8**: Extraction with 2, 3, 4, 5 or 6 M GuHCl **9:** re-suspended IB's after extraction with 2 M urea **10-16**: Extraction with 2, 3, 4, 5, 6, 7 or 8 M urea **Bottom:** UV absorption spectrum after extraction of the IL-5 IB's with 6 M GuHCl (left) and 8 M urea (right).

The refolding protocol established by Patino, E. *et al*. (2011) was then used without changes (s. 3.5.5). Before setting up refolding the extract/protein solution was centrifuged. The buffer of the extraction solution was then exchanged to 50 mM sodium acetate pH 5.0 supplemented with 6 M GuHCl for storage via ultrafiltration and the protein was concentrated to 10-15 mg/ml. About 60-70 mg of denatured and monomeric IL-5 protein per liter bacterial culture could be obtained. 50 mg of the concentrated protein solution were added drop wise (rapid dilution) into one-liter of pre-cooled refolding buffer comprising 100 mM Tris-HCl pH 8.5, 2 M urea, 1 mM reduced glutathione, 0.1 mM oxidized glutathione. The mixture was incubated for at least 72 h at 4°C under mild stirring. The refolding solution was then dialyzed in a ratio of 1:10 against 100 mM Tris buffer (pH 8.5) for 24 h at 4°C and a second time for 4 days at 4°C to substantially lower the urea concentration and allow refolding and dimerization of the IL-5 protein. To remove precipitated protein the refolding solution was centrifuged or/and filtrated using a 0.22 µm filter and stored at 4°C.

About 15-20 mg of dimerized IL-5 protein per liter bacterial culture could be obtained after refolding.

4.1.1.3 Purification of the hIL-5 protein

The gel filtration used in the past, to remove last impurities, requires a time consuming concentration step for the large refolding solution volume and multiple gel filtration runs are needed for preparing large amounts of IL-5 protein. Hence a different chromatography method was tested for an optimized IL-5 production scheme. To reduce the time needed and potential loss of protein during the ultrafiltration different ion exchange chromatography purification schemes were tested as alternative. Strong and weak ion exchange chromatography columns (HiTrap Q FF, DEAE FF, SP XL and CM FF; GE Healthcare) were used and buffers with two different pH values were analyzed for each column. Since the calculated isoelectric point (pI) of IL-5 is 6.8, the IL-5 protein was diluted with buffer having a pH of either 5.0 or 6.0 for subsequent cation exchange chromatography. For the anion exchange chromatography buffers with a pH of either 7.5 or 8.5 were used. The elution profiles and subsequent SDS-PAGE analyses revealed that the IL-5 protein unfortunately did not bind to the ion exchange resins under the conditions tested (s. Figure 20).

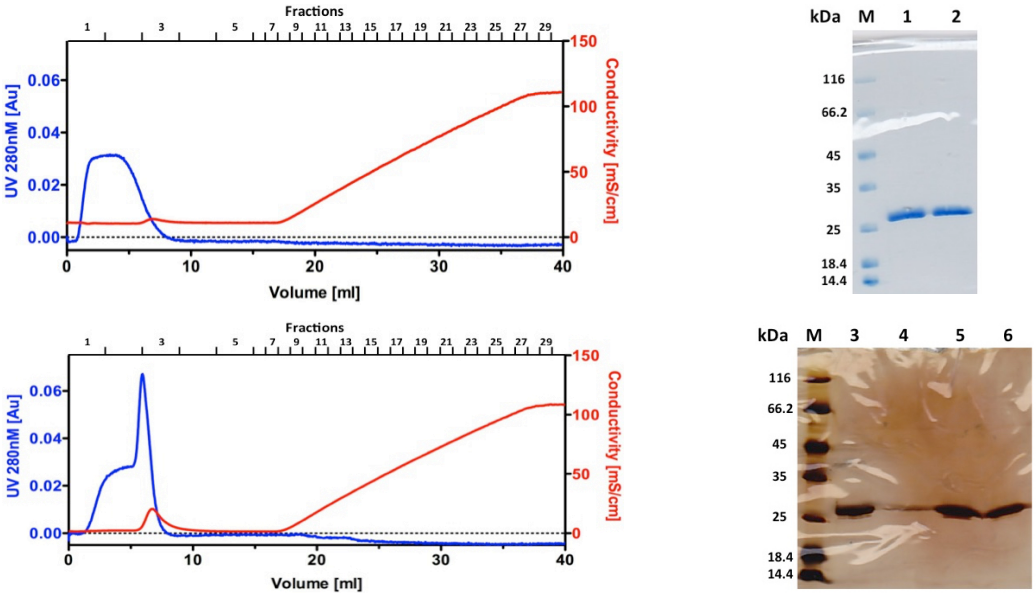

Figure 20: Top: Chromatogram and SDS-PAGE analysis of the cation exchange chromatography (CM FF pH 6.0). **M:** protein standard **1:** IL-5 protein solution before purification **2:** elution fraction 1 **Bottom:** Chromatogram and SDS-PAGE analysis of the anion exchange chromatography (DEAE FF pH 8.5). **M:** protein standard **3:** IL-5 protein solution before purification **4-6:** elution fractions 1-3 **Blue:** UV absorption at 280nm [Au] **Red:** Conductivity [mS/cm]

Thus, the previously employed gel filtration had to be used employing a Superdex 200 column as the first and only purification step for IL-5 (s. 3.6.3). The IL-5 refolding solution was concentrated via ultrafiltration in stirred cells as far as possible and 5 ml quantities were loaded onto the column equilibrated with 100 mM Tris-HCl pH 8.5. Fractions were collected and analyzed via SDS-PAGE (s. Figure 21). Fractions containing highly pure dimeric IL-5 protein were pooled. The gel filtration sufficiently separates dimeric IL-5 protein with a size of around 26kDa from remaining impurities of significantly lower molecular weight.

After optimization of the procedure a yield for dimeric IL-5 of about 9-10 mg/l bacterial culture could be obtained, which presents a 50% improvement compared to the previously used protocol (6 mg/l).

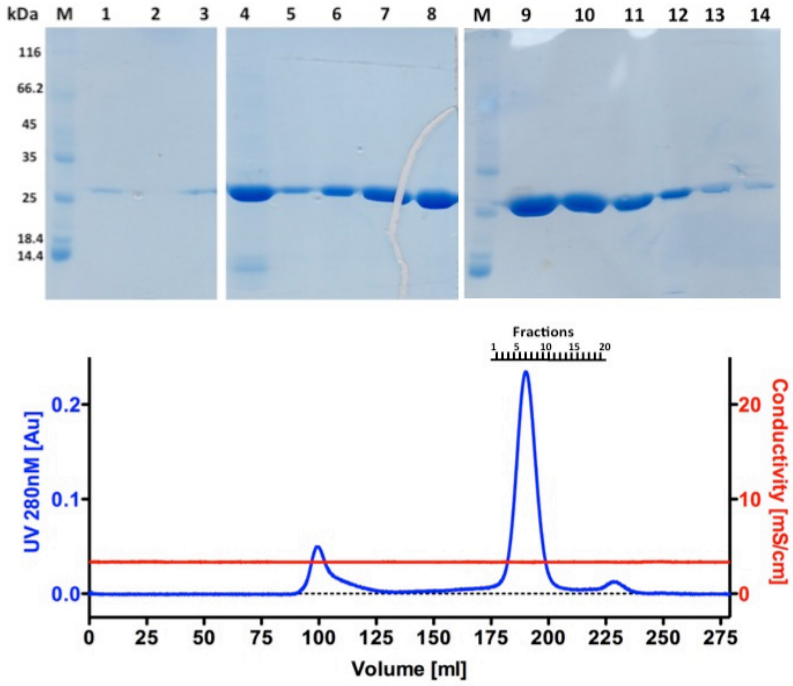

Figure 21: SDS-PAGE analysis and chromatogram of the gel filtration chromatography of the IL-5 protein. Top: SDS-PAGE analysis of the ultra-filtration and gel filtration of the IL-5 protein. **M:** protein standard **1:** IL-5 after refolding / before ultra-filtration **2:** flow through of 1st ultra-filtration **3:** flow through of 2nd ultra-filtration **4:** IL-5 after ultra-filtration / before purification **5-14:** elution fractions 4-13 of the IL-5 gel filtration. **Bottom:** Chromatogram of the gel filtration of the IL-5 protein **Blue:** UV absorption at 280nm [Au] **Red:** Conductivity [mS/cm]

4.1.2 Purification of the Interleukin-5 receptor ectodomain

A similar optimization strategy was performed for the production of the human Interleukin-5 receptor α chain ectodomain (IL-5Rα) as for the IL-5 protein. Again four *E. coli* expression strains were tested for improved expression of the IL-5Rα protein. IL-5Rα is likewise expressed insoluble in inclusion bodies in *E. coli* and therefore also requires *in vitro* refolding to obtain biologically active protein. Therefore, aiming to increase the yield and purity of protein starting material seemed a potential measure to increase the overall yield.

4.1.2.1 Bacterial expression of the ectodomain of hIL-5Rα C66A

The cDNA encoding human IL-5Rα (Uniprot: Q01344-2, 21-335) was cloned in the expression vector pET3d (s. 9.2.2). The variant hIL-5Rα C66A was used as the replacement of the cysteine residue with alanine led to increased protein stability without affecting IL-5 binding (Devos, R. *et al.*, 1994). The four different *E. coli* expression strain cells, i.e. Rosetta (DE3), BL21 Gen-X (DE3), BL21 Star (DE3) and JM109 (DE3) were transformed with the expression vector pET3d hIL-5Rα C66A (s. 3.2.7). Test expression was performed in baffled Erlenmeyer flasks using 400 ml LB-medium supplemented with the respective antibiotic(s) (s. 3.5 + 3.5.1). The cells were incubated at 37°C until an optical density (OD_{600nm}) of 0.6 was reached and protein expression was induced by adding 1 mM IPTG. As the JM109 cells did only grow to an OD_{600nm} of 0.24 within 280 min, these cells were discarded from further analysis. The cells were incubated for 3h at 37°C. After harvesting, cells were lysed and the inclusion bodies were purified by washing (s. 3.5.3). The inclusion bodies were then resuspended in TBS buffer (40ml/g cells wet weight). SDS-PAGE analysis (s. 3.3.1) of the expression and cell lysis revealed that the *E. coli* strain BL21 Star (DE3) ensured the highest expression rate of cell strains tested. To our surprise the *E. coli* strain Rosetta (DE3) used so far showed almost no expression of the IL-5Rα protein in our experiments (s. Figure 22). The *E. coli* strain BL21 Star (DE3) is a BL21 derivate, which exhibits enhanced mRNA stability due to a mutation in the RNaseE gene (ren131).

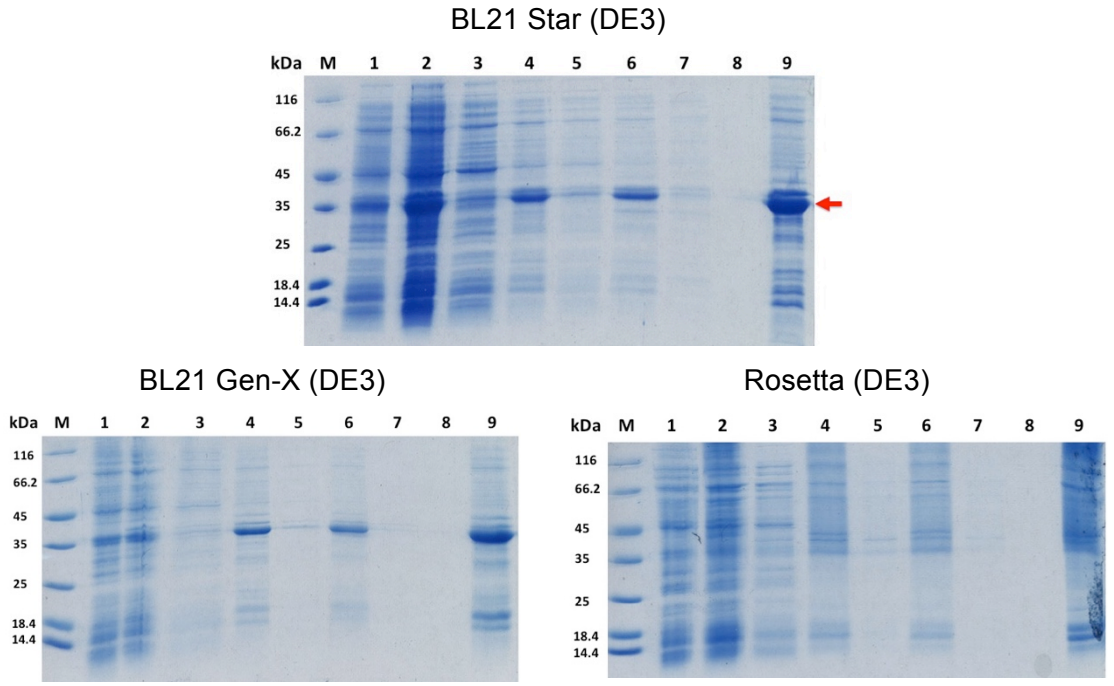

Figure 22: SDS-PAGE analysis of the different *E. coli* strains tested for expression of the ectodomain of IL-5Rα. M: protein standard **1:** before protein expression **2:** after induced protein expression for 3 h. **3:** supernatant after 1st cell lysis step **4:** re-suspended inclusion bodies (IB's) after 1st cell lysis step **5:** supernatant after 2nd cell lysis step **6:** re-suspended IB's after 2nd cell lysis step **7:** supernatant after 1st washing step **8:** supernatant after 2nd washing step **9:** re-suspended IB's after 2nd washing step. The red arrow marks the protein band of the IL-5Rα C66A ectodomain protein.

Hence preparative scale protein expression of IL-5Rα was done using the *E. coli* strain BL21 Star (DE3). Two-liter baffled Erlenmeyer flasks containing 800 ml LB-Medium were inoculated with 20 ml overnight culture supplemented with 100 µg/ml ampicillin. Protein expression (s. 3.5 + 3.5.1) and cell lysis (s. 3.5.3) were done as described above. About 3-4 g bacteria (wet weight) per liter bacterial culture could be obtained resulting in about 1 g of inclusion bodies per liter bacterial culture after cell lysis.

4.1.2.2 Refolding of the hIL-5Rα C66A ectodomain protein

A similar optimization approach for extraction of IL-5Rα protein from inclusion bodies as for IL-5 was performed. Different concentrations of guanidine hydrochloride (GuHCl) and urea were used to specifically extract the IL-5Rα protein from the insoluble inclusion bodies. The goal was to identify conditions that would yield highly pure IL-5Rα protein, free from contaminants that would therefore reduce the number of purification steps.

Similar quantities of IL-5Rα-containing inclusion bodies were resuspended in extraction buffer (50 mM NaOAc pH 5.0 supplemented with either 2-6 M GuHCl or 2-8 M urea; concentration were varied in 1 M steps). The extraction solutions

were incubated for 2 h at room temperature. Afterwards the protein solutions were centrifuged and the supernatant of the different extracts were analyzed by SDS-PAGE (s. Figure 23). Using 4, 5 or 6 M GuHCl, most of the IL-5Rα protein could be solubilized from the inclusion bodies, while using urea for solubilizing IL-5Rα, only at a concentration of 7 or 8 M of urea yielded a minor portion of the IL-5Rα protein in the extract leaving most of the IL-5Rα protein remaining in the inclusion bodies. Thus, protein extraction was done using 50 mM sodium acetate pH 5.0 supplemented with 6 M GuHCl. The suspension was then incubated at room temperature overnight to allow complete extraction of hIL5-Rα from the insoluble inclusion bodies (s. 3.5.3.).

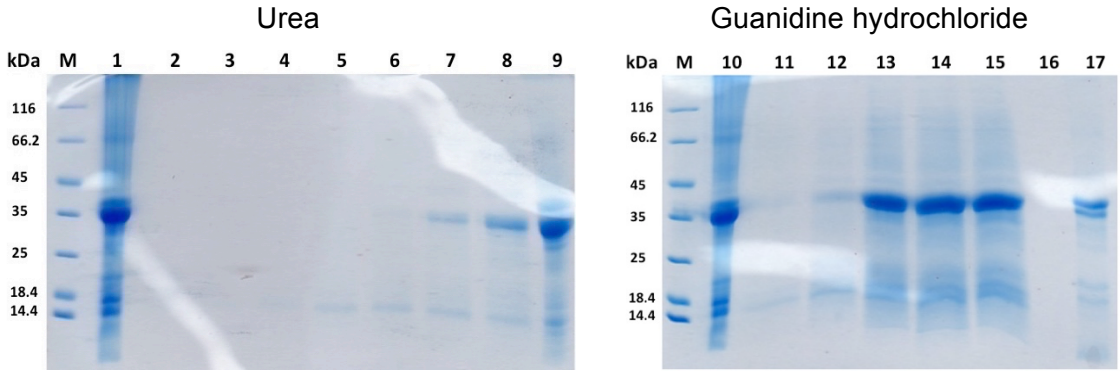

Figure 23: SDS-PAGE analysis of the extract conditions tested for the ectodomain of hIL-5Rα. Left: Extraction using urea. **Right:** Extraction using guanidine hydrochloride. **M:** protein standard **1:** re-suspended IL-5Rα inclusion bodies (IB's) after last washing step **3-8**: Extraction with 2, 3, 4, 5, 6, 7 or 8 M urea **9:** re-suspended IB's after extraction with 8 M urea **10:** re-suspended IL-5Rα inclusion bodies (IB's) after last washing step **11-15**: Extraction with 2, 3, 4, 5, or 6 M GuHCl **16:** empty lane **17:** re-suspended IB's after extraction with 6 M GuHCl

Since the UV absorption spectrum (s. Figure 24) of the IL-5Rα protein solution showed only minor amounts of nucleic acid contaminations the gel filtration under denatured conditions previously used was omitted, as this task was mainly required to remove nucleic acids.

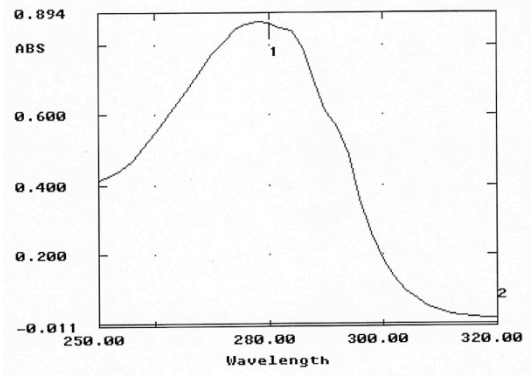

Figure 24: UV absorption spectrum after extraction of the ectodomain of hIL-5Rα IB's using 50 mM sodium acetate buffer (pH 5.0) supplemented with 6 M GuHCl.

The established refolding protocol was used without additional changes (s 3.5.5). Before refolding, the protein solution was cleared by centrifugation (30 min, 4°C, 33.000xg) and concentrated via ultrafiltration (membrane cut-off 10 kDa) until a concentration of 10-15 mg/ml was obtained. About 80-100 mg of denatured IL-5Rα protein per liter bacterial culture used could be obtained. 100 mg of the concentrated protein solution were drop-wise added (rapid dilution) into one-liter pre-cooled refolding buffer comprising 50 mM Tris-HCl pH 9.5, 7.5 M urea and 0.1 mM reduced glutathione. The mixture was incubated for 2 h at room temperature. Then the refolding solution was dialyzed for 24 h at 4°C against 10 volumes of 3 M urea, 50 mM Tris-HCl pH 9.5, supplemented with 1 mg/l $CuSO_4$. Thereafter, urea concentration was decreased every 24 h by exchanging half of the dialysis buffer with 50 mM Tris-HCl pH 9.5 until a urea concentration of 0.75 M was obtained. Refolding was ended by final dialysis against 50 mM Tris-HCl pH 8.1. Precipitated protein was removed by centrifugation (30 min, 4°C, 33.000xg) or/and filtration through a 0.22 µm filter and stored at 4°C. About 50-60 mg of IL-5Rα protein per liter bacterial culture could be obtained after refolding.

4.1.2.3 Anion exchange chromatography of the hIL-5Rα C66A

Before anion exchange chromatography the protein solution of the refolding was concentrated via ultrafiltration using a stirred cell and employing a membrane with cut-off of 10 kDa to a final volume of 40-50 ml. The concentrated refolding solution was applied onto a HiTrap Q-sepharose HP 5 ml column (GE Healthcare) at a flow rate of 1.5 ml/min. The column was equilibrated and washed with 5-10 column volumes (CV), thereafter the protein was eluted employing a linear salt gradient (10 CV, 1.5 ml/min). The elution profile of the anion exchange chromatography showed two separated UV absorbance maxima (s. Figure 25). The SDS-PAGE analysis of these two absorbance maxima revealed that the first maximum only contained pure IL-5Rα protein while the second maximum contained IL-5Rα protein along with other bacterial proteins and impurities (s. Figure 25). The used anion exchange column seems to be capable of separating active and highly pure IL-5Rα protein from inactive and further contaminations.

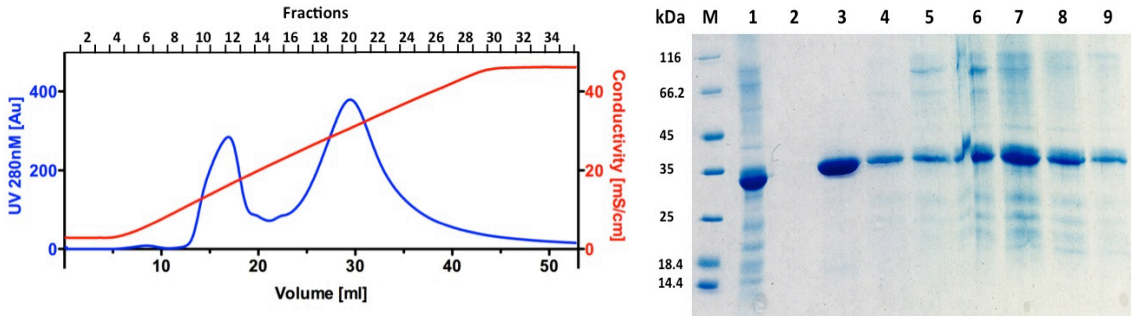

Figure 25: Chromatogram and SDS-PAGE analysis of the anion exchange chromatography of the IL-5Rα protein. M: protein standard **1:** IL-5Rα protein solution before purification **2:** flow through **3:** elution fraction 12 **4:** elution fraction 14 **5:** elution fraction 16 **6:** elution fraction 18 **7:** elution fraction 20 **8:** elution fraction 23 **9:** elution fraction 25 **Blue:** UV absorption at 280nm [Au] **Red:** Conductivity [mS/cm]

To validate this assumption, elution fractions 10-13 of the first absorbance maximum and elution fractions 17-25 of the second maximum were separately pooled and the combined elution fractions were dialyzed against 50 mM Tris-HCl pH 8.1. Half of the pooled fractions were subjected to an IL-5 affinity chromatography as used in the previous purification protocol to determine which of the pooled fractions contained active and pure IL-5Rα protein.

Similar quantities of the first elution maximum (F10-13) and the second (F17-25) of IL-5Rα were loaded onto IL-5 affinity resin. The suspension was transferred into a falcon tube and incubated for 1 h at 4°C under agitation. Then the suspension was transferred into a column (Biorad) and the flow through was collected. The column was washed with buffer and the bound IL-5Rα protein was eluted with 4 M $MgCl_2$ repeatedly added to the column. The elution fractions were dialyzed against buffer (50 mM Tris-HCl pH 8.1) overnight and analyzed via SDS-PAGE (s. Figure 26).

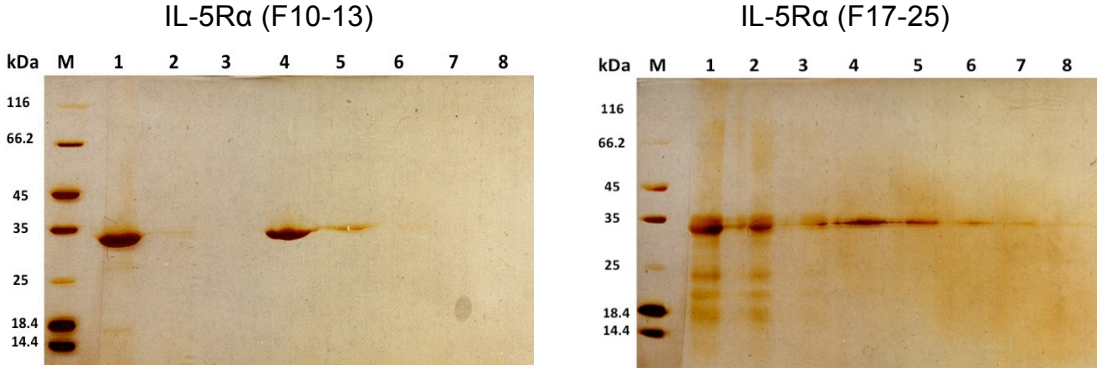

Figure 26: SDS-PAGE analysis of the IL-5 affinity chromatography. Left: Of the pooled fractions 10-13 after the anion exchange chromatography. **Right:** Of the pooled fractions 17-25 after the anion exchange chromatography. **M:** protein standard **1:** IL-5Rα before the IL-5 affinity chromatography **2:** flow through **3:** wash **4-8:** elution fractions 1-5

The first elution maximum of the anion exchange chromatography contained active (i.e. natively folded) and highly pure IL-5Rα protein. No IL-5Rα protein of the first elution maximum was found in the flow through of the IL-5 affinity chromatography and about 75% of the subjected IL-5Rα protein to the column could be recovered. On the contrary most of the IL-5Rα protein from the second elution peak that was subjected to the IL-5 affinity chromatography was found in the flow through, indicating that the second elution maximum contains mostly inactive (misfolded) IL-5Rα protein.

The improved anion exchange chromatography with higher resolution allowed eliminating the IL-5 affinity chromatography done before. With these established optimizations the yield of the IL-5Rα protein could be increased by about three fold from 2-3 mg per liter bacterial culture used to 8-9 mg/l.

4.1.3 Purification of the ectodomain of the common beta chain

The protein purification of the ectodomain of the common beta chain (βc) was previously established using a baculovirus-infected insect cell system. Insect cells have a similar post-translational modification mechanism as mammalian cells and a chaperon-mediated folding system allowing proper folding, disulfide bond formation and protein oligomerization.

4.1.3.1 Recombinant virus generation of βc N346Q

The cDNA encoding for the ectodomain of the human βc (Uniprot: P32927, 17-438) had been cloned into the pAB-bee-8xHis expression vector (s. 9.2.3). The βc N346Q variant was used as mutation of this possible N-glycosylation site did not affect expression yield but significantly improved the quality of the obtained protein crystals (Gustin, S.E. *et al.*, 2001). As previously produced virus for the βc N346Q protein had been stored for a rather long period, new virus stocks were produced. Therefore, the co-transfection of S*f*9 cells with the expression vector pAB-bee-8xHis βc N346Q, a plaque assay to isolate virus clones and their amplifications using TriEx S*f*9 cells were done as described (s. 3.4.3-3.4.7). Western Blot analysis after the second round of virus amplification showed that all six clones picked expressed the βc protein (s. Figure 27). Clone 6 was selected since it showed the highest expression rate of all six clones analyzed. The SDS-PAGE analysis of our expression tests showed a protein band with an apparent molecular weight of about 55 kDa,

which is due to the fact that the dimeric βc protein is dissociating into its monomers under the SDS-PAGE conditions.

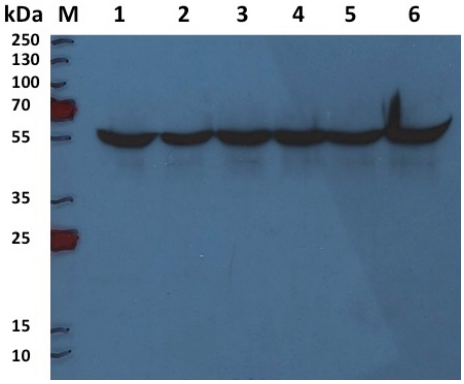

Figure 27: Western Blot of the second virus amplification round of the ectodomain of βc N346Q. M: protein standard **1-6:** clone 1-6

4.1.3.2 Expression and purification of the ectodomain of βc N346Q using High-Five insect cells

The protein expression of βc N346Q was carried out as described under 3.4.8 using High-Five insect cell suspension cultures grown under serum-free conditions. The density of the insect cells was adjusted to $5.5x10^5$ cells/ml. Depending on the expression volume and baculovirus titer the required volume of the supernatant of a serum free virus amplification was added to achieve an multiplicity of infection of 5. Up to 400 ml of expression mixture were incubated in a two-liter culture flask for 5 days at 27°C and 80 rpm. Due to the honeybee melittin signal sequence upstream of the gene of interest natively folded and post-translationally modified protein is transferred into the supernatant via the secretory pathway of the cells. After removal of the cells and debris by centrifugation the cells were dialyzed two times (1:10) overnight against 50 mM Tris-HCl pH 8.1, 500 mM NaCl at 4°C.

The ectodomain of βc N346Q has an octo-histidine sequence at the C-terminus and therefore allows a metal chelate affinity chromatography as the first purification step (s. 3.6.1). The cell medium supernatant was centrifuged and filtered through a 0.22 µm filter to remove debris and then loaded onto a 5 ml HisTrap excel column. The column was washed with ten column volumes (CV) buffer and thereafter with ten CV buffer containing 20 mM imidazole, to remove unspecifically bound proteins and other impurities. The protein was eluted using buffer containing 500 mM imidazole and collected in fractions. SDS-PAGE analysis of the metal chelate affinity chromatography revealed that the elution

fractions contained the βc N346Q protein but also further impurities (s. Figure 28, Top). During dialysis (1:100) of the pooled fractions against 100 mM Tris-HCl pH 8.5 most of the contaminations precipitated. The yield of the βc N346Q protein after the metal chelate affinity chromatography was about 18-20 mg/l insect culture.

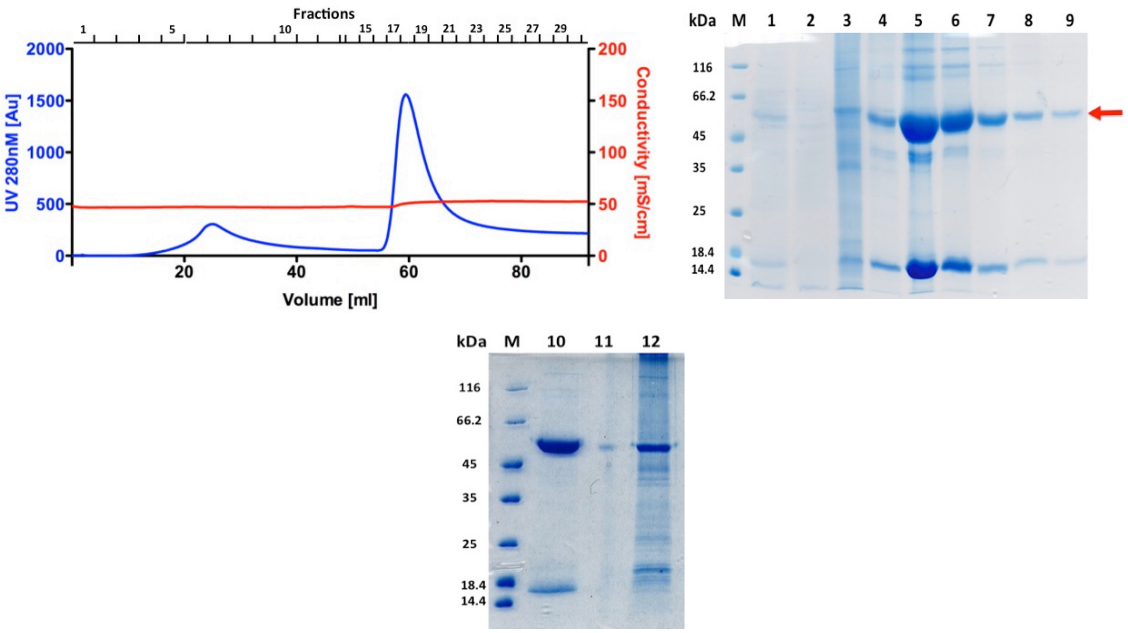

Figure 28: Top: Chromatogram and SDS-PAGE analysis of the metal chelate affinity chromatography of the βc N346Q protein. **Bottom:** SDS-PAGE analysis of the dialyzed βc protein. **M:** protein standard **1:** βc N346Q protein solution before purification **2:** flow through **3:** elution fraction 7 **4-5:** elution fractions 16-17 **6:** elution fraction 20 **7:** elution fraction 23 **8:** elution fraction 26 **9:** elution fraction 29 **10:** dialyzed βc protein solution **11:** empty **12:** precipitation after dialysis. The red arrow marks the protein band of the βc N346Q ectodomain protein; fractions 16-30 were pooled. **Blue:** UV absorption at 280nm [Au] **Red:** Conductivity [mS/cm]

4.1.3.3 Final purification of the ectodomain of βc N346Q via gel filtration

The βc protein solution was already highly pure after IMAC chromatography and contained only one additional contamination of lower molecular weight (s. Figure 28, Bottom). Therefore, a gel filtration was performed as second and final purification step.

The protein solution was centrifuged and concentrated by ultrafiltration down to 2.5-5 ml using stirred cells and centrifugal concentrators. Then the protein solution was filtrated using a 0.22 µm syringe filter before it was loaded onto a Superdex 200 26/70 column (GE Healthcare) using 10 mM HEPES pH 7.4, 150 mM NaCl, 3.4 mM EDTA as buffer. The elution profile and the respective SDS-PAGE analysis showed that βc N346Q could be efficiently separated from

the contamination with lower molecular weight (s. Figure 29). The yield of the highly purified βc N346Q protein using this optimized protocol was 8-9 mg/l insect culture.

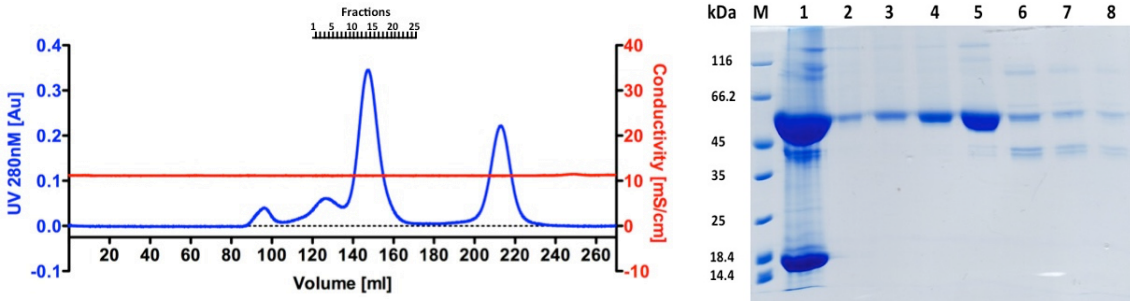

Figure 29: Chromatogram and SDS-PAGE analysis of the gel filtration of the βc N346Q protein. M: protein standard **1:** concentrated βc N34Q protein solution before purification **2-4:** elution fractions 10-12 **5:** elution fraction15 **6-8:** elution fractions 21-23. Fractions 10-20 were pooled. **Blue:** UV absorption at 280nm [Au] **Red:** Conductivity [mS/cm]

4.2 Structural and functional studies of the ternary IL-5 complex

4.2.1 Functional analysis of protein-protein interactions employing surface plasmon resonance (SPR)

To verify the binding parameters of the recombinantly produced proteins (IL-5, IL-5Rα and βc) using the optimized purification protocols with data available in the literature, an *in vitro* interaction analysis using surface plasmon resonance (SPR) was performed.

IL-5 was labeled with biotin (EZ-Link^{TM} Sulfo-NHS-Biotin) using NHS-chemistry as described under 3.3.7 yielding protein that had one biotin molecule attached randomly to a lysine residue. A GLC biosensor chip (Biorad) was activated by perfusing an EDC/sulfo-NHS solution (100 mM/25 mM). The activated biosensor surface was then coated with neutravidin (0.1 mg/ml in 10 mM sodium acetate pH 4.0) until a density of 3000-4000 response units (RU) was obtained. Remaining free activated carboxyl groups were deactivated by perfusing 1 M ethanolamine pH 8.5. The biotinylated IL-5 protein (200 nM, ligand) diluted in running buffer (10 mM HEPES pH 7.4, 150 mM NaCl, 3.4 mM EDTA, 0.005% Tween20) was immobilized until a density of 400 RU was obtained (s. 3.10).

For the analysis of the interaction of IL-5 with the IL-5Rα C66A ectodomain protein, six different concentrations (40 nM or 20 nM log2 dilution) of IL-5Rα C66A were perfused over the sensor surface (s. Figure 30). Analysis of the data was done applying a simple Langmiur 1:1 interaction model. The equilibrium binding constant K_D was calculated using the equation $K_D = k_d/k_a$. Compared to older SPR results obtained for the interaction of the human IL-5Rα C66A protein with IL-5, an almost ten times better affinity was observed (s. Table 18). The increase in affinity can be explained through a combination of a faster association rate and a slower dissociation rate. This result indicates that the proteins produced using the new protocol form the binary complex faster and that the formed complex is more stable.

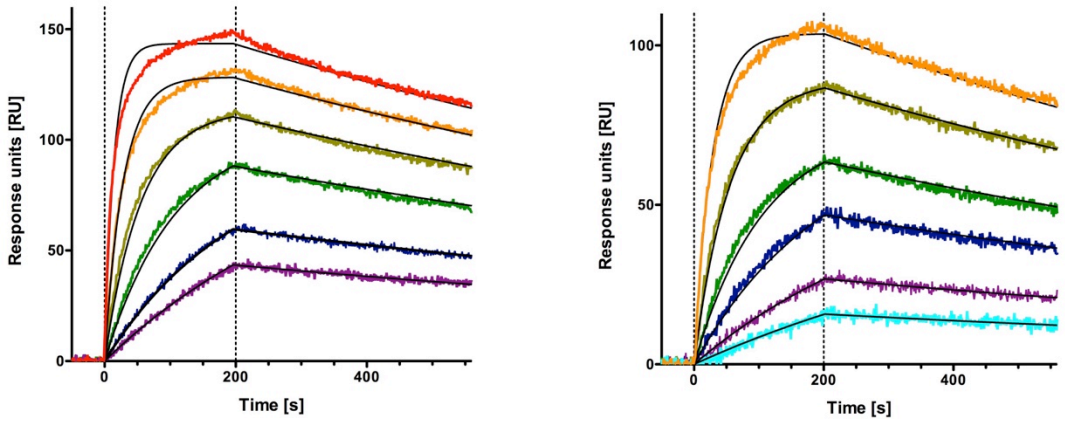

Figure 30: SPR sensorgrams of the interaction of hIL-5Rα C66A ectodomain with hIL-5. Left: SPR sensorgram of the 40 nM log 2 dilutions. **Right**: SPR sensorgram of the 20 nM log 2 dilutions. IL-5Rα concentrations: **40 nM**, **20 nM**, **10 nM**, **5 nM**, **2.5 nM**, **1.25 nM** and **0.625 nM**. (Flow rate: 100 µl/min; association time 200 s; dissociation time 300 s)

Table 18: Summary of the equilibrium binding constant, association and dissociation rate constants using the Langmuir 1:1 interaction model of the IL-5Rα C66A ectodomain protein produced with the optimized protocol compared to the reported values by Patino, E. *et al* (2011). (n=3, Rmax = local)

Receptor protein	k_a [10^6/Ms]	k_d [10^{-4}/s]	K_D (pM)
IL-5Rα C66A	1.8 ± 0.06	6.6 ± 0.4	376 ± 25
IL-5Rα C66A (Patino)	0.5 ± 0.2	0.14± 0.04	3000 ± 40

In addition to the analysis of the IL-5Rα protein, the binding parameters of βc N346Q ectodomain were also analyzed using a so-called co-injection protocol. Here two samples are drawn in sequence from separate vials and then injected consecutively over the sensor surface with no running buffer flow in between. Therefore, a solution of 300 nM IL-5Rα was injected first at a flow rate of 60 µl/min until an equilibrium was achieved for the binding of the ligand IL-5 and the analyte IL-5Rα. Then, in a second injection step, the βc N346Q protein was perfused as a mixture of 2 µM log 2 dilution and 300 nM of IL-5Rα over the transiently formed binary complex. The sensorgram of this co-injection of βc N346Q as the second analyte shows that the βc N346Q protein binds to the binary IL-5•IL-5Rα complex on the chip surface (s. Figure 31, left). Evaluation of the co-injection experiment was done by analyzing the dose-dependent binding of βc to the binary complex (s. Figure 31, right). The equilibrium constant, K_D, can be calculated directly from the sensorgram using the following formula:

$$R_{eq} = \frac{R_{max}\,[A]}{K_D + [A]}$$

with:

R_{eq} = Response at equilibrium

R_{max} = Theoretical maximum response

K_D = Equilibrium constant

[A] = Concentration of analyte

Even though full saturation and the plateau phase were not completely reached, likely due to the short injection time, an estimate of the binding affinity could be obtained. Optimization of the experiment conditions by lowering the constant concentration of the IL-5Rα down to 100 nM did not yield better sensorgrams, but allowed evaluation yielding a similar value for the equilibrium binding constant (s. Table 19).

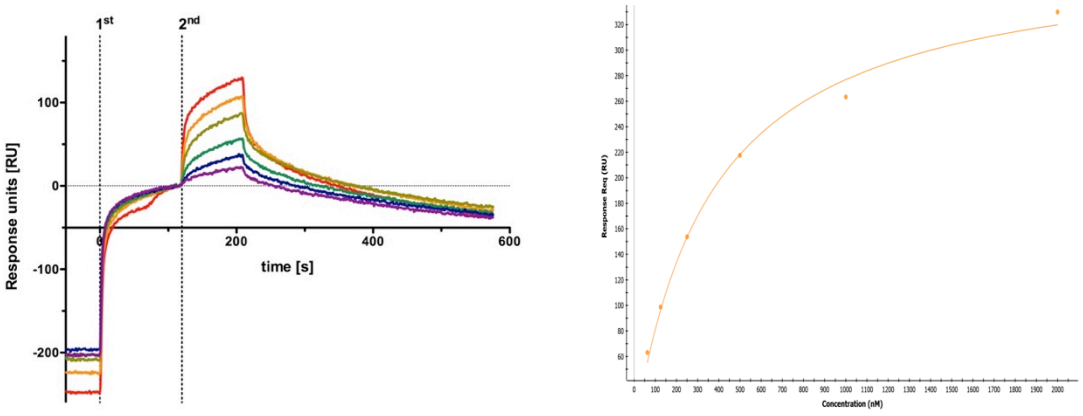

Figure 31: Left: SPR sensorgram of the co-injection experiment highlighting the formation of the IL-5 ternary ligand-receptor complex. **Right:** Equilibrium analysis of the βc N346Q protein. βc N346Q concentrations: **2000 mM**, **1000 mM**, **500 mM**, **250 mM**, **125 mM** and **62.5 mM**. 1st injection (IL-5Rα 300nM constant) 0-110 s. 2nd injection (IL-5Rα 300 nM constant + βc 2 µM log 2 dilution) 110-200 s, dissociation time 300 s. (Flow rate: 100 µl/min)

Table 19: Equilibrium constants using the analysis of the co-injection βc N346Q ectodomain protein with a constant IL-5Rα concentration. (n=3)

Receptor protein	K_D [µM]
IL-5Rα C66A 300 nM	0.5 ± 0.2
IL-5Rα C66A 100 nM	0.8 ± 0.2

4.2.2 Purification of the IL-5 ternary ligand-receptor complex via gel filtration

Our SPR analysis of the interaction of βc N346Q with the binary IL-5•IL-5Rα complex as well as SPR data reported in the literature (Scibek, J.J. *et al.*, 2002) indicated a binding affinity of the βc protein to the IL-5 binary ligand-receptor complex in the submicromolar (<1 µM) range. Together with the data reported for the preparation and purification of the ternary GM-CSF•GM-CSFRα•βc complex (Hansen, G. *et al.*, 2008), an isolation and purification of the ternary hIL-5•hIL-5Rα•βc complex employing gel filtration chromatography seemed therefore possible.

As we assumed the stoichiometry of the IL-5 ternary complex to be similar to that of the hexameric GM-CSF ternary complex, in which a dimeric βc is placed between two GM-CSF•GM-CSFRα assemblies, the ternary IL-5 complex was prepared with a 2:2:4 stoichiometric ratio consisting of two βc chains, two IL-5Rα chains and four IL-5 molecules. This protein mixture was incubated for 72 h at 4°C. Then the protein solution was centrifuged to remove precipitate and loaded onto a Superdex 200 10/300 (GE Healthcare) column. SDS-PAGE analysis showed that the βc N346Q protein and the binary complex however separated during gel filtration (s. Figure 32). This was unexpected as our (and reported) binding data for βc indicated a sufficiently high binding affinity to allow isolation by gel filtration chromatography. Thus, the interaction of βc with the IL-5 binary ligand-receptor complex was analyzed using different setups and interaction analysis methods.

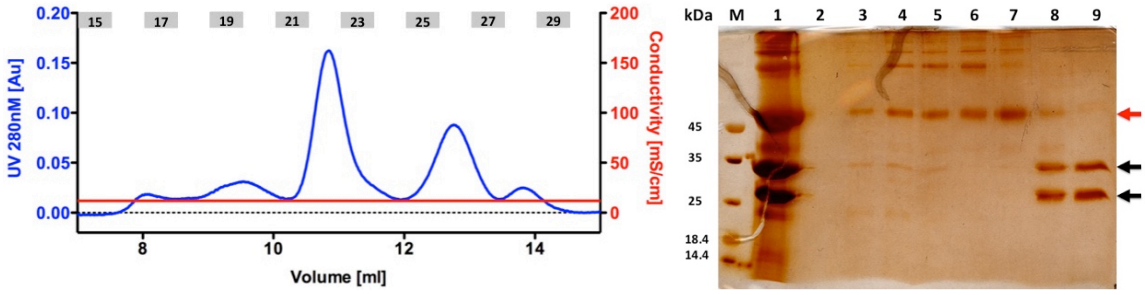

Figure 32: Chromatogram and SDS-PAGE analysis of the purification of the ternary IL-5 complex via gel filtration chromatography. **M:** protein standard **1:** ternary IL-5 complex before purification **2:** elution fraction 16 **3:** elution fraction 17 **4:** elution fraction 18 **5:** elution fraction 19 **6:** elution fraction 20 **7:** elution fraction 22 **8:** elution fraction 26 **9:** elution fraction 28. The red arrow marks the protein band of the βc N346Q ectodomain protein and the black arrows of the binary complex (IL-5•IL-5Rα). **Blue:** UV absorption at 280nm [Au] **Red:** Conductivity [mS/cm]

4.2.3 Functional studies show βc binds to IL-5•IL-5Rα with micromolar affinity

Even though own and literature data indicated that the IL-5•IL-5Rα complex and βc interact with rather high affinities in the submicromolar range our attempts to purify the ternary IL-5 complex via gel filtration chromatography failed. Thus, additional analyses of this interaction were performed employing SPR and a new technique termed micro scale thermophoresis (MST).

The gel filtration chromatography of the ternary IL-5 complex indicates a weaker affinity of the βc N346Q protein towards the binary IL-5 complex as initially suggested from our SPR measurements, hence the setup of the SPR experiment was reconsidered. Our setup might have been biased by avidity effects suggesting a much higher affinity than what would be found in solution, hence a different SPR setup using immobilized βc was performed.

βc N346Q was labeled with biotin (EZ-Link^{TM} Sulfo-NHS-Biotin) using NHS-chemistry as described under 3.3.7 yielding protein that had one biotin molecule attached randomly to a lysine residue. The biotinylated βc protein was immobilized at a density of 700-800 RU on a neutravidin-coated chip surface (GLC, Biorad) similar as done for IL-5 (s. 4.2.1).

For the analysis six different concentrations of purified binary complex starting with 20 µM were perfused over the chip surface (s. Figure 33, left). The SPR data was analyzed applying a simple Langmiur 1:1 interaction model. Compared to the SPR experiments performed before, a 18-fold lower affinity was measured with this setup (s. Table 20). In parallel also wild type βc (βc WT) protein was immobilized and analyzed analogue to βc N346Q. This was done because in the SPR analysis reported by Scibeck, JJ *et al.* (2002), βc WT protein, containing all three potential glycosylation sides, was immobilized on the chip surface. All three N-glycosylation sites are required for the high affinity binding of the βc protein and the binary GM-CSF complex (Niu, L. *et al.*, 2000). The SPR analysis (s. Figure 33, right) of the βc WT protein however revealed an even slightly lower affinity compared to the βc N346Q protein, indicating that for binding of βc to IL-5•IL-5Rα the glycosylation at N346Q is not required or involved (s. Table 20).

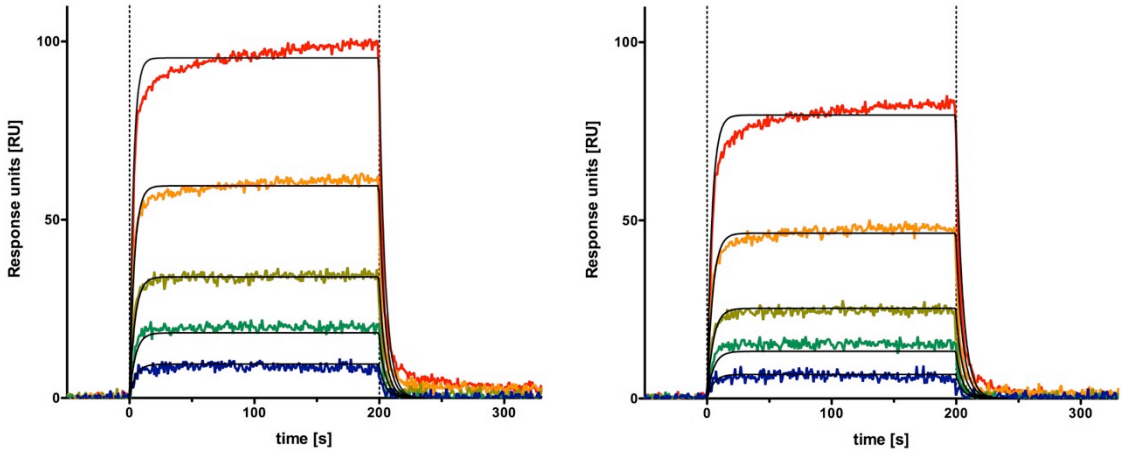

Figure 33: SPR sensorgrams of the interaction analysis of the binary IL-5 complex with βc N346Q or βc WT. Left: βc N346Q immobilized as ligand. **Right:** βc WT immobilized as ligand. Binary IL-5 complex concentrations: **10 µM**, **5 µM**, **2.5 µM**, **1.25 µM** and **0.625 µM**. (Flow rate: 100 µl/min, association time 200 s dissociation time 120 s)

Table 20: Summary of the equilibrium binding constant, association and dissociation rate constants using the Langmuir 1:1 interaction model of the βc ectodomain protein variants. (n=3)

Receptor protein	k_a [10^3/Ms]	k_d [10^{-3}/s]	K_D [µM]
βc N346Q	8.8 ± 0.6	8.0 ± 0.9	9 ± 0.5
βc WT	6.4 ± 0.2	9.1 ± 0.3	14 ± 0.1

In parallel an interaction analysis using the microscale thermophoresis (MST) methodology was performed for the interaction of βc with the binary IL-5 complex. The βc protein was coupled with a fluorescent dye, i.e. Alexa-647 (Thermo Fischer, A20006) as described (s. 3.3.7). In contrast to SPR analysis, in which one of the interaction partners is immobilized on the surface of the biosensor, analysis by MST is performed completely in solution.

For the analysis, log2 dilution series starting with 58 µM as the highest concentration of the IL-5 complex were prepared. To each dilution 86 µM of the fluorescently labeled βc N346Q-647 protein was added (s. 3.11). BSA (0.1 mg/ml) was added to the measuring buffer to minimize unspecific sticking of βc to the glass surface of the capillaries. A thermophoresis temperature gradient of 60% was used to initiate thermophoresis and the fluorescence excitation was performed with 20% LED power.

The first results of the MST analysis showed a sigmoidal curve indicating dose-dependent binding, however the fluorescence signal decreased with increasing protein concentration (s. Figure 34). For reliable and reproducible results, the fluorescence signal should not deviate more than 10%. The calculated affinity of about 5 µM might therefore not be correct and can only serve as a guide value. So far adjustments of the setup failed to obtain consistent fluorescence signals. Hence further optimizations of the MST set up have to be done.

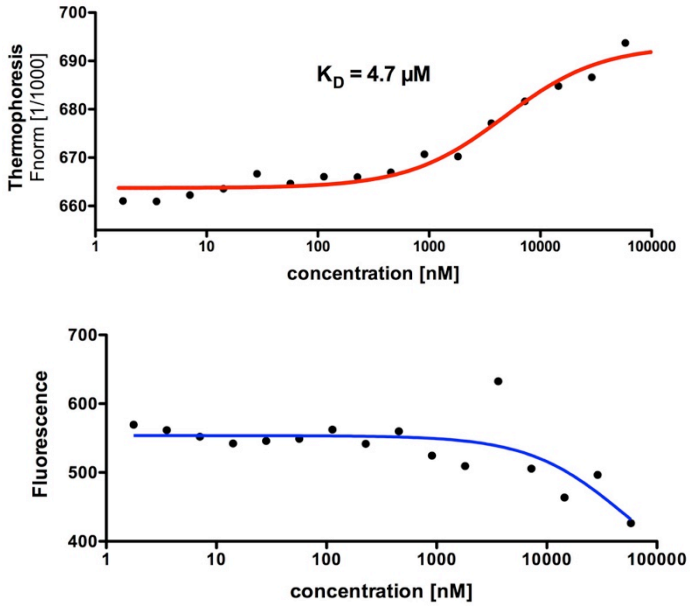

Figure 34: Interaction analysis of βc N346Q and the binary IL-5 complex. Top: Thermophoresis analysis. **Bottom:** Fluorescence signals of the different dilutions.

The affinities obtained by the altered SPR setup as well as MST experiments together suggest however that an isolation of the ternary IL-5 complex via gel filtration is highly unlikely. This is corroborated by the fast dissociation kinetics observed in the altered SPR setup.

4.3 Structural and functional analysis of the ectodomain of hIL-5Rα in its unbound state

In this section a structural and functional analysis of the human Interleukin-5 receptor ectodomain (IL-5Rα) C66A variant in its unbound state was performed, to provide further information helping to answer the question as to what extend the wrench-architecture of the IL-5Rα ectodomain is preformed.

4.3.1 Unfolding analyses of hIL-5Rα $C66A_{ECD}$ indicate a local domain flexibility

Solubility and stability of the IL-5Rα protein were examined, since these two parameters strongly correlate with a protein's probability to crystallize. In our experiments IL-5Rα C66A protein started to precipitate when the concentration exceeded 7-8 mg/ml using buffers close to physiological conditions.

Due to the precipitation of the IL-5Rα at relatively low concentration, a Thermofluor-unfolding experiment was used to screen for buffers providing better solubility and stability conditions. The method is based on the fact that folded and unfolded proteins can be distinguished through exposure to a hydrophobic fluoroprobe (SYPRO Orange, Life Technologies S-6650). The probe is quenched in aqueous solution, but will preferentially bind to the exposed hydrophobic interior of an unfolding protein leading to a sharp decrease in quenching so that a readily detected fluorescence emission can be studied as a function of temperature. Thermally induced unfolding is a generally irreversible unfolding process following a typical two-state model with a sharp transition between the folded and unfolded states, where Tm is defined as the midpoint of temperature of the protein unfolding transition. A higher Tm value compared to the reference Tm value indicates an increase in structural order and reduced conformational flexibility. (Ericsson, U.B. *et al.*, 2006)

The Thermofluor analysis showed for all 40 different buffers tested, as well as the reference, a similar Tm value of about 35°C, indicating that no improvement of the IL-5Rα protein stability could be achieved. Surprisingly the data indicate that the IL-5Rα C66A ectodomain protein is relatively thermally instable. A protein unfolding transition starting around 35°C, only 2°C below the physiological temperature, is rather unusual for a mammalian protein and raise concerns regarding its physiological functionality. However, the Thermofluor analysis only provides information at what temperature unfolding of a protein

starts and not which parts of the protein are involved or whether this is a global unfolding process. The results however could indicate that the wrench-architecture starts to open (unfolds) or that the domain flexibility is increased at 35°C. We measured IL-5Rα also employing differential scanning fluorimetry using a Prometheus NT.48 (Nanotemper) instrument. The conceptual basis for the method is similar to that of the Thermofluor. The Prometheus monitors however the shift of intrinsic tryptophan fluorescence at the emission wavelengths of 330 and 350 nm (dye-free method) to analyze the thermal unfolding path of the sample.

The experiment was performed with IL-5Rα at a concentration of 1 mg/ml in 10 mM HEPES, 150 mM NaCl, 3.4 mM EDTA and 0.005% Tween pH 7.4 (HBSE 150) and temperature was increased by 1°C/min from 20 to 95°C. Figure 35 shows the melting scan and first derivate for the thermal unfolding of IL-5Rα C66A protein. To our surprise two transitions were observed for IL-5Rα, one at 42.3°C and a second at 66.5°C (s. Table 21). One explanation for the two Tm values could be that the wrench-architecture starts to unfold at 42.3°C and at 66.5°C a global unfolding occurs. The first Tm value (42.3°C) is close to the Tm obtained by the thermofluor analysis (35°C). To obtain final proof of this hypothesis, further investigations were needed.

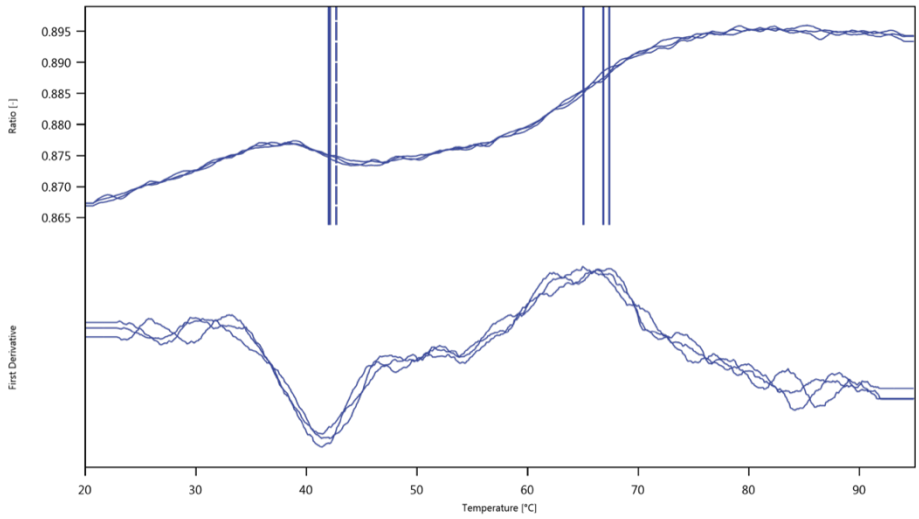

Figure 35: Melting scan and first derivate of the IL-5Rα C66A ectodomain protein of the Prometheus analysis. The melting is shown as fluorescence ratio (y-axis, upper graph) and as its first derivative (y-axis, lower graph) and is plotted against the temperature (x-axis). The vertical lines at the transition points correspond to peak maxima, the Tm. (n=3)

Table 21: Tabular overview of data shown in Figure 35. (n=3)

Receptor protein	Tm 1 [°C]	Tm 2 [°C]
IL-5Rα C66A	42.3 ± 0.4	66.5 ± 1.2

Instead of identifying an optimized buffer condition, stabilizing the IL-5Rα C66A ectodomain protein, the Thermofluor and Prometheus analysis indicated that the wrench-like architecture of IL-5Rα is possible thermolabile. In addition, the flexibility of the ectodomain of the IL-5 receptor seems higher than we suggested from our pervious results and could impede us from finding a suitable crystallization condition.

4.3.2 Crystallization trials of IL-5Rα$_{ECD}$ in the unbound state

Since the buffer screening via the Thermofluor could not identify a buffer composition stabilizing or raising the solubility of the IL-5Rα C66A ectodomain protein, initial crystallization screens were set up with concentrated IL-5Rα protein in 1x PBS buffer.

To select an appropriate protein concentration for the crystallization trials a Pre-Crystallization Test (PCT) was performed. The results from the PCT analysis suggested a concentration of the IL-5Rα protein between 4-5.2 mg/ml for subsequent crystallization trials.

Initial crystallization screens were then set up using sitting drop vapor diffusion method using the Honeybee 963 (Digilab) crystallization robot (Rudolf Virchow Centre, University of Würzburg). Each drop was prepared by mixing 0.3 µl of purified IL-5Rα protein (5.2 mg/ml) and 0.3 µl of crystallization screening reagent solution. Of the reagent solution 40 µl were filled in each well of the 96-well plate (Crystalquick™ LP Plate, Greiner Bio-One) and the plates were sealed using a plastic film. Among almost 900 different conditions screened, two conditions yielded small single needle-like or clusters of plate-like crystals (s. Figure 36).

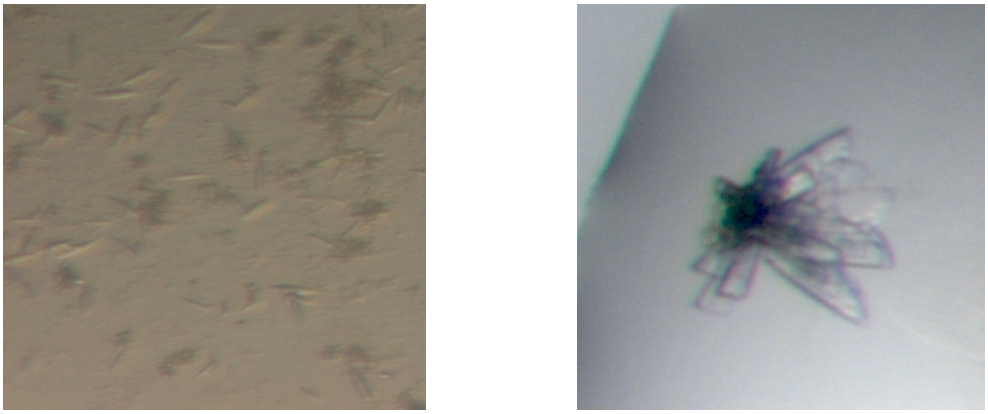

Figure 36: Crystals observed during the crystallization trails of the free hIL-5Rα ectodomain. Left: 0.1 M MES pH 6.5, 1.6 M $MgSO_4$ **Right:** 0.1 M MES pH 6.5, 0.01 M zinc sulfate, 25% PEG 550 mme

For both conditions optimization screens were designed, testing different pH and varying the buffer composition of the initial crystallization condition (s. Appendix page 178, Table 37). The small single needle-like crystals initially observed unfortunately could not be reproduced in further screens. Additional crystallization trials of this condition only yielded precipitate or did not result in any crystals or precipitate, even after extended incubation for more than three months. Further screens of the clusters of plate crystals instead yielded mostly clusters of plate crystals with slightly thinner plates. However, after four weeks of incubation also clusters of cubic crystal were observed under these conditions (s. Figure 37).

Since these crystals showed no diffraction at all, further optimization was not performed. Analysis of the crystals using a UV-Vis microscope suggested that these crystals were salt and not protein. The phosphate in the protein buffer together with the zinc sulfate in the crystallization buffer could be the source of the salt crystals. Therefore, the protein buffer needs to be exchanged to a buffer containing no phosphate before further crystallization trials.

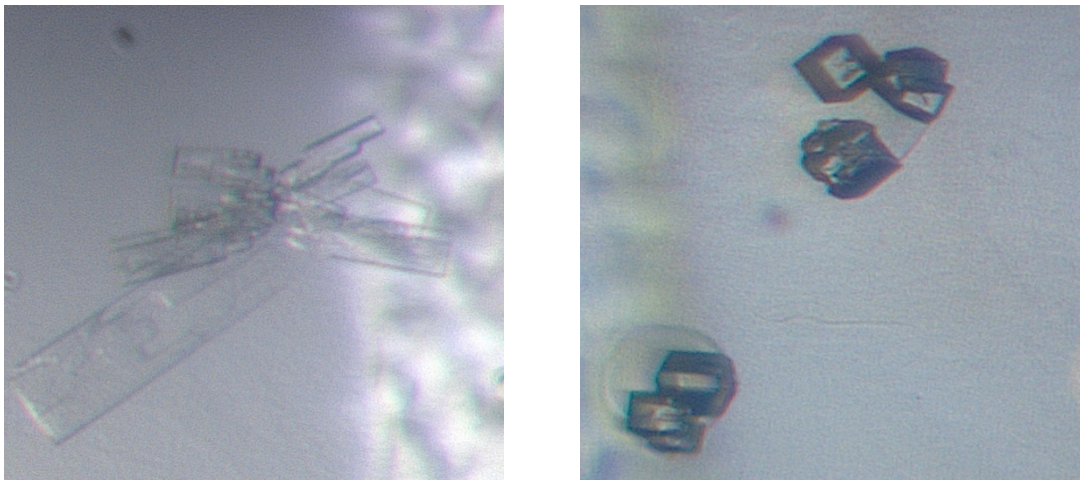

Figure 37: Crystals observed during the sub-screen of the free hIL-5Rα ectodomain. Left: 0.1 M MES pH 6.5, 0.01 M zinc sulfate, 26% PEG 550 mme **Right:** 0.1 M MES pH 6.5, 0.01 M zinc sulfate, 28% PEG 550 mme

Incubating the crystallization trails at 4°C instead of 21°C might be successful (in addition to exchanging the buffer), as our results indicate that the wrench-like architecture of the IL-5Rα is thermolabile and flexible. Lowering the temperature slows down all the processes occurring during crystallization, helping to obtain more densely packed crystals and should also decrease the flexibility of IL-5Rα, which in turn could positively affect the crystallization process.

4.3.3 Establishing a purification protocol for IL-5Rα C66A derived from baculovirus-infected insect cells

Since solubility of IL-5Rα C66A ectodomain is rather low and precipitation of IL-5Rα was observed at concentrations usually used in crystallization, we established a baculovirus insect cell expression system for hIL-5Rα C66A in the framework of a bachelor thesis (Viola Schmitt 2015 "*Expression und Aufreinigung der extrazellulären Domäne des humanen Interleukin‑5 Rezeptors in Insektenzellen*"). These cells can process the four potential glycosylation sites (N-linked) present in the IL-5Rα ectodomain. Glycosylation of the IL-5Rα protein is not required to obtain biologically active protein, but very likely positively affect its solubility, thereby allowing higher protein concentrations during crystallization trails.

4.3.3.1 Recombinant virus generation of IL-5Rα C66A

The cDNA encoding for the ectodomain of human IL-5Rα C66A (Uniprot: Q01344, 21-332) was cloned into the pMK1 expression vector using the restriction enzymes BamHI and XhoI (s. 9.2.2). The N-terminally fused hexahistidine sequence can be cleaved by endoproteolytic hydrolysis using the protease thrombin. The IL-5Rα protein has a calculated molecular weight of 37.8 kDa (without glycosylation). Co-transfection of S*f*9 cells with the expression vector pMK1 hIL-5Rα C66A, a plaque assay to isolate virus clones and their amplifications using TriEx cells were done as described (s 3.4.3-3.4.7). The Western Blot analysis after the second virus amplification round showed that four of the selected six virus clones expressed IL-5Rα in similar amounts (s. Figure 38). Clone 1 was used in the further course, since it showed a slightly higher expression rate compared to the other clones.

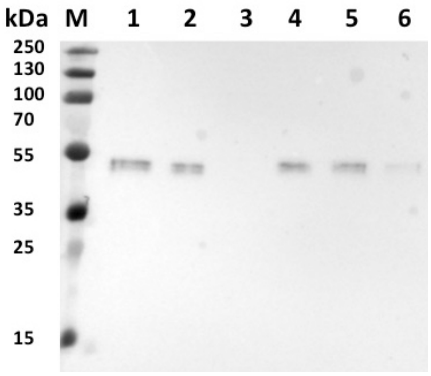

Figure 38: Western Blot of the second virus amplification round of the IL-5Rα C66A ectodomain protein. M: protein standard **1-6:** clone 1-6

4.3.3.2 Semi-preparative production of hIL-5Rα C66A in suspension-adapted High Five insect cells

A first test expression showed that the fatal calf serum (5% v/v FCS, Biochrome) present as supplement in the expression medium could not be completely separated from IL-5Rα protein during purification. Therefore, serum was replaced with 1.5% lipid medium supplement (Sigma) and additionally 0.15% Pluronic (F-68, Sigma) was added to increase the mechanical stability of the cell membrane against hydrodynamic shear forces resulting from cultivating the cells as suspension cultures.

The expression was carried out as described under 3.4.8 using High-Five insect cell suspension cultures grown under serum-free conditions. The insect cells were adjusted to $5.5x10^5$ cells/ml. Depending on the expression volume and titer of the baculovirus used for transfection the required volume of the supernatant of a serum free virus amplification was added to achieve an multiplicity of infection of 5. Up to 400 ml of expression mixture was incubated per two-liter culture flask for 5 days at 27°C and 80 rpm. The natively folded and glycosylated protein is exported out of the cells via the secretory pathway. After centrifugation the protein solution (supernatant) was two times dialyzed overnight against 50 mM Tris-HCl pH 8.1, 500 mM NaCl.

4.3.3.3 Purification of insect-cell derived IL-5Rα C66A using metal chelate affinity chromatography

The N-terminal hexahistidine sequence of the expression construct was used to purify the protein via a metal chelate affinity chromatography (s. 3.6.1) employing a 5 ml HisTrap excel column (GE Healthcare).

The protein solution was centrifuged and filtered through a 0.22 µm filter before being loaded onto the 5 ml HisTrap excel column. Then the column was washed with 10 column volumes of buffer and the protein was eluted using a linear gradient from 0 to 500 mM imidazole. The SDS-PAGE analysis of the metal chelate affinity chromatography revealed an apparent molecular weight for the IL-5Rα protein of about 45 kDa, which is higher than the calculated (37.8 kDa). The protein and its deviating molecular weight could be confirmed by Western Blot analysis (s. Figure 39). The difference might be explained by the glycosylation of the protein. Protein-containing fractions were pooled and

dialyzed against 50 mM Tris-HCl pH 8.1 (1:100) overnight at 4°C for the planed anion exchange chromatography.

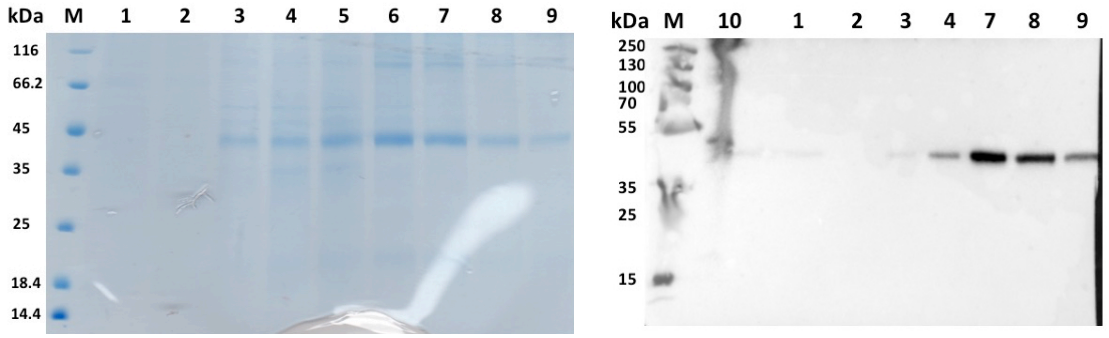

Figure 39: SDS-PAGE (left) and Western Blot analysis (right) of the metal chelate affinity chromatography of the ectodomain of IL-5Rα C66A. M: protein standard **1:** IL-5Rα protein before purification **2:** flow through **3-5:** elution fractions 10-12 **6:** elution fraction 14 **7:** elution fraction 16 **8:** elution fraction 18 **9:** elution fraction 20 **10:** re-suspended insect cell pellet. Fractions 10-21 were pooled.

4.3.3.4 Anion exchange chromatography of insect-cell derived IL-5Rα C66A

The pooled fractions of the IL-5Rα protein derive from insect cell expression still contained minor impurities. The protein was therefore subjected to anion exchange chromatography in analogy to the anion exchange chromatography of the bacterial derived IL-5Rα C66A ectodomain protein (s. 4.1.2.3).

After dialysis IL-5Rα protein solution was applied to a 5 ml HiTrap Q-sepharose HP column (GE Healthcare). The column was washed with 10 column volumes and the protein was eluted with a linear gradient to 500 mM NaCl over 10 column volumes. The chromatogram of the anion exchange chromatography showed two distinct maxima (s. Figure 40). The SDS-PAGE analysis of these two UV absorbance maxima revealed that the first maximum contained mainly the IL-5Rα protein while the second maximum comprised also other proteins and impurities (s. Figure 41, left). Western Blot analysis confirmed that only the first peak contained IL-5Rα protein (s. Figure 41, right). Protein-containing fractions of the first absorbance maximum were pooled and dialyzed overnight at 4°C against PBS. The yield of the IL-5Rα C66A ectodomain was around 2 mg/l insect culture used.

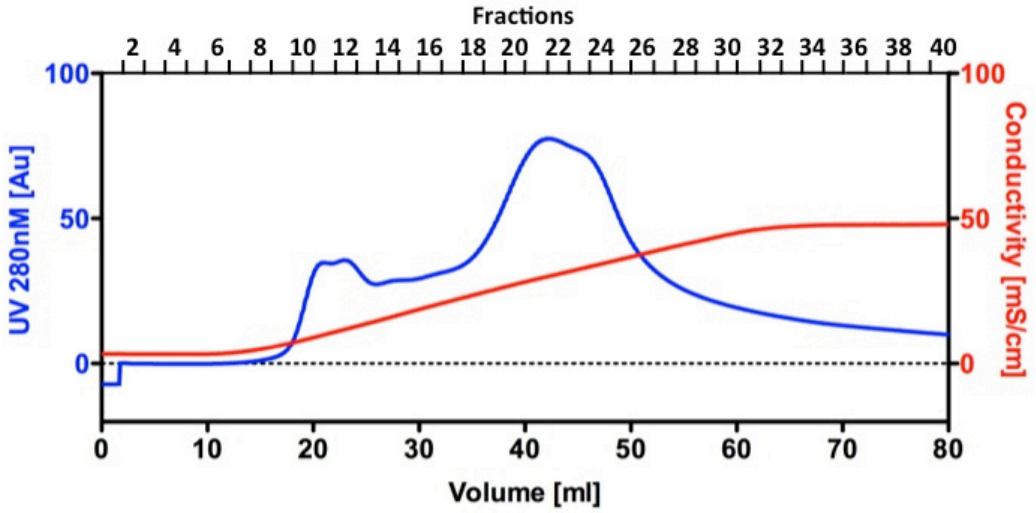

Figure 40: Chromatogram of the anion exchange chromatography of the IL-5Rα protein. Blue: UV absorption at 280nm [Au] **Red:** Conductivity [mS/cm]

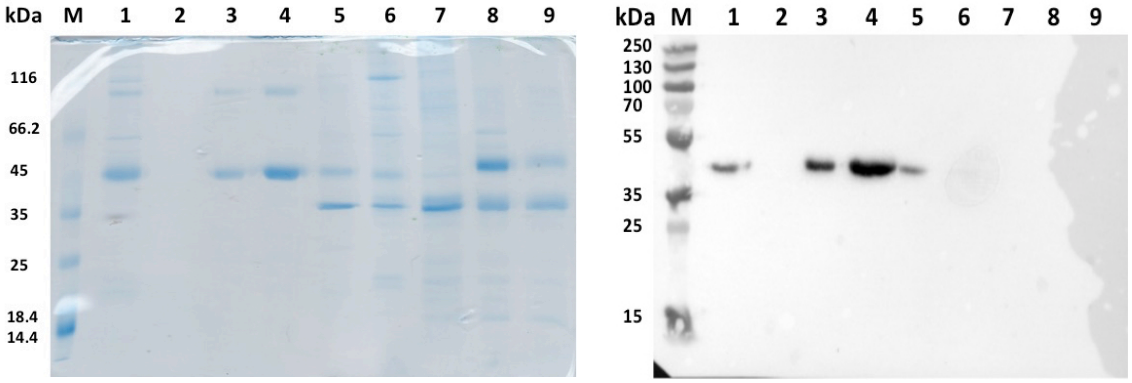

Figure 41: SDS-PAGE (left) and Western Blot analysis (right) of the anion exchange chromatography of the ectodomain IL-5Rα C66A. M: protein standard **1:** IL-5Rα protein before purification **2:** flow through **3:** elution fraction 10 **4:** elution fraction 12 **5:** elution fraction 15 **6:** elution fraction 18 **7:** elution fraction 21 **8:** elution fraction 24 **9:** elution fraction 26. Fractions 10-13 were pooled.

4.3.4 Functional analysis of insect-cell derived IL-5Rα C66A using surface plasmon resonance (SPR)

An *in vitro* interaction analysis employing surface plasmon resonance (SPR) was performed to validate the functionality of the recombinant IL-5Rα C66A protein produced in baculovirus-infected insect cells. Biotinylated IL-5 protein was immobilized (400-450 RU) on a neutravidin-coated GLC sensor chip (Biorad) as described before for the SPR analysis of the bacterial derived IL-5Rα (s. 4.2.1).

For quantitative analysis six different concentrations (log 2 dilution) of insect-cell derived IL-5Rα C66A protein as analyte, starting with 40 nM as the highest concentration, were perfused over the chip surface (s. Figure 42). The SPR

data was analyzed by using a simple Langmuir 1:1 interaction model. Compared to the SPR results obtained for IL-5Rα protein produced in *E. coli* (which was analyzed on the same chip) an identical affinity was obtained for the IL-5Rα protein from insect cell culture (s. Table 22). These results confirm that glycosylation of IL-5Rα C66A is neither required nor impairs high affinity binding to IL-5.

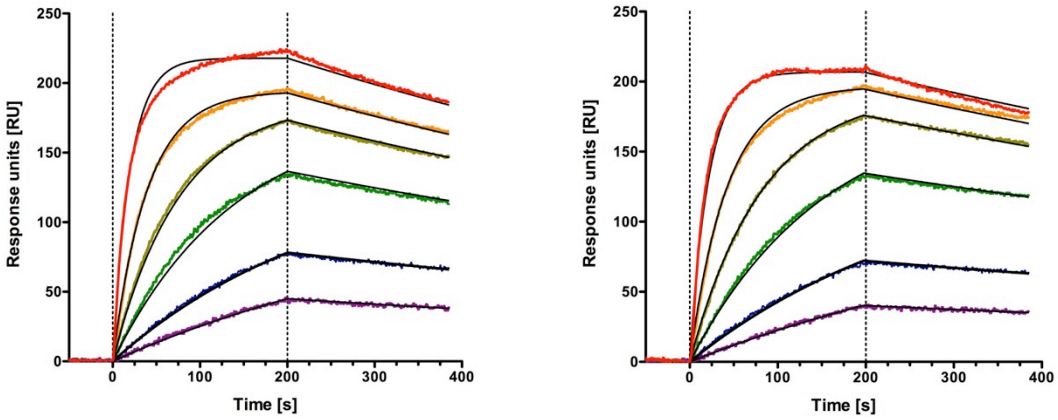

Figure 42: SPR sensorgrams of the differently expressed hIL-5Rα C66A ectodomains. Left: SPR sensorgram of insect-cell derived IL-5Rα C66A. **Right**: SPR sensorgram of bacterial derived IL-5Rα C66A. IL-5Rα concentrations: **40 nM**, **20 nM**, **10 nM**, **5 nM**, **2.5 nM** and **1.25 nM**. (Flow rate: 100 µl/min; association time 200 s; dissociation time 120 s)

Table 22: Summary of the determined equilibrium constant, association and dissociation rate using the Langmuir 1:1 interaction model of the IL-5Rα C66A ectodomain protein produced either using insect or *E. coli* cells. (n=2, Rmax = local)

Receptor protein	k_a [10^6/Ms]	k_d [10^{-4}/s]	K_D [pM]
IL-5Rα C66A (High-Five)	1.1 ± 0.2	9.3 ± 0.4	847 ± 152
IL-5Rα C66A (*E. coli*)	1.0 ± 0.2	7.0 ± 0.3	698 ± 98

4.3.5 Optimization of the IL-5Rα C66A protein yield

Since the overall yield of insect-cell derived IL-5Rα C66A (2 mg/l) was relatively low when compared to βc N346Q (8-9 mg/l) produced in a similar manner, optimization of the protein expression was performed. For optimization we tested different multiplicities of infection (MOI's) and durations of the protein expression.

Therefore, High-Five insect cells were adjusted to 5.5x10^5 cells/ml and mixed 1:1 with fresh serum-free expression medium and incubated for 2 h at 27°C in a 6-well plate. Afterwards the medium was removed and 2 ml of virus mixed with fresh medium, resulting in the desired multiplicity of infection, were added. Multiplicities of infection of 5, 10, 15 and 20 as well as a negative control

containing no virus were tested. Samples were taken after four and five days and analyzed by Western Blot (s. Figure 43).

A multiplicity of infection of five yielded no detectable expression of the IL-5Rα C66A after four days and only a minor protein band is detected after five days. Using a multiplicity of infection of ten or greater instead shows clear IL-5Rα protein expression after four and five days. The results indicated that a multiplicity of infection of 10-15 (instead of 5) and limiting the protein expression to four days (instead of five) should increase the overall yield of the IL-5Rα C66A ectodomain protein.

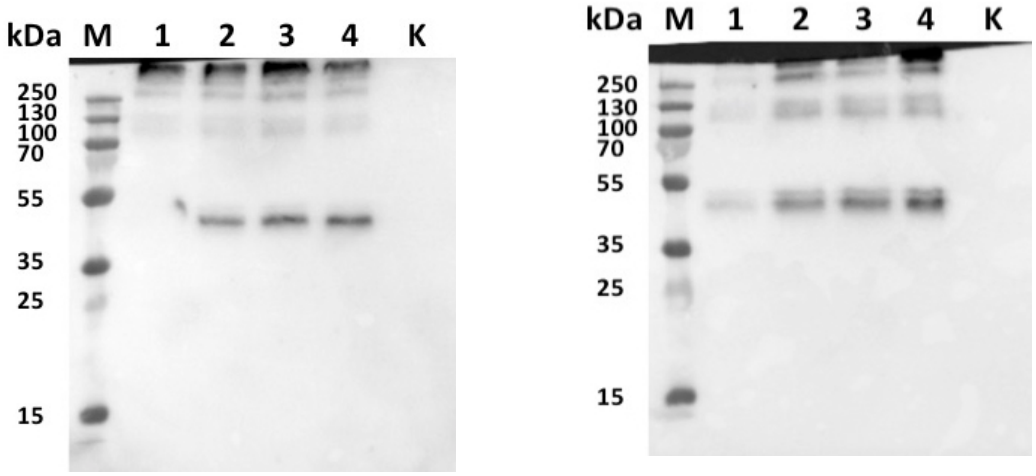

Figure 43: Western Blot analysis of the multiplicity of infection optimization test. Left: Samples analyzed after four days. **Right:** Samples analyzed after five days. **M:** protein standard **1-4:** samples obtained with a multiplicity of infection of 5, 10, 15 or 20 **K:** sample of the negative control with no virus added to the insect cell culture.

The data presented in the next section was published in the following article:
Scheide-Noeth JP, Rosen M, Baumstark D, Dietz H, Mueller TD: **Structural Basis of Interleukin-5 Inhibition by the Small Cyclic Peptide AF17121**. *Journal of molecular biology* 2019, **431**(4):714-731. https://doi.org/10.1016/j.jmb.2018.11.029

4.4 Structure/function analysis of IL-5Rα bound to IL-5 inhibitory peptides

Several approaches have been established to block IL-5 signaling. One of those utilizes small peptides that directly bind to IL-5Rα and competitively block the receptor's interaction with IL-5 (England, B.P. *et al.*, 2000, Ruchala, P. *et al.*, 2004). Two groups of IL-5 inhibiting peptides were identified: monomeric cyclic peptides and disulfide-bridged homodimeric peptides. These peptides block IL-5 signaling *in vitro* very effectively, however little is known about their mechanism of action (Ruchala, P. *et al.*, 2004, Ishino, T. *et al.*, 2005, Ishino, T. *et al.*, 2006, Bhattacharya, M. *et al.*, 2007). Further improvement to potentially render them alternatives to neutralizing antibodies directed against either IL-5 or IL-5Rα in the treatment of eosinophil-mediated diseases, however, would require knowledge about their mechanism of receptor inhibition.

Determining the structure of IL-5Rα C66A bound to either one of the inhibitory peptides will provide information about the flexibility of the wrench-architecture. But even more importantly these structures together with functional analyses will reveal how these small peptides mimic IL-5 when binding to the receptor IL-5Rα. These data have great potential to facilitate rational design of improved IL-5 inhibiting peptides or small-molecule-based pharmacophores yielding novel therapeutics against atopic diseases or the hypereosinophilic syndrome.

4.4.1 Functional analysis of the peptide AF17121 using surface plasmon resonance

The cyclic monomer peptide AF17121 was chosen as the smaller size of the peptide and the less complex inhibition mechanism (1:1 interaction with IL-5Rα) compared to the dimeric peptides (which bind two IL-5Rα molecules) make AF17121 a better starting pharmacophore. The peptide was obtained native and N-terminally biotinylated by chemical synthesis from commercial sources (Centic Biotec).

To determine the affinity of the AF17121 peptide as well as to verify that the obtained AF17121 peptide is active, surface plasmon resonance (SPR) analysis

was performed (s. 3.10). The lyophilized, biotinylated AF17121 was dissolved in PBS and immobilized (100-120 RU) on a neutravidin-coated GLC chip (Biorad) similar to what was described for IL-5 (s. 4.2.1).

For the analysis six different analyte concentrations (log2 dilution) of IL-5Rα C66A with 500 nM as highest concentration were perfused (s. Figure 44). Data was analyzed by applying a simple Langmuir 1:1 interaction model. An affinity of 92 nM was obtained for the interaction of IL-5Rα with AF17121. Compared to the results of the IL-5Rα•IL-5 interaction the IL-5Rα•AF17121 interaction is 20-fold lower. The decreased association rate (k_a) indicates that formation of the IL-5Rα•AF17121 peptide complex is slowed-down compared to the IL-5Rα•IL-5 complex, but complex stability (dissociation rate) is identical for both complexes (s. Table 23).

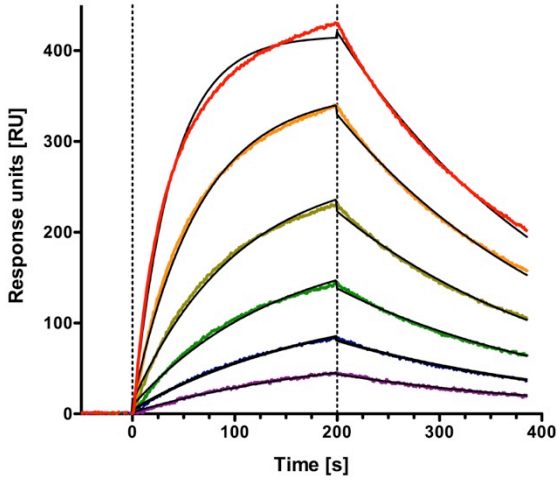

Figure 44: SPR sensorgram of the interaction of hIL-5Rα C66A with AF17121 immobilized. IL-5Rα concentrations: **500 nM**, **250 nM**, **125 nM**, **62.5 nM**, **31.25 nM** and **15.625 nM**. (Flow rate: 100 µl/min; association time 200 s; dissociation time 180 s)

Table 23: Summary of the determined equilibrium constant, association and dissociation rate using the Langmuir 1:1 interaction model of the IL-5Rα C66A ectodomain protein interaction with either AF17121 or IL-5 immobilized on the chip. (n = 3, Rmax = local and Ri = fitted)

Receptor protein	Immobilized	k_a [10^5/Ms]	k_d [10^{-3}/s]	K_D [nM]
IL-5Rα C66A	AF17121	0.5 ± 0.03	4.3 ± 0.1	92 ± 5
IL-5Rα C66A	IL-5	19.0 ± 0.2	1.1 ± 0.3	0.6 ± 0.2

4.4.2 Preparation of the IL-5Rα•AF17121 complex

The purification of IL-5Rα C66A bound to AF17121 was performed using gel filtration. To be able to detect the AF17121 peptide via immunostaining, the biotinylated AF1721 variant was used.

The complex was prepared by mixing IL-5Rα C66A ectodomain and biotinylated AF1721 in a 1:2 molar ratio. The mixture was incubated on ice for 30 min before applying to a Superdex 200 10/300 column (GE Healthcare). The chromatogram showed two UV absorbance maxima (s. Figure 45). The first peak was assumed to contain IL-5Rα protein in complex with AF17121 peptide, while the second peak would then contain AF17121 peptide, which has been used in 2-fold molar excess. This assumption could be confirmed by SDS-PAGE and Dot Blot analysis (s. Figure 46).

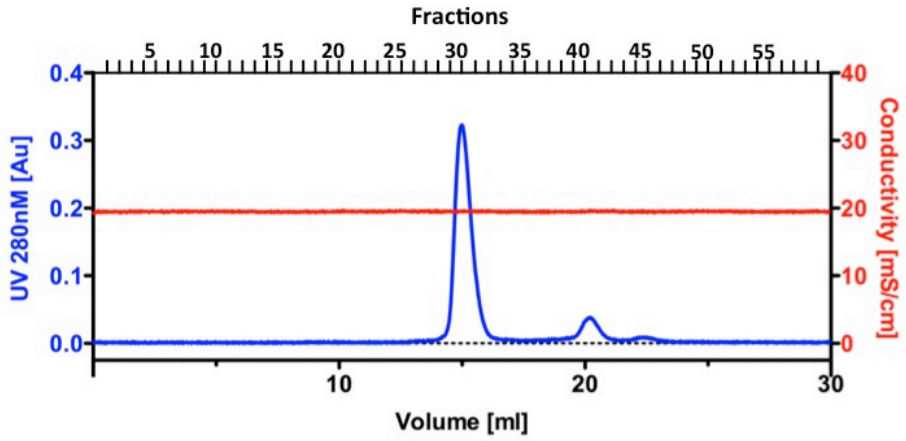

Figure 45: Chromatogram of the gel filtration of the IL-5Rα•AF17121-biotin complex. Blue: UV absorption at 280nm [Au] **Red:** Conductivity [mS/cm]

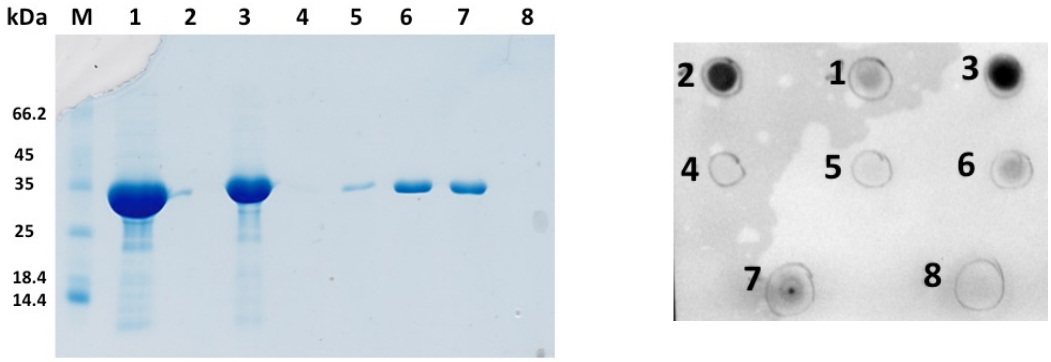

Figure 46: SDS-PAGE (left) and Dot Blot (right) analysis of the gel filtration of the IL-5Rα•AF17121-biotin complex. M: protein standard **1:** IL-5Rα protein before complex preparation **2:** AF17121-biotin before complex preparation **3:** IL5Rα•AF17121 complex before gel filtration **4:** elution fraction 29 **5:** elution fraction 30 **6:** elution fraction 31 **7:** elution fraction 32 **8:** elution fraction 41. Fractions 30-32 were pooled.

IL-5Rα-containing fractions that also comprised AF17121 were pooled and concentrated to about ¼ of the initial volume by ultrafiltration using a membrane with a cut-off of 3 kDa. The purified IL-5Rα•AF17121 complex could be concentrated via ultrafiltration without losing the peptide if the membrane cut-off was 3 kDa or smaller (s. Figure 47).

The obtained results proved the applicability of gel filtration as purification step for the IL-5Rα•peptide complex. Hence for preparative preparation of the complex the native peptide was used and preceded as described above. The molar ratio was set to 1:1.2 (IL-5Rα to peptide) and after incubation on ice for 30 min the protein solution was concentrated by ultrafiltration to 500 µl and stored at 4°C overnight (s. 3.12.1). Gel filtration was performed as described under 3.6.3. The complex was loaded onto a Superdex 200 10/300 column (GE Healthcare) using HBSE 150 as running buffer. Elution fractions were analyzed by SDS-PAGE and fractions of the major elution absorbance maximum were pooled (s. Figure 48).

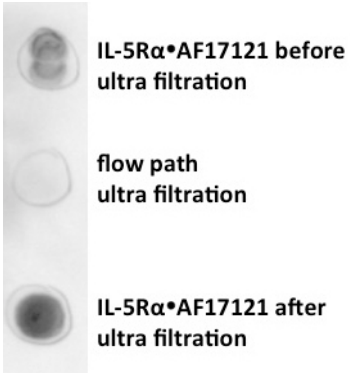

Figure 47: Dot Blot analysis of the ultrafiltration of the IL-5Rα•AF17121-biotin complex.

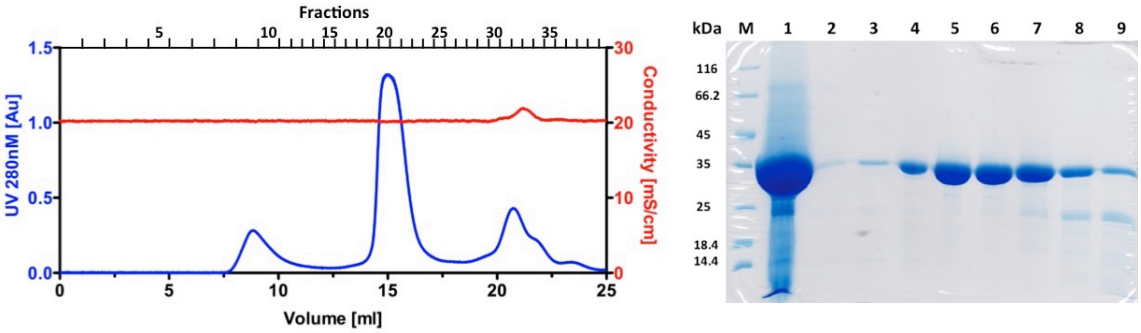

Figure 48: Chromatogram (left) and SDS-PAGE analysis of the gel filtration of the IL-5Rα•AF17121 complex. M: protein standard **1:** IL5Rα•AF17121 complex before purification **2:** elution fraction 18 **3:** elution fraction 19 **4:** elution fraction 20 **5:** elution fraction 21 **6:** elution fraction 22 **7:** elution fraction 23 **8:** elution fraction 24 **9:** elution fraction 25. Fractions 19-25 were pooled. **Blue:** UV absorption at 280nm [Au] **Red:** Conductivity [mS/cm]

To confirm that the complex isolated by gel filtration contained the peptide AF17121 and that the stoichiometry of the complex obeyed 1:1, the complex was analyzed by reversed-phase high-performance liquid chromatography (RP-HPLC). Since the complex was separated by RP-HPLC, the UV absorbance maxima were integrated, and compared to those of individual

reference RP-HPLC experiments performed with identical molar quantities of IL-5Rα C66A and AF17121.

The protein solutions were adjusted to 0.1% TFA (v/v), loaded onto a Phenomenex Jupiter C4 RP-HPLC column. A linear gradient (15 ml 0-100% elution buffer) was used to elute the proteins from the column. Figure 49 shows the elution profiles.

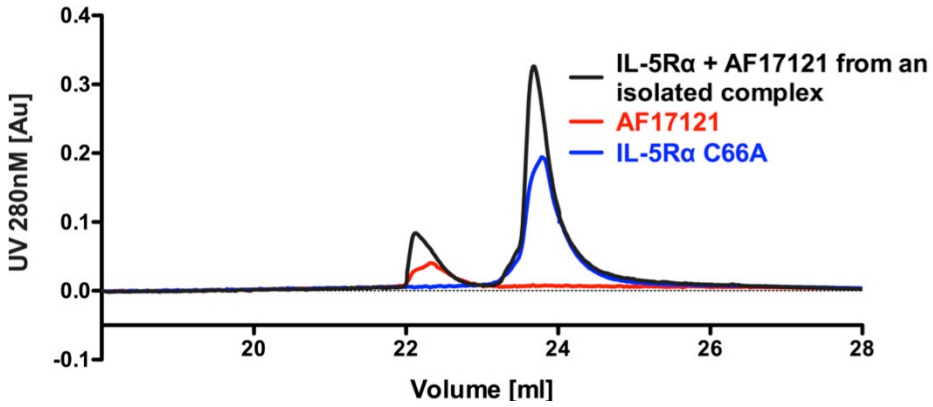

Figure 49: Chromatogram of the reversed-phase high-performance liquid chromatography analysis of the IL-5Rα•AF17121 complex and the single components (IL-5Rα and AF17121). The elution profile range of 18-28 ml is shown.

The volumes of the UV absorbance maxima of the single components and the receptor-peptide complex were calculated using the program Prism (Version 5.0c, GraphPad Software, La Jolla Califronia USA). The peak ratio of the complex (4.6:1) is almost identical to the peak ratio of the single components applied to the analysis in a 1:1 stoichiometric ratio (5:1) (s. Table 24). These results showed that the pooled fractions of the gel filtration of the complex preparation comprised IL-5Rα and AF17121 peptide in the expected 1:1 stoichiometry ratio as assumed.

Table 24: Summary of the calculated volumes under the graph of the complex and single components analyzed via RP-HPLC as well as their corresponding ratios.

	IL-5Rα	AF17121	Ratio
Complex	0.174	0.038	4.58:1
Single components	0.124	0.025	4.96:1
	1.4	1.5	

4.4.3 Crystallization of the IL-5Rα•AF17121 complex

As the structure of the IL-5Rα•AF17121 complex should be determined by X-ray diffraction initial crystallization screens were set up employing the receptor-peptide complex in HBSE 150 buffer (10 mM HEPES pH 7.4, 150 mM NaCl, 3.4 mM EDTA). A Pre-Crystallization Test (PCT, Hampton research, s. 4.3.2) was preformed to select an ideal initial protein concentration for subsequent crystallization trials. However no unambiguous results were obtained, hence a concentration of 5 mg/ml of the purified complex was used in the initial screens.

Initial crystallization screens were performed using sitting drop vapor diffusion setup (s. Figure 50) employing room temperature and using a Honeybee 963 (Digilab) crystallization robot (Rudolf Virchow Centre, University of Würzburg). Each crystallization drop was prepared by mixing 0.3 µl of purified peptide-receptor complex (concentration = 5 mg/ml) and 0.3 µl of the respective reservoir solution. Of the respective reservoir solution 40 µl were filled into each well of the 96-well plate (Crystalquick™ LP Plate, Greiner Bio-One). In two conditions of about 900 different conditions screened, small single crystals grew within 3 weeks (s. Figure 51a-b).

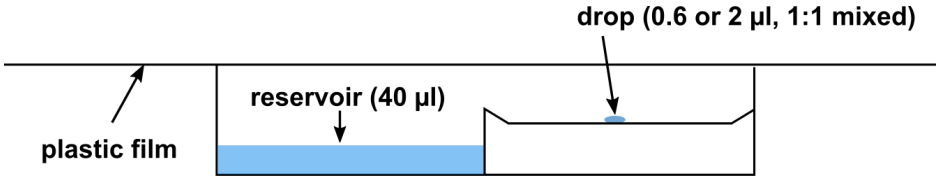

Figure 50: Schematic representation of the vapor-diffusion technique using the sitting drop method used for the crystallization of the peptide-receptor complex.

For both conditions optimization screening was performed, by varying different parameters such as pH value and buffer composition in a systematic manner (s. Appendix page 178, Table 38). However, crystallization could only be reproduced for the crystals that displayed a hexagonal morphology. Optimization screening was then performed with two different drop sizes, 0.3 µl + 0.3 µl and 1 µl + 1 µl. Single crystals of different size, but identical morphology were obtained within 2 weeks (s. Figure 51c-d). These crystals were then used for X-ray data collection.

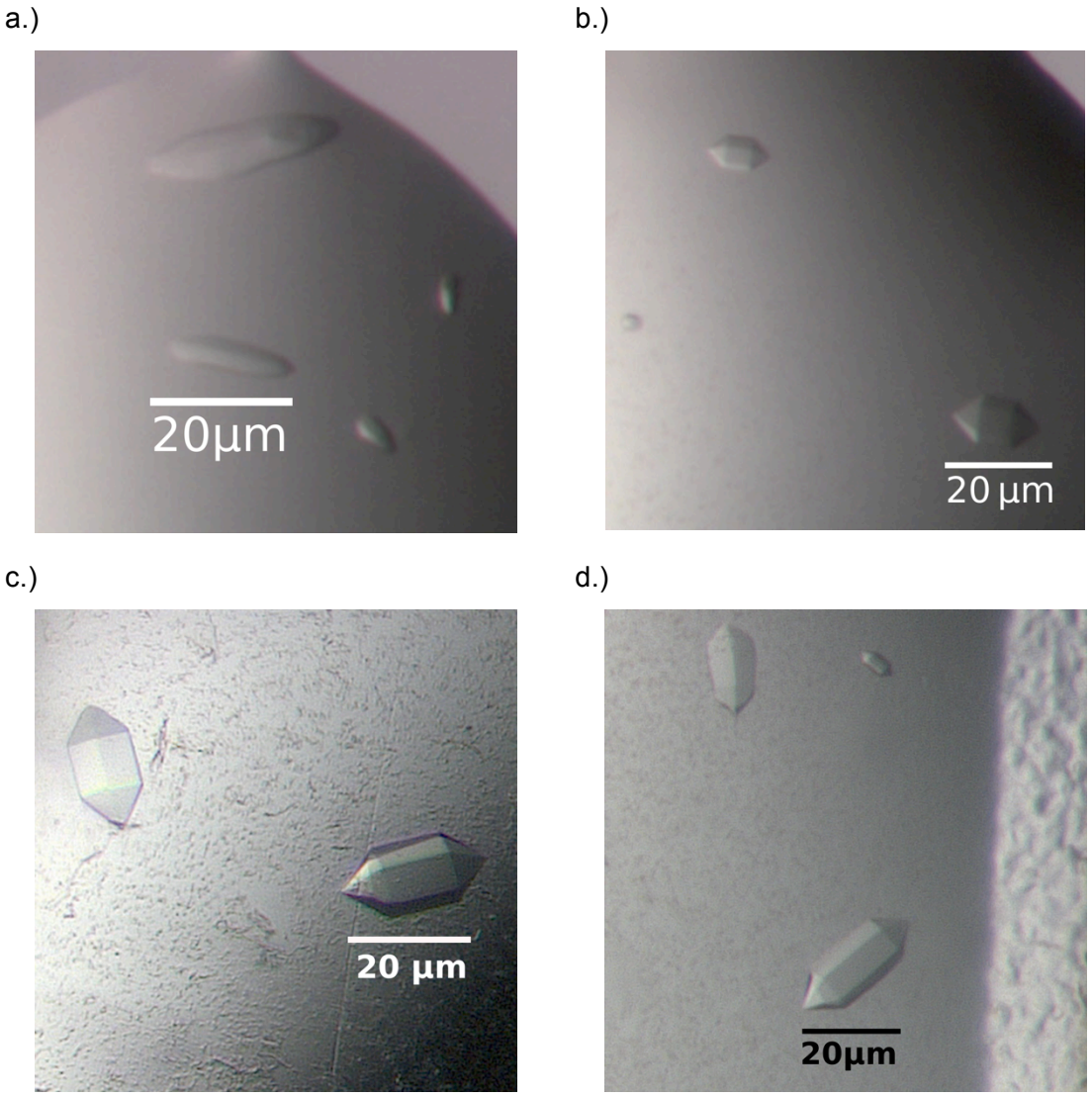

Figure 51: Crystals obtained from initial (a-b) and optimized (c-d) screening of the IL-5Rα•AF17121 peptide complex (after 2-3 weeks). a.) 0.1 M Tris-HCl pH 8. 0, 25% (v/v) PEG 400. **b.)** 0.1 M sodium acetate pH 5.0, 2 % (v/v) PEG 4000, 15% (v/v) 2-methyl-2,4-pentanediol (MPD). **c.)** 0.1 M sodium acetate pH 5.0, 2 % (v/v) PEG 4000, 15% (v/v) MPD; drop size 0.6 µl **d.)** 0.1 M sodium acetate pH 5.0, 2 % (v/v) PEG 4000, 15% (v/v) MPD; drop size 2 µl.

4.4.4 Structure of IL-5Rα•AF17121 receptor-peptide complex shares the wrench-architecture with IL-5•IL-5Rα

Two native data sets were collected from two different single crystals (IL-5Rα•AF17121). A first set was obtained using an X-ray home source (Rigaku MicroMax-007 HF generator, VariMax HF mirror optics and a Rigaku R-AXIS HTC image plate detector, Rudolf Virchow Center, University of Würzburg). Crystals were mounted in a nylon loop and immediately flash-frozen in liquid nitrogen. Crystal-to-detector distance was set to 220 mm, wavelength was 1.54 Å, data were collected by rotating the crystal through 90° (0.5° oscillations) with 600 s exposure per frame at 100 K. The crystal diffracted

to a resolution of 3.0 Å. Data analysis indicated the hexagonal space group $P6_422$ with unit cell parameters *a* = *b* = 137.9 Å, c = 144.1 Å; and α = γ = 90°, and β = 120°.

A second data set was collected at the beamline MX1 at PETRA III (DESY, Hamburg, Germany). Data analysis yielded the same space group ($P6_422$) and angles (α = γ = 90° and β = 120°) as determined before but slightly different unit cell parameters (a = b = 138.13 Å and c = 145.89 Å) were obtained. X-ray diffraction data were indexed, integrated and scaled using *iMOSFLM/MOSFLM* (Battye, T.G. *et al.*, 2011) and *SCALA* (Winn, M.D. et al., 2011) from the *CPP4* program suite. Data collection and processing statistics are summarized in Table 25.

Table 25: Data collection and processing of the IL-5Rα•AF17121 complex

Diffraction source	Home source	DESY PETRA III MX1 – P13
Wavelength (Å)	1.5418	0.97963
Temperature (K)	100	100
Detector	Rigaku R-AXIS HTC	PILATUS 6M-F
Crystal-detector distance (mm)	220	481.78
Rotation range per image (°)	0.5	0.1
Total rotation range (°)	90	180
Exposure time per image (s)	600	0.32
Space group	$P6_422$	$P6_422$
a, *b*, *c* (Å)	137.9, 137.9, 144.1	138.13, 138.13, 145.89
α, β, γ (°)	90, 90, 120	90, 90, 120
Mosaicity (°)	0.55	0.40
Resolution range (Å)	46-3.0 (3.16-3.0)	46-2.8 (2.95-2.8)
Total No. of reflections	179123 (25857)	367694 (56247)
No. of unique reflections	17010 (2406)	20844 (2974)
Completeness (%)	100 (100)	100 (100)
Redundancy	10.5 (10.7)	17.6 (18.9)
$\langle I/\sigma(I)\rangle$	12.4 (1.4[#])	14.5 (2.7)
$R_{r.i.m.}$	0.178 (1.828)	0.164 (3.134)
R_{pim}	0.054 (0.554)	0.040 (0.717)
Overall *B*-factor from Wilson plot ($Å^2$)	41.3	84.7

as data cut-off criteria CC(1/2) was used, which is 0.5 at 3.0 Å. $\langle I/\sigma(I)\rangle$ falls below 2 at a resolution of 3.08 Å.

Phasing was performed employing molecular replacement and the program PHASER (McCoy, A.J. *et al.*, 2007) of the CPP4 program suite. The structure of the IL-5Rα C66A ectodomain protein derived from the binary complex IL-5Rα•IL-5 (PDB ID: 3QT2) was used as template. Each of the three FNIII domains of IL-5Rα was used separately as template during molecular replacement analyses. The preliminary structure data indicated that the IL-5Rα protein is arranged similar as observed in complex with IL-5 suggesting that the wrench-like architecture is likely preformed (s. Figure 52).

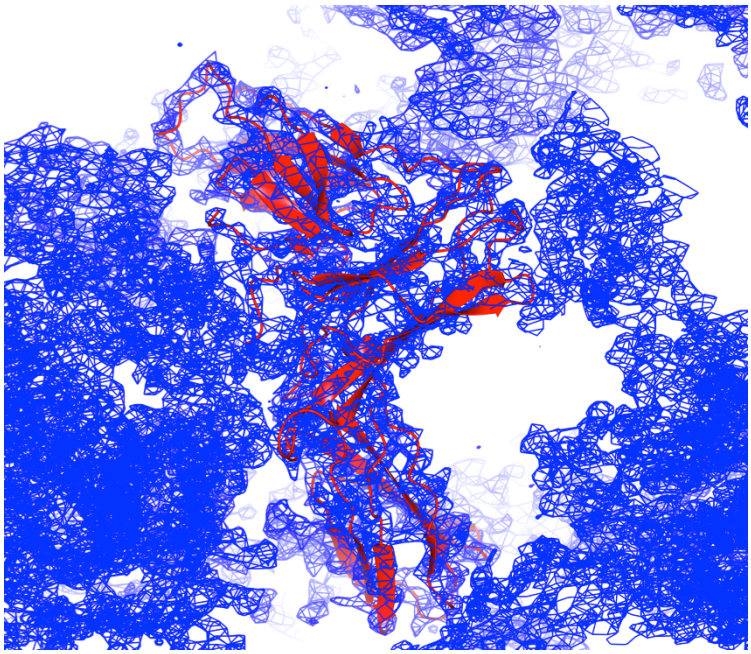

Figure 52: Electron density map of the IL-5Rα•AF1721 complex. The electron density map displays density areas occupied by proteins (blue) in which the IL-5Rα molecule (red ribbon) is placed. Empty areas corresponding to crystal solvent molecules that are not ordered, e.g. water.

The cyclic AF17121 peptide was manually modeled into the electron density map using the tool X-Built of the software suite Quanta (Accelrys MSI) and Coot (Emsley, P. *et al.*, 2010). The structure of the IL-5Rα•AF17121 peptide complex could be determined through repeated rounds of refinement using Refmac5 (Vagin, A.A. *et al.*, 2004) and manual modeling using Coot. Details of the refinement statistics are shown in Table 26.

Table 26: Refinement statistics of the IL-5Rα•AF17121 complex.

Resolution (Å)	43.2 - 2.75 (2.85 - 2.75)
Number of reflections	21878 (2119)
R_{work}/R_{free} (%)	20.2 (33.6) / 22.6 (36.7)
FOM	0.81 (0.72)
TLS groups	2 (group 1: IL-5Rα Lys7 - Arg315; group 2: AF17121 Val1 - Glu18)
Number of atoms	
Protein	2637 (327 residues)
Water	24
Average *B* factors	
Protein (Å^2)	106.2
Water (Å^2)	91.3
RMSD	
Bond lengths (Å)	0.003
Bond angles (°)	0.91
Ramachandran analysis[a]	
Favored (%)	93.5 (306 of 327 residues)
Outliers (%)	1.9 (6 of 327 residues)
Clashscore[b]	7.5
Rotamer outliers (%)	1.4 (4 of 327 residues)

Values in parentheses are for the highest resolution shell
[a] as reported by MolProbity analysis
[b] as reported by Phenix version 1.9.1692 (calculated as 1000 x (number of bad overlaps/number of atoms))

Surprisingly, the architecture of the AF1721 peptide-bound IL-5Rα ectodomain was found basically identical to the wrench-like architecture in the IL-5•IL-5Rα binary complex, providing further evidence that the wrench-like IL-5Rα architecture might be largely preformed. The peptide binds into the cleft formed by the IL-5Rα domains D1 and D2, but in contrast to IL-5, AF17121 shares no contacts with domain D3 (s. Figure 53).

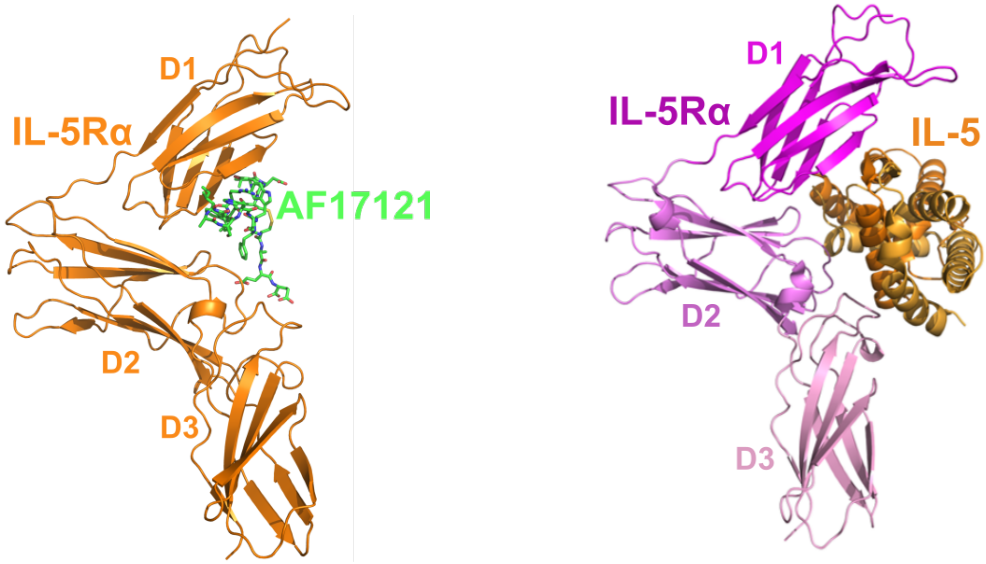

Figure 53: Left: Ribbon plot representation of the crystal structure of the AF17121•IL-5Rα complex [PDB ID: 6H41; Scheide-Noeth, J.P. *et al.* 2019]. **Right:** Crystal structure of the binary complex of IL-5 bound to IL-5Rα [PDB ID: 3QT2; Patino, E. *et al.* 2011].

Structure analysis further revealed that the interface between IL-5Rα and AF17121 comprises of additional polar bonds besides three main chain-main chain groups, i.e. AF17121 Ile8 (amide) to IL-5Rα Val67 (carbonyl), AF17121 Arg6 to IL-5Rα Lys 65 (carbonyl) and Val 67 (amide). The negative charge of Glu3 (AF17121) might engage in a coulomb interaction with the positively charged Lys65 of IL-5Rα (s. Figure 54a). A 13-fold decrease in binding affinity was observed when Asp2 and Glu3 were simultaneously exchanged, indicating that one or both acidic residues are involved in polar interactions with IL-5Rα (Ruchala, P. *et al.*, 2004, Ishino, T. *et al.*, 2006). Two hydrogen bonds between the carboxylate group of AF17121 Glu17 and the amide of IL-5Rα Arg188 as well as the hydroxyl group of Tyr155 fixate the C-terminus in a similar manner (s. Figure 54b). A polar bond might also exist between the guanidinium group of IL-5Rα Arg188 and the C-terminus of AF17121. Exchanging the C-terminal acid residues Glu17 and Glu18 with alanine simultaneously decrease IL-5Rα binding by about 10-fold, similar as observed for Asp2 and Glu3 of AF17121 (Ruchala, P. *et al.*, 2004, Ishino, T. *et al.*, 2006). The loss in binding is however mediated

differently as surface plasmon resonance analysis revealed. Whereas AF17121 D2A/E3A slows done complex formation, AF17121 E17A/E18A increase complex dissociation (Ishino, T. *et al.*, 2006). Structure analysis suggests that "long-range" electrostatic forces between the N-terminal acidic residues of the peptide and a complementary charged patch in IL-5Rα facilitate complex formation rate. In contrast polar bonds (described above) between the C-terminal glutamate residues of the peptide and residues of the receptor stabilize the complex and hence mutation of these residues affects complex dissociation rate. Analysis of the charge distribution of IL-5Rα and AF17121 reveals a highly complementary surface potential for N- and C-terminal acid residues. AF1721 Asp2 and Glu3 are located nearby a small positively charged patch around IL-5Rα Lys65, AF17121 Glu17 and Glu18 are close to a larger positively patch formed by IL-5Rα Lys186, Arg188 and Arg297 (s. Figure 55). Despite their multiple polar bonds to residues of IL-5Rα, the acidic residues do not represent the hot spot of binding of the peptide-receptor interaction as simultaneous exchange of all four acidic residues with alanine resulted in only a 100-fold decrease in binding (Ishino, T. *et al.*, 2006).

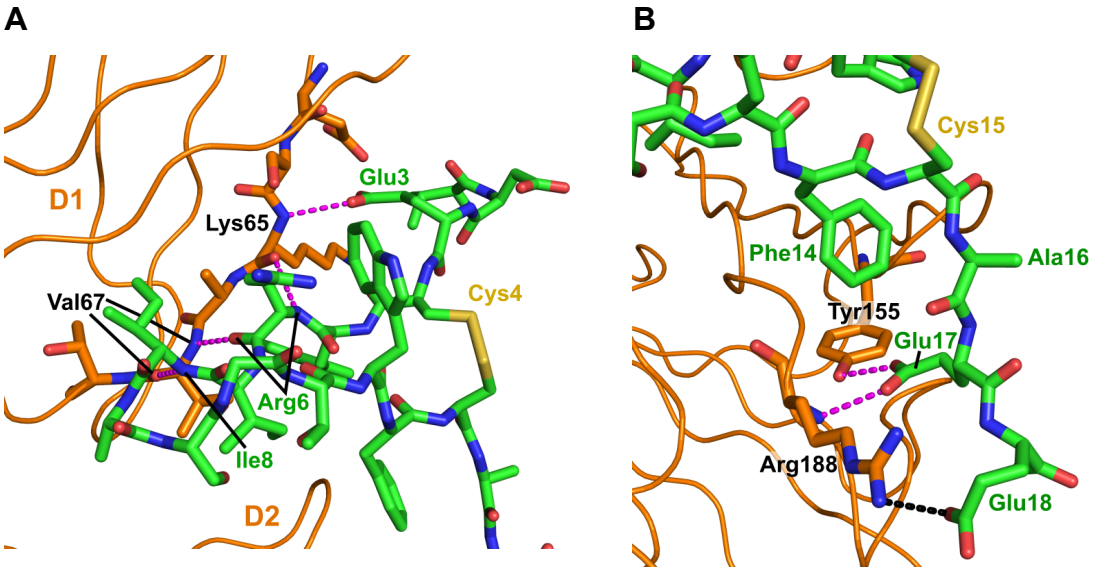

Figure 54: Polar bonds in the AF17121•IL-5Rα interface. A: Hydrogen bonds (indicated as magenta stippled lines) are formed between Arg6 of AF17121 (carbon atoms in green) with Lys65 and Val 67 of IL-5Rα and Ile8 (AF17121) with Val67 (IL-5Rα). At the N-terminus of AF17121 a hydrogen bond is formed between Glu3 and Lys65 of IL-5Rα. **B:** Polar bonds between the C-terminus of AF17121 and IL-5Rα. The carboxylate group of AF17121 Glu17 engages in two hydrogen bonds, i.e. hydroxyl group of Tyr155 and the amide of Arg188 of IL-5Rα. Another polar bond is potentially formed between the C-terminus of AF17121, i.e. Glu18 and the guanidinium group of Arg188 (stippled black line). [PDB ID: 6H41; Scheide-Noeth, J.P. *et al.* 2019*]

* Copyright s. 9.6 (page 179)

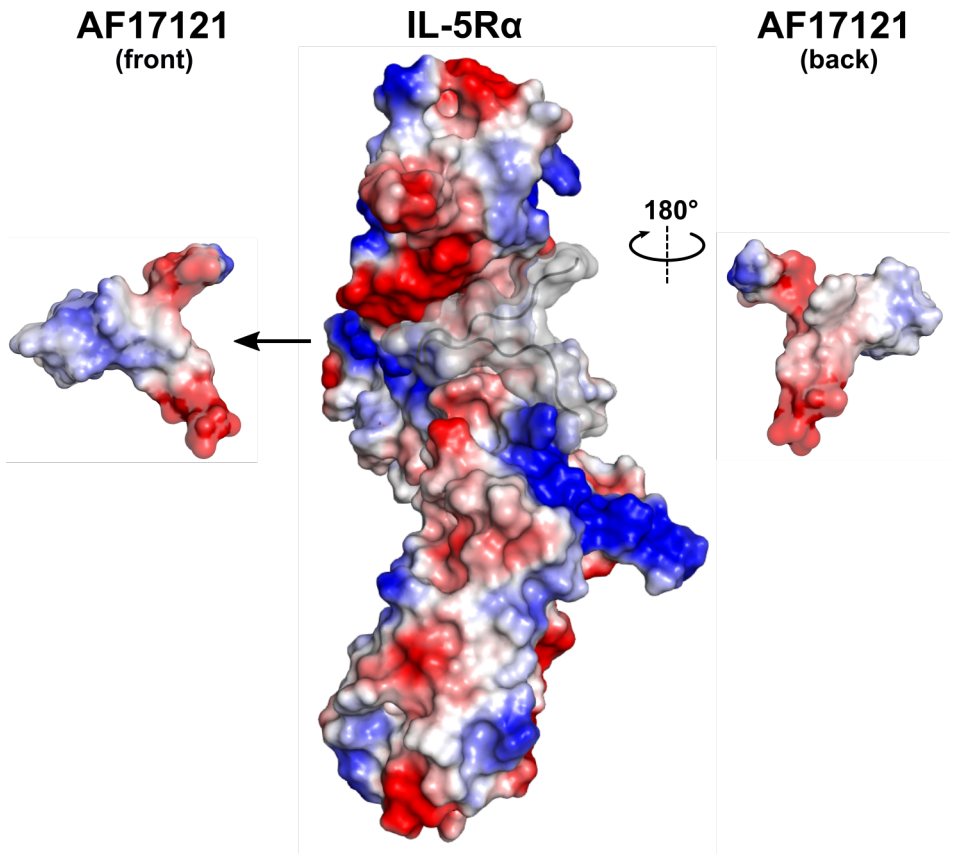

Figure 55: A complementary electrostatic potential of AF17121 and IL-5Rα drives peptide recognition and binding. A simplified electrostatic potential was calculated with PyMOL (vacuum electrostatic potential) and mapped onto the solvent-accessible surface of the two interaction partners to qualitatively visualize the charge distribution at the protein surface. **(Middle panel)** Electrostatic potential map of IL-5Rα, the position of bound AF17121 is indicated by a transparent surface of AF17121 and a Cα-trace of the peptide. **(Left panel)** Electrostatic potential map of AF17121 (front). For visualization the peptide is moved from its bound position by translating the peptide molecule to the left without rotation. **(Right panel)** Electrostatic potential map of AF17121 (back). For visualization the peptide was moved to the right and rotated around the y-axis by 180°. [PDB ID: 6H41; Scheide-Noeth, J.P. *et al.* 2019*]

The guanidinium group of AF17121 Arg6 and the carboxylate group of IL-5Rα Asp55 form a bi-dentate salt bridge, which is shielded from solvent access by several surrounding residues, i.e. Ile8, His11 and Trp13 of AF17121 and Tryp57 of IL-5Rα (s. Figure 56). Studies performed by Ruchala, P *et al.* (2004) showed that replacing Arg6 with alanine or lysine completely abrogated binding *in vitro*. Together with the observation that alanine mutation of Asp55 of IL-5Rα abolished binding of AF17121 (Ishino, T. *et al.*, 2005) led to the suggestion that Arg6 of AF17121 mimics Arg91 of IL-5 (Ishino, T. *et al.*, 2006), which from structure data of the IL-5•IL-5Rα complex is known to also interact with IL-5Rα Asp55 (Patino, E. *et al.*, 2011, Kusano, S. *et al.*, 2012). Comparing the interaction on the molecular level for both arginine residues with IL-5Rα

* Copyright s. 9.6 (page 179)

revealed fundamentally differences. Arg91 together with Arg32 and Arg90 of IL-5 form multiple polar bonds with acidic residues of IL-5Rα, i.e. Glu44, Asp55 and Glu58, resulting in a polar zipper-like interaction (Patino, E. *et al.*, 2011). Arg6 of AF17121 in contrast forms an isolated bi-dentate salt bridge with Asp55 of IL-5Rα. Orientation of the side chain of AF17121 Arg6 is mediated via van der Waals contacts, whereas the side chain of Arg91 is positioned through polar bonds. Highly important for the interaction of AF17121 Arg6 with IL-5Rα Asp55 is the fact that three of the four surrounding residues are of aromatic nature, i.e. His11 and Trp13 of AF17121 and Tyr57 of IL-5Rα. Arrangement and orientation of these residues leads to the formation of a π-π electron stacking system, which very likely strongly potentiate the polar interaction. Mutagenesis studies of Trp13 revealed that not only the size, but also the configuration of the aromatic ring system matters at this position (Bhattacharya, M. *et al.*, 2007). AF17121 His11 possibly coordinates Asp55 of IL-5Rα by forming a hydrogen bond between the imidazole nitrogen and the aspartate carboxylate group. Mutation of His11 to alanine decreased the binding affinity towards IL-5Rα by about 10-fold revealing its significance for the peptide-receptor interaction (Ishino, T. *et al.*, 2006).

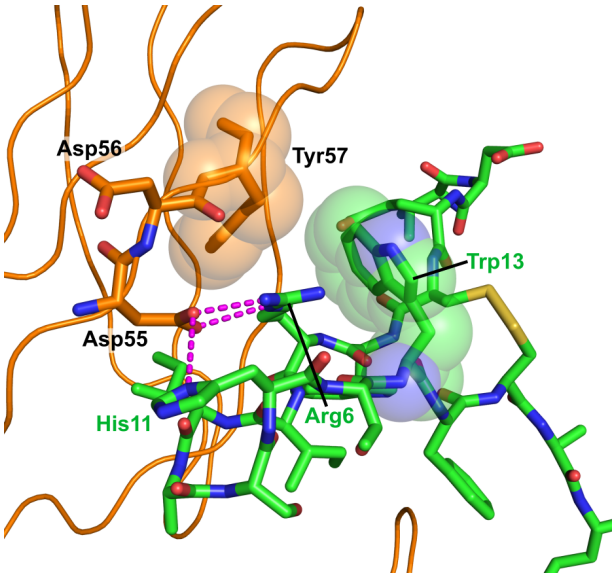

Figure 56: Hot spot polar bond in the AF17121•IL-5Rα interface. The bi-dentate salt bridge (stippled magenta lines) between the guanidinium group of Arg6 and the carboxylate group of IL-5Rα Asp55 is the key determinant of AF17121 binding to IL-5Rα. Its strength is likely potentiated by ππ-stacking interactions with AF17121 Trp13 from the side (transparent van der Waals spheres are shown) and IL-5Rα Tyr57 from the top. AF17121 His11 possibly coordinates IL-5Rα Asp55 with another hydrogen bond and additionally shields the Arg6•Asp55 interaction. [PDB ID: 6H41; Scheide-Noeth, J.P. *et al.* 2019*]

* Copyright s. 9.6 (page 179)

In addition to these polar bonds a number of hydrophobic residues of AF17121 share contacts with IL-5Rα and might thus contribute to binding. Upon complex formation with IL-5Rα the hydrophobic peptide residues Trp5, Ile7, Ile8 and Phe14 become buried (≥ 60% of the solvent accessible surface), with Trp5 and Ile8 sharing the largest total surface area of about 130 $Å^2$ each (s. Figure 57a-c). The contribution to the overall binding energy of these four residues however varies greatly. Trp5 and Ile8 seem not to contribute to binding energy at all, whereas exchanging Ile7 and Phe14 with alanine decreased IL-5Rα affinity by 18- and 10-fold, respectively (Bhattacharya, M. et al., 2007). The structure does not provide a clear explanation for the rather large difference. A π-π stacking interaction between Phe14 and the carboxylate group of IL-5Rα Asp189 might explain the contribution of Phe14 to peptide binding (s. Figure 57a), even though Trp5 engages in a similar interaction with IL-5Rα Gln25 (s. Figure 57b). AF17121 Ile8 seemingly engages in a perfect knob-into-hole interaction with a hydrophobic cleft in domain D1 of IL-5Rα formed by Leu28, Ile49, Try57, Thr68 and Phe74, but mutation to alanine did not alter IL-5Rα binding. On the other hand, a major drop in binding to IL-5Rα was observed for mutation of AF17121 Ile7 to alanine, which forms similar hydrophobic contacts with IL-5Rα Val67 and Trp190 (s. Figure 57c).

The structure shows for the first time the IL-5Rα C66A in complex with a ligand other than the native ligand IL-5. The identical overall architecture of hIL-5Rα in both structures indicates that the wrench-architecture is possibly preformed. The structural data additionally revealed a minimum interaction interface required for small inhibitory molecules/peptides to be specifically recognized by IL-5Rα. The obtained structural information’s provide a starting point for the optimization of already existing IL-5 inhibitors and/or the development of new ones.

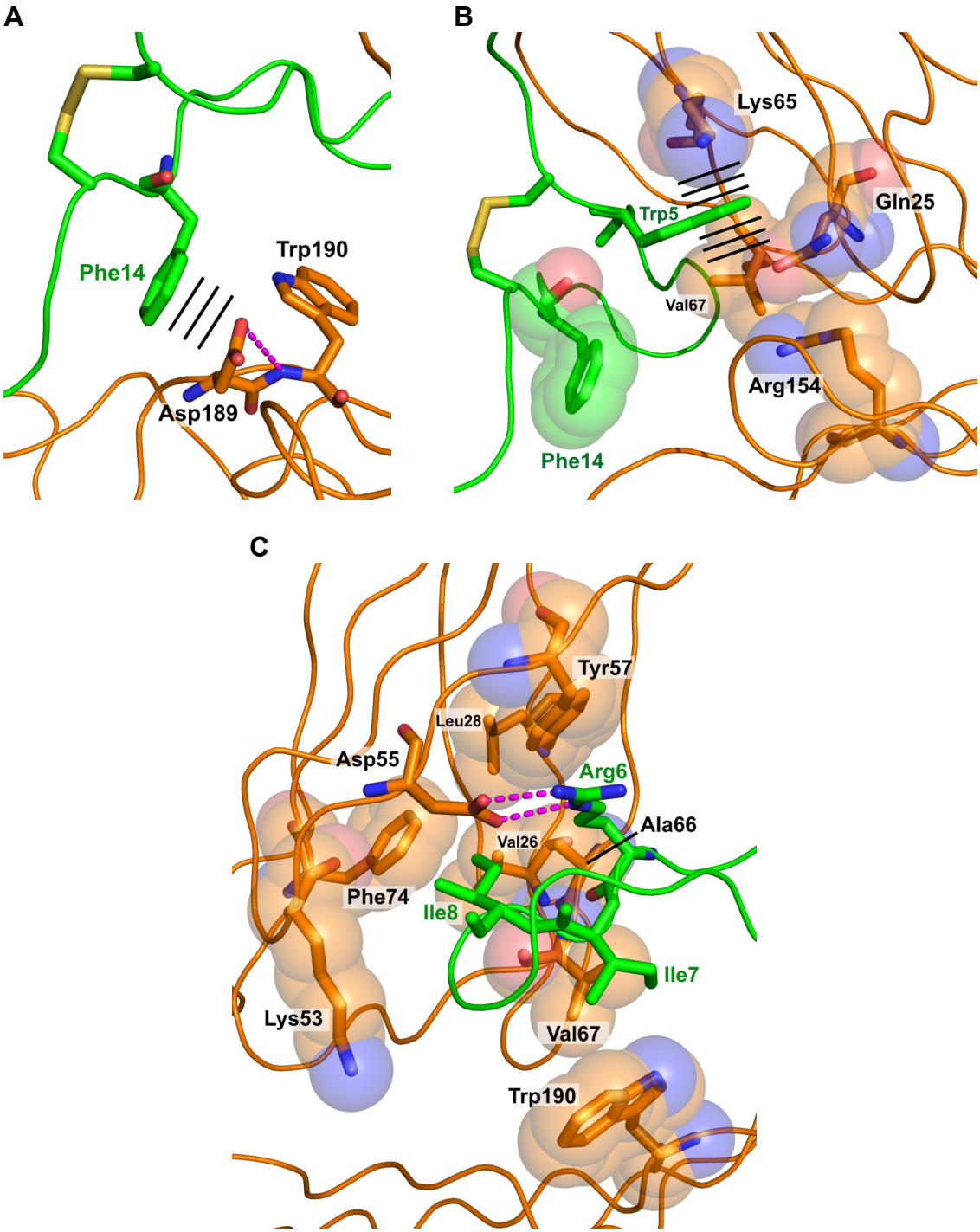

Figure 57: Hydrophobic interaction in the AF17121•IL-5Rα interface. Besides polar bonds, hydrophobic and ππ-stacking (indicated with parallel lines) interactions are found in the AF17121•IL-5Rα complex. **A:** AF17121 Phe14 forms a ππ-stacking interaction with the carboxylate group of IL-5Rα Asp189. This interaction is additionally shielded by IL-5Rα Trp190. **B:** AF17121 Trp5 stacks with the carboxamide group of IL-5Rα Gln25, which stacks with IL-5Rα Arg154. The amine group of Lys65 possibly engages in favorable amine-π electron interactions with AF17121 Trp5. **C:** Isoleucine 7 and 8 of the peptide make hydrophobic contacts with surrounding residues of IL-5Rα. Ile7 is packed between IL-5Rα Val67 and Trp190 and additionally shielded by residues of the peptide. Ile8 makes a knob-into-hole interaction with IL-5Rα Val26, Leu28, Ala66 and Phe74. [PDB ID: 6H41; Scheide-Noeth, J.P. *et al.* 2019*]

* Copyright s. 9.6 (page 179)

4.4.5 Differences and similarities of IL-5Rα recognition between IL-5 and AF17121

To functionally analyze the structure of the IL-5Rα•AF17121 complex and to test how the recognition of AF17121 and IL-5 by IL-5Rα differs, a detailed mutagenesis screening (25 variants of IL-5Rα were prepared) was performed and variants were analyzed by *in vitro* interaction analysis (side-by-side) employing SPR.

Two different types of variants were produced. The first set ("IL-5 binding affecting mutants") comprised IL-5Rα variants that were identified to be important for binding of IL-5Rα to IL-5. The second set ("AF17121 mutants") comprised IL-5Rα variants that were chosen based on the structure of the IL-5Rα•AF17121 complex and that were assumed to contribute to the IL-5Rα•AF17121 interaction (these variants had not been reported in the literature before).

The IL-5Rα C66A variants were generated by site directed introduction of single amino acid mutations (s. 3.2.1) using the corresponding oligonucleotides (s. 3.1.4). The variant proteins were produced and purified according to the protocol in 4.1.2 using the BL21 Gen-X *E. coli* strain. IL-5Rα C66A protein was used as reference under identical conditions. Figure 58 and Figure 59 displays SDS-PAGE analysis of the 25 IL-5Rα variants produced as a summary.

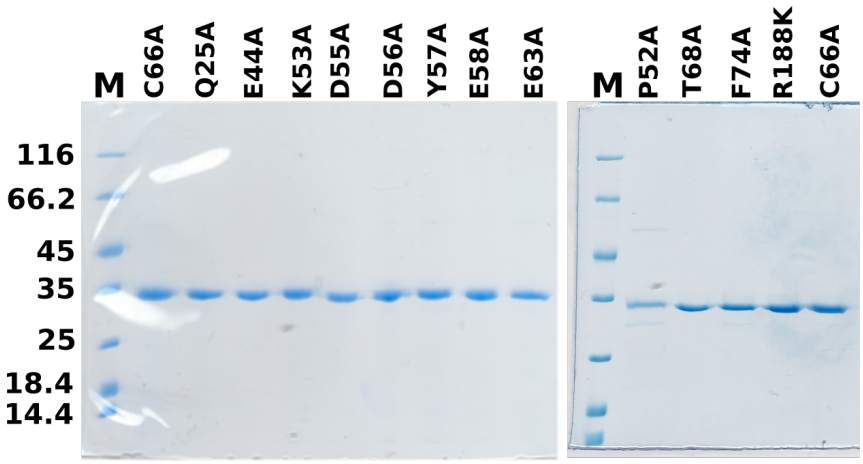

Figure 58: SDS-PAGE analysis of the produced and final purified IL-5Rα variants. 1.5 µg of each IL-5Rα variant were loaded onto the SDS-PAGE.

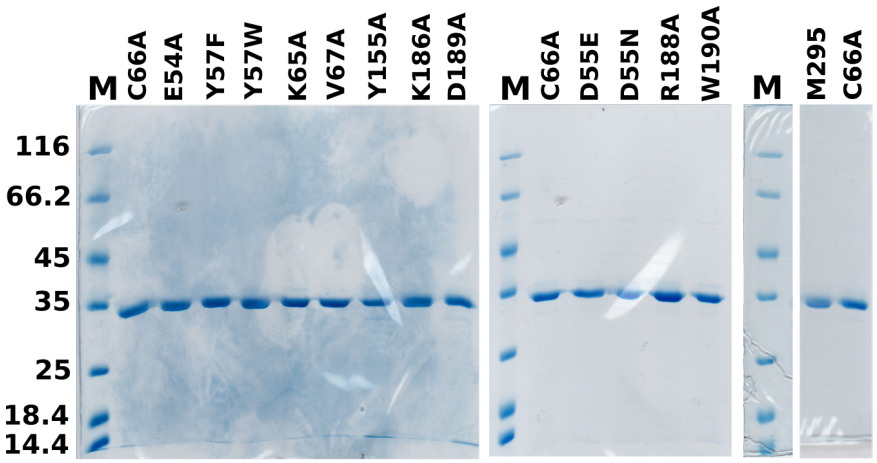

Figure 59: SDS-PAGE analysis of the produced and final purified IL-5Rα variants. 1.5 µg were loaded onto the SDS-PAGE.

The *in vitro* interaction analyses of the IL-5Rα variants were performed using SPR. About 220-240 RU of biotinylated IL-5 protein and 110-130 RU of biotinylated AF17121 peptide were immobilized on a neutravidin-coated GLC sensor chip (Biorad) as described for IL-5 (s. 4.2.1) or for the peptide (s. 4.4.1). For quantitative analysis 12 different concentrations (log 2 dilution) for the analyte IL-5Rα C66A variants were prepared, starting with 250 nM as highest concentration. The analytes were perfused over the chip surface in two different steps (six concentrations per step). To completely remove bound IL-5Rα, the chip surface was regenerated and equilibrated after each measurement. SPR data were analyzed using a simple Langmuir 1:1 interaction model and six analyte concentration were used to deduce the equilibrium constant (K_D), association rate (k_a) and dissociation rate (k_d) if not specified otherwise. To subtract bulk face effects and non-specific interaction a reference flow cell was used for IL-5 and for AF17121 interspots were used.

The evaluation revealed that Asp55, Tyr57 and Arg188 of IL-5Rα are important residues for interaction of IL-5Rα with both ligands, IL-5 and AF17121. Alanine mutation of these residues dramatically reduced binding affinity to IL-5 as well as the peptide. Mutation of Asp55 to either asparagine or glutamic acid showed a smaller loss of affinity for IL-5 when compared to substitution with alanine, this effect was however not observed for AF17121. Exchanging Tyr57 with phenylalanine or tryptophan did not affect binding of AF17121, but significantly (decrease or increase by more than 2-fold) reduced the affinity of IL-5Rα towards IL-5. The same could be observed for the variant Il-5Rα R188K. Replacing Glu44, Glu54 and Asp189 with alanine did neither affect IL-5 nor

peptide binding. Alanine mutations of Asp56, Glu58, Lys186 and Met295 only decreased the interaction of IL-5Rα with IL-5, but not of the peptide. The IL-5Rα variant E63A had no effect on IL-5, but to our surprise significantly increased the affinity of IL-5Rα for the peptide AF17121 (s. Table 27). This observation might provide a hint for potential affinity maturation of the peptide.

Table 27: Relative (rel.) equilibrium constants, association and dissociation rates of the interaction of IL-5Rα variants with either AF17121 or IL-5. (n = 3)

AF17121				IL-5		
rel. k_a	rel. k_d	rel. K_D	Receptor	rel. k_a	rel. k_d	rel. K_D
1.2	1.0	0.80[a]	E44A	0.9	1.7	1.8
1.0	1.4	1.5[a]	E54A	1.1	1.5	1.4
n.b.	n.b.	n.b.	D55A	0.5	25.0	53.0[a]
n.b.	n.b.	n.b.	D55N	0.8	4.0	5.0
n.b.	n.b.	n.b.	D55E	0.9	4.4	4.8
1.1	1.2	1.1[a]	D56A	0.5	21.6	40.7[a]
n.b.	n.b.	n.b.	Y57A	0.2	20.5	91.6[a]
1.0	1.2	1.3[a]	Y57F	1.1	3.2	2.9
1.0	0.9	0.9[a]	Y57W	1.2	5.8	4.5
1.1	1.1	1.0[a]	E58A	0.9	2.3	3.0
1.4	0.7	0.5[a]	E63A	1.0	1.1	1.1
0.6	1.0	1.8[a]	K186A	0.6	11.4	19.3
0.4	1.6	340	R188A	0.5	21.8	49.8[a]
1.2	0.9	0.8	R188K	0.04	5.1	132.5[b,c]
1.3	0.8	0.6[a]	D189A	0.7	0.7	0.9
1.5	0.9	0.7[a]	M295A	0.2	1.9	10.0[b,c]

a: Rmax = local

a: 60 s of dissociation phase used
b: Ri = local fitted
c: five concentrations used

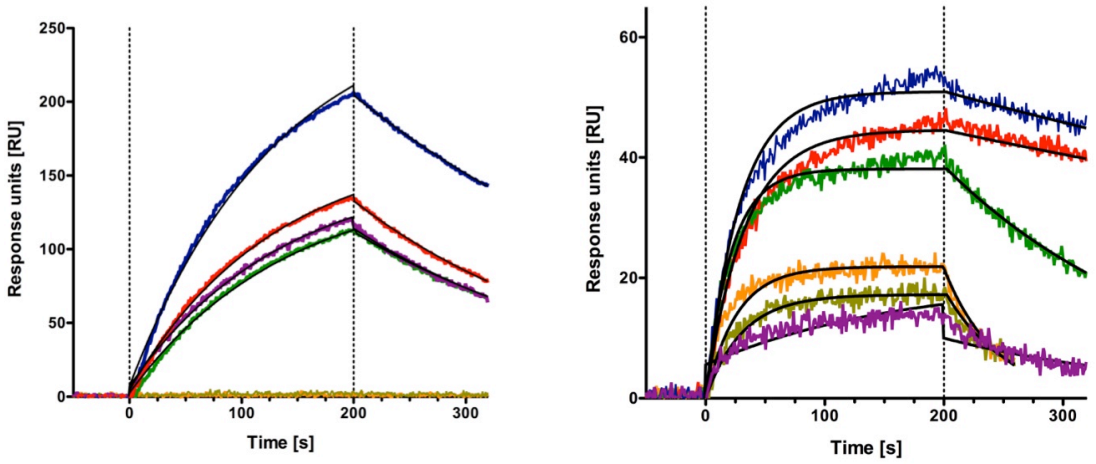

Figure 60: SPR sensorgrams of the interaction of hIL-5Rα C66A variants with AF17121 (left) or IL-5 (right). Biotinylated IL-5 and AF17121 were captured onto a neutravidin-coated GLC sensor surface at densities of about 200 to 250 RU (for IL-5) and about 100 to 150 RU (for AF17121). IL-5Rα variants were perfused as analytes over the biosensor employing six concentrations typically ranging from 250 to 7.8 nM for AF17121 and from 15.6 to 0.5 nM for IL-5. IL-5Rα concentrations: AF17121 62.5 nM and IL-5 15.6 nM are shown respectively. **C66A**, **D55A**, **Y57A**, **Y57W**, **E63A** and **R188K**. (Flow rate: 100 µl/min; association time 200 s; dissociation time 120 s)

Surface plasmon resonance analysis of the second set of IL-5Rα C66A variants revealed that alanine replacement of Gln25, Lyn53, Val67 and Trp190 only affected interaction of IL-5Rα with the peptide. Of these mutations, receptor variant K53A showed a surprisingly increased affinity towards AF17121 due to an increased association and a decreased dissociation rate. The IL-5Rα residues Ile49, Pro52, Thr68 and Phe74 form a hydrophobic pocket, in which the Ile8 of AF17121 is positioned. Contrary to our expectations alanine substitutions of these residues did not only affect the interaction with the peptide but also with IL-5. There is no evidence of direct or indirect interaction of these residues with IL-5 as observed for the peptide. The affinity loss observed for the IL-5Rα variants I49A, P52A and F74A are due to a dramatically reduced association rate for the IL-5 interaction. A similar effect was observed for the interaction of these IL-5Rα variants with AF17121, but reduction of the association rate was less pronounced. The variant I49A showed an increased dissociation rate in addition. The alanine replacement of Thr68 had no effect on interaction with AF17121 but affected IL-5 binding. The variants K65A and Y155A negatively affected the binding of both, IL-5 and AF17121 (s. Table 28).

Table 28: Relative (rel.) equilibrium constants, association and dissociation rates of the interaction of IL-5Rα variants with either AF17121 or IL-5. (n = 3)

AF17121				IL-5		
rel. k_a	rel. k_d	rel. K_D	Receptor	rel. k_a	rel. k_d	rel. K_D
0.8	1.9	2.3	Q25A	0.8	1.4	1.7
0.3	2.6	8.0[b,c]	I49A	0.02	1.3	57.3[a]
0.1	0.6	6.4[a,d]	P52A	0.02	0.9	61.7[a]
1.3	0.3	0.2[a]	K53A	1.1	1.0	0.9
0.5	4.0	8.2	K65A	0.9	3.1	3.2
0.7	3.4	5.0	V67A	0.8	0.9	1.2
1.3	1.0	0.8[a]	T68A	0.5	1.4	3.3[a,b]
0.1	1.1	11.2[b,d]	F74A	0.02	1.3	60.5[a]
0.3	1.6	5.6	Y155A	0.2	3.8	15.5
0.9	2.3	2.8	W190A	1.1	1.2	1.1

a: Rmax = local
b: Rmax = constant
c: four concentrations used
d: three concentrations used

a: Ri = local fitted
b: three concentrations used

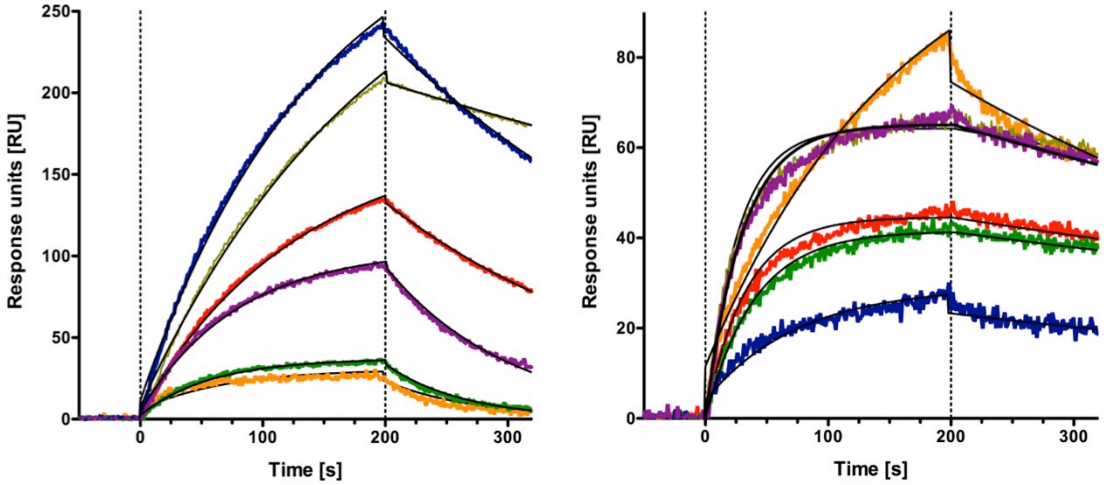

Figure 61: SPR sensorgrams of the interaction of hIL-5Rα variants with AF17121 (left) or IL-5 (right). Biotinylated IL-5 and AF17121 were captured onto a neutravidin-coated GLC sensor surface at densities of about 200 to 250 RU (for IL-5) and about 100 to 150 RU (for AF17121). IL-5Rα variants were perfused as analytes over the biosensor employing six concentrations typically ranging from 250 to 7.8 nM for AF17121 and from 15.6 to 0.5 nM for IL-5. IL-5Rα concentrations: AF17121 62.5 nM and IL-5 15.6 nM are shown respectively. **C66A**, **I49A**, **K53A**, **V67A**, **T68A** and **W190A**. (Flow rate: 100 µl/min; association time 200 s; dissociation time 120 s)

The structure-function analysis conducted in this study confirmed that the peptide-receptor interaction is less polar and differs significantly from the IL-5•receptor interaction, which is based on a large number of intermolecular hydrogen bonds. While there seems to be a similar key element in the recognition epitope, involving Asp55 of IL-5Rα and Arg6 of A17121 or Arg91 of the native ligand IL-5, several residues of IL-5Rα however differ in their importance for binding of the peptide or IL-5.

4.4.6 Is the IL-5Rα wrench-architecture prefixed or formed upon ligand binding?

The results of Patino, E. *et al* (2011) indicated that the wrench-like architecture of the IL-5Rα ectodomain might be preformed and fixed (Patino, E. *et al.*, 2011). The structures of IL-5Rα of the complexes AF17121•IL-5Rα and IL-5•IL-5Rα could be superimposed almost perfectly (r.m.s.d. about 1.4 Å for the Cα-atoms of residues 7 to 313). While an identical architecture when bound to two structurally vastly different ligands seemingly confirms the above-described hypothesis, data from thermal shift assays of IL-5Rα (described under 4.3.1) pointed toward a selection fit binding mechanism. Therefore, to test whether the peptide AF17121 and IL-5 require different flexibility, IL-5Rα variants with mutations in the D1-D2 interface, including L23A, I69A, H71A, L194A, P206A, D208A and L210A that potentially modulate the flexibility of the wrench-architecture were generated. Their impact on AF17121 and IL-5 binding was analyzed by SPR to provide information on binding kinetics.

Generation of the IL-5Rα variants, recombinant expression and purification, as well as SPR analysis were performed as described for the IL-5Rα variants in 4.4.5. Figure 62 shows SDS-PAGE analysis of the IL-5Rα variants produced as a summary.

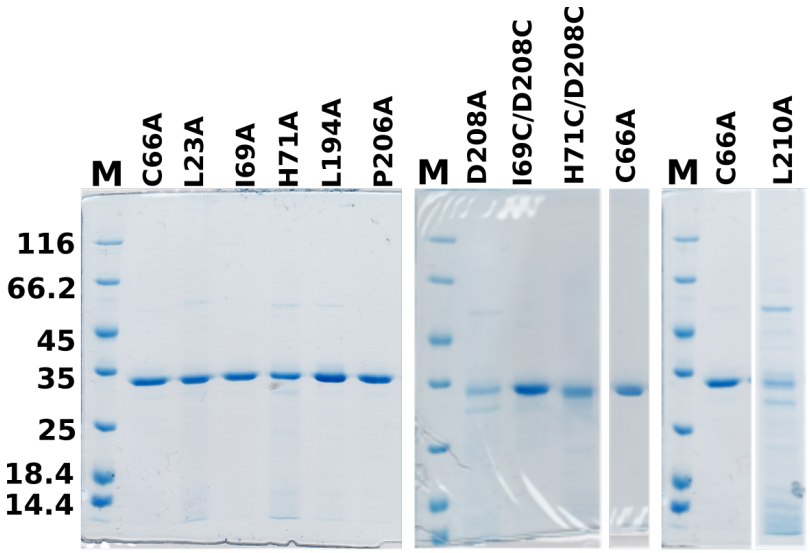

Figure 62: SDS-PAGE analysis of the produced and final purified IL-5Rα variants. 1.5 µg were loaded onto the SDS-PAGE.

The analysis of the IL-5Rα C66A variants provided further evidence towards a preformed wrench-architecture of IL-5Rα (s. Table 29). All alanine "wrench" variants showed similar results for the interaction with IL-5 or the peptide (decrease or no effect on binding), except for Ile69. The variant I69A did not display a loss in affinity for the interaction with IL-5 as reported by Patino *et al.* (2011) but for the peptide. This observation might be explained by the fact that a different (optimized) purification protocol was used, yielding highly purified and active I69A protein. However, substantial loss of binding was observed for the variants H71A, D208A and L210A with IL-5 or the peptide. The loss in binding could be ascribed to a decreased association rate. The results indicate that the formation of the IL-5Rα•AF17121 complex becomes the rate-limiting step, presumably due to disruption of the D1D2 interface leading to a more "open" wrench arrangement. Mutations of Leu194 and Pro206 had no effect on the interaction with IL-5 or the peptide, possibly because neither on of them is fully buried in the interdomain interface.

Given the different size of AF17121 and IL-5, it seemed unlikely that both ligands require similar ectodomain flexibility for binding. Therefore, two double cysteine variants (I69C/D208C and H71C/D208C) were designed that should replace the fixation by hydrogen bonds formed between Asp208 and His71 and Asp208 and Leu70 by a covalent disulfide bond. The disulfide-bridge introduced between the domains D1 and D2 should therefore lead to a closed and non-flexible wrench-like arrangement. If the association rate would then be not affected, opening of the wrench-like architecture prior to binding is not required. However, if binding and potential association would be negatively affected by the disulfide bond between both domains, binding requires a flexible wrench-like architecture. The results showed that a fully rigid wrench- architecture presents a steric constraint for the rather large IL-5 to bind, as the interaction of both variants with IL-5 was strongly reduced, i.e. 84-fold for I69C/D208C and 19-fold for H71C/D208C. In contrast, binding of AF17121 was only impaired for IL-5Rα H71C/D208C, whereas I69C/D208C showed wild type-like binding to AF17121. These results suggest that a larger opening of the IL-5Rα wrench is only required for the larger IL-5 but not for the small peptide AF17121, having the majority of its binding epitope located within domain D1 of IL-5Rα.

Table 29: Relative (rel.) equilibrium constants, association and dissociation rates of the interaction of IL-5Rα variants with either AF17121 or IL-5. (n = 3)

AF17121				IL-5		
rel. k_a	rel. k_d	rel. K_D	Receptor	rel. k_a	rel. k_d	rel. K_D
0.5	2.3	5.2	L23A	0.5	0.9	2.2
0.7	2.0	2.7	I69A	0.7	0.8	1.2
1.0	1.0	0.9	I69C/D208C	0.03	1.5	59.0[a]
0.2	1.1	7.1	H71A	0.07	1.3	19.2[a]
0.03	1.0	31.1[b]	H71C/D208C	0.07	2.6	38.4[a,b]
1.0	1.0	1.0[a]	L194A	1.00	0.9	0.9
1.1	1.0	0.9[a]	P206A	1.00	1.00	1.0
0.09	2.0	23.4[b,c]	D208A	0.08	1.5	18.5[a]
n.b.	n.b.	n.b.	L210A	0.03	1.9	61.6[a]

a: Rmax = local
b: Rmax = constant
c: four concentrations used

a: Ri = local fitted
b: five concentrations used

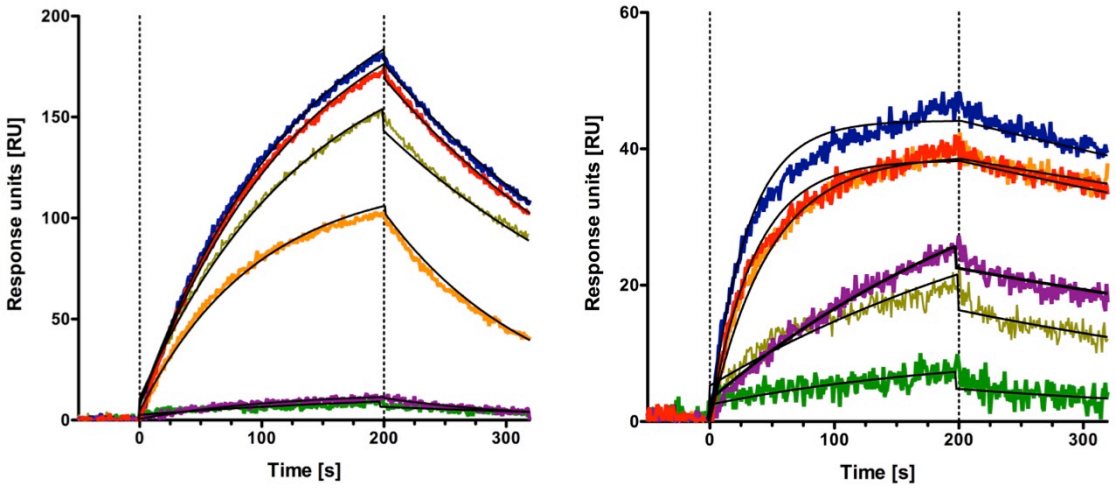

Figure 63: SPR sensorgrams of the interaction of hIL-5Rα C66A variants with AF17121 (left) or IL-5 (right). Biotinylated IL-5 and AF17121 were captured onto a neutravidin-coated GLC sensor surface at densities of about 200 to 250 RU (for IL-5) and about 100 to 150 RU (for AF17121). IL-5Rα variants were perfused as analytes over the biosensor employing six concentrations typically ranging from 250 to 7.8 nM for AF17121 and from 15.6 to 0.5 nM for IL-5. IL-5Rα concentrations: AF17121 62.5 nM and IL-5 15.6 nM are shown respectively. **C66A**, **I69A**, **I69C/D208C**, **H71C/D208C**, **L194A** and **D208A**. **(**Flow rate: 100 µl/min; association time 200 s; dissociation time 120 s)

4.4.7 Mutagenesis study of AF17121: Establishing a recombinant production of the peptide

Although binding of AF17121 to IL-5Rα is remarkably tight, a peptide-based IL-5 inhibitor suitable for pharmaceutical use in treatment of HES would still need improvements with regard to efficacy. Therefore, we wanted to improve binding of the peptide to the receptor by exchanging residues in the peptide using rational structure design and employing the information from the peptide•IL-5Rα complex.

As chemical synthesis of so many peptide variants would have been too costly, we developed a recombinant strategy to produce peptide variants by a biosynthetic expression. A procedure making use of a peptide-protease fusion protein approach was hence established (Shen, A. *et al.*, 2009), which uses intermolecular proteolytic cleavage of the peptide from the protease fusion partner by allosteric activation of the protease with inositol hexakisphosphate (InsP6).

4.4.7.1 Bacterial expression of the AF17121-cysteine protease domain (CPD) fusion protein

The cDNA encoding for AF17121 peptide was cloned upstream of the cysteine protease domain (CPD) gene into the pET22-$CPD_{BamHI\text{-}Leu}$ vector via a two-step PCR (s. 9.2.5). Two overlapping oligonucleotides generated the cDNA encoding the peptide, carrying an additional C-terminal leucine, which is required for recognition and processing by the protease. The DNA encoding the CPD in the expression vector pET22-$CPD_{BamHI\text{-}Leu}$ was replaced by the cDNA encoding AF17121 fused to the CPD.

Transformed *E. coli* BL21 Star (DE3) cells were grown in TB medium and incubated at 37°C until an optical density (OD_{600nm}) of 0.65-0.7 (protein expression was induced with 1 mM IPTG) and the cells were incubated at 18°C overnight (s. 3.5. + 3.5.2). The cell pellet was resuspended in CPD buffer and stored at -20°C. Cell lysis was performed chemically (lysozyme) followed by sonication of the cells. The supernatant was filtrated using fluted filter and incubated overnight at 4°C. If cloudiness was observed after incubation, the protein solution was centrifuged and filtrated using a 0.22 µm filter (s. 3.5.4). SDS-PAGE analysis confirmed expression of the AF17121-CPD protein

showing a protein band at the expected height of ca. 26.1 kDa (s. Figure 64, lane 1-3).

4.4.7.2 Purification of the AF17121-CPD fusion protein

The protease-peptide fusion protein contained a C-terminal hexahistidine sequence that was used for the purification employing a metal chelate affinity chromatography (IMAC, s. 3.6.1).

The filtrated protein solution was loaded onto a 5 ml column. The column was then washed with buffer and the protein was eluted with buffer containing 500 mM imidazole. The SDS-PAGE analysis of the chromatography revealed that most impurities did not bind to the column resin (s. Figure 64). Protein-containing fractions were pooled and dialyzed overnight at 4°C.

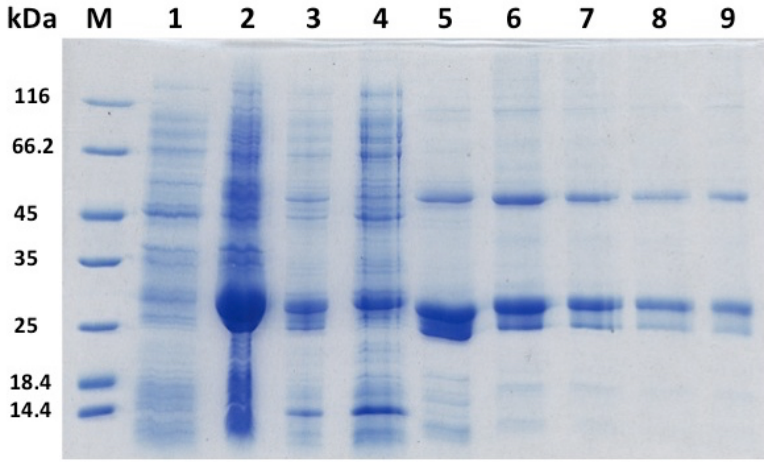

Figure 64: SDS-PAGE analysis of the protein expression, cell lysis and metal chelate affinity chromatography of the AF17121-CPD fusion protein. M: protein standard **1:** before protein induction **2:** after protein induction with 1 mM ITPG **3:** after cell lysis/before IMAC **4:** flow through **5:** elution fraction 2 **6:** elution fraction 5 **7:** elution fraction 6 **8:** elution fraction 7 **9:** elution fraction 8. Elution fractions 2-7 were pooled.

4.4.7.3 Auto-processing of the peptide-protease fusion protein

The intermolecular proteolytic processing of the peptide from its fusion partner (CPD) was done by adding inositol hexakisphosphate (InsP6), which allosterically activates the protease. In contrast to the suggestion by Shen *et al.* (2009) cleaving of the peptide-CPD fusion protein was not done while the fusion-protein was bound to the column, as initial tests indicated ineffective processing of the fusion protein. Hence the auto-processing was performed in solution.

The peptide-CPD fusion protein was concentrated via ultrafiltration until an UV absorbance at 280 nm of 80-90 was obtained. Inositol hexakisphosphate

(1 mM, Santa Cruz) was added to the concentrated protein solution and the mixture was incubated for 1 h at 37°C. The solution was then transferred on ice and centrifuged to remove precipitate. No peptide-CPD fusion protein could be observed in the SDS-PAGE analysis after the auto-processing (s. Figure 65).

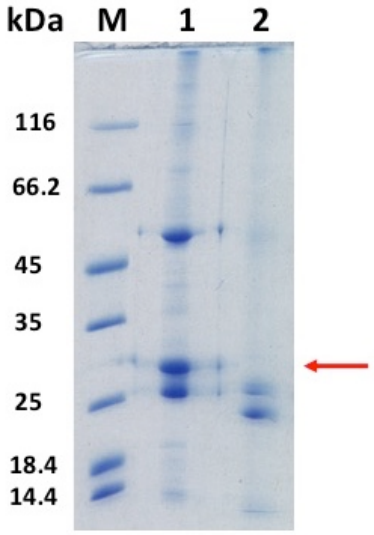

Figure 65: SDS-PAGE analysis of the AF17121-CPD fusion protein before and after proteolytic processing. M: protein standard **1:** AF17121-CPD solution before auto-processing **2:** AF17121-CPD solution after auto-processing. **Red arrow:** AF17121-CPD protein.

4.4.7.4 Purification of AF17121 using gel filtration

As second purification step a gel filtration was established to purify the AF17121 peptide released from the cysteine fusion protein.

After proteolytic processing the protein solution was loaded onto a Superdex Peptide 10/300 column (GE Healthcare, s. 3.6.3). The elution profile showed three UV absorbance maxima. SDS-PAGE analysis of the elution fractions revealed that the first absorbance maximum contained most of the protease fusion protein and other contaminations. The peptide AF17121 was found in the second absorbance maximum (s. Figure 66). The third absorbance maximum probably belongs to the inositol hexakisphosphate (ca. 660 Da), as no protein was found in the SDS-PAGE analysis.

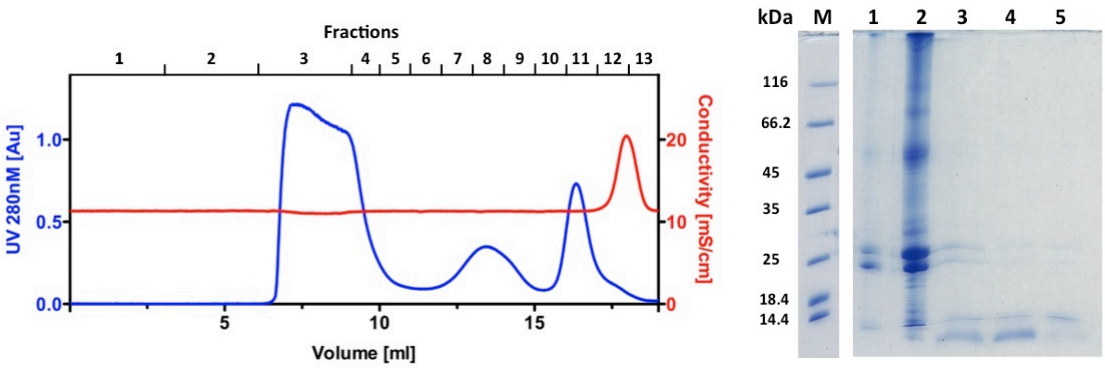

Figure 66: Chromatogram and SDS-PAGE analysis of the first gel filtration of the AF17121 after proteolytic processing. M: protein standard **1:** processed AF17121 CPD solution before gel filtration **2:** elution fraction 3 **3:** elution fraction 7-9 **4:** elution fraction 10 **5:** elution fraction 11. Fractions 7-9 were pooled. **Blue:** UV absorption at 280nm [Au] **Red** Conductivity [mS/cm]

The elution fractions of the AF17121 peptide however still contained further impurities and therefore the pooled fractions were concentrated again via ultrafiltration for a second gel filtration. The elution profile of the second gel filtration showed one major UV absorbance maxima. SDS-PAGE analysis revealed that the absorbance maxima contained highly pure AF17121 peptide (s. Figure 67).

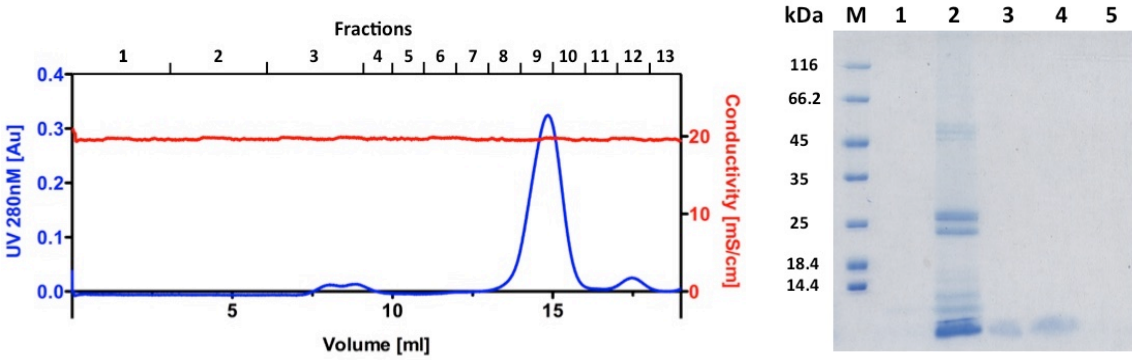

Figure 67: Chromatogram and SDS-PAGE analysis of the 2nd gel filtration of the AF17121 after cleavage. M: protein standard **1:** AF17121 before ultrafiltration **2:** after ultrafiltration **3:** elution fraction 9 **4:** elution fraction 10 **5:** elution fraction 11. Fractions 9-10 were pooled. **Blue:** UV absorption at 280nm [Au] **Red:** Conductivity [mS/cm]

Fractions containing the peptide were pooled and concentrated to about 100 µM by ultrafiltration using a membrane cut-off of 3 kDa. Around 0.7 mg of pure AF17121 peptide could be obtained from one-liter bacterial culture (s. Figure 68).

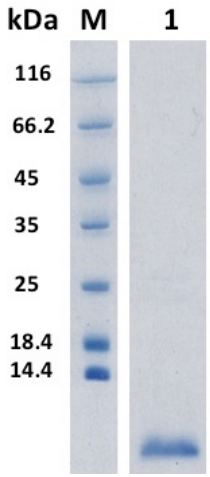

Figure 68: SDS-PAGE analysis of the final purified AF17121 peptide. M: protein standard **1:** AF17121 peptide. 5 µg were loaded onto the SDS-PAGE.

4.4.8 Functional analysis of recombinantly produced AF17121 peptide

To verify that biosynthetically produced AF17121 can bind IL-5Rα as determined for the chemically synthesized peptide, interaction analysis using microscale thermophoresis (MST) was performed. Therefore, the variant ybbR IL-5Rα C66A was produced and purified as described for IL-5Rα C66A. This variant carries a N-terminal ybbR peptide tag (s. 9.2.2), which can be site-specifically labeled with CoA conjugates using the Sfp phosphopantetheinyl transferase (Yin, J. *et al.*, 2005, Yin, J. *et al.*, 2006). For the measurements using MST, ybbR IL-5Rα C66A protein was site-specifically labeled with the fluorescent dye CoA-647 (s. 3.3.8).

16 different concentrations (log 2 dilution) starting with 20 µM as highest concentration of the recombinant produced or chemical synthesis AF17121 peptide with a fixed concentration of CoA-647-ybbR-IL-5Rα (29 nM) were prepared for MST analysis and incubated at room temperature for 5 min. The protein solution was filled into glass capillaries (MO-AK002, NanoTemper) for subsequent MST measurements. The thermophoresis temperature gradient was set to 60% and the fluorescence excitation was performed with 60% of the LED energy (Monolith NT.115, NanoTemper).

MST analysis then revealed for the biosynthetic produced AF17121 peptide an equilibrium constant of 35 ± 3 nM and 35 ± 6 nM for the chemically synthesized peptide. The results show that the biosynthetic purification scheme for AF17121 yields fully cyclized peptide. The leucine added to the C-terminus of the peptide for intermolecular processing of the peptide-protease fusion protein seems to have no negative effect on the binding.

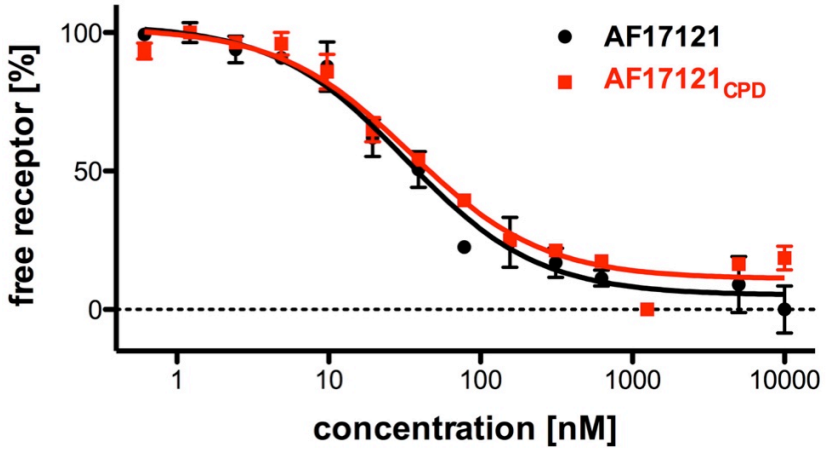

Figure 69: Interaction analysis of the AF17121 peptide obtained by chemical synthesis (AF17121) or recombinantly produced (AF17121$_{CPD}$) with IL-5Rα using MST. LED = 60%, MST power = 60%, Time used for analysis: 14-15 s. Data were fitted using the software Prism yielding the following apparent K_D: AF17121 = 35 ± 6 nM and AF17121$_{CPD}$ = 35 ± 3 nM. (n=2). Thermophoresis experiments were setup making serial dilution series of the different produced AF17121 peptides ranging from 20 µM to 0.6 nM in the presence of 29 nM labeled IL-5Rα. The samples were incubated for 5 min at room temperature. Measurements were performed at 25°C using 10 mM HEPES pH 8.0, 150 mM NaCl, 3.4 mM EDTA, and 0.05% (v/v) Tween20 as buffer.

4.4.9 Structure-based improvement of the AF17121 mediated IL-5 inhibition

Based on the structure data of the IL-5Rα•AF17121 complex and the functional mapping derived from IL-5Rα mutagenesis residues in the peptide were then exchanged in order to obtain peptide variants with improved binding properties for IL-5Rα. Wild type (WT) AF17121 peptide and 21 variants thereof covering 11 selected positions in the 19mer peptide were prepared and their binding to IL-5Rα was determined.

The following 11 positions of AF17121 were analyzed: Glu3, Trp5, Ile7, Ile8, Ala9, Ser10, His11, Thr12, Phe14, Ala16 and Glu17. Glu3 of AF17121 is positioned opposite of Glu63 of the IL-5Rα receptor. Mutation of Glu63 in IL-5Rα to alanine led to increased affinity for AF17121, indicating that residues of the same charge in close proximity is disadvantageous. Glu3 of AF17121 was replaced by glutamine (E3Q). Thr21, Gln25, Val26, Lys65 and Ala66 of IL-5Rα are in contact to Trp5 of AF17121 and form a positively charged area above and a hydrophobic cleft beneath the tryptophan of the peptide. To check if only the hydrophobic contacts of the tryptophan residue are important we replaced Trp5 by a smaller tyrosine (W5Y). Val67, Trp190 and Leu210 of IL-5Rα form a hydrophobic cleft for interaction with Ile7 of AF17121. Ile7 however does not completely fill the hydrophobic cleft and we therefore mutated

Ile7 with large residues such as phenylalanine (I7F), histidine (I7H), leucine (I7L) methionine (I7M) and tyrosine (I7Y). Similar analyses were made for Ile8 of AF17121. Here residues Ile49, Pro52, Thr68 and Phe74 of IL-5Rα form a hydrophobic “pocket” for Ile8. Isoleucine 8 was thus exchanged by phenylalanine (I8F), methionine (I8M) and valine (I8V). As Ala9 of AF17121 is positioned above a hydrophobic cleft created by Val67, Trp190 and Leu210 of IL-5Rα, it was exchanged for phenylalanine (A9F), isoleucine (A9I) and methionine (A9M) to potentially increase the hydrophobic interactions. Trp190 of IL-5Rα is the only residue in close proximity to Ser10 of the peptide. Mutations of Ser10 did not intent to strengthen the hydrophobic interaction with Trp190 but to validate the contribution of the peptide’s flexibility. Therefore, Ser10 was replaced by alanine (S10A), glycine (S10G) and proline (S10P). Whereas glycine might add flexibility to the ring structure, proline should act contrary and make the peptide ring more rigid. Mutation of serine to alanine was performed to test whether the side chain hydroxyl group of Ser10 is involved in β-turn stabilization or folding. Glu54, Asp55 and Asp56 form a negatively charged patch opposite of His11 of the peptide. Exchanging His11 with lysine (H11K) or arginine (H11R) should therefore yield additional polar interactions. As Thr12 is similar positioned opposite a negatively charged patch it was replaced to glutamine (T12Q) or glutamic acid (T12E) to also yield additional polar interactions. Trp190 and Asp189 form a hydrophobic surface area in the peptide epitope at the receptor, which interact with the AF17121 Phe14. We increased the size for hydrophobic interaction by exchanging Phe14 with a tryptophan (F14W). Similar to Ser10 the alanine residue at position 16 was replaced with glycine or proline to increase or decrease the flexibility of the C-terminus. Glutamic acid at position 17 of the peptide interacts with IL-5Rα through the complementary charged Arg188 possibly forming a salt bridge. To analyze whether the negative charge of Glu17 or the salt bridge contributes to the interaction, it was replaced with aspartic acid (E17D).

The AF1721 variants were generated by site directed introduction of single amino acid mutations (s. 3.2.1) using the corresponding oligonucleotides (s. 3.1.4). They were produced and purified as described for wild type AF17121 (s. 4.4.7). Unfortunately, AF17121 variants I7L, A9I, and A9M could not be produced. Table 30 summarizes the yield obtained for each AF17121 variant.

Table 30: Summary of the obtained yields of the AF17121 peptide variants.

Variant	mg/l	Variant	mg/l
wild type	0.71	S10A	0.12
E3Q	0.13	S10G	0.58
W5Y	0.07	S10P	0.90
I7F	0.47	H11K	0.23
I7H	1.10	H11R	0.18
I7M	1.45	T12E	0.24
I7Y	0.41	T12Q	0.66
I8F	0.14	F14W	0.26
I8M	1.55	A16G	1.02
I8V	0.66	A16P	0.20
A9F	0.33	E17D	0.30

The biosynthetically produced peptide variants were then analyzed by interaction analysis using microscale thermophoresis. For each AF17121 variant 16 different concentrations (log 2 dilution) starting with 20 µM as highest concentration were prepared for the MST analysis as described (s. 4.4.8). The measurements were performed at 25°C and 37°C to check to what extent the observed thermal stability of IL-5Rα has an influence on binding of the peptide variants. For the evaluation the average of three duplicates of each variant were used. Figure 70 shows the MST analysis of the wild type (WT), I8F, I8V, S10A and S10G AF17121 peptide variant.

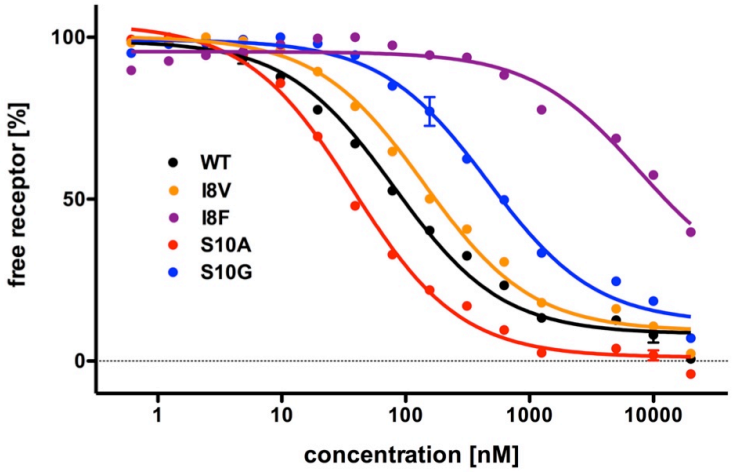

Figure 70: Interaction analysis of the AF17121 wild type (WT) and the variants I8V, I8F, S10A and S10G with IL-5Rα at 25°C using MST. LED = 60%, MST power = 60%, Time used for analysis: 29-30 s. Data was plotted using the software Prism (Graphpad). Data was analyzed using the software MO.Affinity Analysis 2.1.3 (Nanotemper) yielding the following apparent K_D: WT = 85 ± 10 nM, I8V = 127 ± 15 nM, I8F = 8 ± 1 µM, S10A = 25 ± 2 nM and S10G = 424 ± 10 nM, respectively. Thermophoresis experiments were setup making serial dilution series of the different AF17121 variants ranging from 20 µM to 0.6 nM in the presence of 29 nM labeled IL-5Rα. The samples were incubated for 5 min at room temperature. Measurements were performed at 25°C and 37°C using 10 mM HEPES pH 8.0, 150 mM NaCl, 3.4 mM EDTA, and 0.05% (v/v) Tween20 as buffer.

Table 31 summarizes relative equilibrium constants obtained at 25°C and 37°C. For the majority of the AF1721 variants a decrease in affinity was observed instead of an intended increased binding. The results indicate that these positions might be "optimized" i.e. residues that have already the best interaction between the peptide and the receptor. However, mutations of Glu3, Ala9, Thr12, Phe14, Ala16 and Glu17 show that at these positions the interaction might be optimizable since the variants exhibit wild type binding affinity or even showed slightly improvements. To our surprise the AF17121 variant S10A showed an improvement in affinity of 4- to 5-fold, whereas mutation to glycine (S10G) or proline (S10P) resulted in a 5-fold or more than 30-fold decrease, respectively. Hence, neither rigidifying nor relaxing the ring structure of AF17121 did improve binding of the peptide to IL-5Rα.

Table 31: Summary of equilibrium binding (K_D) normalized to the interaction of wild type AF17121 with IL-5Rα C66A derived from *in vitro* interaction analysis using MST. AF17121 WT K_D at 25°C = 85 ± 11 nM and at 37°C = 40 ± 6 nM**.** The changes in binding to IL-5Rα upon mutation are color-coded. Red represents a loss in binding affinity ≥ 5-fold, yellow indicates a loss in affinity by at least 2-fold and ≤ 5-fold. Increase by more than 2-fold are colored green. Blue indicates no change in binding (≥ 0.5-fold and ≤ 2.0)

Variant	25°C	37°C
E3Q	1.0	0.9
W5Y	4.3	6.1
I7F	7.3	16.5
I7H	4.4	9.5
I7M	3.7	5.8
I7Y	3.2	14.6
I8F	94.0	146.8
I8M	189.0	114.5
I8V	1.5	2.0
A9F	1.0	1.0
S10A	0.3	0.2
S10G	5.0	12.9
S10P	32.4	96.6
H11K	6.5	8.9
H11R	2.7	3.8
T12E	1.3	1.6
T12Q	1.6	2.4
F14W	0.7	0.8
A16G	0.8	1.0
A16P	1.0	1.2
E17D	0.9	1.1

To test whether improvements in binding affinity can be translated into enhanced inhibition of IL-5 signaling by the peptide, 12 peptide variants were analyzed in a modified cell proliferation assay employing a TF1 cell clone especially selected to grow IL-5-dependent (Yen, J.J. *et al.*, 1995). The TF-1 competition assays were set up using a defined constant concentration of IL-5 as stimulus and an increasing concentration of AF17121 as competitor (s. 3.9). Figure 71 shows the competition of an exemplary measurement for AF17121 and the variants E3Q, S10A and S10G on TF-1 cells stimulated with 200 pM IL-5. Since the IC_{50} value may vary between experiments depending on experimental conditions, e.g. performance of the cells, the inhibition constant (K_i) was calculated using the following equation (Lazareno, S. *et al.*, 1993):

$$K_i = \frac{IC_{50}}{\frac{[A]}{EC_{50}} + 1}$$

with:

IC_{50} = half maximal inhibitory concentration of the peptide variant

[A] = fixed concentration of agonist (IL-5)

EC_{50} = half maximal effective concentration of agonist (IL-5)

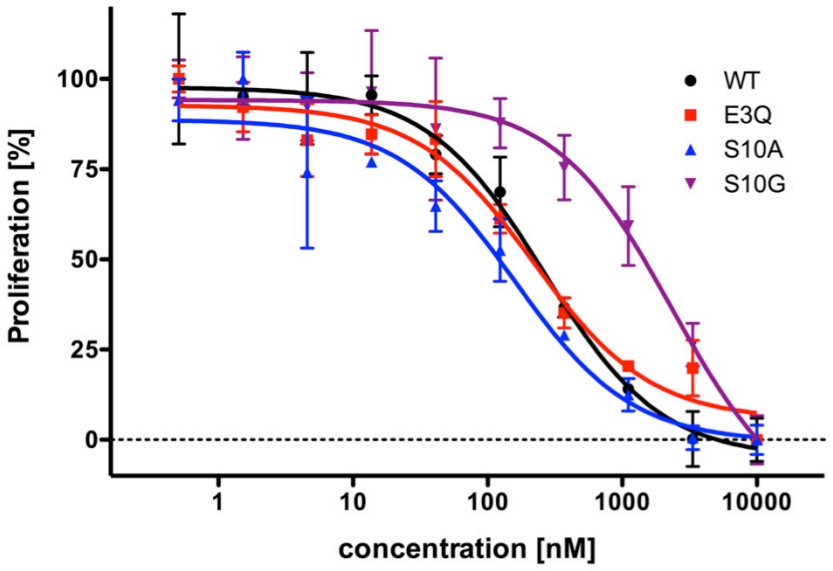

Figure 71: TF1 cell assay showing the IL-5 competition by AF17121 and variants using IL-5 induced cell proliferation as readout. The peptide dose-dependently inhibits proliferation of TF-1 cells induced by a constant concentration of IL-5. Data were fitted using the software Prism yielding IC50 values for the peptides variants: AF17121 WT = 265 ± 48 nM, AF17121 E3Q = 211 ± 52 nM, AF17121 S10A = 168 ± 81 nM and AF17121 S10G = 2332 ± 261 nM, respectively.

The K_i is a normalized value. Table 32 summarizes the obtained relative IC_{50} and K_i values of the analyzed AF17121 peptide variants.

The results of the TF-1 assay were in line with the MST analysis. Most peptide variants show a similar inhibition efficient as wild type AF17121. The results of the duplicate measurements usually differed only slightly except for the AF17121 peptide variants S10A, S10G and T12E. These AF17121 variants were therefore analyzed by SDS-PAGE (s. Figure 72) revealing that the peptides are not as stable as the other peptide variants or wild type AF17121.

Table 32: Summary of the relative IC_{50} and K_i values determined for the competition of IL-5 activity in a TF-1 cell proliferation assay.

	Measurement I		Measurement II	
variant	rel. IC_{50}	rel. K_i	rel. IC_{50}	rel. K_i
E3Q	0.8	0.8	0.5	0.6
I8V	0.9	1.0	0.8[a]	0.9[a]
A9F	0.9	0.8	1.1[a]	1.1[a]
S10A	0.6[a]	0.6[a]	1.2[a]	1.2[a]
S10G	8.8	8.3	12.9	13.0
H11R	1.4	1.2	1.1[a]	1.5[a]
T12E	1.1[a]	1.1[a]	1.7[a]	1.7[a]
T12Q	1.8	1.7	1.7[a]	1.7[a]
F14W	-	-	1.3	1.3
A16G	1.0	0.9	1.2	1.2
A16P	1.3	1.1	1.4[a]	1.4[a]
E17D	1.3	1.1	0.9	0.9

a: Only the second and third plate rows were used.

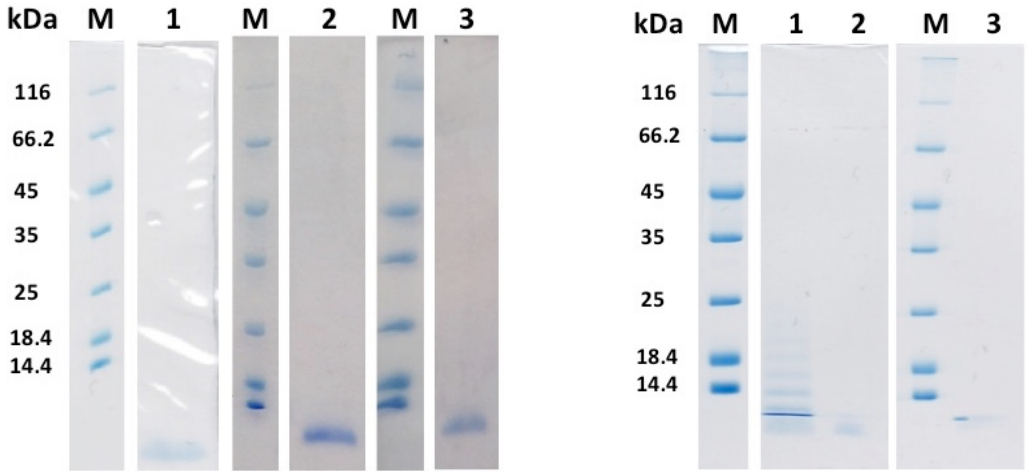

Figure 72: SDS-PAGE analysis of the AF7121 variants S10A, S10G and T12E directly after purification (left) and after longer storage at 4°C (right). M: protein standard **1:** AF17121 S10A **2:** AF17121 S10G **3:** AF17121 T12E

Taken together the results of the MST analysis and the TF-1 cell assay of the AF17121 peptide mutagenesis suggest that the interaction of the peptide with IL-5Rα might be further optimized although the peptide has been identified through an iterative screening of random recombinant peptide-on-plasmid libraries. On the contrary the results also revealed which residues might be already optimal if only proteinogenic amino acid are considered. These positions may therefore be further optimized by the use of non-natural amino acids, which offer a much wider chemical space for exploration than what could have been achieved by our recombinant peptide production approach. The mutation of serine at position 10 to alanine (S10A) currently displays the most promising variant. This was much to our surprise, as in our structure analysis we did not find that Ser10 shares direct contacts with the IL-5Rα ectodomain. This raises the question about the mechanism underlying this affinity enhancement.

Upcoming studies using non-natural amino acids and our novel structure of AF17121 bound to IL-5Rα, will certainly facilitate improving efficacy and other pharmacokinetic parameters to yield novel peptide-based IL-5 inhibitors for future therapies of eosinophil-mediated diseases.

5 DISCUSSION

Interleukin-5 (IL-5) belongs to the class I cytokines and plays an important role in T_H2 immune response development. Helminth infections, certain subtypes of asthma and hypereosinophilic syndromes are diseases characterized by increased levels of eosinophils (blood or tissue eosinophilia, s. reviews: (Klion, A.D. *et al.*, 2004b, Klion, A., 2009, Akuthota, P. *et al.*, 2012, Leru, P.M., 2015, Amin, K. *et al.*, 2016)). As IL-5 controls many aspects of eosinophil life, such as differentiation, migration, proliferation, survival and activation, it is considered an essential key regulator of eosinophils (s. review: (Wen, T. *et al.*, 2016)). Hence, it seems not surprising that the cytokine IL-5 became and still is a highly interesting target for pharmaceutical intervention.

The activity of IL-5 is mediated by the ligand-induced interaction of its cellular receptors; the IL-5 receptor α (IL-5Rα) and the common beta chain (βc). The latter is shared with IL-3 and Granulocyte-Macrophage Colony-Stimulating Factor (GM-CSF). (s. review: (Hercus, T.R. *et al.*, 2013)) Targeting IL-5 or either one of its receptors present current strategies for different therapeutic development. The 3D structures determined in the past for IL-5, the βc ectodomain and particularly for the complex of IL-5Rα bound to IL-5 provided first insights for structure-based design attempts of IL-5 inhibitors. The structure of the IL-5Rα bound to IL-5 revealed that the IL-5Rα adopts a wrench-like architecture (Patino, E. *et al.*, 2011). Whether the wrench-like structure is preformed or the wrench can adopt an open state and a closed state during binding of IL-5 is still unclear. For future structure-based design attempts, the conformational freedom in the IL-5Rα ectodomain is essential, as the drugs that are to be developed will target the free IL-5Rα. To answer this question additional functional and structure analysis need to be performed.

5.1 Recombinant production of the IL-5 protein and the ectodomains of IL-5Rα and βc

In this project the structures of the unbound IL-5Rα ectodomain, in complex with an inhibitory peptide and the ternary IL-5•IL-5Rα•βc complex were planned to be examined via X-ray crystallography. Therefore, large quantities of highly pure proteins are required, making protein production often the limiting step for these analyses. Hence the purification protocols for IL-5 and the extracellular domains of IL-5Rα and βc were optimized.

The IL-5 and IL-5Rα ectodomain protein expressed in *E. coli* were derived in form of insoluble inclusion bodies. Optimization of the protocols included testing (i) different *E. coli* expression strains and (ii) optimized extraction of IL-5Rα and IL-5 using different chaotropic agents to hopefully omit the gel filtration under denaturing conditions used in the past.

The *E. coli* strain Rosetta (DE3) showed the strongest expression for IL-5. A bioinformatic analysis of the cDNA of human IL-5 revealed the presence of several so-called rare codons, which are only limited available in *E. coli*. The Rosetta strain harbors an additional plasmid that encodes for these underrepresented tRNAs in *E. coli*. The extraction was performed using urea instead of guanidine hydrochloride (GuHCl) as chaotropic agent and yielded already highly pure IL-5 protein, allowing to omit the gel filtration otherwise performed under denatured conditions. After refolding the IL-5 protein was purified via gel filtration as the only purification step. The individual optimizations allowed raising the yield of IL-5 by about 50% (9-10 mg per L bacteria culture) compared to previous procedures (6 mg per L bacteria culture). Figure 73 displays the changes applied to the old protocol of IL-5.

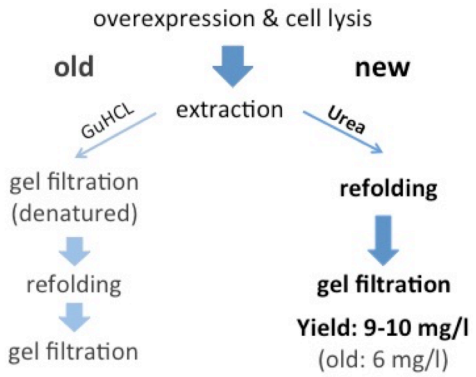

Figure 73: Schematic illustration of the old and new IL-5 purification protocol.

The variant IL-5Rα C66A has been shown to have no negative affect on IL-5 binding but increases the protein stability (Devos, R. *et al.*, 1994). Since high concentrated protein solutions are required for the planned X-ray crystallography, the IL-5Rα C66A variant was chosen. Surprisingly, when using

the *E. coli* strain Rosetta (DE3) previously transformed with the plasmid, almost no expression of the IL-5Rα protein was found. Instead the *E. coli* strain BL21 Star (DE3) was used showing the strongest expression. The Rosetta and BL21 Star cells are both BL21 derivatives. The mutation in the RNaseE gene (ren131) of the BL21 strain reduces endogenous ribonucleases and hence attenuates mRNA degradation, which enhanced mRNA stability and protein yield. The solubilization of the IL-5Rα protein was not changed as extraction of IL-5Rα showed only minor contaminations with nucleic acids. Hence gel filtration under denatured conditions was not required anymore. Anion exchange chromatography was used to separate active IL-5Rα protein from misfolded protein and other contaminations. This was confirmed by analyzing elution fractions containing IL-5Rα using IL-5 affinity chromatography employing an IL-5 affinity resin and by interaction studies using surface plasmon resonance (SPR). The yield of the IL-5Rα ectodomain protein could be increased by more than three-fold (8-9 mg per L bacteria culture) compared to the old protocol (2.5 mg per L bacteria culture). Figure 74 shows the changes applied to the previous protocol used for IL-5Rα production. The increase in yield is also related to the elimination of the IL-5 affinity chromatography. Regeneration of immobilized IL-5Rα with 4M $MgCl_2$, previously used to elute IL-5Rα in the IL-5 affinity chromatography, led to dramatic affinity loss of IL-5Rα for IL-5. This might also explain the higher affinity of IL-5Rα produced with the new method observed in SPR analyses of the IL-5Rα•IL-5 interaction (s. Table 18).

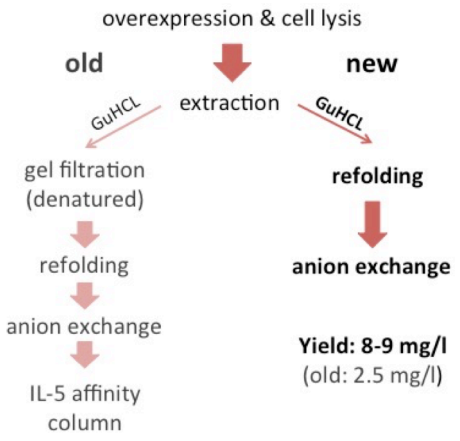

Figure 74: Schematic illustration of the old and new IL-5Rα C66A purification protocol.

Production of the common beta chain (βc) ectodomain was reported using a baculovirus-infected insect cell expression system (Gustin, S.E. *et al.*, 2001). Production of recombinant proteins in an insect cell expression system offers the advantage of post-translational modifications. Furthermore, an efficient secretion system allows transport of the target protein into the cell culture medium, which contains less proteins and proteases compared to the

cytoplasm and therefore reduces aggregation of the target protein. The chaperone system of the complex secretion system ensures proper folding, disulfide bond formation and oligomerization, if the protein has a quaternary structure. Protein yield is often higher in comparison to other eukaryotic expression systems (e.g. mammalian: HEK/CHO). The βc N346Q variant was used as removal of the N-glycosylation site at position 346 by mutation to glutamine significantly improved the quality of the obtained crystals, when βc was crystallized on its own (Gustin, S.E. *et al.*, 2001). However, expression and purification initially revealed that serum (FCS) present in the expression medium could not be fully separated from the βc protein by chromatography. Optimization of the purification therefore comprised expression media without FCS for protein production. Medium supernatant of these FCS-free cell cultures were purified by metal chelate affinity chromatography and showed only a single impurity with significant smaller molecular weight compared to the βc protein. In this case gel filtration could effectively remove this contamination. The overall yield of highly pure βc was 8-9 mg per L insect culture.

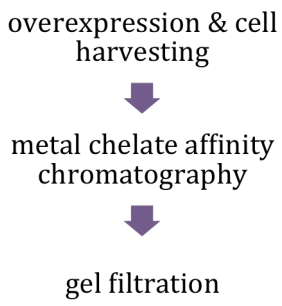

Figure 75: Schematic illustration of the established βc N346Q ectodomain purification protocol.

5.2 Cryo-EM required to determine the structure of the ternary IL-5 complex?

Hansen *et al.* (2008) suggested that the GM-CSF dodecamer formation is an obligate step for full receptor activation. In contrast to the receptor subunits of GM-CSF, IL-5Rα and βc are both associated with Janus kinases (JAK) JAK2 and JAK1, respectively (Ogata, N. *et al.*, 1998). Therefore, dimerization of the IL-5 receptor subunits or a hexamer assembly of the ternary IL-5 complex might be sufficient for downward signaling and hence a dodecameric assembly is not essential to initiate IL-5 signaling. This is different to GM-CSFRα, which does not exist in a kinase-associated form and thus in case of GM-CSF signaling the dodecamer assembly seems to be required. Solving the structure of the ternary IL-5 complex should reveal whether the receptor assembly is identical/similar to that of the ternary GM-CSF complex, or if there are ligand-specific differences.

The functional analysis of the single components of the IL-5 ternary complex via surface plasmon resonance (SPR) showed that the proteins do indeed interact with each other. The SPR analysis of the βc N346Q ectodomain protein as well as data from SPR analysis published in the past (Scibek, J.J. *et al.*, 2002) indicated rather tight binding with an affinity ≤ 1 µM for the binding of IL-5•IL-5Rα to βc. This affinity hence seemed sufficient to allow isolation and purification of the ternary IL-5 complex by gel filtration similar as reported for the preparation and structure analysis of the GM-CSF ternary complex (Hansen, G. *et al.*, 2008). However, SDS-PAGE analysis of the gel filtration performed to isolate the ternary complex IL-5•IL-5Rα•βc showed that all βc protein dissociates and was separated from the binary IL-5 complex. Additional analyses showed that the SPR analysis was biased by avidity effects, thereby suggesting a much higher affinity as if interaction analyses were performed in solution. A measurement using microscale thermophoresis as independent control revealed that binding of βc to the binary complex occurred with micromolar affinity only, indicating an about 10 to 20-fold lower affinity as initially assumed. This could be confirmed with a different SPR analysis employing a different setup with βc immobilized on the sensor surface and using the binary complex as analyte. As the wild type (WT) βc protein, containing all three potential glycosylation sites, was used in the SPR analysis reported by Scibek, J.J. *et al.* (2002), it had to be ruled out that all

N-glycosylation sites are required for full binding affinity. High affinity binding to the GM-CSF receptor needs all N-glycosylation sites of βc to be intact (Niu, L. *et al.*, 2000). The rather low affinities obtained for the interaction of wild-type βc with the binary IL-5 complex (K_D 9 to 14 µM) together with a very fast dissociation (k_d 1.5 to 2 x 10^{-1} s^{-1}) of the ternary complex suggest that isolation of the ternary complex by gel filtration will be very unlikely.

Other possibilities to carry out structure analyses with the proteins produced include the preparation of the ternary IL-5 complex by directly mixing the components in the assumed stoichiometry (hIL-5•hIL-5Rα•βc: 2:2:1) prior to crystallization attempts. Alternatively, and particularly for structure analysis by Cryo-EM, the complex could be stabilized by chemically crosslinking of the components.

5.3 A bi-dentate salt bridge is the key determinant for the strong AF17121•IL-5Rα interaction

Determining the structure of the IL-5Rα ectodomain in complex with the peptide AF17121 revealed how this small molecule inhibits the interaction of IL-5Rα with IL-5. The structure of the IL-5Rα C66A ectodomain bound to the AF17121 peptide showed that the peptide binds into the cleft formed by the domains D1 and D2 in the ectodomain of IL-5Rα. In contrast to the interaction with IL-5 the peptide AF17121 shares no contact with the domain D3. The overall structure of the IL-5Rα ectodomain is highly similar to that of the IL-5Rα in complex with IL-5, suggesting that the wrench-like architecture of the IL-5Rα ectodomain is largely predetermined and possibly also maintained in a preformed conformational state. A structural alignment/superposition of the IL-5Rα ectodomains in complex with AF17121 and IL-5 (Patino, E. *et al.*, 2011) illustrates these observations (s. Figure 76). Orientation and position of the D1 and D2 domains are almost identical and only loop regions pointing away from the ligand differ in conformation.

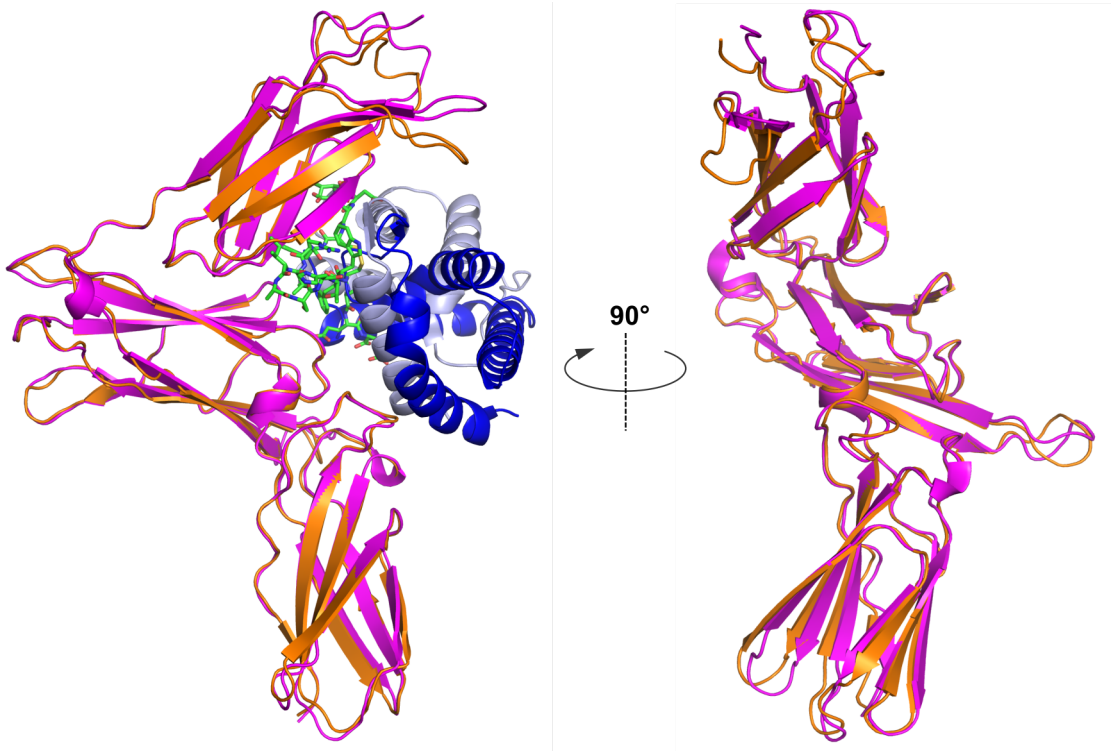

Figure 76: Aligned IL-5Rα ectodomains in complex with the AF17121 peptide and IL-5 (left) and rotated by 90° without AF17121 and IL-5 (right). **IL-5Rα (IL-5)**, **IL-5Rα (AF17121)** and **IL-5** represented as cartoon and the **AF17121** peptide is shown as sticks. **[**PDB ID: 3QT2, 6H41; Patino, E. *et al.* 2011, Scheide-Noeth, J.P. *et al.* 2019*]

* Copyright s. 9.6 (page 179)

A more detailed analysis of the binding site of the peptide AF17121 revealed that the peptide occupies a volume/area in the cleft formed by the domains D1 and D2 in IL-5Rα that is not used for recognition and binding of IL-5 (s. Figure 77).

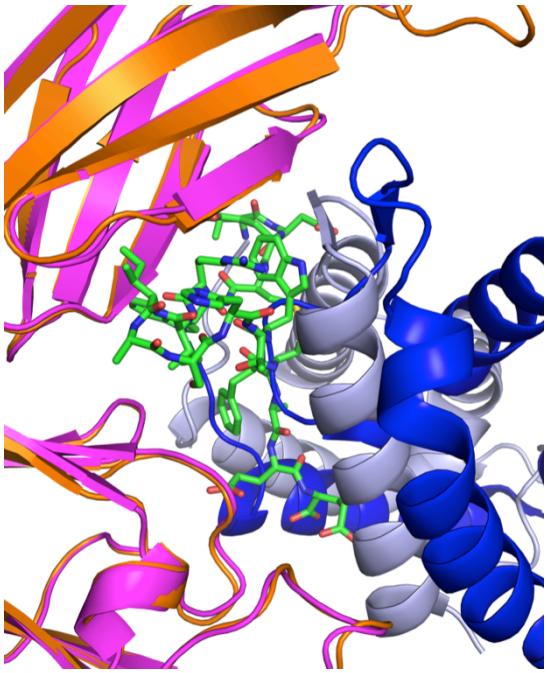

Figure 77: Illustration of the areas occupied by IL-5 and AF17121 in the D1D2 interface of IL-5Rα. IL-5Rα (IL-5), IL-5Rα (AF17121) and IL-5 represented as cartoon and the AF17121 peptide is shown as sticks. **[**PDB ID: 3QT2, 6H41; Patino, E. *et al.* 2011, Scheide-Noeth, J.P. *et al.* 2019]

While IL-5•IL-5Rα interact via eleven direct intermolecular hydrogen bonds formed between the residues of the IL-5Rα D1 domain and IL-5, the peptide only engages in two hydrogen bonds, a bi-dentate salt bridge, with residues of IL-5Rα (D1 domain) (s. Figure 78). This interaction between Arg6 (AF17121) and Asp55 located in the D1 domain of IL-5Rα is strongly shielded by a π-π electron stacking interaction from Trp13 of AF17121, which is positioned such that the indole aromatic ring is placed perpendicular to the bi-dentate salt bridge between Arg6 (AF17121) and Asp55 (IL-5Rα). This explains the importance of these two residues in AF17121 reported in previous studies (Ruchala, P. *et al.*, 2004, Ishino, T. *et al.*, 2006, Bhattacharya, M. *et al.*, 2007). Additional polar interactions were observed between Val67 of IL-5Rα with Arg6 and Ile8 of AF17121 and the residues Tyr155 and Arg188 of IL-5Rα (D2) with Glu17 of AF17121. Other interactions are of non-polar nature.

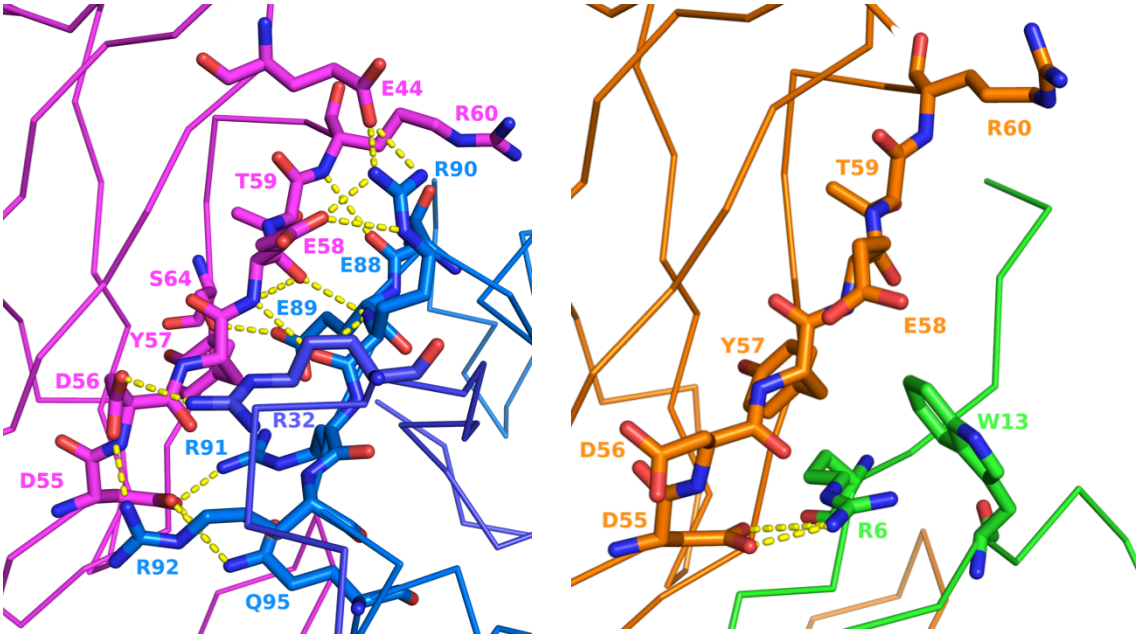

Figure 78: Illustrations of the direct hydrogen bonds formed between the IL-5Rα domain D1 and β-strand 2 of IL-5 (left) and the domain D1 and the AF17121 peptide. **IL-5Rα (IL-5)**, **IL-5Rα (AF17121)**, **IL-5** and the **AF17121** peptide represented as ribbon. Residues involved in hydrogen bond formation are shown as sticks. Hydrogen bonds as stippled lines in yellow. **[**PDB ID: 3QT2 (left), 6H41 (right); Patino, E. *et al.* 2011, Scheide-Noeth, J.P. *et al.* 2019]

5.4 The IL-5Rα ectodomain wrench-like architecture requires a certain degree of flexibility

It is an important question to what extent the IL-5Rα ectodomain displays a conformational flexibility in its unbound state. As structure-based drug design attempts to target the free IL-5Rα protein, rational structure-based design will inevitably fail, if the structure of unbound IL-5Rα deviates from that of IL-5Rα observed in complex with IL-5. It is interesting to note that the previously published structure of IL-3Rα (ectodomain) in complex with a Fab fragment revealed two different conformations, a so-called “closed” and an “open” conformation (Broughton, S.E. *et al.*, 2014). The closed conformation closely resembles a wrench-like architecture as observed for IL-5Rα in complex with IL-5 (Patino, E. *et al.*, 2011) and the peptide AF17121, as well as for the determined structures of GM-CSFRα (Broughton, S.E. *et al.*, 2016) and IL-3Rα (Broughton, S.E. *et al.*, 2018) bound to their ligands (s. Figure 79).

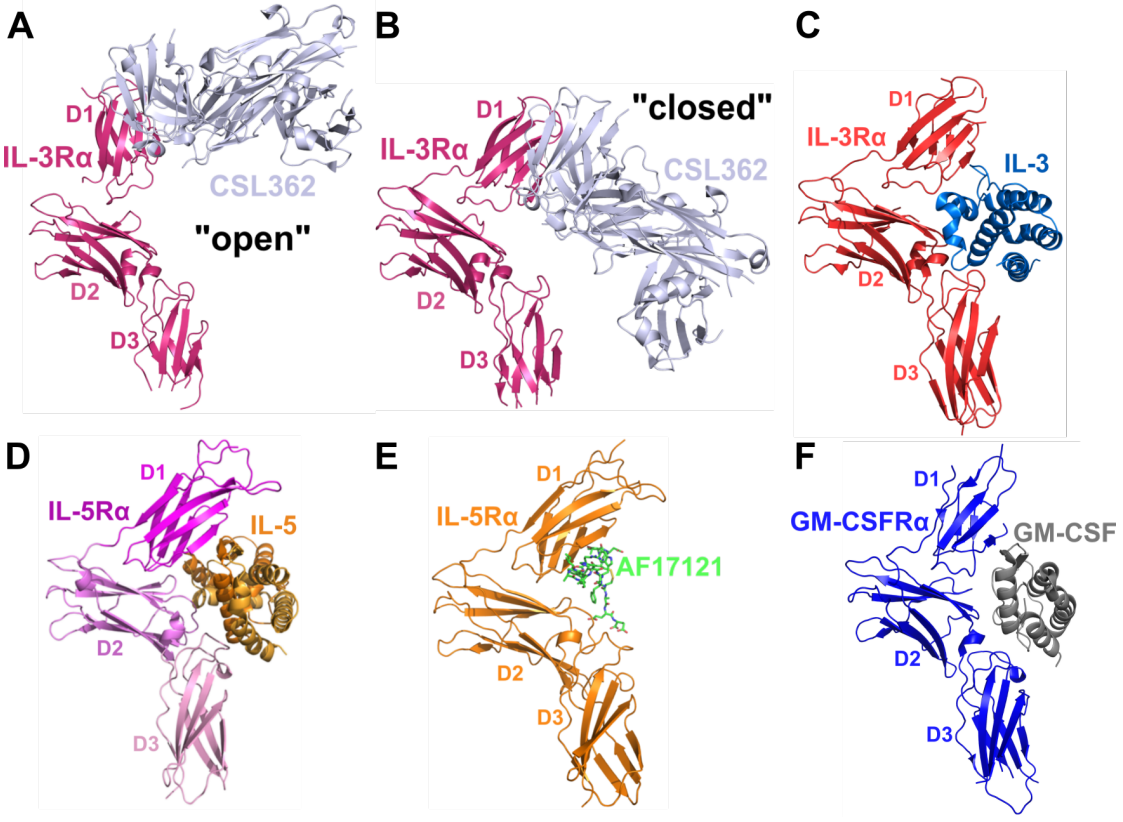

Figure 79: Representation of the receptor α subunit structures of IL-3Rα in complex with the Fab fragment CSL362 in “open” (A) and “closed” (B) conformation and of IL-3Rα (C), IL-5Rα (D) and GM-CSFRα (E) bound to their ligands. The “closed” conformation of IL-3Rα in complex with the Fab fragment CSL362 resembles a wrench-like architecture as observed the binary IL-3, IL-5 and GM-CSF complex. Structures are presented as cartoon. [PDB ID: 4JZJ (A+B), 5UV8 (C), 3QT2 (D), 6H41 (E), 4RS1 (F); Broughton, S.E. *et al.* 2014, Broughton, S.E. *et al.* 2018, Patino, E. *et al.* 2011, Scheide-Noeth, J.P. *et al.* 2019, Broughton, S.E. *et al.* 2016]

The open conformation, however, shows a different orientation of the D1 domain, when compared with the structure of IL-5Rα in complex bound to IL-5. This might offer a hint that the IL-5Rα ectodomain could also arrange in a similar open state. Since the three FNIII domains of IL-5Rα cover more than 170° of the IL-5 torus, a preformed wrench might present an obstacle for ligand binding due to steric hindrance and might slow down complex formation. Therefore, an opening and closing mechanism of the wrench would possibly facilitate ligand-receptor assembly. The fast association rate of the IL-5 ligand-receptor interaction determined *in vitro* suggests however a very fast closing mechanism making a ligand-induced conformational rearrangement unlikely (Patino, E. *et al.*, 2011). Patino *et al.* (2011) provided additional evidence for a preformed wrench through identifying residues involved in the fixation of the IL-5Rα ectodomain D1D2 interface. Mutation of these residues to alanine either resulted in dramatic loss in binding (≥2500-fold) and/or in a strongly reduced association rate of the binary complex formation. As the association rate is strongly affected by conformational alterations during complex formation, this possibly indicates that disruption of the D1D2 interface leads to conformational rearrangement (likely an opening of the wrench), thus the closing of the wrench required becomes the rate-limiting step of the IL-5•IL-5Rα complex formation. (Patino, E. *et al.*, 2011) To test this hypothesis additional functional and structure analyses of IL-5Rα in its unbound state were performed.

In initial trials for structural analysis of free IL-5Rα using X-ray crystallography, IL-5Rα C66A precipitated when protein concentrations exceeded 7-8 mg/ml. Solubility and stability parameters of a protein usually strongly correlate with its tendency to crystallize. Therefore different buffer conditions that potentially stabilize the IL-5Rα protein were examined using a Thermofluor analysis (Ericsson, U.B. *et al.*, 2006). However, none of the buffers tested showed an improvement in protein stability. The analysis instead indicated that the IL-5Rα ectodomain protein possibly unfolds already at 35°C, which would question its conformational stability under physiological conditions. The analysis was therefore repeated using a Prometheus NT.48 device (Nanotemper). While the conceptual basis of this method is similar to that of the Thermofluor analysis, the Prometheus device monitors the shift of intrinsic tryptophan fluorescence

instead of measuring the quenching of a fluorescence dye. The Prometheus analysis then revealed two melting transitions for unfolding of IL-5Rα. A lower Tm point at 42°C might correlate with an unfolding of the wrench, i.e. opening of the D1D2 interface, while the higher melting point found at 65°C could present the globular unfolding of the three Fibronectin type III-like (FNIII) domains. The low Tm obtained in both thermal shift assays possibly indicates that the IL-5Rα ectodomain has a certain degree of intrinsic flexibility. Whether the observed local domain flexibility is also seen for eukaryotic produced IL-5Rα ectodomain protein needs to be analyzed as glycosylation can positively affect protein stability (Rajan, N. *et al.*, 1995).

Therefore, a eukaryotic production scheme for IL-5Rα C66A ectodomain protein was established using baculovirus-infected insect cells (s. Figure 80). The rationale was to obtain IL-5Rα C66A protein that displays enhanced solubility and stability and might therefore exhibit an increased probability to crystallize in the unbound state. Heterogeneous glycosylation, however, can be problematic for structural analysis by protein crystallization. Various enzymes commercially available can be used to homogeneously reduce N-glycosylation. For instance endoglycosidases H and F3 will leave the first N-acetylglucosamine residue attached to the asparagine (Weiner, M.P. *et al.*, 1994), the proximal oligosaccharide can be sufficient to stabilize the protein (Petrescu, A.J. *et al.*, 2004).

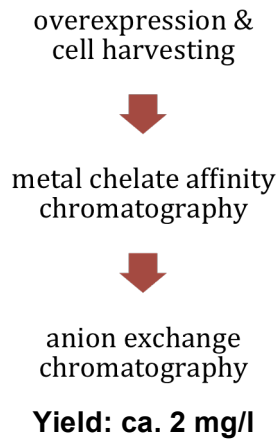

Figure 80: Schematic illustration of the established IL-5Rα C66A ectodomain purification protocol.

Functional analysis using surface plasmon resonance (SPR) showed similar binding properties for insect cell-derived IL-5Rα protein and bacteria-derived IL-5Rα protein with IL-5. These results confirm that the glycosylation of the IL-5Rα ectodomain are not important for the interaction with IL-5, but rather display a stabilizing function (Ishino, T. *et al.*, 2011).

To provide further information of the flexibility of the IL-5Rα wrench-like architecture, functional studies with a set of IL-5Rα variants with mutations in the D1-D2 interface that potentially modulate the flexibility of the

wrench-architecture, but do not directly contact AF17121 or IL-5, were performed in order to determine the required degree of domain flexibility for either ligand. Alanine replacements of Leu23, Ile69, His71, Leu194, Pro206, Asp208 and Leu210 in IL-5Rα similarly affected the interaction of IL-5Rα with IL-5 or the peptide AF17121. Patino, E *et al*. (2011) showed that residues Leu23, Ile69, His71 and Asp208 in IL-5Rα occupy key positions that potentially control and affect the orientation of the two IL-5Rα domains D1 and D2 (s. Figure 81a). The IL-5Rα variants H71A and L210A exhibited a dramatically reduced association rate for the interaction of IL-5Rα with IL-5, while the mutation D208A affected the binding of both the peptide and IL-5. Patino, E *et al.* (2011) described similar effects for the IL-5Rα variant I69A. Even though we could not reproduce the dramatic reduction of the association rate for IL-5Rα I69A, our data on H71A, D208A and L210A suggest that formation of the wrench-like architecture of IL-5Rα becomes the rate-limiting step, likely through disruption of the interface between domain D1 and D2 leading to a more “open” or more flexible wrench-architecture.

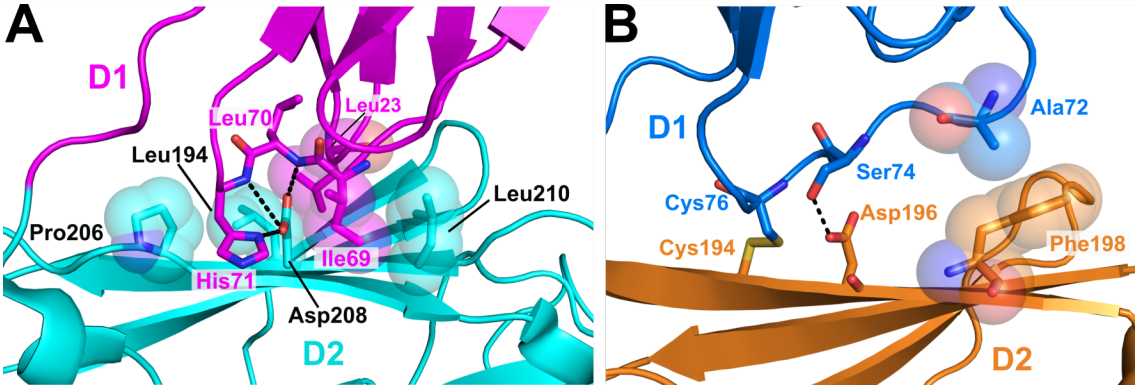

Figure 81: Comparison of the residues involved in the formation of the D1D2 interface in IL-5Rα (A) and IL-3Rα (B). A: Stability of the wrench-architecture and its impact on ligand binding was tested by mutagenesis. Leu23, Ile69, His71, Leu194, Pro206, Asp208 and Leu210 of IL-5Rα were exchanged to alanine, and binding of AF17121 and IL-5 to these variants was analyzed. To test whether a fixed architecture impedes binding of AF17121 or IL-5, the hydrogen bonds (stippled black lines) between Leu70 and His71 and Asp208 were replaced with a disulfide bond. Two IL-5Rα double variants were generated, with Ile69 and Asp208 or His71 and Asp208 being replaced with cysteines. **B:** Asp196 of IL-3Rα forms a hydrogen bond with Ser74 similar as Asp208 of IL-5Rα with Leu70 and His71. Other key features of the D1D2 interface include the Cys76-Cys194 disulfide bond and van der Waals interactions (shown as spheres) between Ala72 and Phe198. **[**PDB ID: 6H41 (A), 4JZJ (B); Scheide-Noeth, J.P. *et al.* 2019*, Broughton, S.E. *et al.* 2014]

* Copyright s. 9.6 (page 179)

IL-5Rα however seems to require a certain degree of flexibility in its ectodomain architecture to allow efficient binding of ligands. This is highlighted by the double variant IL-5Rα I69C/D208C, which contains two cysteine residues that fixate domain D1 and D2 in a closed wrench-like arrangement through a disulfide bond between I69C and D208C (s. Figure 81a). This variant was still able to bind the peptide AF17121 with wild type-like affinity. The strongly decreased association rate of this variant for binding to IL-5 indicates that the ectodomain has to undergo some rearrangements for binding of the larger protein ligand IL-5, though.

Compared to the reported high mobility of the NTD (D1) domain of IL-3Rα (Broughton, S.E. *et al.*, 2014) the flexibility of the D1 domain of IL-5Rα seems to be restricted much stronger. The position of the D1 domain of IL-3Rα in the "closed" form is constrained by a disulfide bond between Cys76 (domain D1) and Cys194 (domain D2), a hydrogen bond between Asp196 (domain D2) and Ser74 (domain D1), and van der Waals interactions between Ala72 (domain D1) and Phe198 (D2) ((Broughton, S.E. *et al.*, 2014), s. Figure 81b). In the "open" conformation the hydrogen bond and van der Waals interactions are not formed. Alanine mutation of Asp196 (IL-3Rα) resulted in only a 4-fold loss of affinity for IL-3, whereas alanine replacement of Asp208 (IL-5Rα) completely abrogates binding to IL-5. Therefore, the high flexibility of the D1 domain of IL-3Rα seems to be required for IL-3 binding. Interestingly the D1 domain of IL-3Rα is highly mobile in the presence of IL-3 (Ref. 2018), even though the IL-3Rα ectodomain adopts in a "wrench-like" conformation when bound to IL-3. The differences in domain flexibility of the D1 domains IL-3Rα and IL-5Rα, but possibly also of GM-CSFRα could explain the very low affinity of IL-3 for IL-3Rα (K_D = 120 nM (Kitamura, T. *et al.*, 1991)) compared to the higher affinities of GM-CSF (K_D = 2-8 nM (Gearing, D.P. *et al.*, 1989)) or IL-5 (K_D = 1 nM (Tavernier, J. *et al.*, 1991)) for their respective α-subunits.

5.5 A similar recognition epitope for AF17121 and IL-5 but with different residues being involved

Functional analysis of the IL-5Rα variants confirmed the interactions seen in the crystal structure and revealed that several residues in the IL-5Rα ectodomain differ with respect to their role for binding to either the peptide AF17121 or the native ligand IL-5. The polar interaction between the Asp55 of IL-5Rα and Arg6 of AF17121 represents the hotspot of binding in the AF17121•IL-5Rα interaction. Mutation of Asp55 to alanine (D55A), asparagine (D55N) or glutamic acid (D55E) completely abrogated binding of AF17121. A complete loss of binding was also observed for IL-5Rα mutations Y57A and L210A. Mutations of Tyr57 to phenylalanine (Y57F) or tryptophan (Y57W), however, showed wild type-like binding of AF17121, indicating that only an aromatic residue at this position is required without specification of its type. Similar to Trp13 of AF17121 the Tyr57 of IL-5-Rα seems to shield the π-π electron interaction of Asp55 of IL-5Rα and Arg6 of AF17121. Mutation of Arg188 (IL-5Rα), which forms hydrogen bonds with AF17121 C-terminus and Glu17, to alanine resulted in a 340-fold loss of affinity for the peptide AF17121. Replacing the arginine with lysine did not affect the peptide-receptor interaction, indicating that a positive charge is sufficient as the lysine side chain is too short to form the same hydrogen bonds as Arg188 (s. Figure 82).

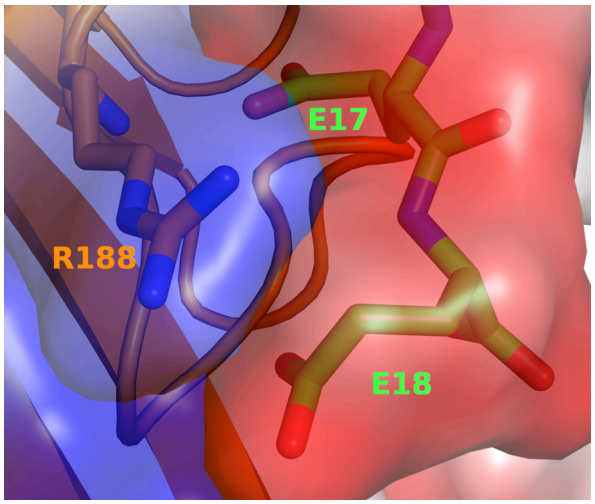

Figure 82: Illustration of the electrostatic distribution of Arg188 of IL-5Rα and Glu17 and 18 of AF17121. Red: negative charged. **Blue:** positive charged.

The IL-5Rα variants K53A and E63A were the only two variants that led to an improved binding affinity of IL-5Rα for AF17121 with a more than 2-fold increase. The alanine mutation of Lys53 removes the large side chain, which most likely facilitates binding due to reduced steric hindrance (s. Figure 83, left). Mutation of Glu63 to alanine removes an electrostatic clash, as Glu63 in IL-5Rα is located directly opposite of Glu3 in AF17121 (s. Figure 83, right).

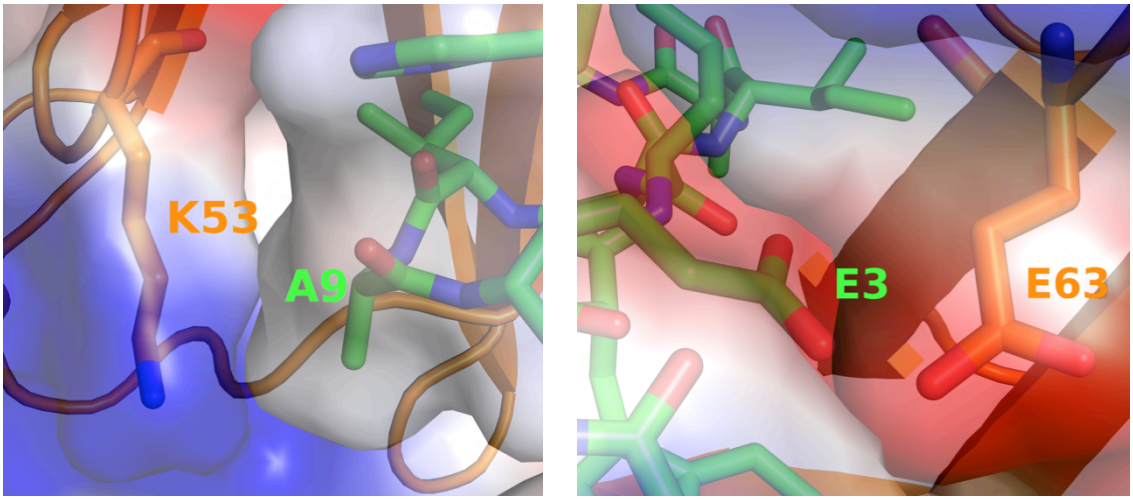

Figure 83: Illustration of the electrostatic distribution of Lys53 of IL-5Rα and AF17121 (left) and of Glu63 of IL-5Rα and Glu3 of AF17121 (right). Red: negative charged. **Blue:** positive charged. **Grey:** uncharged/hydrophobic.

The results of the functional analysis together with the structure data for the IL-5Rα•AF17121 complex might allow an "optimization" of the inhibitory AF17121 peptide and can serve as a starting point for the development of new IL-5 small molecule inhibitors. Mutations showing a decreased affinity indicate that the residue's properties are already optimized for the local interaction. To improve binding of the peptide to IL-5Rα, residues of AF17121 near such residues of IL-5Rα should therefore be exchanged with residues maintaining the residues properties but possibly increase the number of polar or hydrophobic interactions. Exchanges showing improved affinity suggest that the local interactions can be further improved, possibly by transferring the properties of the mutated residue to the peptide.

In summary, the results clearly show that the two structurally distinct IL-5Rα ligands, AF17121 and IL-5, are recognized and bound vastly different (s. Figure 84), although the finding of a seemingly identical interaction pairing, i.e. AF17121 Arg6—IL-5Rα Asp55 compared with IL-5 Arg91—IL-5Rα Asp55 suggested otherwise at first. Thus, the result of IL-5 neutralization by the peptide AF17121 is less a direct competition (mimic) for the very same residues at IL-5Rα, but the implementation of a steric hindrance to block IL-5 from access to its binding site.

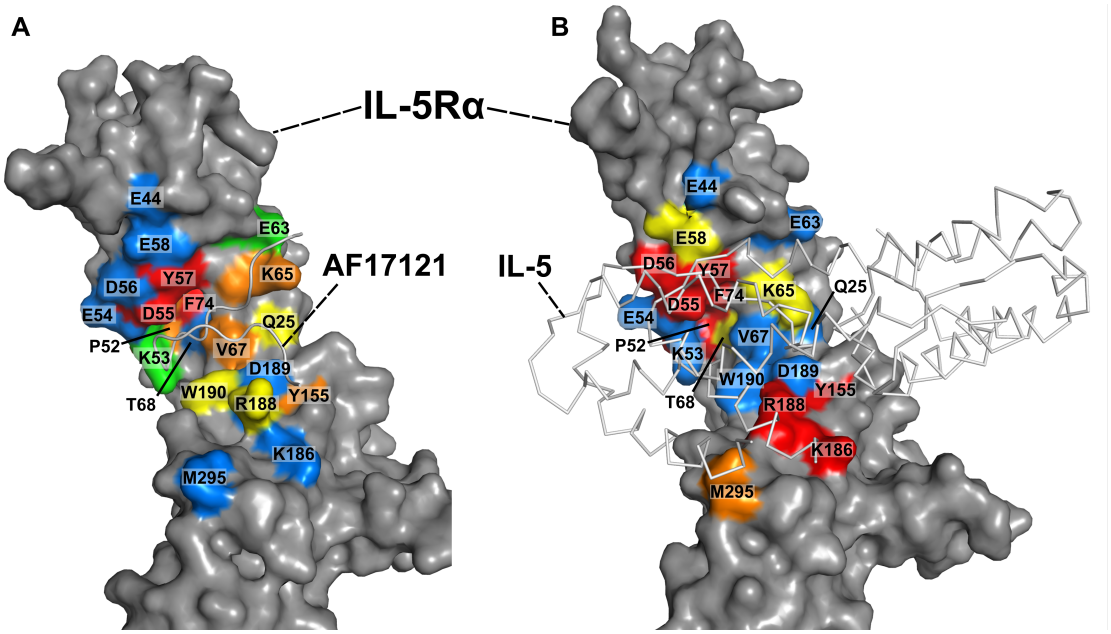

Figure 84: The functional epitope of AF17121 and IL-5 at IL-5Rα differ. The contribution of individual residues to binding of either AF17121 **(A)** of IL-5 **(B)** were determined by mutagenesis of IL-5Rα and subsequent *in vitro* interaction analysis. **A:** Surface representation of IL-5Rα, the binding site of the peptide is indicated; AF17121 is shown as ribbon plot. The interface with mutated residues color-coded according to their contribution to overall binding of AF17121. Residues marked in red represent a loss in binding affinity larger than 10-fold, residues colored orange indicate a loss in affinity by at least 5-fold (and < 10-fold) and in yellow by at least 2-fold (and < 5-fold). Residues marked in green showed an increase by more than 2-fold. Residues colored in blue do not change the binding affinity if mutated to alanine. **B:** as in **(A)** but for the analysis of binding of IL-5 to IL-5Rα variants. [PDB ID: 6H41 (left), 3QT2 (right); Scheide-Noeth, J.P. *et al.* 2019*, Patino, E. *et al.* 2011]

* Copyright s. 9.6 (page 179)

5.6 A rational design approach to AF17121 variants with improved IL-5Rα binding

Although binding of AF17121 to IL-5Rα is remarkably strong with an affinity in the 100 nM range, a peptide inhibitor suitable for pharmaceutical use in treatment of HES and asthma might benefit from an improved binding affinity. Therefore, we replaced residues in AF17121 with the aim to improve binding of the peptide to the receptor using the structure of the peptide•IL-5Rα complex and the data derived from functional mapping of the IL-5Rα mutagenesis study. As chemical synthesis of a larger number of peptide variants would have been too costly, a strategy for recombinant production of the peptides by a biosynthetic expression procedure was developed. We established a peptide-protease fusion protein approach, which allows intramolecular proteolysis of the peptide from the fusion protease partner through an allosteric activation of the protease with a small molecule (Shen, A. *et al.*, 2009). Endoproteases are therefore not required and thus the potential risk of unspecific hydrolysis caused through endoproteases is avoided. In addition, expression of the fusion approach can improve the expression yield and solubility of the peptide. Expression of only the peptide would have possibly failed, due to the small size of the peptide leading very likely to degradation of the peptide. Besides enhanced solubility the protease domain fusion also provides a steric barrier, thereby favoring formation of intramolecular instead of intermolecular disulfide bonds, which would likely led to aggregation. The purification protocol illustrated in Figure 85 enabled us to produce about 0.7 mg/l of pure, cyclic monomeric AF17121 peptide.

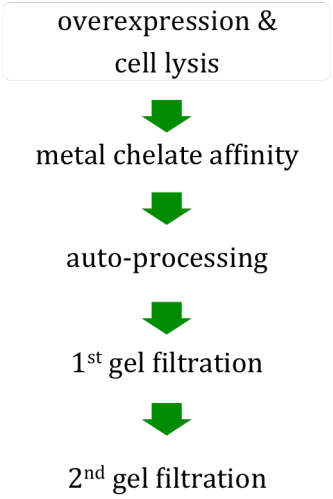

Figure 85: Schematic illustration of the established AF17121 peptide purification protocol

The functional analysis using MST of chemically or biosynthetically produced AF17121 showed similar binding affinities to IL-5Rα, thereby confirming that the biosynthetic produced peptide is correctly processed (cyclic). The binding of recombinant AF17121 to IL-5Rα was not affected by the leucine added to the

C-terminus of the peptide. The leucine was required for processing of the cleavage site by the fusion protease.

The mutagenesis study of AF17121 comprised of 21 variants covering 11 by analysis of the structure data selected positions. The analysis however yielded only very few variants with improved binding to IL-5Rα, even though *in silico* modeling predicted otherwise. These unexpected results might be due to the fact that the peptide was identified via screening of recombinant peptide-on-plasmid libraries. In addition, the peptide design did only utilize the static picture of the final state of the AF17121•IL-5Rα complex, but it could not take the complex formation pathway into account. The results nevertheless provided useful information, that can be used in further optimization approaches. Residues like Trp5, Ile7, Ile8 and His11 seem already optimally filling the cleft in the IL-5Rα binding pocket while Glu3, Ala9, Ser10, Thr12, Phe14, Ala16 and Glu17 are possibly positions suitable for optimization. The geometry of the residues in AF17121 seems to also play an important role since mutations of Trp5, Ile7 and Ile8 with other hydrophobic residues showed a significant decrease in affinity except for the I8V variant. Exchange of His11 with another positively charged residue such as arginine or lysine did not lead to an affinity improvement although suggested from potential formation of additional complementary interactions with the negatively charged residues Glu54, Asp55 and Asp56 in IL-5Rα (s. Figure 86). Mutation of Glu3 to glutamine showed only a slightly improved affinity compared to the mutation of Glu63 to alanine in IL-5Rα, which significantly increased binding of IL-5Rα towards AF17121, indicating that steric hindrance also negatively affects the interaction as these two residues face each other (s. Figure 83, right). Replacing Glu3 with a shorter residue like threonine or alanine might therefore increase the affinity more significantly. Increasing the hydrophobic surface by exchanging the alanine at position 9 for phenylalanine did not affect binding. Instead of

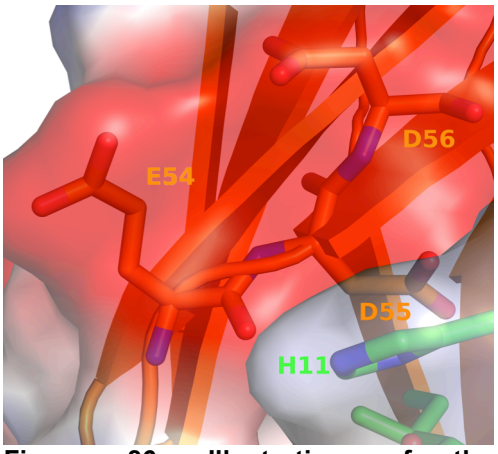

Figure 86: Illustration of the electrostatic distribution of Glu54, Asp55 and 56 of IL-5Rα and His11 of AF17121. Red: negative charged. **Grey:** uncharged/hydrophobic. **Blue:** positive charged.

increasing the hydrophobic surface introducing a negatively charged residue at position 9 of AF17121 might result in complementary interactions with the positively charged residue Lys53 in IL-5Rα (s. Figure 83, left). AF17121 variants T12Q, T12E, F14W, A16G and A16P, albeit chosen because of potential additional hydrophobic or polar interactions with IL-5Rα or increasing/lowering the flexibility of AF17121, did neither improve nor diminish binding significantly. Exchanging Glu17 of AF17121 with aspartic acid might not lead to the formation of a hydrogen bond with Arg188 of IL-5Rα as seen for Glu17 (AF17121) and Arg188 (IL-5Rα), but the complementary interactions are maintained. Since the AF17121 variant E17D showed wild type binding, the hydrogen bond possibly only contributes little to the overall interaction. The influence of modulating backbone flexibility and conformation was also analyzed for the serine at position 10 of AF17121 similar to Ala16. Both mutations of Ser10 to glycine (S10G) or proline (S10P) resulted in a significant decrease in affinity. Exchanging Ser10 with alanine, however, showed a significant 4- to 5-fold improvement in binding. The removal of unfavorable van der Waals contacts of the serine hydroxyl group with the aromatic ring of Trp190 located just beneath Ser10 could explain the observed affinity gain of AF17121 S10A. Figure 87 illustrates positions of the peptide that, based on the AF17121 mutagenesis study using proteinogenic amino acids, showed an increase (green) or decrease (red) in binding to IL-5Rα or had no affect (blue).

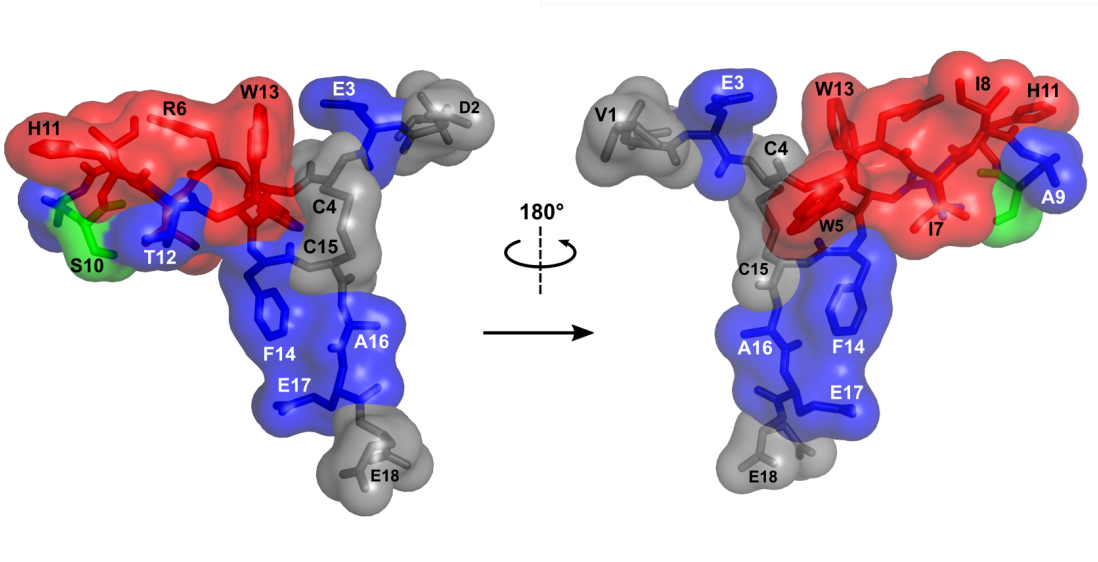

Figure 87: Illustration of the effects on binding towards IL-5Rα of the various residues in AF17121. Red: decrease in binding (more than 2-fold). **Blue:** no significant change in binding. **Green:** increase in binding (more than 2-fold). **Grey**: not analyzed.

The recombinant production scheme however severely limited testing a large number of peptides as an exchange was only possibly to one of the other 19 proteinogenic amino acids. Unfortunately, this also precluded a full sampling of the chemical space as was suggested by the structure-based design using the AF17121•IL-5Rα crystal structure. The use of non-natural amino acids could be particularly beneficial for the positions seemingly showing optimal fitting/filling as they extend the possibilities to alter the functional groups of these residues while preserving their basic chemical properties. D-amino acids can for example additionally increase the resistance to endopeptidases and/or the affinity and limit flexibility different to using proline. Modifications of the peptide bonds can also increase plasma stability of the peptide (Vlieghe, P. *et al.*, 2010).

Generating a multivariant that, combing all individual mutations, showed improvement in binding, could provide another step towards a therapeutically more effective IL-5 inhibitor. The multivariant will certainly yield additional information on the question whether or not the effects of the individual mutations are additive or even synergetic.

Another approach to improve the affinity of the AF17121 peptide could be the generation of a dimeric or multimeric variant. We could recently confirm that the IL-5 inhibitor peptide AF20016, which is a disulfide-bridged homodimer, can bind two interleukin-5 receptor α moieties in solution, as reported by England, B.P. *et al.* (2000). In contrast to AF17121, the dimeric peptide AF20016 binds IL-5Rα with an affinity exceeding 1 nM and therefore blocks IL-5Rα much more efficient than what is observed for AF17121. The affinity of AF20016 is almost identical to the natural ligand IL-5. Dimerization of the AF17121 peptide might result in a similar affinity enhancement, either by enabling simultaneous binding to two receptor molecules located in close proximity at the cell surface or by a mechanism called local concentration enhancement. In the latter the second binding element is held in close proximity and after dissociation a fast rebinding will significantly slowdown the final dissociation of the peptide-receptor complex (s. review: (Handl, H.L. *et al.*, 2004)).

Currently neutralizing antibodies developed against all components involved in IL-5 receptor activation; e.g. the ligand IL-5 (mepolizumab and reslizumab, (Hart, T.K. *et al.*, 2001, Kips, J.C. *et al.*, 2003)), the IL-5 receptor IL-5Rα (benralizumab, (Koike, M. *et al.*, 2009)) as well as βc/CDw131 (CSL311,

(Panousis, C. *et al.*, 2016)) are hitting the clinics. Their effectiveness in abrogating IL-5 signaling, which decreases eosinophil count and relieves from disease symptoms, has finally led to FDA/EMA approval of mepolizumab (in 2015), reslizumab (in 2016) and benralizumab (in 2017) for the therapy of severe eosinophilic asthma (s. review: (Roufosse, F., 2018)). Disadvantages of these IL-5 neutralizing antibodies however include for example complex and costly production, targeting of the drug potentially limited by its size and possible immunogenic activity upon long-term application. Peptides such as AF17121 can overcome some of these disadvantages including: (i) easier targeting into tissues due to their smaller size, (ii) less immunogenic, (iii) lower manufacturing cost, (iv) higher activity per unit mass and (v) longer storablility at room temperature. Major drawbacks of peptides however include: (i) low oral bioavailability (which also applies for antibodies), (ii) a short half-life due to rapid clearance from the circulation by the liver and kidneys and (iii) high sensitivity to proteolytic degradation. To overcome these drawbacks and limitations of peptides various chemical strategies have been developed, including those mentioned above: i.e. using non-natural/D-amino acids, amide bond replacement between two amino acids (e.g. NH-amide alkylation), and/or blocking N- or C-terminal ends by N-acylation. (s. review: (Vlieghe, P. *et al.*, 2010)). After optimizing the peptide's affinity to IL-5Rα and thereby increasing its efficacy to block IL-5 signaling future developments might have to take those pharmacokinetic parameters into account. Addressing all these points might finally yield a peptide-based IL-5 inhibitor or small-molecule-based pharmacophore highly effective to be used in novel therapy setups to fight hypereosinophilic or atopic diseases.

6 SUMMARY

The cytokine interleukin-5 (IL-5) is part of the T_H2-mediated immune response. As a key regulator of eosinophilic granulocytes (eosinophils), IL-5 controls multiple aspects of eosinophil life. Eosinophils play a pathogenic role in the onset and progression of atopic diseases as well as hypereosinophilic syndrome (HES). Here, cytotoxic proteins and pro-inflammatory mediators stored in intracellular vesicles termed granula are released upon activation thereby causing local inflammation to fight the pathogen. However, if such inflammation persists, tissue damage and organ failure can occur. Due to the close relationship between eosinophils and IL-5 this cytokine has become a major pharmaceutical target for the treatment of atopic diseases or HES. As observed with other cytokines, IL-5 signals by assembling a heterodimeric receptor complex at the cell surface in a stepwise mechanism. In the first step IL-5 binds to its receptor IL-5Rα (CD125). This membrane-located complex then recruits the so-called common beta chain βc (CD131) into a ternary ligand-receptor complex, which leads to activation of intracellular signaling cascades. Based on this mechanism various strategies targeting either IL-5 or IL-5Rα have been developed allowing to specifically abrogate IL-5 signaling. In addition to the classical approach of employing neutralizing antibodies against IL-5/IL-5Rα or antagonistic IL-5 variants, two groups comprising small 18 to 30mer peptides have been discovered, that bind to and block IL-5Rα from binding its activating ligand IL-5. Structure-function studies have provided detailed insights into the architecture and interaction of IL-5•IL-5Rα and βc. However, structural information for the ternary IL-5 complex as well as IL-5 inhibiting peptides is still lacking.

In this thesis three areas were investigated. Firstly, to obtain insights into the second receptor activation step, i.e. formation of the ternary ligand-receptor complex IL-5•IL-5Rα•βc, a high-yield production for the extracellular domain of βc was established to facilitate structure determination of the ternary ligand-receptor assembly by either X-ray crystallography or cryo-electron microscopy.

In a second project structure analysis of the ectodomain of IL-5Rα in its unbound conformation was attempted. Data on IL-5Rα in its ligand-free state would provide important information as to whether the wrench-like shaped

ectodomain of IL-5Rα adopts a fixed preformed conformation or whether it is flexible to adapt to its ligand binding partner upon interaction. While crystallization of free IL-5Rα failed, as the crystals obtained did not diffract X-rays to high resolution, functional analysis strongly points towards a selection fit binding mechanism for IL-5Rα instead of a rigid and fixed IL-5Rα structure. Hence IL-5 possibly binds to a partially open architecture, which then closes to the known wrench-like architecture. The latter is then stabilized by interactions within the D1-D2 interface resulting in the tight binding of IL-5.

In a third project X-ray structure analysis of a complex of the IL-5 inhibitory peptide AF17121 bound to the ectodomain of IL-5Rα was performed. This novel structure shows how the small cyclic 18mer peptide tightly binds into the wrench-like cleft formed by domains D1 and D2 of IL-5Rα. Due to the partial overlap of its binding site at IL-5Rα with the epitope for IL-5 binding, the peptide blocks IL-5 from access to key residues for binding explaining how the small peptide can effectively compete with the rather large ligand IL-5. While AF17121 and IL-5 seemingly bind to the same site at IL-5Rα, functional studies however showed that recognition and binding of both ligands differ. With the structure for the peptide-receptor complex at hand, peptide design and engineering could be performed to generate AF17121 analogies with enhanced receptor affinity. Several promising positions in the peptide AF17121 could be identified, which could improve inhibition capacity and might serve as a starting point for AF17121-based peptidomimetics that can yield either superior peptide-based IL-5 antagonists or small-molecule-based pharmacophores for future therapies of atopic diseases or the hypereosinophilic syndrome.

7 ZUSAMMENFASSUNG

Das Zytokin Interleukin-5 (IL-5) nimmt eine zentrale Rolle im Zellzyklus von eosinophlien Granulozyten (Eosinophile) ein, indem es beispielsweise die Differenzierung, Aktivierung und Apoptose dieser Zellen steuert. Als Immunantwort auf Pathogene kommt es zur Aktivierung von Eosinophilen. Dieses führt zur Freisetzung von in intrazellulären Vesikeln (Granula) gespeicherten zytotoxischen Proteinen und proinflammatorischen Mediatoren, wodurch lokale Entzündungen verursacht werden, um den Erreger zu bekämpfen. Fehlregulationen (übermäßige Produktion) von eosinophilen Granulozyten können zu Gewebeschäden und Organversagen führen, wenn diese über einen längeren Zeitraum bestehen, und sind insbesondere mit dem Ausbruch und Fortschreiten von atopischen Erkrankungen sowie dem Hypereosinophilen Syndrom (HES) assoziiert. IL-5 muss, um die Eosinophilen aktivieren zu können, an einen heterodimeren Transmembranrezeptor binden. Im ersten Schritt bindet IL-5 an seinen zytokin-spezifischen Rezeptor IL-5Rα (CD125). Dieser membrangebundene Komplex rekrutiert dann die sogenannte gemeinsame („*common*“) beta-Kette βc (CD131) in einen ternären Liganden-Rezeptorkomplex, was zur Aktivierung von intrazellulären Signalkaskaden führt. Aufgrund dieser engen Beziehung zwischen Eosinophilen und IL-5 ist dieses Zytokin in den Fokus der pharmazeutischen Industrie für die Behandlung atopischer Erkrankungen oder HES gerückt. Bisherige Therapien basieren auf der Unterdrückung der Immunreaktion durch Corticosteroide, neutralisierende gegen IL-5/IL-5Rα gerichtete Antikörper oder antagonistische IL-5 Varianten. Eine alternative Therapiemöglichkeit stellen IL-5 inhibierende Peptide dar, welche an IL-5Rα binden und hierbei die Bindung des aktivierenden Liganden (IL-5) hemmen. Derzeit stehen Strukturen vom binären IL-5•IL-5Rα Komplex und von βc im ungebundenen Zustand zur Verfügung. Zudem konnten wichtige Wechselwirkungen im binären Komplex identifiziert werden. Allerdings sind vom ternären IL-5 Komplex und den IL-5 inhibierenden Peptiden keinerlei Strukturdaten bekannt.

Um im Rahmen dieser Arbeit Einblicke in den zweiten Rezeptoraktivierungsschritt, d.h. die Bildung des ternären Ligand-Rezeptor Komplexes IL-5•IL-5Rα•βc, zu erhalten, wurde ein Herstellungsverfahren für die extrazelluläre Domäne von βc etabliert. Zusammen mit den optimierten

Reinigungsverfahren für IL-5 und IL-5Rα konnte hiermit eine gute Grundlage für zukünftige Strukturanalysen des ternären IL-5 Komplexes geschaffen werden. In einem zweiten Projekt wurde versucht, die Struktur der Ektodomäne von IL-5Rα in ihrem freien Zustand aufzuklären. Diese Strukturdaten würden wichtige Informationen darüber liefern, ob die bisher bekannte „Schraubenschlüssel"-Architektur der IL-5Rα Ektodomäne in einer rigiden, vorgebildeten Konformation vorliegt, oder ob die Architektur der Ektodomäne bei Bindung flexibel an ihren Liganden angepasst wird. Während die Kristallisation von IL-5Rα ohne einen Bindepartner fehlschlug, deuten neue Funktionsanalysen auf einen „*selection fit binding mechanism*" für IL-5Rα hin. Der relativ große Ligand IL-5 bindet daher sehr wahrscheinlich an eine teilweise „offene" Rezeptorkonformation, die erst nach Bindung die bekannte „Schraubenschlüssel"-Architektur annimmt. In einem dritten Projekt wurde eine Strukturanalyse des Komplexes des IL-5 inhibierenden AF17121 Peptids gebunden an die Ektodomäne von IL-5Rα durchgeführt. Anhand dieser neuen Struktur lässt sich erklären, wie das kleine zyklische 18mer Peptid effektiv mit dem wesentlich größeren Liganden IL-5 um die Bindung am Rezeptor konkurrieren kann. Aufgrund der Überlappung der Bindestellen von AF17121 und IL-5 am Rezeptor IL-5Rα blockiert das Peptid den Zugang von IL-5 an seinen Rezeptor. Obwohl AF17121 und IL-5 in einem ähnlich Strukturbereich in IL-5Rα binden, zeigen funktionelle Studien, dass sich Erkennung und Bindung beider Liganden unterscheiden. Mit der vorliegenden Struktur vom Peptid-Rezeptor Komplex konnte ein strukturbasiertes Peptid-Design durchgeführt und so AF17121 Varianten mit verbesserter Rezeptorbindung erzeugt werden. Dabei wurden mehrere Positionen im Peptid AF17121 identifiziert, die dessen Inhibierungseigenschaften möglicherweise verbessern. Somit konnte ein weiterer Grundstein für die Entwicklung von effektiveren Peptid-basierten IL-5 Antagonisten oder sogar nicht-peptidischen Inhibitoren für zukünftige Therapieansätze gegen atopische Erkrankungen oder HES gelegt werden.

8 REFERENCES

Abbas AK, Lichtman AH, Pillai S: **Cellular and Molecular Immunology** 8th Edition edn: Elsevier Saunders; 2015.

Adachi T, Choudhury BK, Stafford S, Sur S, Alam R: **The differential role of extracellular signal-regulated kinases and p38 mitogen-activated protein kinase in eosinophil functions**. *Journal of immunology* 2000, **165**(4):2198-2204.

Akuthota P, Weller PF: **Eosinophils and disease pathogenesis**. *Seminars in hematology* 2012, **49**(2):113-119.

Amin K, Janson C, Bystrom J: **Role of Eosinophil Granulocytes in Allergic Airway Inflammation Endotypes**. *Scandinavian journal of immunology* 2016, **84**(2):75-85.

Anderson GP: **Endotyping asthma: new insights into key pathogenic mechanisms in a complex, heterogeneous disease**. *Lancet* 2008, **372**(9643):1107-1119.

Battye TG, Kontogiannis L, Johnson O, Powell HR, Leslie AG: **iMOSFLM: a new graphical interface for diffraction-image processing with MOSFLM**. *Acta crystallographica Section D, Biological crystallography* 2011, **67**(Pt 4):271-281.

Bazan JF: **Structural design and molecular evolution of a cytokine receptor superfamily**. *Proceedings of the National Academy of Sciences of the United States of America* 1990, **87**(18):6934-6938.

Bel EH, Wenzel SE, Thompson PJ, Prazma CM, Keene ON, Yancey SW, Ortega HG, Pavord ID, Investigators S: **Oral glucocorticoid-sparing effect of mepolizumab in eosinophilic asthma**. *The New England journal of medicine* 2014, **371**(13):1189-1197.

Bhattacharya M, Pillalamari U, Sarkhel S, Ishino T, Urbina C, Jameson B, Chaiken I: **Recruitment pharmacophore for interleukin 5 receptor alpha antagonism**. *Biopolymers* 2007, **88**(1):83-93.

Bjermer L, Lemiere C, Maspero J, Weiss S, Zangrilli J, Germinaro M: **Reslizumab for Inadequately Controlled Asthma With Elevated Blood Eosinophil Levels: A Randomized Phase 3 Study**. *Chest* 2016, **150**(4):789-798.

Bleecker ER, FitzGerald JM, Chanez P, Papi A, Weinstein SF, Barker P, Sproule S, Gilmartin G, Aurivillius M, Werkstrom V *et al*: **Efficacy and safety of benralizumab for patients with severe asthma uncontrolled with high-dosage inhaled corticosteroids and long-acting beta2-agonists (SIROCCO): a randomised, multicentre, placebo-controlled phase 3 trial**. *Lancet* 2016, **388**(10056):2115-2127.

Bochner BS, Schleimer RP: **The role of adhesion molecules in human eosinophil and basophil recruitment**. *The Journal of allergy and clinical immunology* 1994, **94**(3 Pt 1):427-438; quiz 439.

Brizzi MF, Zini MG, Aronica MG, Blechman JM, Yarden Y, Pegoraro L: **Convergence of signaling by interleukin-3, granulocyte-macrophage colony-stimulating factor, and mast cell growth factor on JAK2 tyrosine kinase**. *The Journal of biological chemistry* 1994, **269**(50):31680-31684.

Broide DH, Paine MM, Firestein GS: **Eosinophils express interleukin 5 and granulocyte macrophage-colony-stimulating factor mRNA at sites of allergic inflammation in asthmatics**. *The Journal of clinical investigation* 1992, **90**(4):1414-1424.

Broughton SE, Dhagat U, Hercus TR, Nero TL, Grimbaldeston MA, Bonder CS, Lopez AF, Parker MW: **The GM-CSF/IL-3/IL-5 cytokine receptor family: from ligand**

recognition to initiation of signaling. *Immunological reviews* 2012, **250**(1):277-302.

Broughton SE, Hercus TR, Hardy MP, McClure BJ, Nero TL, Dottore M, Huynh H, Braley H, Barry EF, Kan WL *et al*: **Dual mechanism of interleukin-3 receptor blockade by an anti-cancer antibody**. *Cell reports* 2014, **8**(2):410-419.

Broughton SE, Hercus TR, Nero TL, Dottore M, McClure BJ, Dhagat U, Taing H, Gorman MA, King-Scott J, Lopez AF *et al*: **Conformational Changes in the GM-CSF Receptor Suggest a Molecular Mechanism for Affinity Conversion and Receptor Signaling**. *Structure* 2016, **24**(8):1271-1281.

Broughton SE, Hercus TR, Nero TL, Kan WL, Barry EF, Dottore M, Cheung Tung Shing KS, Morton CJ, Dhagat U, Hardy MP *et al*: **A dual role for the N-terminal domain of the IL-3 receptor in cell signalling**. *Nature communications* 2018, **9**(1):386.

Butterfield JH: **Treatment of hypereosinophilic syndromes with prednisone, hydroxyurea, and interferon**. *Immunology and allergy clinics of North America* 2007, **27**(3):493-518.

Butterfield JH, Sharkey SW: **Control of hypereosinophilic syndrome-associated recalcitrant coronary artery spasm by combined treatment with prednisone, imatinib mesylate and hydroxyurea**. *Experimental and clinical cardiology* 2006, **11**(1):25-28.

Butterworth AE, Wassom DL, Gleich GJ, Loegering DA, David JR: **Damage to schistosomula of Schistosoma mansoni induced directly by eosinophil major basic protein**. *Journal of immunology* 1979, **122**(1):221-229.

Carr PD, Conlan F, Ford S, Ollis DL, Young IG: **An improved resolution structure of the human beta common receptor involved in IL-3, IL-5 and GM-CSF signalling which gives better definition of the high-affinity binding epitope**. *Acta crystallographica Section F, Structural biology and crystallization communications* 2006, **62**(Pt 6):509-513.

Carr PD, Gustin SE, Church AP, Murphy JM, Ford SC, Mann DA, Woltring DM, Walker I, Ollis DL, Young IG: **Structure of the complete extracellular domain of the common beta subunit of the human GM-CSF, IL-3, and IL-5 receptors reveals a novel dimer configuration**. *Cell* 2001, **104**(2):291-300.

Castro M, Zangrilli J, Wechsler ME, Bateman ED, Brusselle GG, Bardin P, Murphy K, Maspero JF, O'Brien C, Korn S: **Reslizumab for inadequately controlled asthma with elevated blood eosinophil counts: results from two multicentre, parallel, double-blind, randomised, placebo-controlled, phase 3 trials**. *The Lancet Respiratory medicine* 2015, **3**(5):355-366.

Chu VT, Beller A, Rausch S, Strandmark J, Zanker M, Arbach O, Kruglov A, Berek C: **Eosinophils promote generation and maintenance of immunoglobulin-A-expressing plasma cells and contribute to gut immune homeostasis**. *Immunity* 2014, **40**(4):582-593.

Chusid MJ, Dale DC, West BC, Wolff SM: **The hypereosinophilic syndrome: analysis of fourteen cases with review of the literature**. *Medicine* 1975, **54**(1):1-27.

Collins PD, Marleau S, Griffiths-Johnson DA, Jose PJ, Williams TJ: **Cooperation between interleukin-5 and the chemokine eotaxin to induce eosinophil accumulation in vivo**. *The Journal of experimental medicine* 1995, **182**(4):1169-1174.

Cook R, Applebaum, R., Cusimano, D.: **Biological and biophysical characteristics of SB 240563, a high affinity humanized monoclonal antibody to IL-5**. *Am J Crit Care Med* 1998.

Cools J, DeAngelo DJ, Gotlib J, Stover EH, Legare RD, Cortes J, Kutok J, Clark J, Galinsky I, Griffin JD *et al*: **A tyrosine kinase created by fusion of the PDGFRA and FIP1L1 genes as a therapeutic target of imatinib in idiopathic hypereosinophilic syndrome**. *The New England journal of medicine* 2003, **348**(13):1201-1214.

Corren J, Weinstein S, Janka L, Zangrilli J, Garin M: **Phase 3 Study of Reslizumab in Patients With Poorly Controlled Asthma: Effects Across a Broad Range of Eosinophil Counts**. *Chest* 2016, **150**(4):799-810.

Coutant G, Bletry O, Prin L, Hauteville D, de Puyfontaine O, Abgrall JF, Godeau P: **[Treatment of hypereosinophilic syndromes of myeloproliferative expression with the combination of hydroxyurea and interferon alpha. Apropos of 7 cases]**. *Annales de medecine interne* 1993, **144**(4):243-250.

Cwirla SE, Balasubramanian P, Duffin DJ, Wagstrom CR, Gates CM, Singer SC, Davis AM, Tansik RL, Mattheakis LC, Boytos CM *et al*: **Peptide agonist of the thrombopoietin receptor as potent as the natural cytokine**. *Science* 1997, **276**(5319):1696-1699.

Dahl C, Hoffmann HJ, Saito H, Schiotz PO: **Human mast cells express receptors for IL-3, IL-5 and GM-CSF; a partial map of receptors on human mast cells cultured in vitro**. *Allergy* 2004, **59**(10):1087-1096.

David JR, Butterworth AE, Vadas MA: **Mechanism of the interaction mediating killing of Schistosoma mansoni by human eosinophils**. *The American journal of tropical medicine and hygiene* 1980, **29**(5):842-848.

de Vos AM, Ultsch M, Kossiakoff AA: **Human growth hormone and extracellular domain of its receptor: crystal structure of the complex**. *Science* 1992, **255**(5042):306-312.

Denburg JA, Silver JE, Abrams JS: **Interleukin-5 is a human basophilopoietin: induction of histamine content and basophilic differentiation of HL-60 cells and of peripheral blood basophil-eosinophil progenitors**. *Blood* 1991, **77**(7):1462-1468.

Dent LA, Strath M, Mellor AL, Sanderson CJ: **Eosinophilia in transgenic mice expressing interleukin 5**. *The Journal of experimental medicine* 1990, **172**(5):1425-1431.

Devos R, Guisez Y, Cornelis S, Verhee A, Van der Heyden J, Manneberg M, Lahm HW, Fiers W, Tavernier J, Plaetinck G: **Recombinant soluble human interleukin-5 (hIL-5) receptor molecules. Cross-linking and stoichiometry of binding to IL-5**. *The Journal of biological chemistry* 1993, **268**(9):6581-6587.

Devos R, Guisez Y, Plaetinck G, Cornelis S, Tavernier J, van der Heyden J, Foley LH, Scheffler JE: **Covalent modification of the interleukin-5 receptor by isothiazolones leads to inhibition of the binding of interleukin-5**. *European journal of biochemistry* 1994, **225**(2):635-640.

Egan RW, Athwal D, Bodmer MW, Carter JM, Chapman RW, Chou CC, Cox MA, Emtage JS, Fernandez X, Genatt N *et al*: **Effect of Sch 55700, a humanized monoclonal antibody to human interleukin-5, on eosinophilic responses and bronchial hyperreactivity**. *Arzneimittel-Forschung* 1999, **49**(9):779-790.

Ehrlich P: **Ueber die Specifischen granulationen des Blutes [in German]**. *Arch Anant Physiol* 1879, **3**:571–579.

Emsley P, Lohkamp B, Scott WG, Cowtan K: **Features and development of Coot**. *Acta crystallographica Section D, Biological crystallography* 2010, **66**(Pt 4):486-501.

England BP, Balasubramanian P, Uings I, Bethell S, Chen MJ, Schatz PJ, Yin Q, Chen YF, Whitehorn EA, Tsavaler A *et al*: **A potent dimeric peptide antagonist of interleukin-5 that binds two interleukin-5 receptor alpha chains**. *Proceedings of the National Academy of Sciences of the United States of America* 2000, **97**(12):6862-6867.

Ericsson UB, Hallberg BM, Detitta GT, Dekker N, Nordlund P: **Thermofluor-based high-throughput stability optimization of proteins for structural studies**. *Analytical biochemistry* 2006, **357**(2):289-298.

Fahy JV, Fleming HE, Wong HH, Liu JT, Su JQ, Reimann J, Fick RB, Jr., Boushey HA: **The effect of an anti-IgE monoclonal antibody on the early- and late-phase responses to allergen inhalation in asthmatic subjects**. *American journal of respiratory and critical care medicine* 1997, **155**(6):1828-1834.

Feng Y, Klein BK, McWherter CA: **Three-dimensional solution structure and backbone dynamics of a variant of human interleukin-3**. *Journal of molecular biology* 1996, **259**(3):524-541.

FitzGerald JM, Bleecker ER, Nair P, Korn S, Ohta K, Lommatzsch M, Ferguson GT, Busse WW, Barker P, Sproule S *et al*: **Benralizumab, an anti-interleukin-5 receptor alpha monoclonal antibody, as add-on treatment for patients with severe, uncontrolled, eosinophilic asthma (CALIMA): a randomised, double-blind, placebo-controlled phase 3 trial**. *Lancet* 2016, **388**(10056):2128-2141.

Flood-Page P, Swenson C, Faiferman I, Matthews J, Williams M, Brannick L, Robinson D, Wenzel S, Busse W, Hansel TT *et al*: **A study to evaluate safety and efficacy of mepolizumab in patients with moderate persistent asthma**. *American journal of respiratory and critical care medicine* 2007, **176**(11):1062-1071.

Fort MM, Cheung J, Yen D, Li J, Zurawski SM, Lo S, Menon S, Clifford T, Hunte B, Lesley R *et al*: **IL-25 induces IL-4, IL-5, and IL-13 and Th2-associated pathologies in vivo**. *Immunity* 2001, **15**(6):985-995.

Foster PS, Hogan SP, Ramsay AJ, Matthaei KI, Young IG: **Interleukin 5 deficiency abolishes eosinophilia, airways hyperreactivity, and lung damage in a mouse asthma model**. *The Journal of experimental medicine* 1996, **183**(1):195-201.

Furuta GT, Nieuwenhuis EE, Karhausen J, Gleich G, Blumberg RS, Lee JJ, Ackerman SJ: **Eosinophils alter colonic epithelial barrier function: role for major basic protein**. *Am J Physiol Gastrointest Liver Physiol* 2005, **289**(5):G890-897.

Garrett JK, Jameson SC, Thomson B, Collins MH, Wagoner LE, Freese DK, Beck LA, Boyce JA, Filipovich AH, Villanueva JM *et al*: **Anti-interleukin-5 (mepolizumab) therapy for hypereosinophilic syndromes**. *The Journal of allergy and clinical immunology* 2004, **113**(1):115-119.

Gauvreau GM, Boulet LP, Cockcroft DW, Fitzgerald JM, Carlsten C, Davis BE, Deschesnes F, Duong M, Durn BL, Howie KJ *et al*: **Effects of interleukin-13 blockade on allergen-induced airway responses in mild atopic asthma**. *American journal of respiratory and critical care medicine* 2011, **183**(8):1007-1014.

Gearing DP, King JA, Gough NM, Nicola NA: **Expression cloning of a receptor for human granulocyte-macrophage colony-stimulating factor**. *The EMBO journal* 1989, **8**(12):3667-3676.

Gleich GJ, Adolphson CR: **The eosinophilic leukocyte: structure and function**. *Advances in immunology* 1986, **39**:177-253.

Gleich GJ, Frigas E, Loegering DA, Wassom DL, Steinmuller D: **Cytotoxic properties of the eosinophil major basic protein**. *Journal of immunology* 1979, **123**(6):2925-2927.

Goh YP, Henderson NC, Heredia JE, Red Eagle A, Odegaard JI, Lehwald N, Nguyen KD, Sheppard D, Mukundan L, Locksley RM *et al*: **Eosinophils secrete IL-4 to facilitate liver regeneration**. *Proceedings of the National Academy of Sciences of the United States of America* 2013, **110**(24):9914-9919.

Griffin JH, Leung J, Bruner RJ, Caligiuri MA, Briesewitz R: **Discovery of a fusion kinase in EOL-1 cells and idiopathic hypereosinophilic syndrome**. *Proceedings of the National Academy of Sciences of the United States of America* 2003, **100**(13):7830-7835.

Gustin SE, Church AP, Ford SC, Mann DA, Carr PD, Ollis DL, Young IG: **Expression, crystallization and derivatization of the complete extracellular domain of the beta(c) subunit of the human IL-5, IL-3 and GM-CSF receptors**. *European journal of biochemistry* 2001, **268**(10):2905-2911.

Guthridge MA, Stomski FC, Thomas D, Woodcock JM, Bagley CJ, Berndt MC, Lopez AF: **Mechanism of activation of the GM-CSF, IL-3, and IL-5 family of receptors**. *Stem cells* 1998, **16**(5):301-313.

Hage T, Sebald W, Reinemer P: **Crystal structure of the interleukin-4/receptor alpha chain complex reveals a mosaic binding interface**. *Cell* 1999, **97**(2):271-281.

Haldar P, Brightling CE, Hargadon B, Gupta S, Monteiro W, Sousa A, Marshall RP, Bradding P, Green RH, Wardlaw AJ *et al*: **Mepolizumab and exacerbations of refractory eosinophilic asthma**. *The New England journal of medicine* 2009, **360**(10):973-984.

Haldar P, Pavord ID, Shaw DE, Berry MA, Thomas M, Brightling CE, Wardlaw AJ, Green RH: **Cluster analysis and clinical asthma phenotypes**. *American journal of respiratory and critical care medicine* 2008, **178**(3):218-224.

Hall DJ, Cui J, Bates ME, Stout BA, Koenderman L, Coffer PJ, Bertics PJ: **Transduction of a dominant-negative H-Ras into human eosinophils attenuates extracellular signal-regulated kinase activation and interleukin-5-mediated cell viability**. *Blood* 2001, **98**(7):2014-2021.

Hamann KJ, Gleich GJ, Checkel JL, Loegering DA, McCall JW, Barker RL: **In vitro killing of microfilariae of Brugia pahangi and Brugia malayi by eosinophil granule proteins**. *Journal of immunology* 1990, **144**(8):3166-3173.

Handl HL, Vagner J, Han H, Mash E, Hruby VJ, Gillies RJ: **Hitting multiple targets with multimeric ligands**. *Expert opinion on therapeutic targets* 2004, **8**(6):565-586.

Hansen G, Hercus TR, McClure BJ, Stomski FC, Dottore M, Powell J, Ramshaw H, Woodcock JM, Xu Y, Guthridge M *et al*: **The structure of the GM-CSF receptor complex reveals a distinct mode of cytokine receptor activation**. *Cell* 2008, **134**(3):496-507.

Haque A, Ouaissi A, Joseph M, Capron M, Capron A: **IgE antibody in eosinophil- and macrophage-mediated in vitro killing of Dipetalonema viteae microfilariae**. *Journal of immunology* 1981, **127**(2):716-725.

Hart TK, Cook RM, Zia-Amirhosseini P, Minthorn E, Sellers TS, Maleeff BE, Eustis S, Schwartz LW, Tsui P, Appelbaum ER *et al*: **Preclinical efficacy and safety of mepolizumab (SB-240563), a humanized monoclonal antibody to IL-5, in**

cynomolgus monkeys. *The Journal of allergy and clinical immunology* 2001, **108**(2):250-257.

Hayashida K, Kitamura T, Gorman DM, Arai K, Yokota T, Miyajima A: **Molecular cloning of a second subunit of the receptor for human granulocyte-macrophage colony-stimulating factor (GM-CSF): reconstitution of a high-affinity GM-CSF receptor**. *Proceedings of the National Academy of Sciences of the United States of America* 1990, **87**(24):9655-9659.

Hercus TR, Dhagat U, Kan WL, Broughton SE, Nero TL, Perugini M, Sandow JJ, D'Andrea RJ, Ekert PG, Hughes T *et al*: **Signalling by the betac family of cytokines**. *Cytokine & growth factor reviews* 2013, **24**(3):189-201.

Horie S, Okubo Y, Hossain M, Sato E, Nomura H, Koyama S, Suzuki J, Isobe M, Sekiguchi M: **Interleukin-13 but not interleukin-4 prolongs eosinophil survival and induces eosinophil chemotaxis**. *Internal medicine* 1997, **36**(3):179-185.

Huebner K, Isobe M, Croce CM, Golde DW, Kaufman SE, Gasson JC: **The human gene encoding GM-CSF is at 5q21-q32, the chromosome region deleted in the 5q-anomaly**. *Science* 1985, **230**(4731):1282-1285.

Ihle JN: **Interleukin-3 and hematopoiesis**. *Chemical immunology* 1992, **51**:65-106.

Ip WK, Wong CK, Wang CB, Tian YP, Lam CW: **Interleukin-3, -5, and granulocyte macrophage colony-stimulating factor induce adhesion and chemotaxis of human eosinophils via p38 mitogen-activated protein kinase and nuclear factor kappaB**. *Immunopharmacology and immunotoxicology* 2005, **27**(3):371-393.

Ishino T, Economou NJ, McFadden K, Zaks-Zilberman M, Jost M, Baxter S, Contarino MR, Harrington AE, Loll PJ, Pasut G *et al*: **A protein engineering approach differentiates the functional importance of carbohydrate moieties of interleukin-5 receptor alpha**. *Biochemistry* 2011, **50**(35):7546-7556.

Ishino T, Harrington AE, Zaks-Zilberman M, Scibek JJ, Chaiken I: **Slow-dissociation effect of common signaling subunit beta c on IL5 and GM-CSF receptor assembly**. *Cytokine* 2008, **42**(2):179-190.

Ishino T, Pillalamarri U, Panarello D, Bhattacharya M, Urbina C, Horvat S, Sarkhel S, Jameson B, Chaiken I: **Asymmetric usage of antagonist charged residues drives interleukin-5 receptor recruitment but is insufficient for receptor activation**. *Biochemistry* 2006, **45**(4):1106-1115.

Ishino T, Urbina C, Bhattacharya M, Panarello D, Chaiken I: **Receptor epitope usage by an interleukin-5 mimetic peptide**. *The Journal of biological chemistry* 2005, **280**(24):22951-22961.

Ito T, Suzuki S, Kanaji S, Shiraishi H, Ohta S, Arima K, Tanaka G, Tamada T, Honjo E, Garcia KC *et al*: **Distinct structural requirements for interleukin-4 (IL-4) and IL-13 binding to the shared IL-13 receptor facilitate cellular tuning of cytokine responsiveness**. *The Journal of biological chemistry* 2009, **284**(36):24289-24296.

Kazura JW, Grove DI: **Stage-specific antibody-dependent eosinophil-mediated destruction of Trichinella spiralis**. *Nature* 1978, **274**(5671):588-589.

Kim S, Marigowda G, Oren E, Israel E, Wechsler ME: **Mepolizumab as a steroid-sparing treatment option in patients with Churg-Strauss syndrome**. *The Journal of allergy and clinical immunology* 2010a, **125**(6):1336-1343.

Kim S, Prout M, Ramshaw H, Lopez AF, LeGros G, Min B: **Cutting edge: basophils are transiently recruited into the draining lymph nodes during helminth infection**

via IL-3, but infection-induced Th2 immunity can develop without basophil lymph node recruitment or IL-3. *Journal of immunology* 2010b, **184**(3):1143-1147.

Kips JC, O'Connor BJ, Langley SJ, Woodcock A, Kerstjens HA, Postma DS, Danzig M, Cuss F, Pauwels RA: **Effect of SCH55700, a humanized anti-human interleukin-5 antibody, in severe persistent asthma: a pilot study**. *American journal of respiratory and critical care medicine* 2003, **167**(12):1655-1659.

Kita H: **The eosinophil: a cytokine-producing cell?** *The Journal of allergy and clinical immunology* 1996, **97**(4):889-892.

Kitamura T, Sato N, Arai K, Miyajima A: **Expression cloning of the human IL-3 receptor cDNA reveals a shared beta subunit for the human IL-3 and GM-CSF receptors**. *Cell* 1991, **66**(6):1165-1174.

Klion A: **Hypereosinophilic syndrome: current approach to diagnosis and treatment**. *Annual review of medicine* 2009, **60**:293-306.

Klion AD, Law MA, Noel P, Kim YJ, Haverty TP, Nutman TB: **Safety and efficacy of the monoclonal anti-interleukin-5 antibody SCH55700 in the treatment of patients with hypereosinophilic syndrome**. *Blood* 2004a, **103**(8):2939-2941.

Klion AD, Nutman TB: **The role of eosinophils in host defense against helminth parasites**. *The Journal of allergy and clinical immunology* 2004b, **113**(1):30-37.

Klion AD, Robyn J, Akin C, Noel P, Brown M, Law M, Metcalfe DD, Dunbar C, Nutman TB: **Molecular remission and reversal of myelofibrosis in response to imatinib mesylate treatment in patients with the myeloproliferative variant of hypereosinophilic syndrome**. *Blood* 2004c, **103**(2):473-478.

Klion AD, Rothenberg ME, Murray JJ, Singh A, Simon HU: **Safety and tolerability of anti-IL-5 monoclonal antibody (Mepolizumab) therapy in patients with HES: A multicenter, randomized, double-blind, placebo-controlled trial.** *Blood* 2006, **108**(11):762A-762A.

Klose CS, Artis D: **Innate lymphoid cells as regulators of immunity, inflammation and tissue homeostasis**. *Nature immunology* 2016, **17**(7):765-774.

Koike M, Nakamura K, Furuya A, Iida A, Anazawa H, Takatsu K, Hanai N: **Establishment of humanized anti-interleukin-5 receptor alpha chain monoclonal antibodies having a potent neutralizing activity**. *Human antibodies* 2009, **18**(1-2):17-27.

Kolbeck R, Kozhich A, Koike M, Peng L, Andersson CK, Damschroder MM, Reed JL, Woods R, Dall'acqua WW, Stephens GL *et al*: **MEDI-563, a humanized anti-IL-5 receptor alpha mAb with enhanced antibody-dependent cell-mediated cytotoxicity function**. *The Journal of allergy and clinical immunology* 2010, **125**(6):1344-1353 e1342.

Kopf M, Brombacher F, Hodgkin PD, Ramsay AJ, Milbourne EA, Dai WJ, Ovington KS, Behm CA, Kohler G, Young IG *et al*: **IL-5-deficient mice have a developmental defect in CD5+ B-1 cells and lack eosinophilia but have normal antibody and cytotoxic T cell responses**. *Immunity* 1996, **4**(1):15-24.

Kunicka JE, Talle MA, Denhardt GH, Brown M, Prince LA, Goldstein G: **Immunosuppression by glucocorticoids: inhibition of production of multiple lymphokines by in vivo administration of dexamethasone**. *Cellular immunology* 1993, **149**(1):39-49.

Kusano S, Kukimoto-Niino M, Hino N, Ohsawa N, Ikutani M, Takaki S, Sakamoto K, Hara-Yokoyama M, Shirouzu M, Takatsu K *et al*: **Structural basis of interleukin-**

5 dimer recognition by its alpha receptor. *Protein science : a publication of the Protein Society* 2012, **21**(6):850-864.

Laemmli UK: **Cleavage of structural proteins during the assembly of the head of bacteriophage T4**. *Nature* 1970, **227**(5259):680-685.

Lam C, Shah KJ, Mansukhani R: **Targeting Interleukin-5 in Patients With Severe Eosinophilic Asthma: A Clinical Review**. *P & T : a peer-reviewed journal for formulary management* 2017, **42**(3):196-201.

Lantz CS, Boesiger J, Song CH, Mach N, Kobayashi T, Mulligan RC, Nawa Y, Dranoff G, Galli SJ: **Role for interleukin-3 in mast-cell and basophil development and in immunity to parasites**. *Nature* 1998, **392**(6671):90-93.

LaPorte SL, Juo ZS, Vaclavikova J, Colf LA, Qi X, Heller NM, Keegan AD, Garcia KC: **Molecular and structural basis of cytokine receptor pleiotropy in the interleukin-4/13 system**. *Cell* 2008, **132**(2):259-272.

Lazareno S, Birdsall NJ: **Estimation of competitive antagonist affinity from functional inhibition curves using the Gaddum, Schild and Cheng-Prusoff equations**. *British journal of pharmacology* 1993, **109**(4):1110-1119.

Le Beau MM, Epstein ND, O'Brien SJ, Nienhuis AW, Yang YC, Clark SC, Rowley JD: **The interleukin 3 gene is located on human chromosome 5 and is deleted in myeloid leukemias with a deletion of 5q**. *Proceedings of the National Academy of Sciences of the United States of America* 1987, **84**(16):5913-5917.

Leckie MJ, ten Brinke A, Khan J, Diamant Z, O'Connor BJ, Walls CM, Mathur AK, Cowley HC, Chung KF, Djukanovic R *et al*: **Effects of an interleukin-5 blocking monoclonal antibody on eosinophils, airway hyper-responsiveness, and the late asthmatic response**. *Lancet* 2000, **356**(9248):2144-2148.

Lee JJ, McGarry MP, Farmer SC, Denzler KL, Larson KA, Carrigan PE, Brenneise IE, Horton MA, Haczku A, Gelfand EW *et al*: **Interleukin-5 expression in the lung epithelium of transgenic mice leads to pulmonary changes pathognomonic of asthma**. *The Journal of experimental medicine* 1997, **185**(12):2143-2156.

Leru PM: **Eosinophilia and Hypereosinophilic Disorders - Update on Etiopathogeny, Classification and Clinical Approach**. *Romanian journal of internal medicine = Revue roumaine de medecine interne* 2015, **53**(4):289-295.

Lierman E, Folens C, Stover EH, Mentens N, Van Miegroet H, Scheers W, Boogaerts M, Vandenberghe P, Marynen P, Cools J: **Sorafenib is a potent inhibitor of FIP1L1-PDGFRalpha and the imatinib-resistant FIP1L1-PDGFRalpha T674I mutant**. *Blood* 2006, **108**(4):1374-1376.

Lim KG, Wan HC, Resnick M, Wong DT, Cruikshank WW, Kornfeld H, Center DM, Weller PF: **Human eosinophils release the lymphocyte and eosinophil active cytokines, RANTES and lymphocyte chemoattractant factor**. *International archives of allergy and immunology* 1995, **107**(1-3):342.

Lopez AF, Begley CG, Williamson DJ, Warren DJ, Vadas MA, Sanderson CJ: **Murine eosinophil differentiation factor. An eosinophil-specific colony-stimulating factor with activity for human cells**. *The Journal of experimental medicine* 1986, **163**(5):1085-1099.

Lopez AF, Sanderson CJ, Gamble JR, Campbell HD, Young IG, Vadas MA: **Recombinant human interleukin 5 is a selective activator of human eosinophil function**. *The Journal of experimental medicine* 1988, **167**(1):219-224.

Lotfi R, Lotze MT: **Eosinophils induce DC maturation, regulating immunity**. *J Leukoc Biol* 2008, **83**(3):456-460.

Lupardus PJ, Birnbaum ME, Garcia KC: **Molecular basis for shared cytokine recognition revealed in the structure of an unusually high affinity complex between IL-13 and IL-13Ralpha2**. *Structure* 2010, **18**(3):332-342.

Mach N, Lantz CS, Galli SJ, Reznikoff G, Mihm M, Small C, Granstein R, Beissert S, Sadelain M, Mulligan RC *et al*: **Involvement of interleukin-3 in delayed-type hypersensitivity**. *Blood* 1998, **91**(3):778-783.

Maneechotesuwan K, Yao X, Ito K, Jazrawi E, Usmani OS, Adcock IM, Barnes PJ: **Suppression of GATA-3 nuclear import and phosphorylation: a novel mechanism of corticosteroid action in allergic disease**. *PLoS medicine* 2009, **6**(5):e1000076.

McCoy AJ, Grosse-Kunstleve RW, Adams PD, Winn MD, Storoni LC, Read RJ: **Phaser crystallographic software**. *Journal of applied crystallography* 2007, **40**(Pt 4):658-674.

Mellman I, Steinman RM: **Dendritic cells: specialized and regulated antigen processing machines**. *Cell* 2001, **106**(3):255-258.

Metcalf D: **Hematopoietic cytokines**. *Blood* 2008, **111**(2):485-491.

Milburn MV, Hassell AM, Lambert MH, Jordan SR, Proudfoot AE, Graber P, Wells TN: **A novel dimer configuration revealed by the crystal structure at 2.4 A resolution of human interleukin-5**. *Nature* 1993, **363**(6425):172-176.

Mishra A, Hogan SP, Lee JJ, Foster PS, Rothenberg ME: **Fundamental signals that regulate eosinophil homing to the gastrointestinal tract**. *The Journal of clinical investigation* 1999, **103**(12):1719-1727.

Molfino NA, Gossage D, Kolbeck R, Parker JM, Geba GP: **Molecular and clinical rationale for therapeutic targeting of interleukin-5 and its receptor**. *Clinical and experimental allergy : journal of the British Society for Allergy and Clinical Immunology* 2012, **42**(5):712-737.

Murphy KM, Weaver C: **Janeway's Immunobiology**, 9th Edition edn: Garland Science; 2017.

Nishinakamura R, Miyajima A, Mee PJ, Tybulewicz VL, Murray R: **Hematopoiesis in mice lacking the entire granulocyte-macrophage colony-stimulating factor/interleukin-3/interleukin-5 functions**. *Blood* 1996, **88**(7):2458-2464.

Niu L, Heaney ML, Vera JC, Golde DW: **High-affinity binding to the GM-CSF receptor requires intact N-glycosylation sites in the extracellular domain of the beta subunit**. *Blood* 2000, **95**(11):3357-3362.

Ogata N, Kouro T, Yamada A, Koike M, Hanai N, Ishikawa T, Takatsu K: **JAK2 and JAK1 constitutively associate with an interleukin-5 (IL-5) receptor alpha and betac subunit, respectively, and are activated upon IL-5 stimulation**. *Blood* 1998, **91**(7):2264-2271.

Ortega HG, Liu MC, Pavord ID, Brusselle GG, FitzGerald JM, Chetta A, Humbert M, Katz LE, Keene ON, Yancey SW *et al*: **Mepolizumab treatment in patients with severe eosinophilic asthma**. *The New England journal of medicine* 2014, **371**(13):1198-1207.

Owen WF, Rothenberg ME, Petersen J, Weller PF, Silberstein D, Sheffer AL, Stevens RL, Soberman RJ, Austen KF: **Interleukin 5 and phenotypically altered eosinophils in the blood of patients with the idiopathic hypereosinophilic syndrome**. *The Journal of experimental medicine* 1989, **170**(1):343-348.

Panousis C, Dhagat U, Edwards KM, Rayzman V, Hardy MP, Braley H, Gauvreau GM, Hercus TR, Smith S, Sehmi R *et al*: **CSL311, a novel, potent, therapeutic**

monoclonal antibody for the treatment of diseases mediated by the common beta chain of the IL-3, GM-CSF and IL-5 receptors. *mAbs* 2016, **8**(3):436-453.

Parkin J, Cohen B: **An overview of the immune system**. *Lancet* 2001, **357**(9270):1777-1789.

Parrillo JE, Fauci AS, Wolff SM: **Therapy of the hypereosinophilic syndrome**. *Annals of internal medicine* 1978, **89**(2):167-172.

Patino E, Kotzsch A, Saremba S, Nickel J, Schmitz W, Sebald W, Mueller TD: **Structure analysis of the IL-5 ligand-receptor complex reveals a wrench-like architecture for IL-5Ralpha**. *Structure* 2011, **19**(12):1864-1875.

Pavord ID, Korn S, Howarth P, Bleecker ER, Buhl R, Keene ON, Ortega H, Chanez P: **Mepolizumab for severe eosinophilic asthma (DREAM): a multicentre, double-blind, placebo-controlled trial**. *Lancet* 2012, **380**(9842):651-659.

Pazdrak K, Stafford S, Alam R: **The activation of the Jak-STAT 1 signaling pathway by IL-5 in eosinophils**. *Journal of immunology* 1995, **155**(1):397-402.

Pegorier S, Wagner LA, Gleich GJ, Pretolani M: **Eosinophil-derived cationic proteins activate the synthesis of remodeling factors by airway epithelial cells**. *Journal of immunology* 2006, **177**(7):4861-4869.

Pelaia G, Vatrella A, Busceti MT, Gallelli L, Preiano M, Lombardo N, Terracciano R, Maselli R: **Role of biologics in severe eosinophilic asthma - focus on reslizumab**. *Therapeutics and clinical risk management* 2016, **12**:1075-1082.

Petrescu AJ, Milac AL, Petrescu SM, Dwek RA, Wormald MR: **Statistical analysis of the protein environment of N-glycosylation sites: implications for occupancy, structure, and folding**. *Glycobiology* 2004, **14**(2):103-114.

Proudfoot AE, Fattah D, Kawashima EH, Bernard A, Wingfield PT: **Preparation and characterization of human interleukin-5 expressed in recombinant Escherichia coli**. *The Biochemical journal* 1990, **270**(2):357-361.

Quelle FW, Sato N, Witthuhn BA, Inhorn RC, Eder M, Miyajima A, Griffin JD, Ihle JN: **JAK2 associates with the beta c chain of the receptor for granulocyte-macrophage colony-stimulating factor, and its activation requires the membrane-proximal region**. *Molecular and cellular biology* 1994, **14**(7):4335-4341.

Raedler D, Ballenberger N, Klucker E, Bock A, Otto R, Prazeres da Costa O, Holst O, Illig T, Buch T, von Mutius E *et al*: **Identification of novel immune phenotypes for allergic and nonallergic childhood asthma**. *The Journal of allergy and clinical immunology* 2015, **135**(1):81-91.

Rajan N, Tsarbopoulos A, Kumarasamy R, O'Donnell R, Taremi SS, Baldwin SW, Seelig GF, Fan X, Pramanik B, Le HV: **Characterization of recombinant human interleukin 4 receptor from CHO cells: role of N-linked oligosaccharides**. *Biochemical and biophysical research communications* 1995, **206**(2):694-702.

Rankin SM, Conroy DM, Williams TJ: **Eotaxin and eosinophil recruitment: implications for human disease**. *Molecular medicine today* 2000, **6**(1):20-27.

Rawlings JS, Rosler KM, Harrison DA: **The JAK/STAT signaling pathway**. *Journal of cell science* 2004, **117**(Pt 8):1281-1283.

Rioux JD, Stone VA, Daly MJ, Cargill M, Green T, Nguyen H, Nutman T, Zimmerman PA, Tucker MA, Hudson T *et al*: **Familial eosinophilia maps to the cytokine gene cluster on human chromosomal region 5q31-q33**. *American journal of human genetics* 1998, **63**(4):1086-1094.

Rothenberg ME, Hogan SP: **The eosinophil**. *Annual review of immunology* 2006, **24**:147-174.

Rothenberg ME, Pomerantz JL, Owen WF, Jr., Avraham S, Soberman RJ, Austen KF, Stevens RL: **Characterization of a human eosinophil proteoglycan, and augmentation of its biosynthesis and size by interleukin 3, interleukin 5, and granulocyte/macrophage colony stimulating factor**. *The Journal of biological chemistry* 1988, **263**(27):13901-13908.

Roufosse F: **Targeting the Interleukin-5 Pathway for Treatment of Eosinophilic Conditions Other than Asthma**. *Frontiers in medicine* 2018, **5**:49.

Roufosse F, Schandene L, Sibille C, Willard-Gallo K, Kennes B, Efira A, Goldman M, Cogan E: **Clonal Th2 lymphocytes in patients with the idiopathic hypereosinophilic syndrome**. *British journal of haematology* 2000, **109**(3):540-548.

Rozwarski DA, Diederichs K, Hecht R, Boone T, Karplus PA: **Refined crystal structure and mutagenesis of human granulocyte-macrophage colony-stimulating factor**. *Proteins* 1996, **26**(3):304-313.

Ruchala P, Varadi G, Ishino T, Scibek J, Bhattacharya M, Urbina C, Ryk DV, Uings I, Chaiken I: **Cyclic peptide interleukin 5 antagonists mimic CD turn recognition epitope for receptor alpha**. *Biopolymers* 2004, **73**(5):556-568.

Sanderson CJ: **Interleukin-5, eosinophils, and disease**. *Blood* 1992, **79**(12):3101-3109.

Sano M, Leff AR, Myou S, Boetticher E, Meliton AY, Learoyd J, Lambertino AT, Munoz NM, Zhu X: **Regulation of interleukin-5-induced beta2-integrin adhesion of human eosinophils by phosphoinositide 3-kinase**. *American journal of respiratory cell and molecular biology* 2005, **33**(1):65-70.

Scheide-Noeth JP, Rosen M, Baumstark D, Dietz H, Mueller TD: **Structural Basis of Interleukin-5 Inhibition by the Small Cyclic Peptide AF17121**. *Journal of molecular biology* 2019, **431**(4):714-731.

Scibek JJ, Evergren E, Zahn S, Canziani GA, Van Ryk D, Chaiken IM: **Biosensor analysis of dynamics of interleukin 5 receptor subunit beta(c) interaction with IL5:IL5R(alpha) complexes**. *Analytical biochemistry* 2002, **307**(2):258-265.

Shamri R, Xenakis JJ, Spencer LA: **Eosinophils in innate immunity: an evolving story**. *Cell and tissue research* 2011, **343**(1):57-83.

Shen A, Lupardus PJ, Morell M, Ponder EL, Sadaghiani AM, Garcia KC, Bogyo M: **Simplified, enhanced protein purification using an inducible, autoprocessing enzyme tag**. *PloS one* 2009, **4**(12):e8119.

Stout BA, Bates ME, Liu LY, Farrington NN, Bertics PJ: **IL-5 and granulocyte-macrophage colony-stimulating factor activate STAT3 and STAT5 and promote Pim-1 and cyclin D3 protein expression in human eosinophils**. *Journal of immunology* 2004, **173**(10):6409-6417.

Straumann A, Bauer M, Fischer B, Blaser K, Simon HU: **Idiopathic eosinophilic esophagitis is associated with a T(H)2-type allergic inflammatory response**. *The Journal of allergy and clinical immunology* 2001, **108**(6):954-961.

Sutherland GR, Baker E, Callen DF, Campbell HD, Young IG, Sanderson CJ, Garson OM, Lopez AF, Vadas MA: **Interleukin-5 is at 5q31 and is deleted in the 5q-syndrome**. *Blood* 1988, **71**(4):1150-1152.

Takatsu K: **[Role of interleukin-5 in immune regulation and inflammation]**. *Nihon rinsho Japanese journal of clinical medicine* 2004, **62**(10):1941-1951.

Tavernier J, Devos R, Cornelis S, Tuypens T, Van der Heyden J, Fiers W, Plaetinck G: **A human high affinity interleukin-5 receptor (IL5R) is composed of an IL5-specific alpha chain and a beta chain shared with the receptor for GM-CSF**. *Cell* 1991, **66**(6):1175-1184.

Tominaga A, Takaki S, Koyama N, Katoh S, Matsumoto R, Migita M, Hitoshi Y, Hosoya Y, Yamauchi S, Kanai Y *et al*: **Transgenic mice expressing a B cell growth and differentiation factor gene (interleukin 5) develop eosinophilia and autoantibody production**. *The Journal of experimental medicine* 1991, **173**(2):429-437.

Uings IJ, Balasubramanian P, McLoughlin PG, Yin Q, Dash L, Beresford A, Kearney S, Barrett RW, McKinnon M, England BP: **Modified peptide antagonists of interleukin 5 exhibit extended in vivo persistence but restricted species specificity**. *Cytokine* 2001, **15**(1):10-19.

Vagin AA, Steiner RA, Lebedev AA, Potterton L, McNicholas S, Long F, Murshudov GN: **REFMAC5 dictionary: organization of prior chemical knowledge and guidelines for its use**. *Acta crystallographica Section D, Biological crystallography* 2004, **60**(Pt 12 Pt 1):2184-2195.

Valent P, Klion AD, Horny HP, Roufosse F, Gotlib J, Weller PF, Hellmann A, Metzgeroth G, Leiferman KM, Arock M *et al*: **Contemporary consensus proposal on criteria and classification of eosinophilic disorders and related syndromes**. *The Journal of allergy and clinical immunology* 2012, **130**(3):607-612 e609.

Varricchi G, Bagnasco D, Borriello F, Heffler E, Canonica GW: **Interleukin-5 pathway inhibition in the treatment of eosinophilic respiratory disorders: evidence and unmet needs**. *Current opinion in allergy and clinical immunology* 2016, **16**(2):186-200.

Verstovsek S, Giles FJ, Quintas-Cardama A, Manshouri T, Huynh L, Manley P, Cortes J, Tefferi A, Kantarjian H: **Activity of AMN107, a novel aminopyrimidine tyrosine kinase inhibitor, against human FIP1L1-PDGFR-alpha-expressing cells**. *Leukemia research* 2006, **30**(12):1499-1505.

Vlieghe P, Lisowski V, Martinez J, Khrestchatisky M: **Synthetic therapeutic peptides: science and market**. *Drug discovery today* 2010, **15**(1-2):40-56.

Walsh GM, Sexton DW, Blaylock MG: **Corticosteroids, eosinophils and bronchial epithelial cells: new insights into the resolution of inflammation in asthma**. *The Journal of endocrinology* 2003, **178**(1):37-43.

Walter MR, Cook WJ, Ealick SE, Nagabhushan TL, Trotta PP, Bugg CE: **Three-dimensional structure of recombinant human granulocyte-macrophage colony-stimulating factor**. *Journal of molecular biology* 1992, **224**(4):1075-1085.

Weiner MP, Costa GL: **Rapid PCR site-directed mutagenesis**. *PCR methods and applications* 1994, **4**(3):S131-136.

Weller PF, Bubley GJ: **The idiopathic hypereosinophilic syndrome**. *Blood* 1994, **83**(10):2759-2779.

Wen T, Rothenberg ME: **The Regulatory Function of Eosinophils**. *Microbiology spectrum* 2016, **4**(5).

Wenzel SE: **Asthma phenotypes: the evolution from clinical to molecular approaches**. *Nature medicine* 2012, **18**(5):716-725.

Wenzel SE, Wang L, Pirozzi G: **Dupilumab in persistent asthma**. *The New England journal of medicine* 2013, **369**(13):1276.

Wilkins MR, Gasteiger E, Bairoch A, Sanchez JC, Williams KL, Appel RD, Hochstrasser DF: **Protein identification and analysis tools in the ExPASy server**. *Methods in molecular biology* 1999, **112**:531-552.

Wills-Karp M, Karp CL: **Biomedicine. Eosinophils in asthma: remodeling a tangled tale**. *Science* 2004, **305**(5691):1726-1729.

Winn MD, Ballard CC, Cowtan KD, Dodson EJ, Emsley P, Evans PR, Keegan RM, Krissinel EB, Leslie AG, McCoy A *et al*: **Overview of the CCP4 suite and current developments**. *Acta crystallographica Section D, Biological crystallography* 2011, **67**(Pt 4):235-242.

Woerly G, Roger N, Loiseau S, Capron M: **Expression of Th1 and Th2 immunoregulatory cytokines by human eosinophils**. *International archives of allergy and immunology* 1999, **118**(2-4):95-97.

Wong CK, Ip WK, Lam CW: **Interleukin-3, -5, and granulocyte macrophage colony-stimulating factor-induced adhesion molecule expression on eosinophils by p38 mitogen-activated protein kinase and nuclear factor-[kappa] B**. *American journal of respiratory cell and molecular biology* 2003, **29**(1):133-147.

Woodruff PG, Modrek B, Choy DF, Jia G, Abbas AR, Ellwanger A, Koth LL, Arron JR, Fahy JV: **T-helper type 2-driven inflammation defines major subphenotypes of asthma**. *American journal of respiratory and critical care medicine* 2009, **180**(5):388-395.

Wrighton NC, Farrell FX, Chang R, Kashyap AK, Barbone FP, Mulcahy LS, Johnson DL, Barrett RW, Jolliffe LK, Dower WJ: **Small peptides as potent mimetics of the protein hormone erythropoietin**. *Science* 1996, **273**(5274):458-464.

Wu CY, Fargeas C, Nakajima T, Delespesse G: **Glucocorticoids suppress the production of interleukin 4 by human lymphocytes**. *European journal of immunology* 1991, **21**(10):2645-2647.

Yamada Y, Rothenberg ME, Lee AW, Akei HS, Brandt EB, Williams DA, Cancelas JA: **The FIP1L1-PDGFRA fusion gene cooperates with IL-5 to induce murine hypereosinophilic syndrome (HES)/chronic eosinophilic leukemia (CEL)-like disease**. *Blood* 2006, **107**(10):4071-4079.

Yanofsky SD, Baldwin DN, Butler JH, Holden FR, Jacobs JW, Balasubramanian P, Chinn JP, Cwirla SE, Peters-Bhatt E, Whitehorn EA *et al*: **High affinity type I interleukin 1 receptor antagonists discovered by screening recombinant peptide libraries**. *Proceedings of the National Academy of Sciences of the United States of America* 1996, **93**(14):7381-7386.

Yen JJ, Hsieh YC, Yen CL, Chang CC, Lin S, Yang-Yen HF: **Restoring the apoptosis suppression response to IL-5 confers on erythroleukemic cells a phenotype of IL-5-dependent growth**. *Journal of immunology* 1995, **154**(5):2144-2152.

Yin J, Lin AJ, Golan DE, Walsh CT: **Site-specific protein labeling by Sfp phosphopantetheinyl transferase**. *Nature protocols* 2006, **1**(1):280-285.

Yin J, Straight PD, McLoughlin SM, Zhou Z, Lin AJ, Golan DE, Kelleher NL, Kolter R, Walsh CT: **Genetically encoded short peptide tag for versatile protein labeling by Sfp phosphopantetheinyl transferase**. *Proceedings of the National Academy of Sciences of the United States of America* 2005, **102**(44):15815-15820.

Ying S, Humbert M, Barkans J, Corrigan CJ, Pfister R, Menz G, Larche M, Robinson DS, Durham SR, Kay AB: **Expression of IL-4 and IL-5 mRNA and protein product by CD4+ and CD8+ T cells, eosinophils, and mast cells in bronchial biopsies**

obtained from atopic and nonatopic (intrinsic) asthmatics. *Journal of immunology* 1997, **158**(7):3539-3544.

9 APPENDIX

9.1 Abbreviations

The used one- and three letter abbreviations of the amino acids correspond to the recommendations of the IUPAC-IUB Commission on Biochemical Nomenclature.

aa	Amino acid
ADA	2-[(2-amino-2-oxoethyl)-(carboxymethyl)amino]acetic acid
Amp^R	Ampicillin resistance
APS	Ammonium-persulphate
BICINE	2-(Bis(2-hydroxyethyl)amino)acetic acid
BSA	Bovine serum albumin
Cam^R	Chloramphenicol resistance
CAPS	3-(Cyclohexylamino)-1-propanesulfonic acid
cDNA	complementary DNA
CHES	2-(Cyclohexylamino)ethanesulfonic acid
CNBr	Cyanogen bromide
CRM	Cytokine recognition motif
CV	Column volume
Da	Dalton
ddH_2O	osmosis water
DNA	Deoxyribonucleic acid
dNTP	Deoxyribose nucleoside triphosphate (Deoxynucleotide)
DTT	Dithiothreitol
E. coli	*Escherichia coli*
EC_{50}	Half maximal effective concentration
ECD	Ectodomain
EDC	1-Ethyl-3-(3-dimethyl-aminopropyl)-carbodiimid
EDTA	Ethylenediaminetetraacetic acid
FCS	Foetal calf serum
FN-III	Fibronectin type III-like domain
GM-CSF	Granulocyte-Macrophage Colony-Stimulating Factor
GM-CSFRα	Granulocyte-Macrophage Colony-Stimulating Factor receptor α
GuHCl	Guanidine hydrochloride
HEPES	3-[4-(2-Hydroxyethyl)piperazin-1-yl]propane-1-sulfonic acid
HES	Hypereosinophilic syndrome
His_6	Hexahistidine tag
IB	Inclusion bodies
IC_{50}	Half maximal inhibitory concentration
IL-3	Interleukin-3
IL-3Rα	Interleukin-3 receptor α
IL-5	Interleukin-5
IL-5Rα	Interleukin-5 receptor α
IPTG	Isopropyl-beta-D-thiogalactopyranoside
JAK	Janus kinase
k_a	Association rate
Kan^R	Kanamycin resistance

K_D	Equilibrium binding constant
k_d	Dissociation rate
kDa	Kilo Dalton
K_i	Inhibition constant
LB	Luria Broth
MES	2-morpholin-4-ylethanesulfonic acid
MOI	Multiplicity of Infection
MOPS	3-Morpholinopropane-1-sulfonic acid
MPD	2-Methyl-2,4-pentanediol
mRNA	Messenger ribonucleic acid
MTT	3-(4,5-Dimethylthiazol-2-yl)-2,5-diphenyltetrazolium-bromid
MW	Molecular weight
MWCO	Molecular weight cut off
NaAc	Sodium acetate
NHS	N-Hydroxysulfosuccinimide
OD_{600}	Optical density at 600 nm
ORF	Open reading frame
P/S	Penicillin/Streptomycin
PAGE	Polyacrylamide gel electrophoresis
PBS	Phosphate-buffered saline
PCR	Polymerase chain reaction
PDB ID	Protein data bank identification code (www.rcsb.org)
PEG	Polyethylene glycol
PIPES	1,4-Piperazinediethanesulfonic acid
RP-HPLC	Reversed-phase high-performance liquid chromatography
rpm	Revolutions per minute
RU	Response units
SDS	Sodium dodecyl sulphate
SOB	Super Optimal Broth
SPR	Surface plasmon resonance
TAE	Tris-acetate-ethylenediaminetetraacetate
TAPS	3-{[1,3-dihydroxy-2-(hydroxymethyl)propan-2yl]amino}propane-1-sulfonic acid
TB	Terrific Broth
TCA	Trichloroacetic acid
TEMED	N,N,N',N'-Tetramethylethylenediamine
TFA	Tri-fluoro acetic acid
T_H2	Type 2 helper T cells
Tris-HCl	Tris (-hydroxylmethyl)-aminoethane
v/v	Volume/volume
w/v	Weight/volume
WT	Wild type
βc	Common beta chain

9.2 cDNA sequences and the respective amino acid sequences

9.2.1 Human Interleukin-5

Section of the vector **pET3d** for expression of human Interleukin-5 in *E. coli* cells. The cDNA sequence and the corresponding amino acid sequence of the encoded ORF (open reading frame) are shown:

cDNA hIL-5

```
4089 ATGGCACCTACTGAAATTCCCACTAGTGCATTGGTGAAAGAGACCTTGGCACTGCTTTCT
   1  M  A  P  T  E  I  P  T  S  A  L  V  K  E  T  L  A  L  L  S

4149 ACTCATCGAACTCTGCTGATAGCCAATGAGACTCTCCGGATTCCTGTTCCTGTACATAAA
  21  T  H  R  T  L  L  I  A  N  E  T  L  R  I  P  V  P  V  H  K

4209 AATCACCAACTGTGCACTGAAGAAATCTTTCAGGGAATAGGCACACTCGAGAGTCAAACT
  41  N  H  Q  L  C  T  E  E  I  F  Q  G  I  G  T  L  E  S  Q  T

4269 GTGCAAGGGGGTACTGTGGAAAGACTATTCAAAAACTTGTCCTTAATAAAGAAATACATC
  61  V  Q  G  G  T  V  E  R  L  F  K  N  L  S  L  I  K  K  Y  I

4329 GATGGCCAAAAAAAAAAaGTGTGGAGAAGAACGTCGCCGTGTAAACCAATTCCTAGACTAT
  81  D  G  Q  K  K  K  C  G  E  E  R  R  R  V  N  Q  F  L  D  Y

4389 CTGCAGGAGTTTCTTGGTGTAATGAACACCGAGTGGATTATTGAAAGTTGA
 101  L  Q  E  F  L  G  V  M  N  T  E  W  I  I  E  S  *
```

9.2.2 Human Interleukin-5 receptor α variant C66A

Section of the vector **pET3d** for expression of human Interleukin-5 receptor α in *E. coli* cells. The cDNA sequence and the corresponding amino acid sequence of the encoded ORF are shown:

cDNA hIL-5Rα Mutation: C66A

```
4089 atggcagacttacttcctgatgaaaagatttcacttctcccacctgtcaatttcaccattaaagttactggtttggctcaagtt
   1  M  A  D  L  L  P  D  E  K  I  S  L  L  P  P  V  N  F  T  I  K  V  T  G  L  A  Q  V

4179 caatggaaaccaaatcctgatcaagagcaaaggaatgttaatctagaatatcaagtgaaaataaacgctccaaaagaagatgac
  31  Q  W  K  P  N  P  D  Q  E  Q  R  N  V  N  L  E  Y  Q  V  K  I  N  A  P  K  E  D  D

4269 accagaatcactgaaagcaaagctgtaaccatcctccacaaaggcttttcagcaagtgtgcggaccatcctgcagaacgaccac
  61  T  R  I  T  E  S  K  A  V  T  I  L  H  K  G  F  S  A  S  V  R  T  I  L  Q  N  D  H

4359 ctggccagcagctgggcttctgctgaacttcatgccccaccagggtctcctggaacctcaattgtgaatttaacttgcaccaca
  91  L  A  S  S  W  A  S  A  E  L  H  A  P  P  G  S  P  G  T  S  I  V  N  L  T  C  T  T

4449 acagaagacaattattcacgtttaaggtcataccaagtttcccttcactgcacctggcttgttggcacagatgcccctgaggac
 121  T  E  D  N  Y  S  R  L  R  S  Y  Q  V  S  L  H  C  T  W  L  V  G  T  D  A  P  E  D

4539 tattttctctactataggtatggctcttggactgaagaatgccaagaatacagcaaagacacactggggagaaatatcgcatgc
 151  Y  F  L  Y  Y  R  Y  G  S  W  T  E  E  C  Q  E  Y  S  K  D  T  L  G  R  N  I  A  C

4629 cccaggacttttatcctcagcaaagggcgtgactggcttgcggtgcttgttaacggctccagcaagcactctgctatcaggccc
 181  P  R  T  F  I  L  S  K  G  R  D  W  L  A  V  L  V  N  G  S  S  K  H  S  A  I  R  P

4719 cagctgtttgcccttcacgccattgatcaaataaatcctccactgaatgtcacagcagagattgaaggaactcgtctctctatc
 211  Q  L  F  A  L  H  A  I  D  Q  I  N  P  P  L  N  V  T  A  E  I  E  G  T  R  L  S  I

4809 gagaaaccagtgtctgctttccaatccattgctttgattatgaagtaaaaatacacaatacaaggaatggatatttgcagata
 241  E  K  P  V  S  A  F  P  I  H  C  F  D  Y  E  V  K  I  H  N  T  R  N  G  Y  L  Q  I

4899 ttgatgaccaatgcattcatctcaataattgatgatctttctaagtacgatgttcaagtgagagcagcagtgagctccatgtgc
 271  L  M  T  N  A  F  I  S  I  I  D  D  L  S  K  Y  D  V  Q  V  R  A  A  V  S  S  M  C

4989 gcagggctctggagtgagtggagccaacctatttatgtggggttctcaagatag
 301  A  G  L  W  S  E  W  S  Q  P  I  Y  V  G  F  S  R  *
```

Section of the vector **pET28b-ybbR** for expression of human Interleukin-5 receptor α in *E. coli* cells. The cDNA sequence and the corresponding amino acid sequence of the encoded ORF are shown:

cDNA hIL-5Rα Mutation: C66A ybbR-Tag sequence

Section of the vector **pMK1** for expression of human Interleukin-5 receptor α in insect cells. The cDNA sequence and the corresponding amino acid sequence of the encoded ORF are shown:

cDNA hIL-5Rα Mutation: C66A His_6-Tag Thrombin sequence

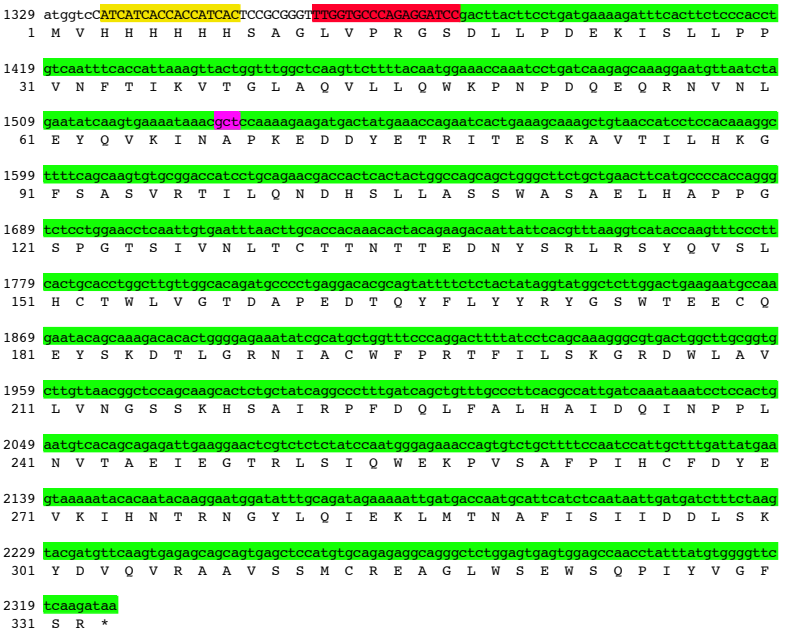

9.2.3 Common beta chain variant N346Q

Section of the vector **pAB-bee-8xHis** for expression of the human common beta chain in insect cells. The cDNA sequence and the corresponding amino acid sequence of the encoded ORF are shown:

cDNA βc | Mutation: N346Q | His_6-Tag | Honeybee signal sequence

```
4143 atgaaattcttagtcaacgttgcccttgtttttatggtcgtatacatttcttacatctatGCGGCCGCTTGGGAGCGTTCCCTGGCTGGTGCTGAGGAAACCATC
   1  M  K  F  L  V  N  V  A  L  V  F  M  V  V  Y  I  S  Y  I  Y  A  A  A  W  E  R  S  L  A  G  A  E  E  T  I

4248 CCCCTGCAGACCCTGCGCTGCTACAACGACTACACCTCCCACATCACTTGCCGTTGGGCTGACACCCAGGACGCTCAGCGTCTGGTCAACGTGACCCTGATCCGT
  36  P  L  Q  T  L  R  C  Y  N  D  Y  T  S  H  I  T  C  R  W  A  D  T  Q  D  A  Q  R  L  V  N  V  T  L  I  R

4353 CGTGTGAACGAGGACCTGCTGGAACCCGTGTCCTGCGACCTGTCCGACGACATGGCCTTGGAGCGCTTGCCCCCACCCTCGTTGCGTGCCCCGTCGTTGCGTGATC
  71  R  V  N  E  D  L  L  E  P  V  S  C  D  L  S  D  D  M  P  W  S  A  C  P  H  P  R  C  V  P  R  R  C  V  I

4458 CCCTGCCAGTCCTTCGTGGTCACCGACGTGGACTACTTCAGCTTCCAGCCCGACCGTCCCCTGGGCACCCGTCTGACCGTGACTCTGACCCAGCACGTGCAGCCC
 106  P  C  Q  S  F  V  V  T  D  V  D  Y  F  S  F  Q  P  D  R  P  L  G  T  R  L  T  V  T  L  T  Q  H  V  Q  P

4563 CCCGAGCCTCGTGACCTGCAGATCTCTACCGACCAGGACCACTTCCTGCTGACTTGGAGCGTGGCCCTGGGTTCCCCCCAGTCTCACTGGCTGTCTCCCGGCGAC
 141  P  E  P  R  D  L  Q  I  S  T  D  Q  D  H  F  L  L  T  W  S  V  A  L  G  S  P  Q  S  H  W  L  S  P  G  D

4668 CTGGAGTTCGAGGTGGTGTACAAGCGTCTGCAGGACTCCTGGGAGGACGCTGCTATCCTGCTGTCCAACACCTCCCAGGCTACCCTGGGTCCCGAGCACCTGATG
 176  L  E  F  E  V  V  Y  K  R  L  Q  D  S  W  E  D  A  A  I  L  L  S  N  T  S  Q  A  T  L  G  P  E  H  L  M

4773 CCCTCTTCCACCTACGTGGCCCGTGTGCGTACCCGTCTGGCTCCTGGTTCCCGTCTGTCCGGTCGTCCCTCCAAGTGGTCCCCCGAAGTGTGCTGGGACTCTCAG
 211  P  S  S  T  Y  V  A  R  V  R  T  R  L  A  P  G  S  R  L  S  G  R  P  S  K  W  S  P  E  V  C  W  D  S  Q

4878 CCTGGCGACGAGGCTCAGCCCCAGAACCTGGAATGCTTCTTCGACGGTGCTGCTGTGCTGTCCTGCTCCTGGGAAGTGCGCAAGGAAGTGGCTTCCTCTGTCTCC
 246  P  G  D  E  A  Q  P  Q  N  L  E  C  F  F  D  G  A  A  V  L  S  C  S  W  E  V  R  K  E  V  A  S  S  V  S

4983 TTCGGCCTGTTCTACAAGCCCTCCCCCGACGCTGGTGAAGAGGAATGCTCCCCCGTGCTGCGCGAGGGACTGGGTTCTCTGCACACCCGTCACCACTGCCAGATC
 281  F  G  L  F  Y  K  P  S  P  D  A  G  E  E  E  C  S  P  V  L  R  E  G  L  G  S  L  H  T  R  H  H  C  Q  I

5088 CCCGTGCCCGACCCTGCTACCCACGGCCAGTACATCGTGTCCGTGCAGCCTCGTCGTGCTGAGAAGCACATCAAGTCCTCCGTGAACATCCAGATGGCTCCCCCA
 316  P  V  P  D  P  A  T  H  G  Q  Y  I  V  S  V  Q  P  R  R  A  E  K  H  I  K  S  S  V  N  I  Q  M  A  P  P

5193 TCCCTGCAAGTGACCAAGGACGGCGACTCCTACTCCCTGCGTTGGGAGACTATGAAGATGCGTTACGAGCACATCGACCACACCTTCGAGATCCAGTACCGCAAG
 351  S  L  Q  V  T  K  D  G  D  S  Y  S  L  R  W  E  T  M  K  M  R  Y  E  H  I  D  H  T  F  E  I  Q  Y  R  K

5298 GACACCGCTACCTGGAAGGACTCCAAGACCGAGACTCTGCAGAACGCTCACTCCATGGCTCTGCCCGCTCTGGAACCCTCCACCCGTTACTGGGCTCGTGTGCGT
 386  D  T  A  T  W  K  D  S  K  T  E  T  L  Q  N  A  H  S  M  A  L  P  A  L  E  P  S  T  R  Y  W  A  R  V  R

5403 GTGCGCACCTCCCGTACCGGTTACAACGGTATCTGGTCCGAGTGGTCCGAAGCTCGTTCCTGGGACACCGAGTCCGAATTCgtcgagcaccaccaccaccaccac
 421  V  R  T  S  R  T  G  Y  N  G  I  W  S  E  W  S  E  A  R  S  W  D  T  E  S  E  F  V  E  H  H  H  H  H  H

5508 caccactaa
 456  H  H  *
```

9.2.4 Common beta chain wild type

Section of the vector **pMK1** for expression of the human common beta chain in insect cells. The cDNA sequence and the corresponding amino acid sequence of the encoded ORF are shown:

cDNA βc wt | His_6-Tag | Thrombin sequence

```
1260 atgcccatgttaagcgctattgttttatatgtgcttttggcggcggcggcgcattctgcctttgcggccatggtccATCATCACCACCATCACTCCGCGGGTTTG
   1  M  P  M  L  S  A  I  V  L  Y  V  L  L  A  A  A  A  H  S  A  F  A  A  M  V  H  H  H  H  H  H  S  A  G  L

1365 GTGCCCAGAGGATCGTGGGAGCGTTCCCTGGCTGGTGCTGAGGAAACCATCCCCCTGCAGACCCTGCGCTGCTACAACGACTACACCTCCCACATCACTTGCCGT
  36  V  P  R  G  S  W  E  R  S  L  A  G  A  E  E  T  I  P  L  Q  T  L  R  C  Y  N  D  Y  T  S  H  I  T  C  R

1470 TGGGCTGACACCCAGGACGCTCAGCGTCTGGTCAACGTGACCCTGATCCGTCGTGTGTGAACGAGGACCTGCTGGAACCCGTGTCCTGCGACCTGTCCGACGACATG
  71  W  A  D  T  Q  D  A  Q  R  L  V  N  V  T  L  I  R  R  V  N  E  D  L  L  E  P  V  S  C  D  L  S  D  D  M

1575 CCTTGGAGCGCTTGCCCCCACCCTCGTTGCGTGCCCCGTCGTTGCGTGATCCCCTGCCAGTCCTTCGTGGTCACCGACGTGGACTACTTCAGCTTCCAGCCCGAC
 106  P  W  S  A  C  P  H  P  R  C  V  P  R  R  C  V  I  P  C  Q  S  F  V  V  T  D  V  D  Y  F  S  F  Q  P  D

1680 CGTCCCCTGGGCACCCGTCTGACCGTGACTCTGACCCAGCACGTGCAGCCCCCCGAGCCTCGTGACCTGCAGATCTCTACCGACCAGGACCACTTCCTGCTGACT
 141  R  P  L  G  T  R  L  T  V  T  L  T  Q  H  V  Q  P  P  E  P  R  D  L  Q  I  S  T  D  Q  D  H  F  L  L  T

1785 TGGAGCGTGGCCCTGGGTTCCCCCCAGTCTCACTGGCTGTCTCCCGGCGACCTGGAGTTCGAGGTGGTGTACAAGCGTCTGCAGGACTCCTGGGAGGACGCTGCT
 176  W  S  V  A  L  G  S  P  Q  S  H  W  L  S  P  G  D  L  E  F  E  V  V  Y  K  R  L  Q  D  S  W  E  D  A  A

1890 ATCCTGCTGTCCAACACCTCCCAGGCTACCCTGGGTCCCGAGCACCTGATGCCCTCTTCCACCTACGTGGCCCGTGTGCGTACCCGTCTGGCTCCTGGTTCCCGT
 211  I  L  L  S  N  T  S  Q  A  T  L  G  P  E  H  L  M  P  S  S  T  Y  V  A  R  V  R  T  R  L  A  P  G  S  R

1995 CTGTCCGGTCGTCCCTCCAAGTGGTCCCCCGAAGTGTGCTGGGACTCTCAGCCTGGCGACGAGGCTCAGCCCCAGAACCTGGAATGCTTCTTCGACGGTGCTGCT
 246  L  S  G  R  P  S  K  W  S  P  E  V  C  W  D  S  Q  P  G  D  E  A  Q  P  Q  N  L  E  C  F  F  D  G  A  A

2100 GTGCTGTCCTGCTCCTGGGAAGTGCGCAAGGAAGTGGCTTCCTCTGTCTCCTTCGGCCTGTTCTACAAGCCCTCCCCCGACGCTGGTGAAGAGGAATGCTCCCCC
 281  V  L  S  C  S  W  E  V  R  K  E  V  A  S  S  V  S  F  G  L  F  Y  K  P  S  P  D  A  G  E  E  E  C  S  P

2205 GTGCTGCGCGAGGGACTGGGTTCTCTGCACACCCGTCACCACTGCCAGATCCCCGTGCCCGACCCTGCTACCCACGGCCAGTACATCGTGTCCGTGCAGCCTCGT
 316  V  L  R  E  G  L  G  S  L  H  T  R  H  H  C  Q  I  P  V  P  D  P  A  T  H  G  Q  Y  I  V  S  V  Q  P  R

2310 CGTGCTGAGAAGCACATCAAGTCCTCCGTGAACATCCAGATGGCTCCCCCATCCCTGAACGTGACCAAGGACGGCGACTCCTACTCCCTGCGTTGGGAGACTATG
 351  R  A  E  K  H  I  K  S  S  V  N  I  Q  M  A  P  P  S  L  N  V  T  K  D  G  D  S  Y  S  L  R  W  E  T  M

2415 AAGATGCGTTACGAGCACATCGACCACACCTTCGAGATCCAGTACCGCAAGGACACCGCTACCTGGAAGGACTCCAAGACCGAGACTCTGCAGAACGCTCACTCC
 386  K  M  R  Y  E  H  I  D  H  T  F  E  I  Q  Y  R  K  D  T  A  T  W  K  D  S  K  T  E  T  L  Q  N  A  H  S

2520 ATGGCTCTGCCCGCTCTGGAACCCTCCACCCGTTACTGGGCTCGTGTGCGTGTGCGCACCTCCCGTACCGGTTACAACGGTATCTGGTCCGAGTGGTCCGAAGCT
 421  M  A  L  P  A  L  E  P  S  T  R  Y  W  A  R  V  R  V  R  T  S  R  T  G  Y  N  G  I  W  S  E  W  S  E  A

2625 CGTTCCTGGGACACCGAGTCCTAA
 456  R  S  W  D  T  E  S  *
```

9.2.5 AF17121

Section of the vector **pET22b-CPD$_{BamHI-Leu}$** for expression of the AF17121-CPD fusion protein in *E. coli* cells. The cDNA sequence and the corresponding amino acid sequence of the encoded ORF are shown:

cDNA AF17121 cDNA CPD His$_6$-Tag

```
5205 ATGgttgacgaatgctggcgtatcATCGCTTCCCACacctggttctgcgctgaagaactcGGATCCGGAAAAATACTCCATAATCAAAAT
   1  M  V  D  E  C  W  R  I  I  A  S  H  T  W  F  C  A  E  E  L  G  S  G  K  I  L  H  N  Q  N

5295 GTTAATAGCTGGGGCCCGATTACGGTTACACCAACGACAGATGGTGGTGAAACCCGCTTCGACGGTCAAATCATCGTTCAAATGGAAAAC
  31  V  N  S  W  G  P  I  T  V  T  P  T  T  D  G  G  E  T  R  F  D  G  Q  I  I  V  Q  M  E  N

5385 GACCCGGTAGTAGCAAAAGCGGCAGCCAATTTAGCAGGTAAACATGCTGAAAGCAGTGTGGTGGTGCAGCTCGATTCAGACGGCAACTAT
  61  D  P  V  V  A  K  A  A  A  N  L  A  G  K  H  A  E  S  S  V  V  V  Q  L  D  S  D  G  N  Y

5475 CGCGTGGTGTATGGCGATCCGTCAAAACTGGATGGAAAGCTACGTTGGCAGTTGGTGGGGCATGGTCGCGACCACTCAGAAACTAACAAT
  91  R  V  V  Y  G  D  P  S  K  L  D  G  K  L  R  W  Q  L  V  G  H  G  R  D  H  S  E  T  N  N

5565 ACTCGCTTAAGTGGTTACAGTGCCGATGAGTTGGCCGTGAAATTGGCCAAGTTCCAACAGTCGTTTAATCAAGCCGAAAACATCAACAAC
 121  T  R  L  S  G  Y  S  A  D  E  L  A  V  K  L  A  K  F  Q  Q  S  F  N  Q  A  E  N  I  N  N

5655 AAACCGGATCACATCAGTATTGTTGGTTGTTCTTTGGTGAGTGACGACAAGCAAAAAGGCTTTGGTCATCAGTTTATTAACGCGATGGAT
 151  K  P  D  H  I  S  I  V  G  C  S  L  V  S  D  D  K  Q  K  G  F  G  H  Q  F  I  N  A  M  D

5745 GCGAATGGTCTTCGTGTCGATGTCTCTGTTCGTAGTTCTGAACTGGCCGTAGACGAGGCGGGACGTAAGCATACCAAGGACGCGAATGGC
 181  A  N  G  L  R  V  D  V  S  V  R  S  S  E  L  A  V  D  E  A  G  R  K  H  T  K  D  A  N  G

5835 GATTGGGTTCAAAAGGCAGAAAACAACAAAGTTTCGCTAAGCTGGGACGCGCAAGGTCTCGAGCACCACCACCACCACCACTGA
 211  D  W  V  Q  K  A  E  N  N  K  V  S  L  S  W  D  A  Q  G  L  E  H  H  H  H  H  H  *
```

9.3 Molecular weights and molar extinction coefficients

9.3.1 Molecular weight and extinction coefficients of Interleukin-5 receptor α variants

Table 33: Overview of the molecular weights and molar extinction coefficients calculated with ExPASy ProtParam tool of the IL-5Rα variants produced in this study.

IL-5Rα C66A variant	Molecular weight [Da]	Extinction coefficient ε_{280} [M-1 cm-1]
L23A	35998.6	69245
Q25A	35983.6	69245
E44A	35982.7	69245
I49A	35998.6	69245
P52A	36014.7	69245
K53A	35983.6	69245
E54A	35982.7	69245
D55A	35996.7	69245
D55N	36039.7	69245
D55E	36054.7	69245
D56A	35996.7	69245
Y57A	35948.6	67755
Y57F	36024.7	67755
Y57W	36063.7	73255
E58A	35982.7	69245
E63A	35982.7	69245
K65A	35983.6	69245
V67A	36012.6	69245
T68A	36010.7	69245
I69A	35998.6	69245
I69C/D208C	36018.7	69370
H71A	359746	69245
H71C/D208C	35994.7	69370
F74A	35964.6	69245
Y155A	35948.6	67755
K186A	35983.6	69245
R188A	35955.6	69245
R188K	36012.7	69245
D189A	35996.7	69245
W190A	35925.6	63745
L194A	35998.6	69245
P206A	36014.7	69245
D208A	35996.7	69245
L210A	35998.6	69245
M295A	35980.6	69245

9.3.2 Molecular weight and extinction coefficients of AF17121-CPD fusion protein variants

Table 34: Overview of the molecular weights and molar extinction coefficients calculated with ExPASy ProtParam tool of AF17121-CPD fusion protein variants produced in this study.

AF17121-CPD variant	Molecular weight [Da]	Extinction coefficient ε_{280} [M-1 cm-1]
E3Q	26124.80	37595
W5Y	26102.78	33585
I7F	26159.83	37595
I7H	26149.80	37595
I7M	26143.85	37595
I7L	26125.81	37595
I7L	26125.81	37595
I7Y	26175.83	39085
I8F	26159.83	37595
I8M	26143.85	37595
I8V	26111.70	37595
I8V	26111.70	37595
I8Y	26175.83	39085
A9F	26201.90	37595
A9F	26201.90	37595
A9I	26167.90	37595
A9M	26185.93	37595
S10A	26109.80	37595
S10G	26095.79	37595
S10P	26135.85	37595
H11K	26116.85	37595
H11R	26144.86	37595
T12E	26153.82	37595
T12Q	26152.84	37595
F14W	26164.85	43095
A16G	26111.79	37595
A16P	26151.85	37595
E17D	26111.79	37595
E18G	26053.75	37595

9.3.3 Molecular weight and extinction coefficients of AF17121 peptide variants

Table 35: Overview of the molecular weights and molar extinction coefficients calculated with ExPASy ProtParam tool of AF17121peptide variants produced in this study.

AF17121 variant	Molecular weight [Da]	Extinction coefficient ε_{280} [M-1 cm-1]
E3Q	2307.60	11125
W5Y	2285.57	7115
I7F	2342.63	11125
I7H	2332.59	11125
I7M	2326.64	11125
I7L	2308.61	11125
I7L	2358.63	12615
I7Y	2342.63	11125
I8F	2326.64	11125
I8M	2294.50	11125
I8V	2358.63	12615
I8V	2384.71	11125
I8Y	2350.69	11125
A9F	2368.73	11125
A9F	2292.61	11125
A9I	2278.58	11125
A9M	2318.65	11125
S10A	2299.64	11125
S10G	2327.66	11125
S10P	2336.62	11125
H11K	2335.64	11125
H11R	2347.65	16625
T12E	2294.58	11125
T12Q	2334.65	11125
F14W	2294.58	11125
A16G	2236.55	11125
A16P	2307.60	11125
E17D	2285.57	7115
E18G	2342.63	11125

9.4 Thermofluor buffer composition

Table 36: List of the buffers and their pH values used in the Thermofluor screen.
Reference buffer: 1x PBS buffer (137 mM NaCl, 2.7 mM KCl, 10 mM Na_2HPO_4, 2 mM KH_2PO_4 pH 7.4)

Well	Buffer (100mM)	pH	Well	Buffer (100mM)	pH
A1	Citric acid	4.5	**E1**	Sodium cacodylate	6.0
A2	Bis-Tris	7.0	**E3**	Bis-Tris propane	7.0
A3	Imidazole	6.5	**E3**	MOPS	7.0
A4	HEPES	8.0	**E4**	BICINE	9.0
A5	Tris-HCl	8.5	**E5**	Glycyl-glycine	8.5
A6	Reference buffer		**E6**	Reference buffer	
B1	Acetate	4.6	**F1**	Sodium cacodylate	6.5
B2	ADA	6.5	**F2**	PIPES	6.5
B3	Imidazole	8.0	**F3**	MOPS	7.5
B4	HEPES	8.5	**F4**	Tris-HCl	7.0
B5	Tris-HCl	9.0	**F5**	CHES	9.0
B6	Reference buffer		**F6**	Water	
C1	MES	5.5	**G1**	Bis-Tris	5.5
C2	ADA	7.0	**G2**	PIPES	7.0
C3	Sodium potassium phosphate	6.8	**G3**	HEPES	7.0
C4	BICINE	8.0	**G4**	Tris-HCl	7.5
C5	TAPS	8.0	**G5**	CHES	9.5
C6	Reference buffer		**G6**	Water	
D1	MES	6.5	**H1**	Bis-Tris	6.5
D2	Bis-Tris propane	6.0	**H2**	PIPES	7.5
D3	Sodium potassium phosphate	7.5	**H3**	HEPES	7.5
D4	BICINE	8.5	**H4**	Tris-HCl	8.0
D5	TAPS	9.0	**H5**	CAPS	9.8
D6	Reference buffer		**H6**	Water	

9.5 Buffer composition of the sub-screens

Table 37: Summary of the buffer composition of the sub-screen for the free IL-5Rα protein.

A-D: 0.1 M MES pH 6.5/0.1 M MOPS pH 7.0, 0.01 M $ZnSO_4$, 21-32% PEG 550 mme

	1	2	3	4	5	6	7	8	9	10	11	12
A	pH 6.5 21% PEG	pH 6.5 21% PEG	pH 6.5 22% PEG	pH 6.5 22% PEG	pH 6.5 23% PEG	pH 6.5 23% PEG	pH 6.5 24% PEG	pH 6.5 24% PEG	pH 6.5 25% PEG	pH 6.5 25% PEG	pH 6.5 26% PEG	pH 6.5 26% PEG
B	pH 6.5 27% PEG	pH 6.5 27% PEG	pH 6.5 28% PEG	pH 6.5 28%PEG	pH 6.5 29% PEG	pH 6.5 29% PEG	pH 6.5 30% PEG	pH 6.5 30% PEG	pH 6.5 31% PEG	pH 6.5 31% PEG	pH 6.5 32% PEG	pH 6.5 32% PEG
C	pH 7.0 21% PEG	pH 7.0 21% PEG	pH 7.0 22% PEG	pH 7.0 22%PEG	pH 7.0 23% PEG	pH 7.0 23% PEG	pH 7.0 24% PEG	pH 7.0 24% PEG	pH 7.0 25% PEG	pH 7.0 25%PEG	pH 7.0 26% PEG	pH 7.0 26% PEG
D	pH 7.0 27% PEG	pH 7.0 27% PEG	pH 7.0 28% PEG	pH 7.0 28%PEG	pH 7.0 29% PEG	pH 7.0 29% PEG	pH 7.0 30% PEG	pH 7.0 30% PEG	pH 7.0 31% PEG	pH 7.0 31%PEG	pH 7.0 32% PEG	pH 7.0 32% PEG
E	pH 5.5 0.6 M	pH 5.5 0.6 M	pH 5.5 0.8 M	pH 5.5 0.8 M	pH 5.5 1 M	pH 5.5 1 M	pH 5.5 1.2 M	pH 5.5 1.2 M	pH 5.5 1.4 M	pH 5.5 1.4 M	pH 5.5 1.6 M	pH 5.5 1.6 M
F	pH 6.0 0.6 M	pH 6.0 0.6 M	pH 6.0 0.8 M	pH 6.0 0.8 M	pH 6.0 1 M	pH 6.0 1 M	pH 6.0 1.2 M	pH 6.0 1.2 M	pH 6.0 1.4 M	pH 6.0 1.4 M	pH 6.0 1.6 M	pH 6.0 1.6 M
G	pH 6.5 0.6 M	pH 6.5 0.6 M	pH 6.5 0.8 M	pH 6.5 0.8 M	pH 6.5 1 M	pH 6.5 1 M	pH 6.5 1.2 M	pH 6.5 1.2 M	pH 6.5 1.4 M	pH 6.5 1.4 M	pH 6.5 1.6 M	pH 6.5 1.6 M
H	pH 7.0 0.6 M	pH 7.0 0.6 M	pH 7.0 0.8 M	pH 7.0 0.8 M	pH 7.0 1 M	pH 7.0 1 M	pH 7.0 1.2 M	pH 7.0 1.2 M	pH 7.0 1.4 M	pH 7.0 1.4 M	pH 7.0 1.6 M	pH 7.0 1.6 M

E-H: 0.1 M MES pH 5.5-6.5/0.1 M MOPS pH 7.0, 0.6-1.6 M $MgSO_4$

Table 38: Summary of the buffer composition of the sub-screen for the IL-5Rα•AF17121 complex.

A-D: 0.1 M Tris pH 7.0-8.5, 10-35% PEG 400

	1	2	3	4	5	6	7	8	9	10	11	12
A	pH 7.0 10% PEG	pH 7.0 10% PEG	pH 7.0 15% PEG	pH 7.0 15% PEG	pH 7.0 20% PEG	pH 7.0 20% PEG	pH 7.0 25% PEG	pH 7.0 25% PEG	pH 7.0 30% PEG	pH 7.0 30% PEG	pH 7.0 35% PEG	pH 7.0 35% PEG
B	pH 7.5 10% PEG	pH 7.5 10% PEG	pH 7.5 15% PEG	pH 7.5 15% PEG	pH 7.5 20% PEG	pH 7.5 20% PEG	pH 7.5 25% PEG	pH 7.5 25% PEG	pH 7.5 30% PEG	pH 7.5 30% PEG	pH 7.5 35% PEG	pH 7.5 35% PEG
C	pH 8.0 10% PEG	pH 8.0 10% PEG	pH 8.0 15% PEG	pH 8.0 15% PEG	pH 8.0 20% PEG	pH 8.0 20% PEG	pH 8.0 25% PEG	pH 8.0 25% PEG	pH 8.0 30% PEG	pH 8.0 30% PEG	pH 8.0 35% PEG	pH 8.0 35% PEG
D	pH 8.5 10% PEG	pH 8.5 10% PEG	pH 8.5 15% PEG	pH 8.5 15% PEG	pH 8.5 20% PEG	pH 8.5 20% PEG	pH 8.5 25% PEG	pH 8.5 25% PEG	pH 8.5 30% PEG	pH 8.5 30% PEG	pH 8.5 35% PEG	pH 8.5 35% PEG
E	pH 4.5 1% PEG 10% MPD	pH 4.5 1% PEG 10% MPD	pH 4.5 2% PEG 10% MPD	pH 4.5 2% PEG 10% MPD	pH 5.0 3% PEG 10% MPD	pH 5.0 3% PEG 10% MPD	pH 5.0 4% PEG 10% MPD	pH 5.0 4% PEG 10% MPD	pH 5.5 5% PEG 10% MPD	pH 5.5 5% PEG 10% MPD	pH 5.5 6% PEG 10% MPD	pH 5.5 6% PEG 10% MPD
F	pH 4.5 1% PEG 15% MPD	pH 4.5 1% PEG 15% MPD	pH 4.5 2% PEG 15% MPD	pH 4.5 2% PEG 15% MPD	pH 5.0 3% PEG 15% MPD	pH 5.0 3% PEG 15% MPD	pH 5.0 4% PEG 15% MPD	pH 5.0 4% PEG 15% MPD	pH 5.5 5% PEG 15% MPD	pH 5.5 5% PEG 15% MPD	pH 5.5 6% PEG 15% MPD	pH 5.5 6% PEG 15% MPD
G	pH 4.5 1% PEG 20% MPD	pH 4.5 1% PEG 20% MPD	pH 4.5 2% PEG 20% MPD	pH 4.5 2% PEG 20% MPD	pH 5.0 3% PEG 20% MPD	pH 5.0 3% PEG 20% MPD	pH 5.0 4% PEG 20% MPD	pH 5.0 4% PEG 20% MPD	pH 5.5 5% PEG 20% MPD	pH 5.5 5% PEG 20% MPD	pH 5.5 6% PEG 20% MPD	pH 5.5 6% PEG 20% MPD
H	pH 4.5 1% PEG 25% MPD	pH 4.5 1% PEG 25% MPD	pH 4.5 2% PEG 25% MPD	pH 4.5 2% PEG 25% MPD	pH 5.0 3% PEG 25% MPD	pH 5.0 3% PEG 25% MPD	pH 5.0 4% PEG 25% MPD	pH 5.0 4% PEG 25% MPD	pH 5.5 5% PEG 25% MPD	pH 5.5 5% PEG 25% MPD	pH 5.5 6% PEG 25% MPD	pH 5.5 6% PEG 25% MPD

E-H: 0.1 M sodium acetate pH 4.5-5.5, 1-6% PEG 4000, 10-25% MPD

9.6 Copyright clearance

Parts of this thesis were published in the following article:

Scheide-Noeth JP, Rosen M, Baumstark D, Dietz H, Mueller TD: **Structural Basis of Interleukin-5 Inhibition by the Small Cyclic Peptide AF17121**. *Journal of molecular biology* 2019, **431**(4):714-731.
https://doi.org/10.1016/j.jmb.2018.11.029

Including the following figures:

Figure 54, Figure 55, Figure 56, Figure 57, Figure 76, Figure 81a and Figure 84

Furthermore, I would like to acknowledge the permission by the publishers to reuse/republish the following figures in my doctoral thesis:

Figure 1:

JANEWAY'S IMMUNOBIOLOGY 9E by Kenneth Murphy and Casey Weaver. Copyright © 2017 by Garland Science, Taylor & Francis Group, LLC. Used by permission of W. W. Norton & Company, Inc.

Figure 6:

Republished with permission of Dove Medical Press, from Pelaia G *et al.*, **Role of biologics in severe eosinophilic asthma - focus on reslizumab**. *Therapeutics and clinical risk management,* Copyright © 2016, **12**:1075-1082; permission conveyed through Copyright Clearance Center, Inc.

Figure 7, Figure 8 and Figure 11:

Reprinted from Patino E *et al.*: **Structure analysis of the IL-5 ligand-receptor complex reveals a wrench-like architecture for IL-5Ralpha**. *Structure*, Copyright © 2011, **19**(12):1864-1875, with premission from Elsevier.

Figure 13:

Reprinted from Hansen G *et al.*: **The structure of the GM-CSF receptor complex reveals a distinct mode of cytokine receptor activation**. *Cell,* Copyright © 2008, **134**(3):496-507, with premission from Elsevier.

Figure 3 and Figure 14:

Reprinted from Hercus TR *et al.*: **Signalling by the betac family of cytokines**. *Cytokine & growth factor reviews,* Copyright © 2013, **24**(3):189-201, with premission from Elsevier.

10 CURRICULUM VITAE

11 LIST OF PUBLICATIONS

Scheide-Noeth JP, Rosen M, Baumstark D, Dietz H, Mueller TD: **Structural Basis of Interleukin-5 Inhibition by the Small Cyclic Peptide AF17121**. *Journal of molecular biology* 2019, **431**(4):714-731. https://doi.org/10.1016/j.jmb.2018.11.029

12 ACKNOWLEDGEMENT

I would like to acknowledge and thank many people who helped me to get this far. First of all, I am very thankful to my mentor Prof. Dr. Thomas Müller for giving me the opportunity to start my scientific career in the field of protein biochemistry and structure biology. I enjoyed working on such an interesting and versatile topic. I would like to thank him for the good support, the constant willingness to discuss and his numerous suggestions and ideas that have contributed to the progress of this work.

I'm thankful to Prof. Dr. Hermann Schindelin and PD Dr. Heike Hermanns to act as members of my supervisory committee and for their fruitful input and critical revision of my work.

Furthermore, I would like to thank all former and current colleagues of the work group and the entire chair for the pleasant working atmosphere and the good cooperation. A special thanks goes to Eva-Maria Muth, Jens Lautenschläger, Dr. Mathias Kottmair for entertaining moments, helpful discussions and activities outside the lab.

I would like to thank Maximilian Rosen, David Baumstark, Viola Schmitt and Harald Dietz for the trust they put into me to complete their thesis under my supervision and the great cooperation!

I also would like to thank all the administrative staff of the Graduate School of Life Sciences (GSLS) for the organization of different workshops, symposia and retreats, and the effort they take to provide further training for us. I am also thankful for the fruitful discussions during these events and would like to thank all doctorate students of the GSLS.

I would like to thank Dr. Jochen Kuper and Dr. Wolfgang Kölmel for the introduction to automated protein crystallization and X-ray crystallography.

I would like to thank my friends for reminding me that there is also a life outside of work. I would like to thank my family for the continued support and the constant faith in me.

My greatest thanks go to my wife Sandra Nöth, who bravely passed through all the ups and downs, especially during the final time and that I can rely on her at all times.

13 AFFIDAVIT

I hereby confirm that my thesis entitled “Activation of the Interleukin-5 receptor and its inhibition by cyclic peptides” is the result of my own work. I did not receive any help or support from commercial consultants. All sources and / or materials applied are listed and specified in the thesis.

Furthermore, I confirm that this thesis has not yet been submitted as part of another examination process neither in identical nor in similar from.

Place, Date Signature

Eidesstattliche Erklärung

Hiermit erkläre ich an Eides statt, die Dissertation “Aktivierung des IL-5 Rezeptors und dessen Inhibierung durch zyklische Peptide” eigenständig, d.h. insbesondere selbstständig und ohne Hilfe eines kommerziellen Promotionsberaters, angefertigt und keine anderen als die von mir angegeben Quellen und Hilfsmittel verwendet zu haben.

Ich erkläre außerdem, dass die Dissertation weder in gleicher noch in ähnlicher Form bereits in einem anderen Prüfungsverfahren vorgelegen hat.

Ort, Datum Unterschrift